PROGRESS REPORT
ON NUCLEAR DATA RESEARCH IN THE EURATOM COMMUNITY

for the period January 1 to December 31, 1965

Submitted by the Joint Euratom Nuclear Data and Reactor Physics Committee

(Secretariat : Central Bureau for Nuclear Measurements, Euratom, Geel, Belgium)

February 1966

EUROPEAN AMERICAN NUCLEAR DATA COMMITTEE

EANDC(E) 66 "U"

PROGRESS REPORT

ON NUCLEAR DATA RESEARCH IN THE EURATOM COMMUNITY

for the period January 1 to December 31, 1965

Submitted by the Joint Euratom Nuclear Data
and Reactor Physics Committee

(Secretariat : Central Bureau for Nuclear
Measurements, Euratom, Geel, Belgium)

February, 1966

EUROPEAN AMERICAN NUCLEAR DATA COMMITTEE

INDEX

1. KERNFORSCHUNGSZENTRUM KARLSRUHE (GERMANY), INSTITUT FÜR ANGEWANDTE KERNPHYSIK

1.1. 3 MeV Van de Graaff

1.1.1. High Resolution Resonance Spectroscopy

G. Rohr, J. Nebe

Total neutron cross sections with high resolution have been made in the energy region of about 18 - 220 KeV using two sorts of detectors together with a 1 ns pulsed Van de Graaff generator and a thick ^{7}Li target. For the lower energy region up to 50 KeV the boron slab detector was used in the following manner. Around the boron slab four well-shielded NaI(Tl)-detectors were mounted perpendicular to the neutron beam. With this arrangement the background is not time correlated and can be measured in a very simple and accurate manner. The instrumental time resolution for the four parallel connected NaI(Tl)-detectors was measured as 2.8 ns with the 478 keV γ-ray from the lithium target. The overall time resolution of the spectrometer is influenced by the above mentioned instrumental uncertainty, the channel width, and the transit time spread of the detected neutrons in the boron slab. Gaussian functions were assumed for the shape of the two first uncertainties, the third depends upon the detection efficiency which is an exponential function of penetration. All three functions were folded together to give the overall time resolution of the spectrometer.

Above 50 keV the proton recoil detector with two photomultipliers in coincidence was used. The instrumental time resolution was measured with the Compton spectrum of the 478 keV γ-ray from the lithium target, but accepting pulses equivalent to the neutron pulses, at which the highest pulses correspond to pulses of known neutron energy. The half width of time resolution changes from 4 to 2.9 ns with neutron energy from 30 to 300 keV. The overall time resolution of the spectrometer was determined in the same way as for the boron slab. With the correct information for the background and the energy resolution of the spectrometer a

new technique in determining the resonance parameters was used. Measured cross sections were compared with the cross sections of the R-matrix multilevel formula taking into account the finite energy resolution. In this manner one can assign resonance parameters even for resonances which are not completely resolved.

The total neutron cross section with a resolution of 0.39 ns/m (for 220 keV) was measured for the following materials:

Vanadium	18 - 220 keV
Manganese	50 - 260 keV
Iron	54 - 250 keV

Some of the results are given in figs. 1.1.-1.6. A few new resonances in vanadium and manganese were detected. Using the new technique for analysing resonance parameters the spin of more resonances than hitherto known could be determined. The results for vanadium are given in table 1.1. The analysis of the resonance parameters is in progress.

Table 1.1.: Resonance Parameters for Vanadium

E(keV)	Γ_n (keV)	l	J
21.65	0.79	0	3
29.45	0.191	0	4
39.30	0.57	0	3
48.20	0.15	0	4
49.55	0.63	0	3
52.0	0.115	0	4
53.0	0.98	0	3
62.9	3.8	0	3
68.1	4.7	0	4
83.0	1.2	0	4
87.8	3.2	0	4
110.8	0.25	0	3
113.5	0.11	0	4
114.8	0.08	0	3
116.6	2.4	0	4
118.7	0.115	0	3
118.7	20.5	0	4
134.7	3.3	0	4
141.2	3.8	0	3
145.7	1.5	0	3
152.6	3.0	0	4

1.1.2. Measurement of Radiative Capture Cross Sections

D. Kompe

The large liquid scintillator tank (800 l) for radiative capture cross section measurements was completed and installed together with shielding, collimator, sample changer, and electronics at the 10 ns-flight-path of the 3 MeV Van de Graaff. Some tests were made: We measured a timing resolution of 2.8 ns. Resolution for γ-ray energy was

46 % for 0.66 MeV (^{137}Cs)
36 % for 0.84 MeV (^{54}Mn)
15 % for 2.50 MeV (^{60}Co)

Average capture cross section measurements in the energy range from 10 to 100 keV on Au, In, Ta, Ag, Mo, W, Nb are planned for the beginning of the year 1966.

1.1.3. Fast Neutron Life Time Measurements

H. Miessner, E. Arai

Fast neutron life time measurements in the keV region were carried out in order to measure ("selfshielded") effective neutron cross sections, which are very important for fast reactor design. A short burst (1-10 ns) of nearly monoenergetic neutrons is injected into assemblies of Pb and ^{238}U, and the decay of the neutron field in the block is measured. Due to moderation effects this decay is not exactly exponential (fig. 1.7.), but by means of age theory one can calculate a moderation correction function F(t), which corrects the measured neutron density $n_{obs}(t)$ in the following way

$$n_{obs}(t) \;/\; F(t) \sim \exp{-\alpha t}.$$

The corrected neutron density decays exactly exponentially (fig. 1.7.) with a decay constant α, which is given by

$$\alpha = v.\Sigma_a^{eff} + vB^2 \;/\; 3\Sigma_t^{eff} + C_T B^4.$$

α is measured as a function of the buckling B^2 (fig. 1.8.) and in this way Σ_a^{eff} and Σ_t^{eff} are obtained (table 1.2.). The effective cross sections are related to the "infinite dilution" average values $\langle\sigma_a\rangle$ and $\langle\sigma_t\rangle$ by selfshielding factors f_c and f_t calculated by Abagjan (1) :

$$\sigma_a^{eff} = f_c.\langle\sigma_a\rangle \qquad \sigma_t^{eff} = f_t.\langle\sigma_t\rangle$$

Table 1.2. shows σ_a^{eff} and σ_t^{eff} measured by this method in comparison with $\langle\sigma_a\rangle$ and $\langle\sigma_t\rangle$ measured by other methods and the calculated f-factors.

Table 1.2.: Effective cross sections

Material	Neutron Energy (keV)	$\langle\sigma_a\rangle$(b)	f_c	$f_c \cdot \langle\sigma_a\rangle$(b)	σ_a^{eff}(b)
Pb	30 ± 6	-	-	-	-
^{238}U	30 ± 6	0.50(2)	0.90	0.45	0.44 ± 0.03
^{238}U	7.5 ± 0.8	0.64(2)	0.63	0.40	0.43 ± 0.04

Material	Neutron Energy (keV)	$\langle\sigma_t\rangle$(b)	f_t	$f_t \cdot \langle\sigma_t\rangle$(b)	σ_t^{eff}(b)
Pb	30 ± 6	10.0(3)	1.00	10.0	9.6 ± 0.5
^{238}U	30 ± 6	14.0(4)	0.97	13.6	14.5 ± 0.5
^{238}U	7.5 ± 0.8	15.8(4)	0.73	11.7	12.0 ± 0.8

(1) Abagjan, L.P. et al.: INDSWG 17(1964)
(2) Schmidt, J.J.: KFK 120 (1963)
(3) Hughes and Schwartz: BNL 325
(4) Allan: EANDC-UK-35L(1964)

1.1.4. Measurements of Activation Cross Sections

W. Pönitz

The activation cross section of ^{197}Au was measured at 30 and 64 keV neutron energy. Two different methods were used at 30 keV:

1. The neutron source-strength of the $^{7}Li(p,n)^{7}Be$ reaction was determined from the ^{7}Be activity. Both α-activities (^{198}Au from the gold probe and ^{7}Be from the ^{7}Li-target) were measured using a 4 x 3 in NaI(Tl) crystal. The different γ-efficiencies were corrected by theoretical calculations.

2. The neutron flux was measured by the manganese bath technique. The ^{198}Au activity was determined using the $4\pi\beta-\gamma$-coincidence method. Many corrections were carried out. The average result is

$$\sigma_{act}^{Au}(30keV) = \sigma_{n,\gamma}^{Au}(30keV) = (0.600 \pm 0.009)\ \text{barn}$$

For 64 keV neutron energy the result is

$$\sigma^{Au}_{act}\ (64\ keV) = \sigma^{Au}_{n,\gamma}\ (64\ keV) = (0.361 \pm 0.008)\ barn.$$

The result at 30 keV was used to normalise energy dependent measurements of other experimentators (1 - 5). The result is shown in fig. 1.9. This cross section was used to measure some other activation cross sections (tabel 1.3.) and isomeric cross section ratios. Fig. 1.10. shows the n,γ-cross section of indium which is a combination of the four partial activation cross sections.

The isomeric cross section ratios were used to determine p-wave- and spin dependent s-wave-strength functions. The results are

^{103}Rh $S(1) = (3.2 \pm 1.5) \cdot 10^{-4}$

^{109}Ag $S(1) = 2.0 \cdot 10^{-4}$

^{103}Rh $S(0,1)/S(0,0) = 3.0 \pm 1.5$

^{115}In $S(0,5)/S(0,4) = 3.1 \pm 1.5$

The isomeric cross section ratios R of Rh and Ag show a behavior like a threshold detector (see fig. 1.11.).

Table 1.3.: Activation cross sections

Activity	Half live	σ_{act}(7.8keV) (barn)	σ_{act}(30keV) (barn)	σ_{act}(64keV) (barn)
$^{110}Ag^{m}$	250 d	0.05	0.04	0.06
$^{114}In^{m}$	50 d	1.12	0.61	0.45
$^{116}In^{m}$	54 min	1.19	0.640	0.383
$^{122}Sb^{g}$	28 d	0.72	0.34	0.28
$^{124}Sb^{g}$	60 d	0.52	0.23	0.18

(1) J.F. Barry, J. of Nucl. Energy A/B, 18, 491 (1964).
(2) K.K. Harris et al., Nucl. Phys. 69, 37 (1965).
(3) E. Haddad et al., EANDC-33 "U" (1963).
(4) J.H. Gibbons et al., Phys. Rev. 122, 182 (1961).
(5) V.A. Konks et al., Sov. Phys. JETP 19, 59 (1964).

1.1.5. Fission Cross Sections

W. Gilboy, G. Knoll

The absolute fission cross section of ^{235}U is being measured in the neutron energy range 10 - 150 keV using the $^{7}Li(p,n)^{7}Be$ reaction. The neutron source intensity will be established by reference to the induced ^{7}Be activity. An experiment to measure the fission cross sections of ^{239}Pu, ^{240}Pu, ^{241}Pu relative to ^{235}U in the same energy range is due to begin in January 1966 when the first Pu-foils will be delivered by CBNM, Geel.

1.1.6. Operation of the Machine

H. Miessner, B. Reuter

The pulsed 3 MeV Van de Graaff worked without any serious breakdowns since April, 1965, and only routine repairs were necessary. The total weekly operation time of the machine is about 100 hrs; 80 % of this time is effectively used as measuring time.

1.2. (n,γ)-Spectroscopy

W. Michaelis, C. Weitkamp, U. Fanger, G. Markus, H. Schmidt

In the period covered by this report (n,γ)-reactions on the following target nuclei were investigated at the FR 2: ^{73}Ge, ^{87}Sr and ^{164}Dy. The subject of these experiments is the investigation of quadrupole vibrational states with multiple phonon characteristics in the case of ^{74}Ge and ^{88}Sr and the examination of the Nilsson theory and the superfluid model in the case of the deformed nucleus ^{165}Dy. Precision measurements of the capture gamma ray spectrum have been performed over the whole energy range by means of a 4 cm^2 x 0.5 cm lithium-drifted germanium detector. Considerable aid in analysis of the level structure is provided by double and triple coincidence measurements with 4"Ø x 5" NaI(Tl) detectors and a 5-crystal-pair spectrometer which is capable of working in coincidence with a large single crystal spectrometer. Data were processed using the Karlsruhe Multiple Input Data Acquisition System (MIDAS).

1.2.1. ^{74}Ge: The target was ^{73}Ge enriched to 86.1 %. 148 gamma transistions have been observed with the germanium detector.

Several coincidence relationships could be established. The level scheme obtained involves 38 excited states in the energy range from 0 to 4400 keV. The neutron binding energy of ^{74}Ge was determined to be (10202 ± 10)keV.

1.2.2. ^{88}Sr: High resolution measurements revealed 146 gamma transitions from a natural strontium sample. Information on high energy transitions which have to be attributed to ^{88}Sr was obtained from a triple sum coincidence experiment with a window set at the binding energy of ^{88}Sr. A major number of cascade relationships could be settled. 15 energy levels were observed in the energy range from 0 to 5325 keV. The binding energy was found to be (11110 ± 4) keV.

1.2.3. ^{165}Dy: The sample was ^{164}Dy enriched to 92.7 %. Along with conventional coincidence experiments an attempt was made to operate a lithium-drifted germanium diode in coincidence with a 4"Ø x 5" NaI(Tl) detector. The position of several gamma transitions in the level scheme could be established. As to the low-lying Nilsson orbitals $7/2^+$ (633), $1/2^-$ (521), $5/2^-$ (512), and $5/2^-$ (523) the results of previous investigations from curved crystal and (d,p)-measurements are confirmed. The Nilsson state 3/2- (521) up to now tentatively assigned to the level at 605 keV obviously occurs at 1108 keV. The 658 keV state most probably has spin $5/2^-$ and seems to be collective in nature. As to levels at 1167 and 1590 keV the hitherto existing data preclude a definite assignment. Further analysis of the experimental data is in progress.

Detailed results of the (n,γ)-experiments have been published in refs. (1 - 6).

(1) C. Weitkamp, W. Michaelis, H. Schmidt, U. Fanger and G. Markus, Proc. Int. Conf. on the Study of Nuclear Structure with Neutrons, Antwerp (1965)

(2) C. Weitkamp, W. Michaelis, H. Schmidt and U. Fanger, submitted to Zeitschr. f. Physik

(3) H. Schmidt, W. Michaelis, G. Markus and C. Weitkamp, Proc. Int. Conf. on the Study of Nuclear Structure with Neutrons, Antwerp (1965)

(4) H. Schmidt, W. Michaelis, G. Markus and C. Weitkamp, submitted to Zeitschr. f. Physik

(5) G. Markus, W. Michaelis, H. Schmidt and C. Weitkamp, Proc. Int. Conf. on the Study of Nuclear Structure with Neutrons, Antwerp (1965)

(6) G. Markus, W. Michaelis, H. Schmidt and C. Weitkamp, submitted to Zeitschr. f. Physik.

1.3. Slow Neutron Inelastic Scattering

1.3.1. Scattering Law Measurements

W. Gläser, F. Carvalho, G. Ehret, R. Merkel

1.3.1.1. Free H_2O Molecules

Improved measurements of the double differential scattering cross section for water vapour in a temperature and density range of 230 - 270° C and 8 - 15 mg/cm^3 have been completed for several incident energies between 18 and 70 meV. The energy and momentum transfer range for which data have been processed is now

$$0 \leq \beta \leq 2 \text{ and } 0.05 < \alpha < 6 \quad (\beta = \hbar\omega / k_B T; \alpha = \hbar^2 k^2 / 2M_p k_B T).$$

Part of the derived scattering law values $S(\alpha,\beta)$ are represented in fig. 1.12. The curves are best fits to the experimental data. Using Krieger-Nelkin theory these results can be described only with an energy dependent mass ($M_{eff} \geq 1.9\ M_p$).

1.3.1.2. Zirconium Hydride

Zirconium hydride scattering runs with improved signal-to-background ratio and with incident energies of 18, 35, 64, and 90 meV have been made. The range of scattering angles was between 30 and 150 degrees. A rough analysis of the optical band yields a line width of 30 meV, independent from scattering angle. The main effort of the data processing was still on the acoustical modes.

The reconstruction of the measured scattering law $S(\alpha,\beta)$, sometimes including modified line shapes for the high energy mode (1), by using LEAP-ADDELT calculations yielded no satisfactory agreement. Effort is made now on multiple scattering corrections for the data.

(1) S.S. Pan and F.J. Webb, Nucl. Sci. Eng. 23, 194 (1965).

1.3.1.3. Graphite

Double differential scattering cross sections of graphite have

been measured at 260° C. Two types of graphite of different origins and densities (ρ = 2.05 and 1.57, respectively) were studied. The incident energies were 18, 35, 72, and 95 meV, the scattering angles covered the range from 22 to 150 degrees. The raw data obtained is being processed now.

1.3.2. Other Experiments

W. Gläser, F. Carvalho, P. von Blankenhagen

1.3.2.1. H_2O

Experimental studies of small energy transfers in H_2O (20° C) covering a wide range of momentum transfer down to $\kappa = 0.2$ Å^{-1} have been started (incident energy = 7.5 meV, smallest scattering angle = 5.5 degrees). Earlier results on diffusive motions in H_2O have been verified (2).

(2) K.E. Larsson, Inelastic Scattering, Vol. II, P. 3, IAEA, Vienna, 1965.

1.3.2.2. Amonium Halides

Preliminary measurements of the scattering properties of some amonium halides (NH_4C, NH_4Br, NH_4J) below and above the highest phase transition in the solid have been done for a relative large range of the (κ,ω)-plane. It is intended to extract from these data quantitative information on the degree of freedom of the rotational motion of the NH_4 ion.

1.3.2.3. Vanadium

Considerable amount of double differential scattering data has been collected for room temperature vanadium. An effort is done in the direction of correcting for multiple scattering events. Besides an analytical computation of elastic double scattering correction factors for infinite plane geometry, a Fortran program has been written also for inelastic-elastic double scattering processes. Finally measurements were done with a sample geometry designed to give minimum multiple scattering.

1.4. New Developments in Instrumentation

1.4.1. On-Line Computers

G. Krüger et al.

1.4.1.1. On-Line Computer Facility at the FR 2 Reactor

The real-time data processing system MIDAS (1) (Multiple

Input Data Acquisition System) was in continuous operation until October, 1965. The facility has proven its performance and reliability. After restart of the FR 2 with a new fuel loading the neutron flux will increase by a factor of 5 - 7. As a consequence, the experiments will furnish much higher data rates to the data handling system. Therefore, an extended MIDAS was designed which is nearly completed now (fig. 1.13.). This MIDAS 66 (2) consists of two computers, a CDC 160-A and a CDC 8090, both fully compatible with each other. Each computer has its own private core storage of 8 K - 12 bit words. They share an additional memory with a capacity of 16 K. Some pieces of peripheral equipment were newly designed:

An Exchange Unit facilitates cooperation of the two processors. The Real-Time Clock (time-of-the-day clock) is computer-independent and provides an absolute time base for the computers to control their real-time environment.
The Channel Control enables or disables the different data communication lines between the experiments and the computer input.
The System Control monitors some basic electronic functions of the computers and the I/O interface. It alarms the operator when a serious malfunction happens.
The switchbox is a network which connects the data channel, the drum control, and the display units. One of the activities of the box is the generation of steady display pictures without interfering with the computer operations.
To connect experiments from outside the reactor building a fast (100 kHz) data transmission system has been implemented.

An IBM 1311 disc file unit increases the direct access storage considerably. A new software procedure allows on-line accumulation of 256 K channels of one or more multiparameter experiments on the disc. Therefore, the combination CDC 160-A/IBM 1311 will be used as a 256 K multichannel analyzer for counting rates up to 2500 events/s. This procedure also has advantages for the accumulation of the raw data stored event-by-event onto magnetic tape. An Operating System for the symmetrical double computer system is being developed.

1.4.1.2. On-Line Computer CAE 510 at the Van de Graaff Accelerator

The CAE 510 is a microprogrammed machine with an 8 K 18 bit core memory. The memory cycle is 6 μs. The computer-experiment interface consists of a special data channel CAE 592, a 12 word derandomizer and buffer, and a transfer control unit. A 1 nanosecond time coder manufactured by Intertechnique, Paris, is used as an imput device mainly for the measurement of neutron cross sections by time-of-flight in the intermediate energy range. The system was going in full operation during the reported period.

(1) G. Krüger und G. Zipf: MESPRO 64 - das Betriebssystem für die integrierte Computeranlage MIDAS, KFK 371 (1965).
(2) G. Krüger, G. Dimmler, G. Zipf, H. Hanak und R. Merkel: Ein Doppelcomputersystem zur integrierten Datenverarbeitung am FR 2, Kerntechnik (in press).

1.4.2. The Neutron Flash Tube

A. Schmidt

The tube has been operated over extended periods with a neutron output of approximately 5 x 10^8 n/pulse, the pulse duration being 2 μs. The maximum pulse frequency is 5 00 s^{-1}. Target life tests have been performed with 1.2 mg/in^2 titanium targets which gave a constant neutron output of the flash tube in excess of 100 h using an average loading of 0.5 mA/cm^2 at the target sheath. Further development work at the neutron flash tube will be devoted to shorter neutron pulses.

1.4.3. A High Resolution Time-of-Flight Spectrometer at the Karlsruhe Cyclotron

S. Cierjacks et al.

A neutron time-of-flight spectrometer was constructed using the isochronous cyclotron as a pulsed neutron source of very high intensity and extremly short pulse length. With a special type of a deflection-bunching system (see fig. 1.14.) consisting of two pairs of electrostatic deflector plates the natural pulse sequence frequency of 33 MHz was reduced to 20 kHz. From this, however, follows a current reduction of a factor of 30 only.
The following performance data of the spectrometer have been determined:

Neutron pulse length $\leq$ 1.5 ns.
Neutron intensity ($E_n \geq$ 200 keV) at the detector station: $(5 \pm 2)10^4$ n/cm^{2}s using deuterons (40 MeV$\leq E_d \leq$50 MeV) and a thick natural uranium target.

From the present length of the flight path of 57 m a resolution of $\leq$ 0.03 ns/m can be deduced.

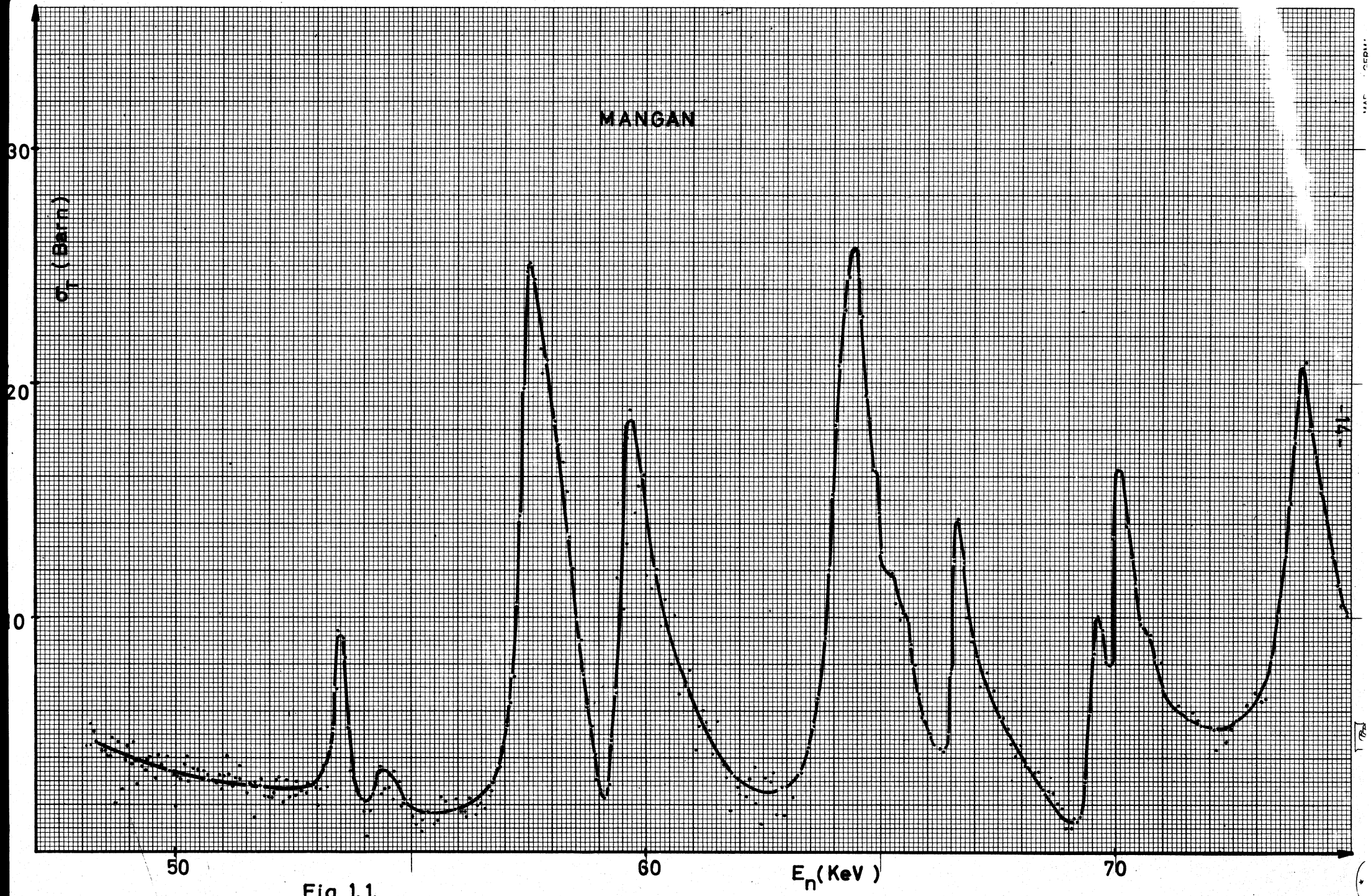

Fig. 1.1.

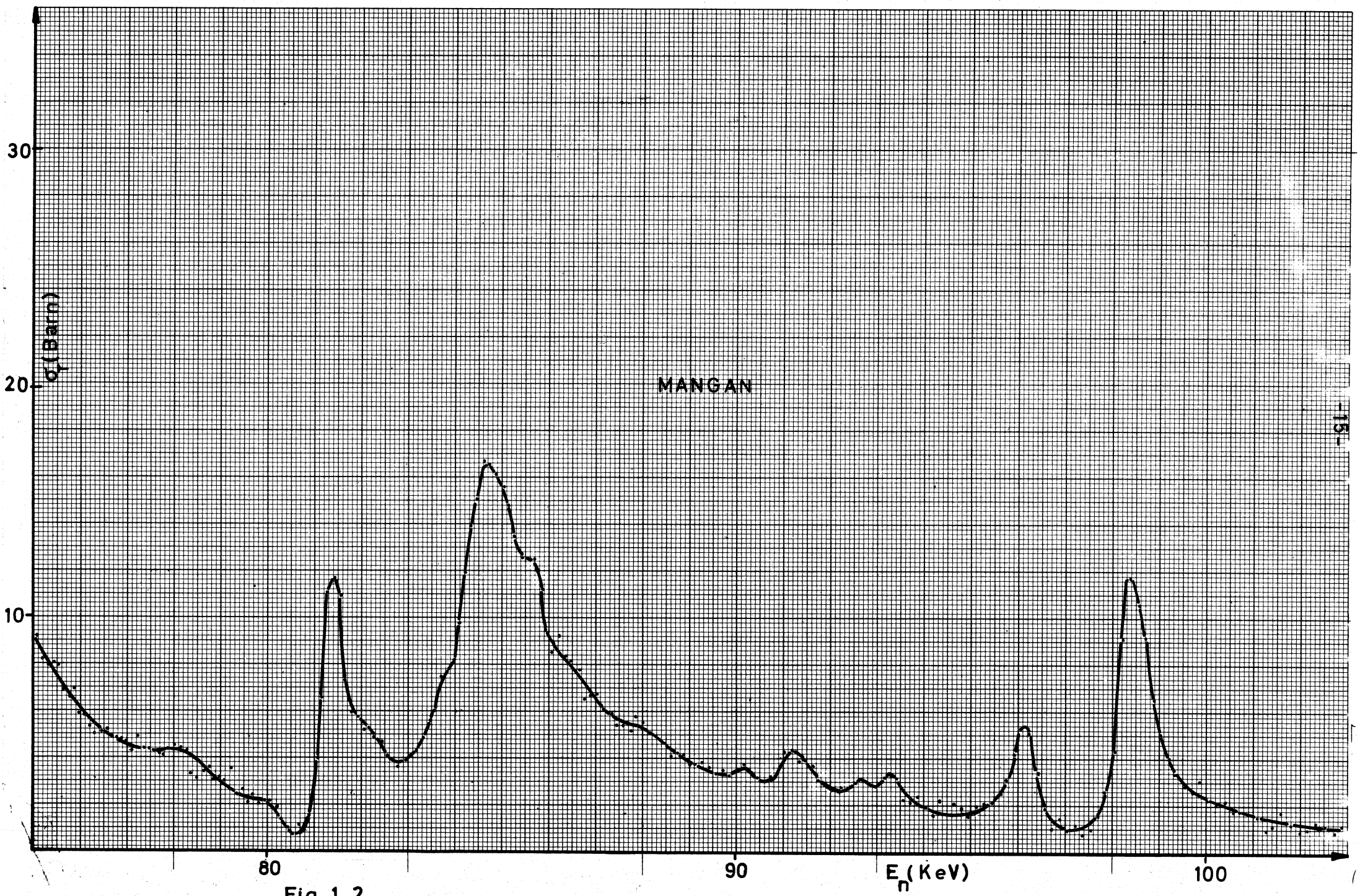

Fig. 1. 2.

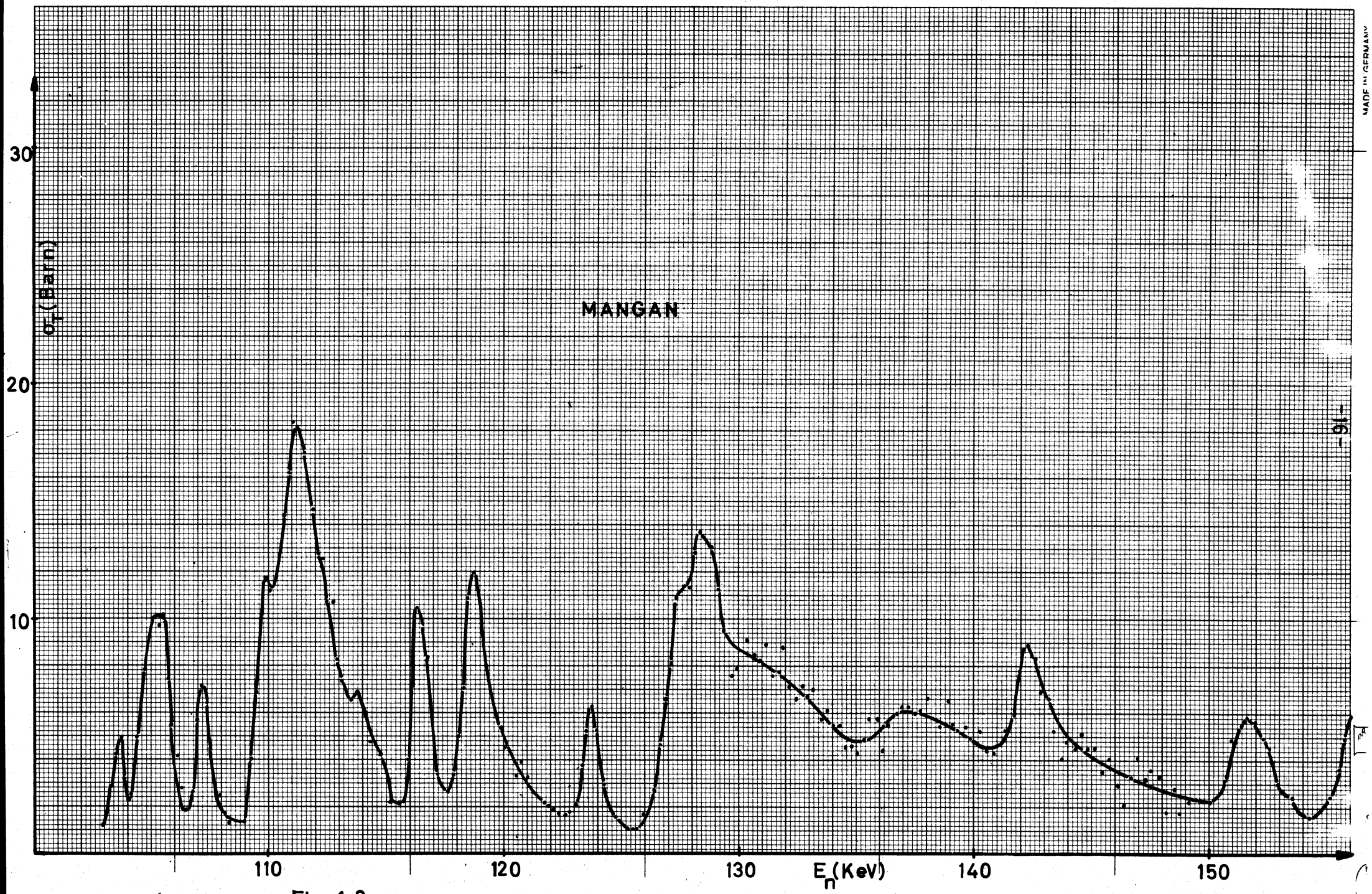

Fig. 1.3.

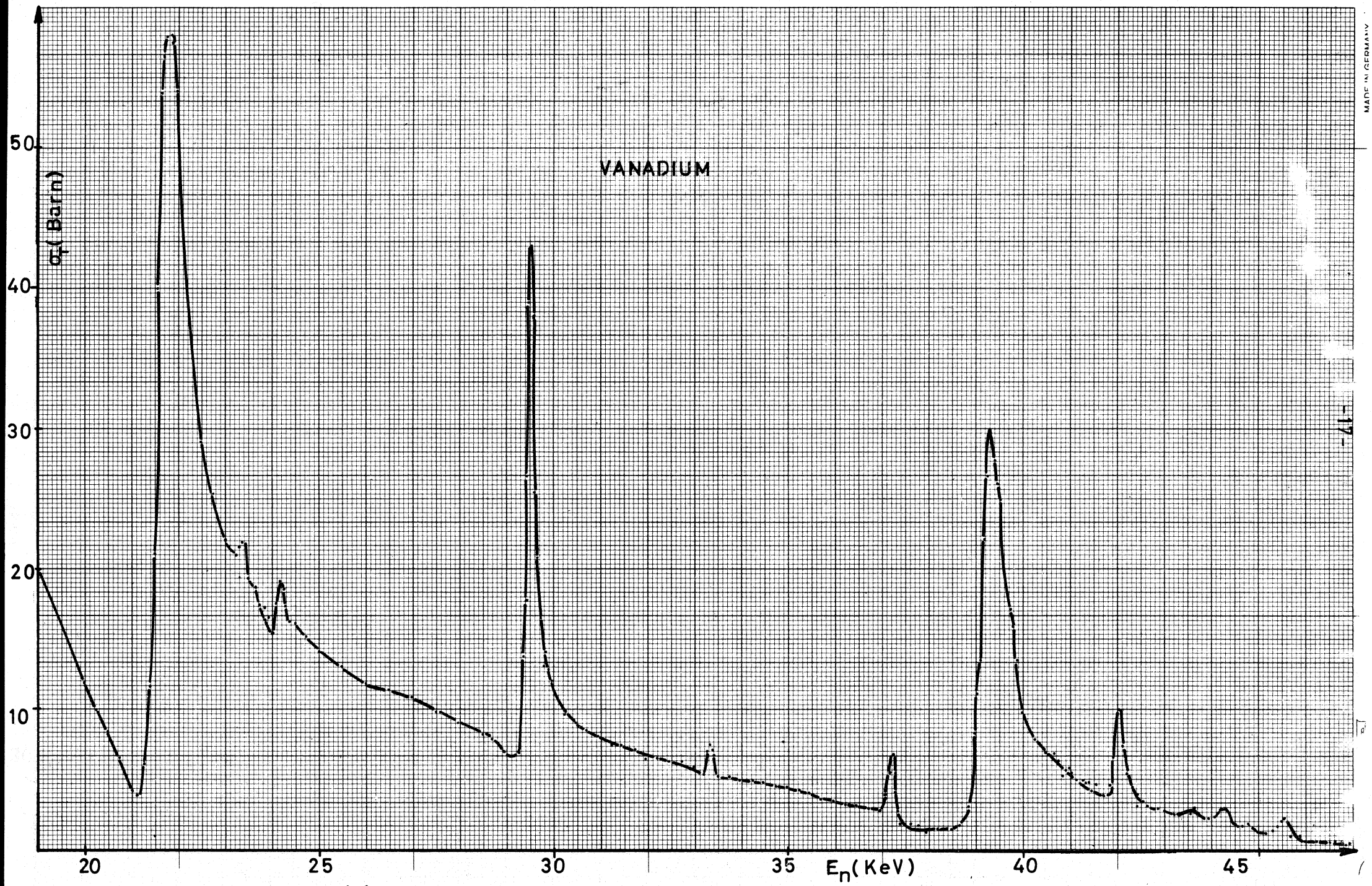

Fig. 1.4.

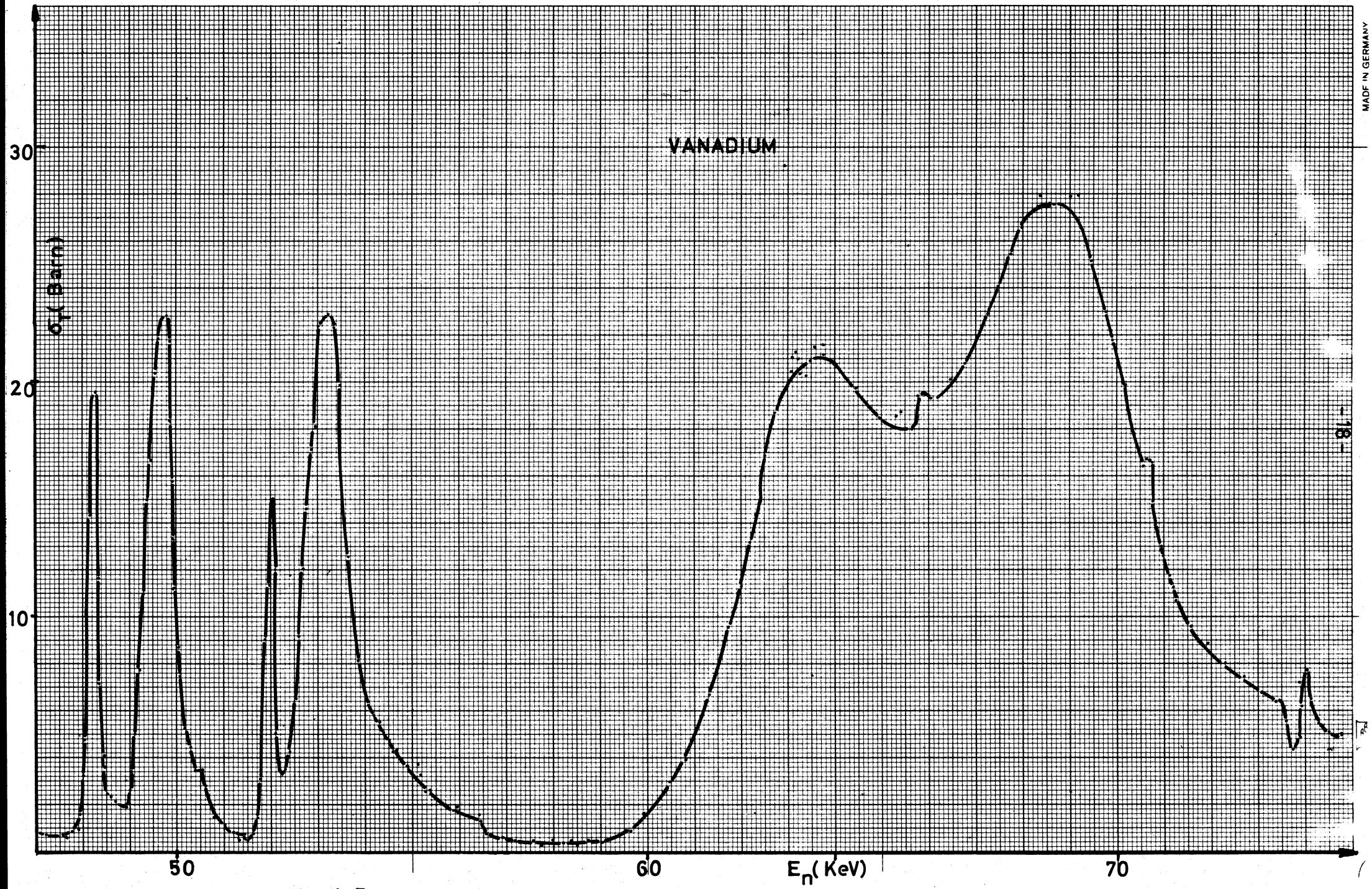

Fig. 1. 5.

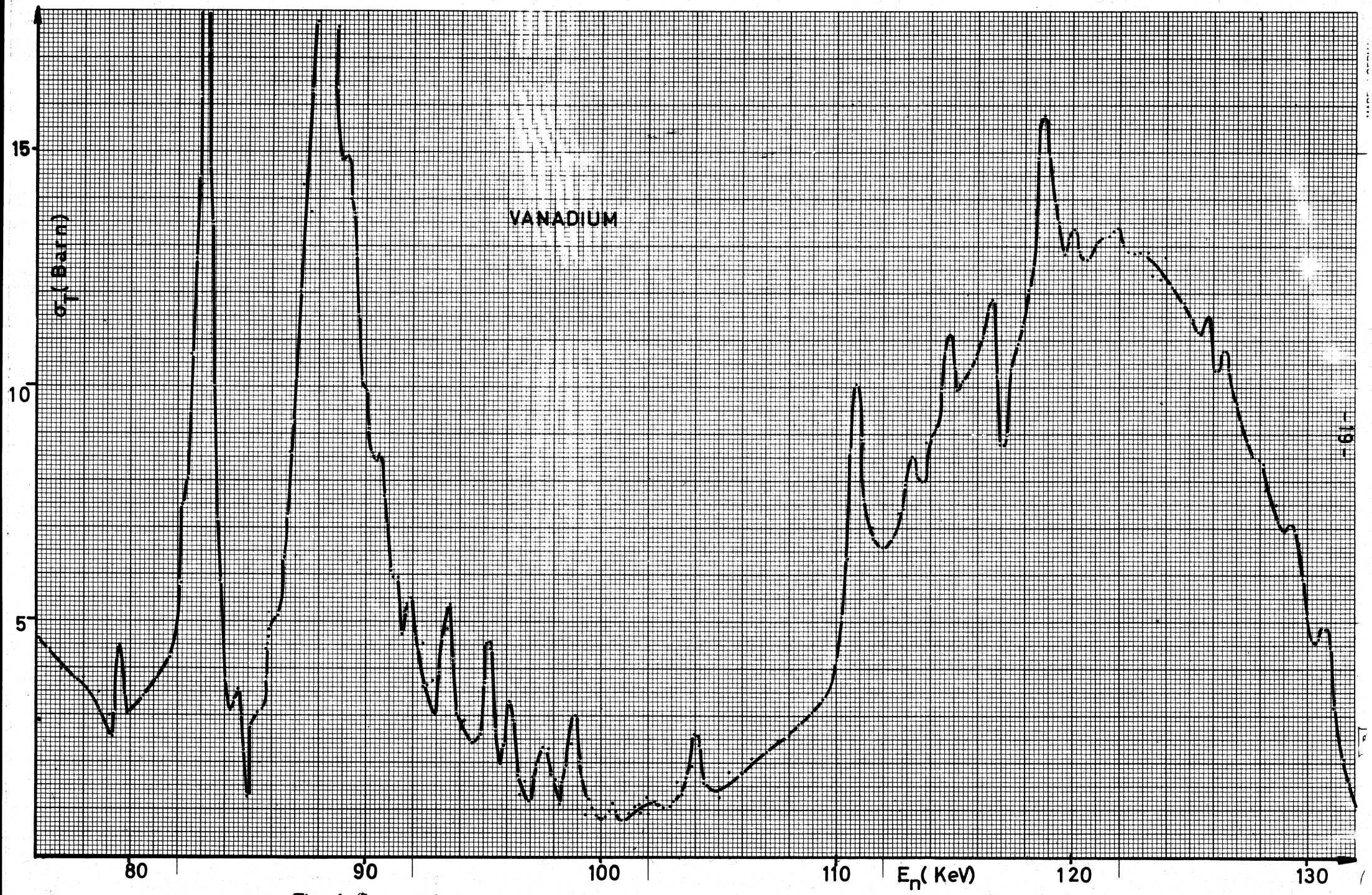

Fig. 1. 6.

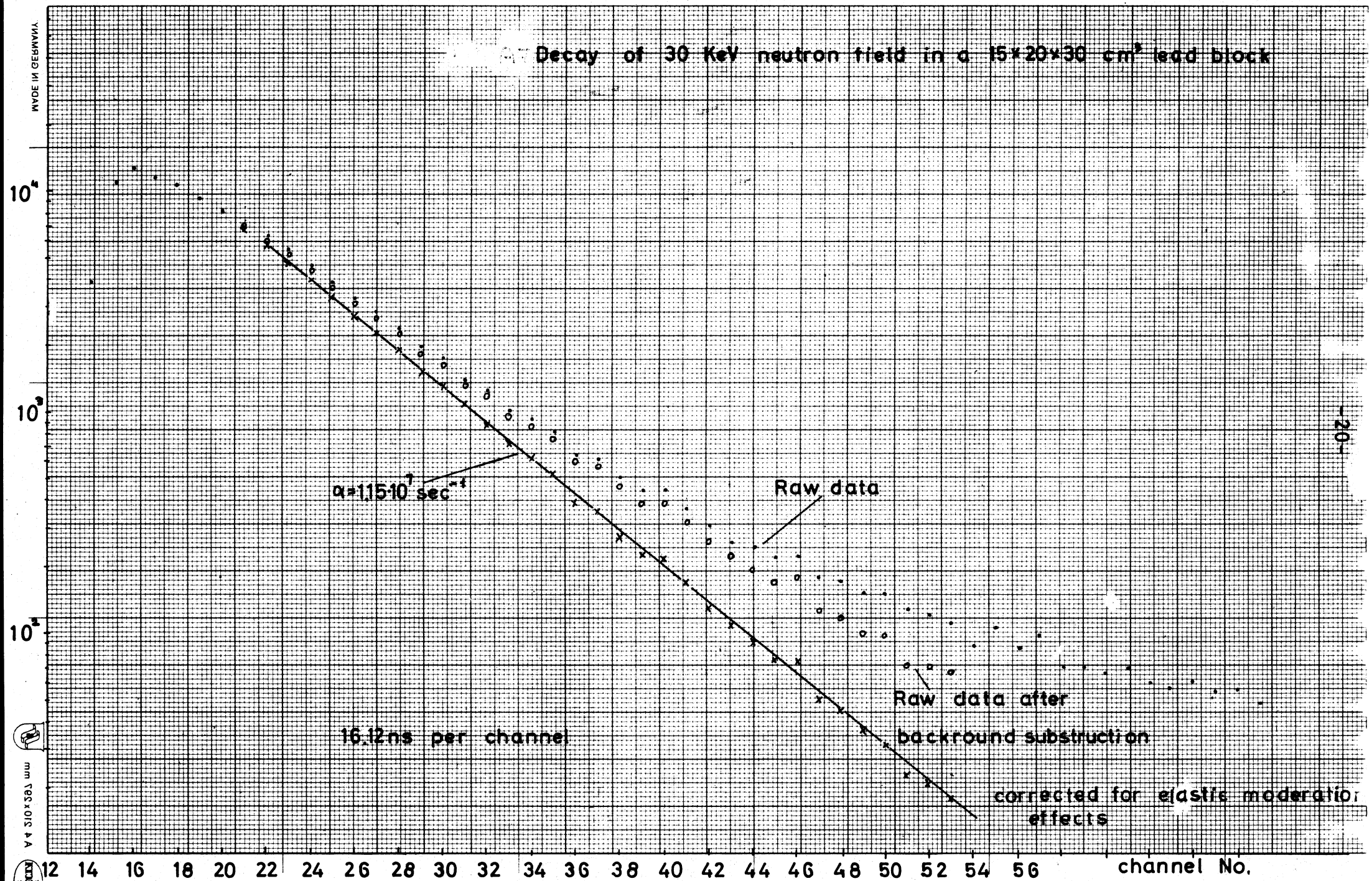
Decay of 30 KeV neutron field in a 15×20×30 cm³ lead block
10⁴
10³
10²
α=1.15·10⁷ sec⁻¹
Raw data
Raw data after
backround substruction
corrected for elastic moderation
effects
16.12ns per channel
12 14 16 18 20 22 24 26 28 30 32 34 36 38 40 42 44 46 48 50 52 54 56
channel No.

Fig. 1.7.

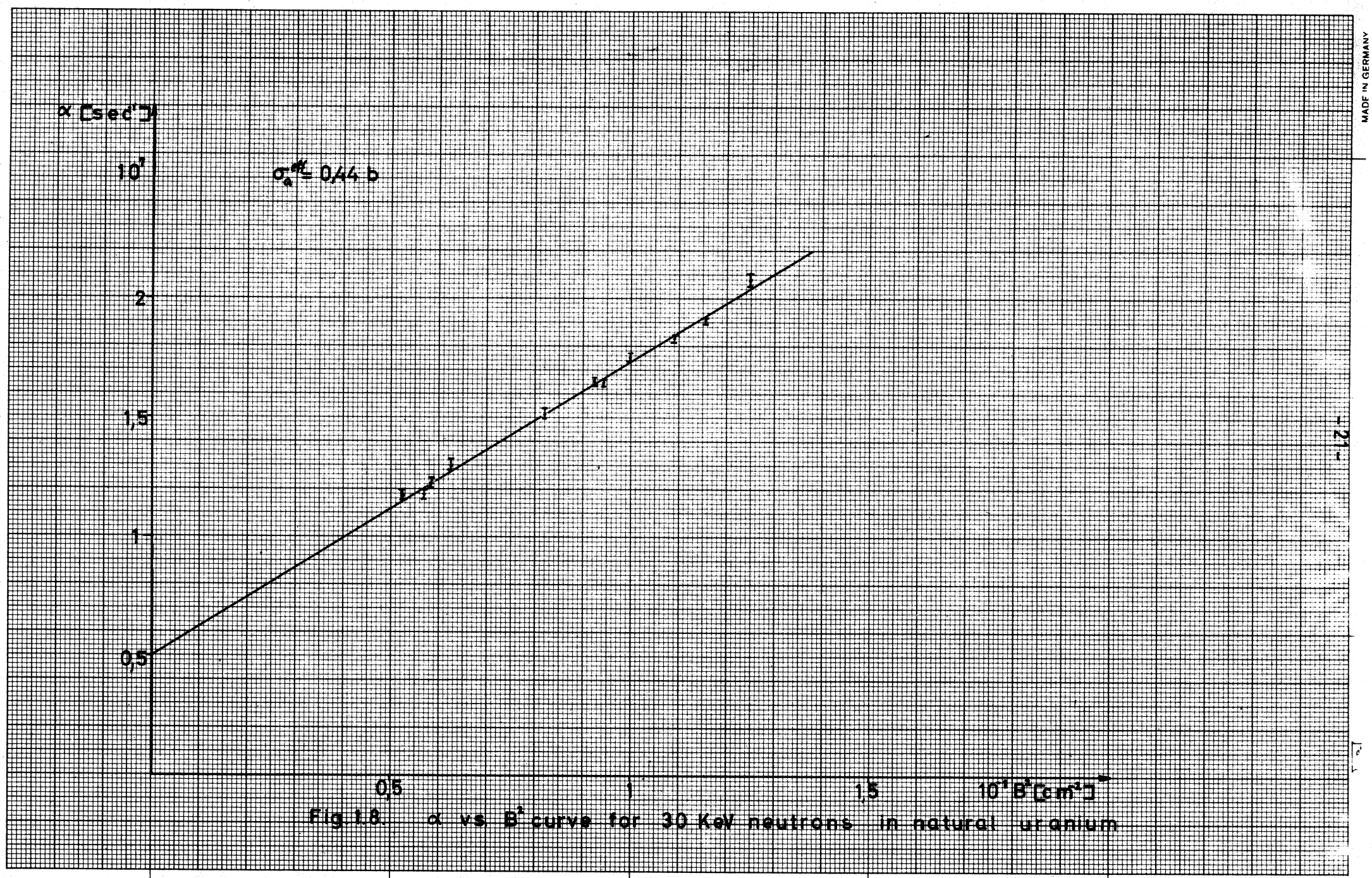

Fig. 1.8. α vs. B^2 curve for 30 KeV neutrons in natural uranium

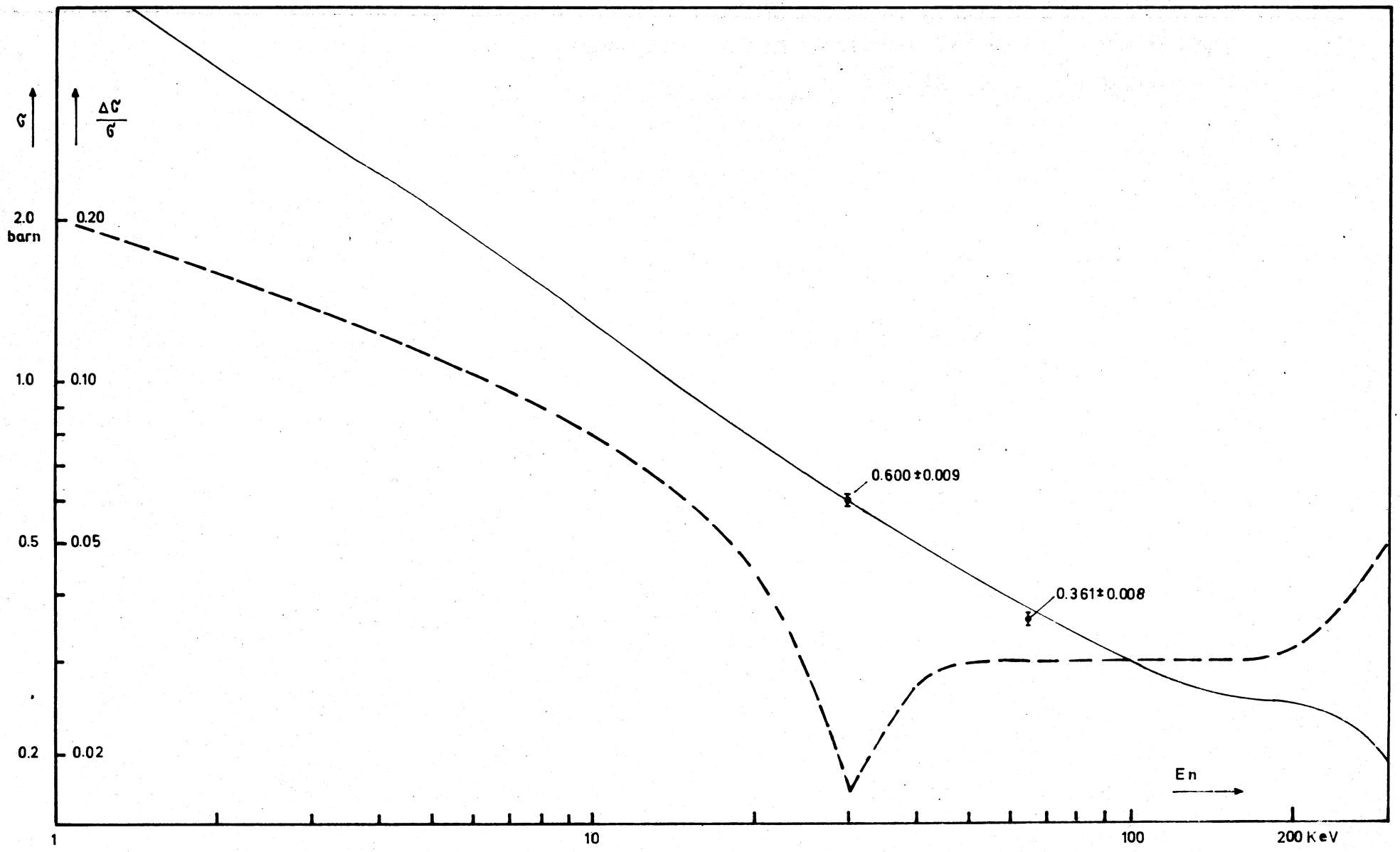

Fig. 1. 9. The Average (n,γ)- Cross Section of Au^{197}.

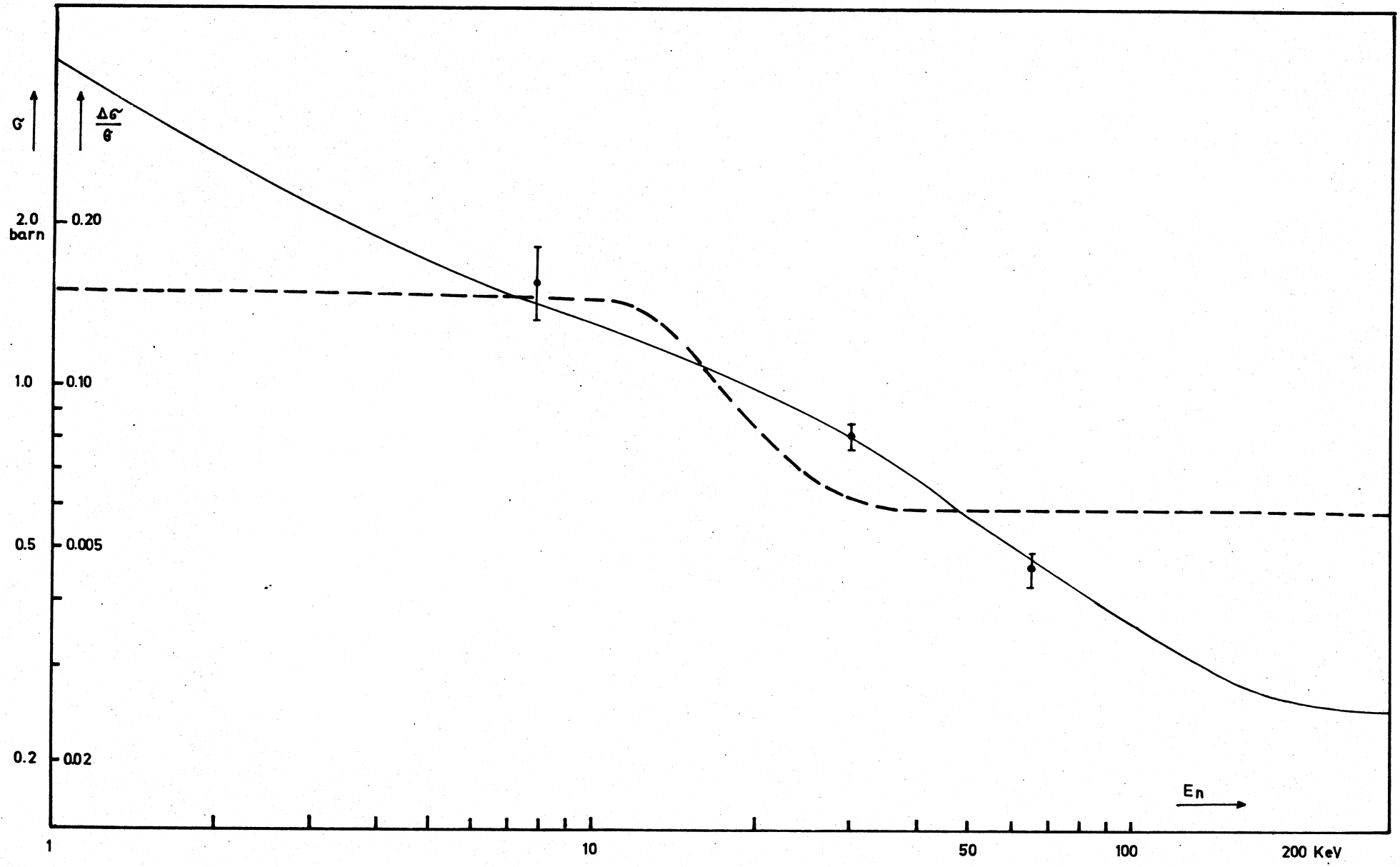

Fig.1.10. The Average (n,γ)- Cross Section of Indium.

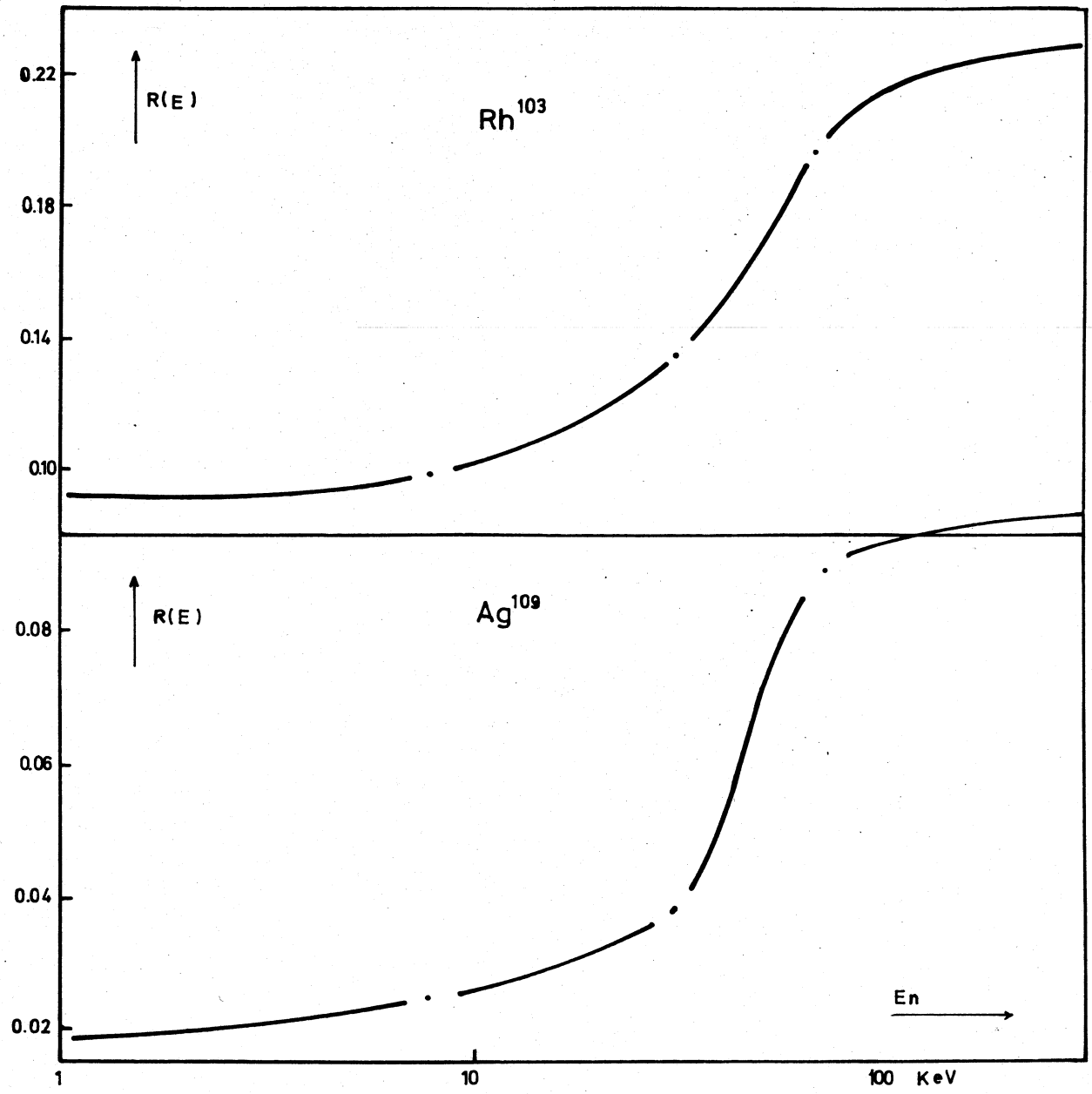

Fig.1.11. The Isomeric Cross Section Ratios of Rh and Ag.

Scattering Law of the H_2O-Molecule (Temperature 539°K, density 12mg/cm^3; best fit to the experimental data)

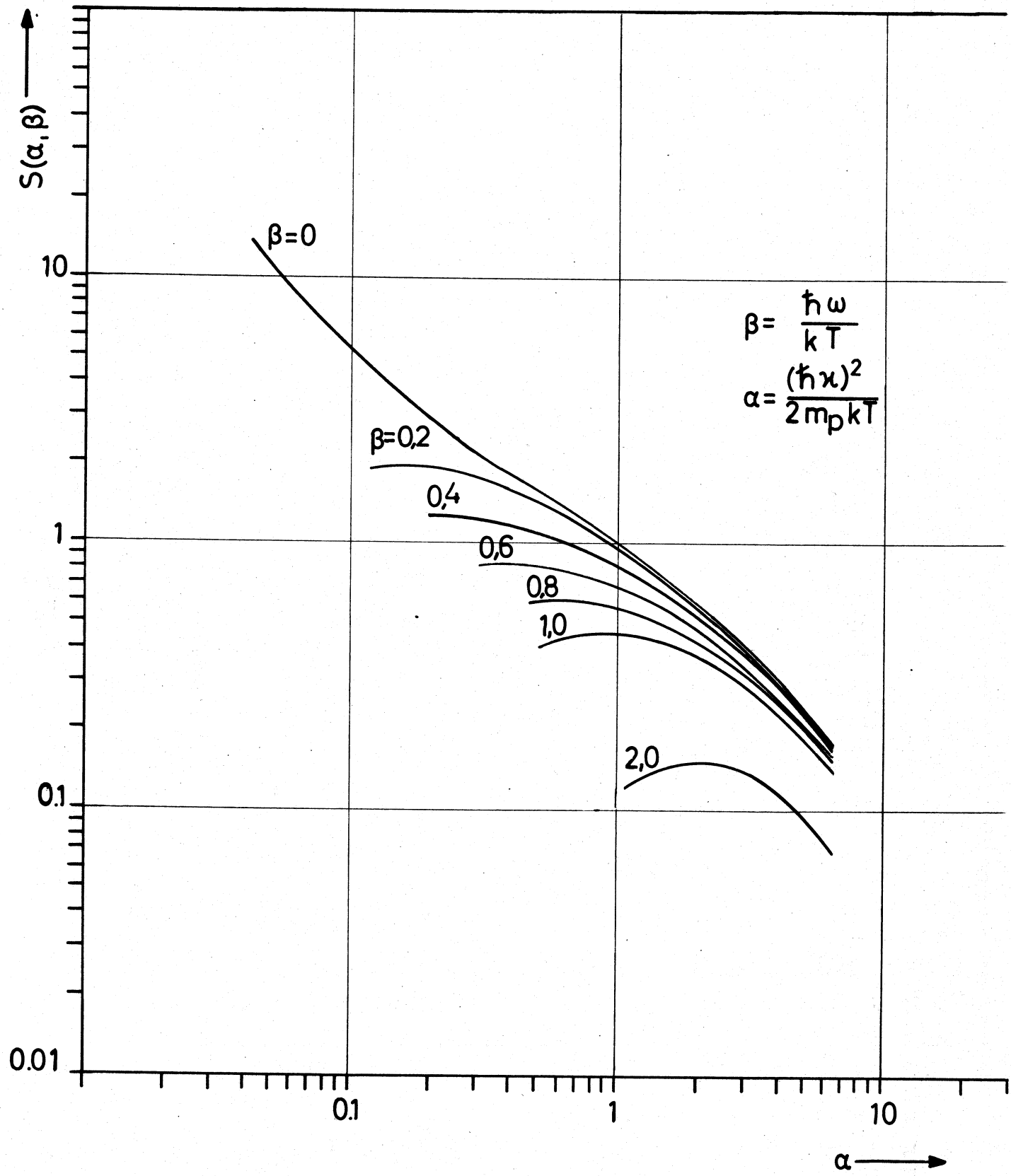

Fig. 1. 12.

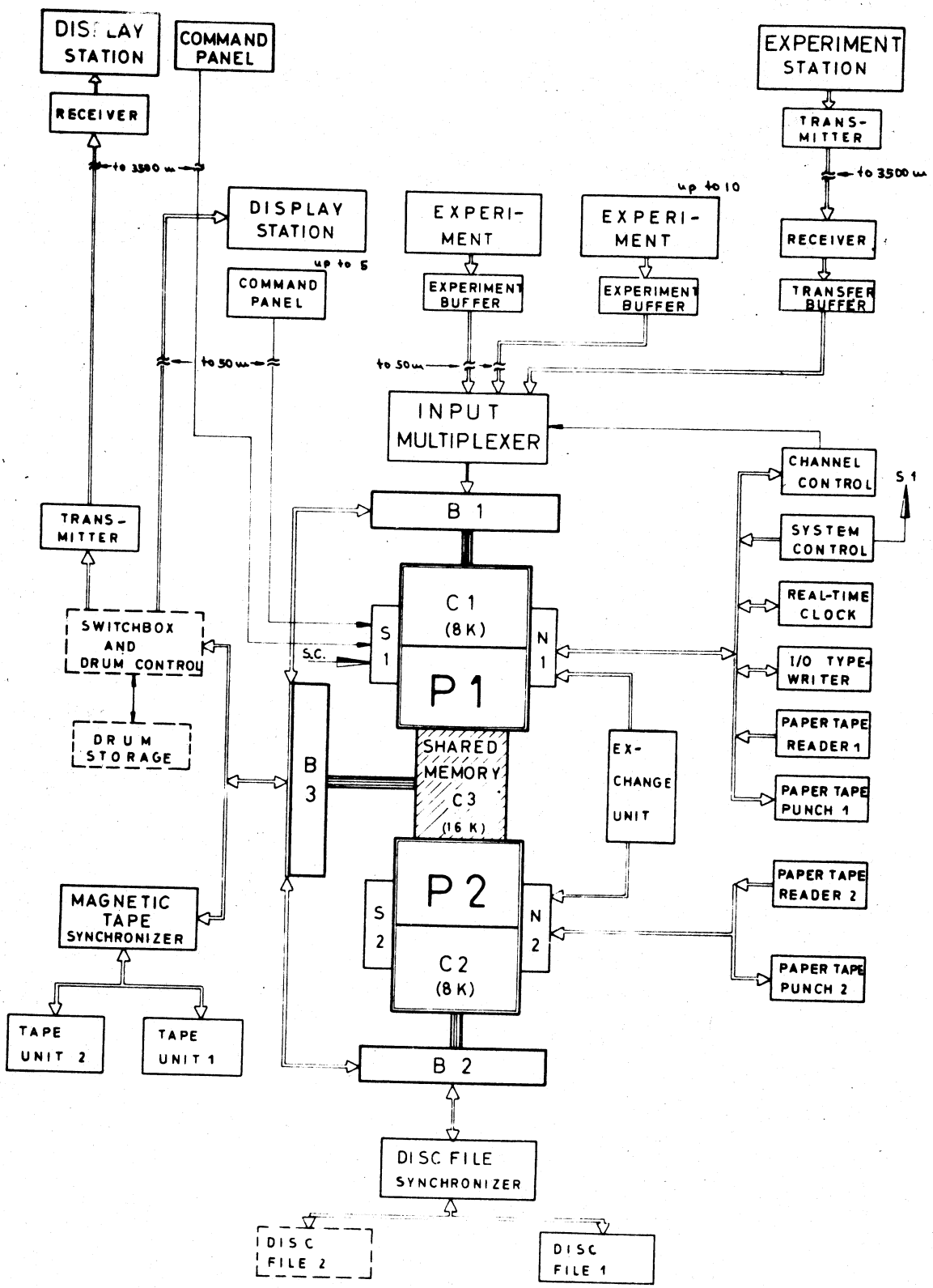

Fig.1.13. Symmetrical two-Computer System MIDAS 66

C1,C2 private memories of the processors (P1,P2) - C3 shared memory

B1,B2 buffered data channels of the computers,

B3 buffered data channel of the additional memory, the computers can override the B3 channel control and use the peripheral equipment connected with this channel.

N1,N2 unbuffered data channels used to exchange small amounts of information.

S1,S2 special input channels; S1 connects the command panels (remote program selector boards) with the computer 1.

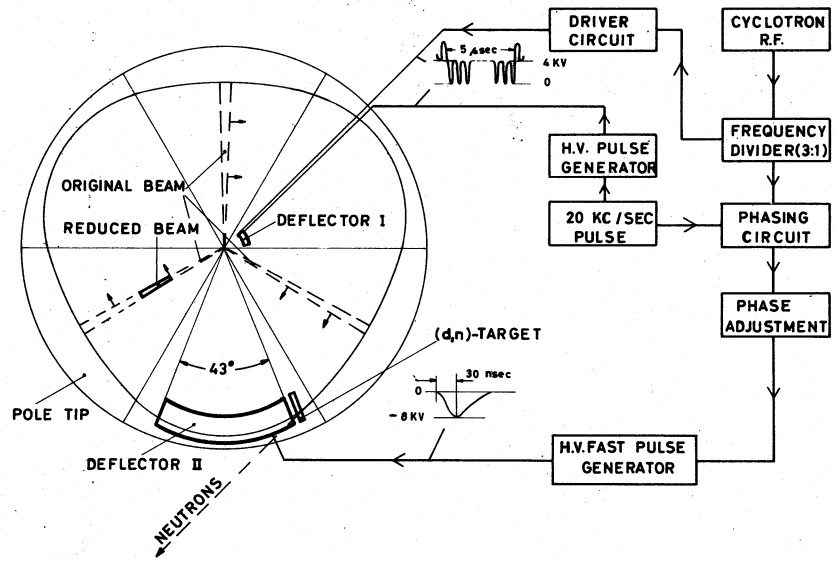

Fig.1.14. Scheme of bunching-deflection system

2. PHYSIK-DEPARTMENT DER TECHNISCHEN HOCHSCHULE MÜNCHEN (GERMANY)

2.1. Neutron Beam Experiments

2.1.1. Absolute Determination of Coherent Cross Sections by the Neutron Gravity Refractometer

L. Koester, N. Nücker, W. Trüstedt

The coherent scattering length of mercury has been determined as $a_{coh} = +(12.69 \pm 0.02) \cdot 10^{-13}$ cm (1). After the elimination of the low angle scattering in the neutron windows, reflectivity measurements on inorganic and organic liquids have shown that the critical height of the total reflection may evaluated from the reflection curve with an accuracy of about $2 \cdot 10^{-4}$. With a new water level all along the experimental facility (ca. 110 m), the difference in height between the entrance slit and the reflection mirror can be measured with an accuracy of approximately ± 0.02 mm. The total error of the scattering length may be estimated to be smaller than 0.05 % in favorable cases.

Measurements with organic compounds for the determination of the scattering length of H and C, and on molten metals are in progress.

(1) Koester L., Z. f. Physik, 182, 328 (1965).

2.1.2. Determination of Incoherent and Free Cross Sections

J.P. Niklaus, R. Simson, W. Triftshäuser and W. Schmatz

With the previously (1,2) described filter difference method the free cross sections of lead and silicon have been determined (average neutron wave length 0.09 Å). To obtain from these values the coherent scattering cross sections of the same elements the incoherent scattering cross sections have been measured by a scattering device. The results are given in table 2.1.

Table 2.1.: Cross sections (barn)

	Si	Pb
σ_{free}	2.022 ± 0.003	10.58 ± 0.03
σ_{inc}	$(15 \pm 1.3)\ 10^{-3}$	$<30 \times 10^{-3}$ or $(15 \pm 15)\ 10^{-3}$
$\sigma_{coh} = 4\pi\ a^2_{coh,K}$	2.153 ± 0.005	10.65 ± 0.05
$4\pi(a_{coh,K}+Za_{el})^2$	2.173 ± 0.005	10.93 ± 0.05

$a_{coh,K}$ is the scattering length of the nucleus, a_{el} the scattering length of the electron (Foldy (3)). The results will be published (4). Additionally σ_{inc} of aluminium has been redetermined. The value is (10 ± 1.7)mb in agreement with (5). In the case of natural copper we have found σ_{inc} = (590 ± 40)mb in agreement with the result of Reating et al (6).

(1) Progress Report on Nuclear Data Research in the Euratom Community - EANDC (E) 57 "U" (1965), p. 21.
(2) W. Triftshäuser, Z. Physik 186, 23 (1965).
(3) Foldy L.L., Rev. Mod. Phys. 30, 471 (1958).
(4) J.P. Niklaus, R. Simson, W. Triftshäuser and W. Schmatz, to be published in Z. Physik (1966).
(5) R. Scherm and W. Schmatz, Z. Naturforschung 19a, 354 (1964).
(6) D.T. Reating, W.J. Neidhardt and A.N. Goland, Phys. Rev. 111, 261 (1958).

2.1.3. Total cross sections of Er and Cu (at 300°K and 77°K)

K. Knorr

Using a mechanical velocity selector, total cross sections for subthermal neutrons ($\lambda \approx 5$-20 Å) are being determined. The specific energy of the neutrons was found by comparison with cross sections of Au foils ($1/v$ extrapolation from 97.8 b for 25.3 meV). The measured values of Er with estimated errors are given in table 2.2. and fig. 2.1. A metal foil of 220 mg/cm^2 with a specified purity of 99 % was used. The error of cross sections caused by the impurities of Gd, Sm, Eu, and Dy is <1 % (examination by a γ-spectrometer). The values of Cu (metal foil of 2.70 g/cm^2 and a specified purity of 99.98 %) are given in table 2.3. and fig. 2.2.

Table 2.2.: σ_{tot} of Er

E (MeV)	(Å)	(b)	error (%)
2.504	5.71	513.9+	2
1.875	6.61	577.5	2
1.434	7.56	653.1	2
0.971	9.17	781.0	2
0.667	11.07	939.2	2
0.492	12.09	1090.8	2
0.343	15.44	1325.0	4

+probably with Bragg scattering

Table 2.3.: σ_{tot} of Cu

E (MeV)	(Å)	(b) 300°K	(b) 77°K	error (%)
2.064	6.30	---	13.53	1.5
1.828	6.69	---	14.35	1.5
1.618	7.11	15.68	15.31	1.5
1.405	7.63	---	16.34	1.5
1.184	8.31	---	17.84	1.5
0.958	9.24	20.21	19.72	1.5
0.663	11.1	24.23	---	3
0.497	12.8	27.96	---	3
0.348	15.3	34.23	---	3

2.1.4. Time Dependance of the β-Activity of the Total Thermal Fission Products of ^{233}U, ^{235}U, and ^{239}Pu

H. Seyfarth

In a methane flow 4π-proportional counter the mean number of β-particles per second and fission was measured for times of 5.10^{-2} ... $3.6\ 10^{4}$s after fission. Results showing the time dependance and the mean total number of β-particles per fission of ^{233}U and ^{235}U are published in Proceedings of the Symposium on the Physics and Chemistry of Fission, Salzburg 1965, Paper SM 60/61.

Results for ^{239}Pu will be published in 1966. There also will be published some investigations concerning the number of conversion electrons emitted by the decay of isomeric states of the fission products up to $3.6.10^{4}$ s after fission.

2.2. Fission Physics

With the fission particle mass spectrometer, constructed by Ewald et al. (1), the following experiments have been done since the last issue of this report:
(H. Ewald, E. Koneeny, H. Gunther, G. Siegert, H. Göbel, K. Hetwer, K. Kürzinger, L. Winter).

2.2.1. Primary Distributions of Nuclear Charge for Fission Fragment Masses 130 to 137 from Thermal Fission of ^{235}U

The measurements which were reported in this report of Feb. 1965 and in (2) have been continued for the mass region from A = 130 to A = 137 with improved experimental methods.

The fission fragments impinge upon a β-sensitive nuclear emulsion in which the β-tracks from each fission product are registrated. Since the stable end products of the isobaric decay chains are known, and since each β-track can be correlated to a particular fission fragment track, it is possible to determine not only the mean primary nuclear charge Z_p, but also the distribution of charge about this mean value.

The measurements yield the following Z_p values with an error of 0.4 %:

A	130	131	132	133	134	135	136	137
Z_p	50.1	51.0	50.0	51.6	52.0	51.9	52.9	53.2

The distributions of these Z_p values have a mean 1/e width of 1.3 charge units. These measurements will be continued for heavier masses.

2.2.2. Dependence on Excitation Energy of Nuclear Charge Distribution of Separated Fission Fragment Masses

With the experimental procedure mentioned above, the fission particles with masses 138 and 139 were investigated at different kinetic energies after prompt neutron emmission. Since the sum of kinetic and excitation energy is almost constant, fission particles of different excitation energy have been caught in β-sensitive emulsions.

In mass no. 138, with increasing excitation energy, the FWHM of the distribution increases and the ratio of even-even to odd-odd nuclei strongly decreases. In mass no. 139, with even-odd and odd-even nuclei, these effects are relatively small. The measurements will be done also in the region of closed nuclear shells. The results of these experiments are to be published.

2.2.3. Response of Semiconductor Surface Barrier Detectors to Fission Fragments

With the technique developed in (3) the pulse height defect and resolution for fission fragments and their variation with energy, mass, incident angle, and bias voltage for 7 different counters have been investigated. The results are published in Nucl. Instr. and Meth. 36 (1965).

2.2.4. Scattering of Fission Fragments

The value of the scattering parameter of Born is increased one order of magnitude in the scattering of fission fragments separated according to energy and mass. The theories of G. Molière and Nigam Sundaresam and Wu (NSW) yield different distributions here. No direct comparison with the experimental results is possible, because the fission particles are not fully ionized, but some value between the ionic and the nuclear charge should be the effective one for scattering. Within these limits, only in the theorie of Molière is it possible to find an effective charge for which the theoretical and experimental curves have the same width. The distributions of the NSW theorie are always too small.

(1) E. Ewald, E. Koneeny, H. Opower, H. Rösler, Z. Naturforschg 19a (1964).
(2) E. Koneeny, H. Opower, H. Gunther, H. Göbel, Proceedings of the Symposium on the Physics and Chemistry of Fission, Salzburg 1965, paper SM-60/33.
(3) E. Koneeny, H. Opower, G. Siegert, Z. Naturforschg 20a (1965).

2.3. Measurement of Internal Conversion Electrons Following Neutron Capture

T. v. Egidy, E. Bieber, Th. W. Elze, H. Mahlein, W. Kaiser, B. Dutta

The betaspectrometer is described in (1 - 4). By measurement of the energy and intensity of internal conversion electrons following neutron capture, one gets much information on the level scheme. The spectra are given on a punch tape and the energy and intensity is determined by a computer. The best resolution was 0.07 %.

2.3.1. ^{150}Sm (5)

337 K-conversion lines, 48 L-conversion lines, 6 M-conversion lines and one N-conversion line were found in the energy region from 3 keV to 8 MeV. The multipolarities of these lines were determined. A level scheme with the levels given in table 2.4. was constructed.

Table 2.4.: Levels of ^{150}Sm

Level (keV)	Spin Parity	Level (keV)	Spin Parity
333.95	2+	1504.7	2(3,4)+
740.6	0+	1556,9	2+
773.4	4+	1642.7	3+
892.2	2+	1672.3	3-
1046.3	2+	1822.0	1- or 2,3+
1071.5	3-	1957.7	2,3-
1083.0	2-	2150	1+
1165.8	2+	2268	2,3-
1170.3	(0-4)+	2456	2,3+
1193.8	2+	2497	2,3,4+
1256.6	2,3,4+	2507	1- 5-
1278.9	2,3+	3051	1- or 2-5+
1357.8	3(4,5)-	7983	3,4-
1449.3	4+		

2.3.2. ^{198}Au

About 100 lines between 3 keV and 7 MeV were found.

2.3.3. ^{160}Tb

22 line were measured and the multipolarities were determined. The 63.69 keV line is a E2 transition, the 64.11 keV line is a M1 transition and the 75.05 keV line is a E1 transition.

2.3.4. H Capture Line and ^{28}Si 1780 keV Line

In the conversion electron spectra of ^{150}Sm, ^{198}Au and ^{165}Dy following neutron capture near the reactor core, the H capture line and a line of ^{28}Si in external conversion from the gamma background appeared. The energies were determined very exactly to (2224.4 ± 0.9) keV for the H capture line and (1778.3 ± 0.7) keV for the ^{28}Al-^{28}Si line.

(1) T. v. Egidy, Ann. Physik (Lpz), 7.F., 9, 221 (1962).
(2) E. Bieber, T. v. Egidy, O.W.B. Schult, Z. Physik 170, 465 (1962).
(3) W. Nörenberg, Z. angew. Physik 17, 452 (1964).
(4) E. Bieber, Z. Physik (1965-66).
(5) Th. W. Elze, to be published (1966).

2.4. Cross Section Determinations by Activation Techniques

2.4.1. Measurement of some Averaged Cross Sections for n,p- and n,α-Reactions

G. Rau

The cross section averaged over the fission neutron spectrum N (E) is defined as

$$(1)\ \langle\sigma\rangle = \int_0^\infty \sigma\ (E)\ N(E)\ dE \ \Big/ \int_0^\infty N(E)\ dE$$

with N(E) having the shape as given by Watt (1) or in a more elaborate form by Cranberg (2). Because the fast neutron spectrum above 1.5 MeV has about the same shape as N(E), that means

$$(2)\quad \varphi'(E) = \text{const}.N(E),$$

and since for n,p- and n,α-reactions the influence of neutrons below 1.5 MeV is negligible because of the Coulomb potential barrier, we can write instead of (1):

$$(3)\ \langle\sigma\rangle = \int_0^\infty \sigma\ (E)\ \varphi'(E)\ dE \ \Big/ \text{const} \int_0^\infty N(E)\ dE.$$

This way, for several isotopes the averaged cross section has been measured.

The samples were irradiated under Cd shielding in order to reduce interfering activities caused by thermal activation. In some cases it was even necessary to use enriched isotopes in order to obtain measurable effects.

The determination of the fast neutron flux has been done by the reactions $^{58}Ni(n,p)\ ^{58}Co$, $\langle\sigma\rangle$ = 95 mb (3) for irradiation times below one day, or because of the ^{58}Co burnup (4) with the reaction $^{46}Ti(n,p)^{46}Sc$, $\langle\sigma\rangle$= 12.6 mb (5), for higher irradiation times.

Short time irradiations from 15 seconds up to one day were performed in the pneumatic rabbit system of the FRM, the irradiation position being only 1.5 cm from the uranium zone; for long time irradiations, a position within the core was available. For each reaction, five to ten samples were irradiated and measured.

Measurements of the induced activities were performed with a 3"x3" NaI (Tl)-crystal, the total absorption peak efficiency of which had been determined by means of several absolute

calibrated radioisotopes.

The results of the measurements are given in table 2.5. Column 1 gives the reaction, column 2 the measured averaged cross section, column 3 the Q-value of the reaction, column 4 the half life of the induced activity, column 5 the gamma energy which has been used for determination of activity, column 6 gives the corresponding gamma abundance, already corrected for internal conversion, column 7 gives the reaction used for determination of the fast neutron flux, and column 8 gives values of other authors for comparison (6 - 8).

Decay schemes, gamma abundances, and half lives were taken from (9 - 11); the Q-values were either obtained from (12) or calculated by the energy level schemes of the nuclei.

In the case of ^{53}V, its half life given in literature with 2.0 resp. 1.7 minutes did not seem very credible. It was remeasured and found to be (1.52 $\pm$ 0.015)min.

Comparison of the measured cross sections with those of other authors gave good agreement except for the case of $\langle\sigma\rangle_{n,\alpha}$ (^{68}Zn), where the discrepancy is about a factor of two. In nine cases, no comparable data were found in literature.

For (n,p)reactions, plotting $\langle\sigma\rangle$ against $Q_{n,p}$ in single logarithmical display, one gets straight lines for constant Z, the slope of which changes only slightly with different Z-values. It is intended to derive an empirical formula for predicting roughly averaged cross sections by its Z and $Q_{n,p}$ alone.

References

(1) Watt, B.E.: Phys. Rev. 87, 1037 (1952).
(2) Cranberg, L., et al.: Phys. Rev. 103, 662 (1956).
(3) Hertlein, F: Ann. d. Phys. 12, 57 (1963).
(4) Hoog, C.H., L.D. Weber: IDO 16744 (1962).
(5) Köhler, W.: to be published in Nukleonik.
(6) Depuyd, M., and M. Nève de Mévergnies: Journal of Nuclear Energy Parts A/B, 16, 477 (1962).
(7) Boldeman, J.W.: Journal of Nuclear Energy, Parts A/B, 18, 417 (1964).
(8) Rochlin, R.S.: Nucleonics 17, Nr. 1, 54 (1959).

(9) Nuclear Data Sheets, National Research Council, Washington D.C.
(10) Strominger, D. et al.: Mod. Rev. Phys. 30 (1958).
(11) Bakhru, H.: Nuclear Phys. 52, 125 (1964).
(12) Lawrence, E.O.: URCL 5419 (1959).

Table 2.5.: Averaged Cross Sections

Reaction	$\langle\sigma\rangle$ (mb)	$Q_{n,x}$ (MeV)	$t_{1/2}$	E_γ (MeV)	h_γ (%)	Reference reaction	of other authors (mb)
$^{27}Al(n,\alpha)^{24}Na$	0.61 ± 0.028	-3.14	14.97 h	1.37 2.75	100 100	$^{58}Ni(n,p)$	0.63 ± 0.03 (6)
$^{34}S(n,p)^{34}P$	0.26 ± 0.022	-4.32	12.4 s	2.1	25	$^{58}Ni(n,p)$	no value available
$^{41}K(n,p)^{41}Ar$	1.78 ± 0.14	-1.71	110 m	1.29	100	$^{58}Ni(n,p)$	no value available
$^{41}K(n,\alpha)^{38}Cl$	0.61 ± 0.032	-0.10	37.29 m	2.16	47	$^{58}Ni(n,p)$	no value available
$^{52}Cr(n,p)^{52}V$	0.92 ± 0.037	-3.26	3.76 m	1.44	100	$^{58}Ni(n,p)$	no value available
$^{53}Cr(n,p)^{53}V$	0.37 ± 0.026	-2.75	1.52 m	1.01	100	$^{58}Ni(n,p)$	no value available
$^{54}Cr(n,p)^{54}V$	$(4.88 \pm 0.83).10^{-3}$	-6.52	55 s	2.21	100	$^{58}Ni(n,p)$	no value available
$^{64}Zn(n,p)^{64}Cu$	26.9 ± 1.2	+0.22	12.8 h	$0.51(\beta^+)$	38	$^{58}Ni(n,p)$	27 ± 1.2 (7)
$^{66}Zn(n,p)^{66}Cu$	0.56 ± 0.034	-1.85	5.1 m	1.04	9	$^{58}Ni(n,p)$	no value available
$^{67}Zn(n,p)^{67}Cu$	0.96 ± 0.067	+0.21	60.0 h	0.182	37.2	$^{58}Ni(n,p)$	0.9 ± 0.1 (7)
$^{68}Zn(n,p)^{68}Cu$	$(13.1 \pm 1.9).10^{-3}$	-3.80	30 s	1.08	95.2	$^{58}Ni(n,p)$	no value available
$^{68}Zn(n,\alpha)^{65}Ni$	$(6.25 \pm 0.38).10^{-2}$	+0.82	2.564 h	1.49	17.2	$^{58}Ni(n,p)$	$3.4.10^{-2}$ (8)
$^{92}Mo(n,p)^{92}Nb$	6.74 ± 0.27	+0.304	10.1 d	0.93+0.90	98 + 1	$^{46}Ti(n,p)$	6.2 ± 0.4 (7)
$^{95}Mo(n,p)^{95}Nb$	0.138 ± 0.006	-0.148	35.0 d	0.76	99	$^{46}Ti(n,p)$	0.13 ± 0.01 (7)
$^{98}Mo(n,\alpha)^{95}Zr$	$(14 \pm 1.3).10^{-3}$	+3.62	65 d	0.73+0.76	55+43	$^{46}Ti(n,p)$	no value available

2.4.2. Determination of σ (2200 m/s) for $^{30}Si\ (n,\gamma)\ ^{31}Si$

W. Köhler, K. Knopf

For the calibration of counting systems for the reaction $^{31}P(n,p)^{31}Si$ the reaction $^{30}Si\ (n,\gamma)^{31}Si$ is used in some cases (request list EANDC 43 "U"). By means of a rotating disc thin gold and silicon oxyd layers have been activated in the water reflector of the reactor. The ^{198}Au activity has been counted by $\beta-\gamma$-coincidence technique (1), the ^{31}Si-activity has been determined by $4\pi\beta$-counting using the efficiency tracing method (2).

If one assumes $\sigma_o = (98.8 \pm 0.3)$b for gold one gets $\sigma_o = (103 \pm 3)$mb for $^{30}Si\ (n,\gamma)^{31}Si$. The older value in literature is $\sigma_o = (110 \pm 10)$mb (3).

(1) W. Köhler, Z. f. Naturforschg. 20a, 1170 (1965).
(2) W. Köhler, K. Knopf, to be published.
(3) BNL 325.

2.4.3. Determination of σ(2200 m/s) for $^{35}Cl(n,p)^{35}S$

W. Köhler, K. Knopf

In connection with the search for good reactions to measure the fast flux density we examined the reaction $^{35}Cl(n,p)^{35}S$. At the time of writing this article the measurements are not yet finished, but the thermal activation cross section has been determined.

Using the value of $\sigma_o = (37.4 \pm 0.2)$b for $^{59}Co\ (n,\gamma)^{60}Co$ (Vaninbroukx 1965), the cross section is $\sigma_o = (0.37 \pm 0.02)$b. This value does not agree with the values in BNL 325, $\sigma_o = (0.19 \pm 0.04)$b, nor with the value of Seren, Friedlander and Turkel (1) but it lies within the limits of error of the values of
Gilbert, Roggen and Rossel $\sigma_o = (0.30 \pm 0.09)$b (2) and
Maurer $\sigma_o = (0.34 \pm 0.08)$b (3) (if one uses for $^{55}Mn\ (n,\gamma)^{56}Mn$ $\sigma_o = 13.2$ instead of the older value 11.2 b).

(1) L. Seren, H.N. Friedlander, S.H. Turkel, Phys. Rev. 72, 888 (1947).
(2) A. Gilbert, F. Roggen, J. Rossel, Helv. Phys. Acta 17, 97 (1944).
(3) W. Maurer, Z. f. Naturforschg. 4a, 150 (1959).

2.4.4. Resonance Activation Integral Cross Sections for the (n,γ) Reactions of ^{55}Mn, ^{41}K and ^{51}V

H. Schmelz, W. Köhler

By simultaneous irradiations of the samples and thin gold foils with Cd-covers of 1 mm thickness in the pneumatic irradiations facility and by determining the activity after the irradiation, the resonance activation integral cross section I_{res} has been determined. The lower limit of the integral cross section is the cadmium cut-off for the given geometry, in our case 0.68 eV.

With the σ_o-values given in table 2.6. the $1/\sqrt{v}$ -contribution to the resonance activation integral has been calculated and subtracted to obtain I_{res}.

Table 2.6.: Resonance integrals

Reaction	$_o$(barn)	I_{res}(0.68)(barn)	I'_{res} (barn)
^{55}Mn (n,γ)	13.3 ± 0.2	12.6 ± 0.5	7.55 ± 0.6
^{41}K (n,γ)	1.2 ± 0.1	0.96 ± 0.05	0.51 ± 0.09
^{51}V (n,γ)	4.5 ± 0.5	2.17 ± 0.1	0.46 ± 0.3
reference values:			
^{197}Au(n,γ)	98.6 ± 0.3	1543 ± 20	1507 ± 20

A determination by cadmium ratio measurements has been done, too. In this method the standard deviations are greater (two irradiations instead of one for the single value), but the mean values agree with the other values within the limits of error.

The value of ^{55}Mn agrees with the measurement of Dahlberg (1964) I' = (8.16 ± 0.6)b (1), but it does not agree with that of Vidal (1965) I' = (10.5 ± 1.1)b (2).

(1) R. Dahlberg, K. Jirlow, E. Johannson, Reactor Sci. Techn. 14, 33 (1961).
(2) R. Vidal, CEA internal report MIN 73 (1965).

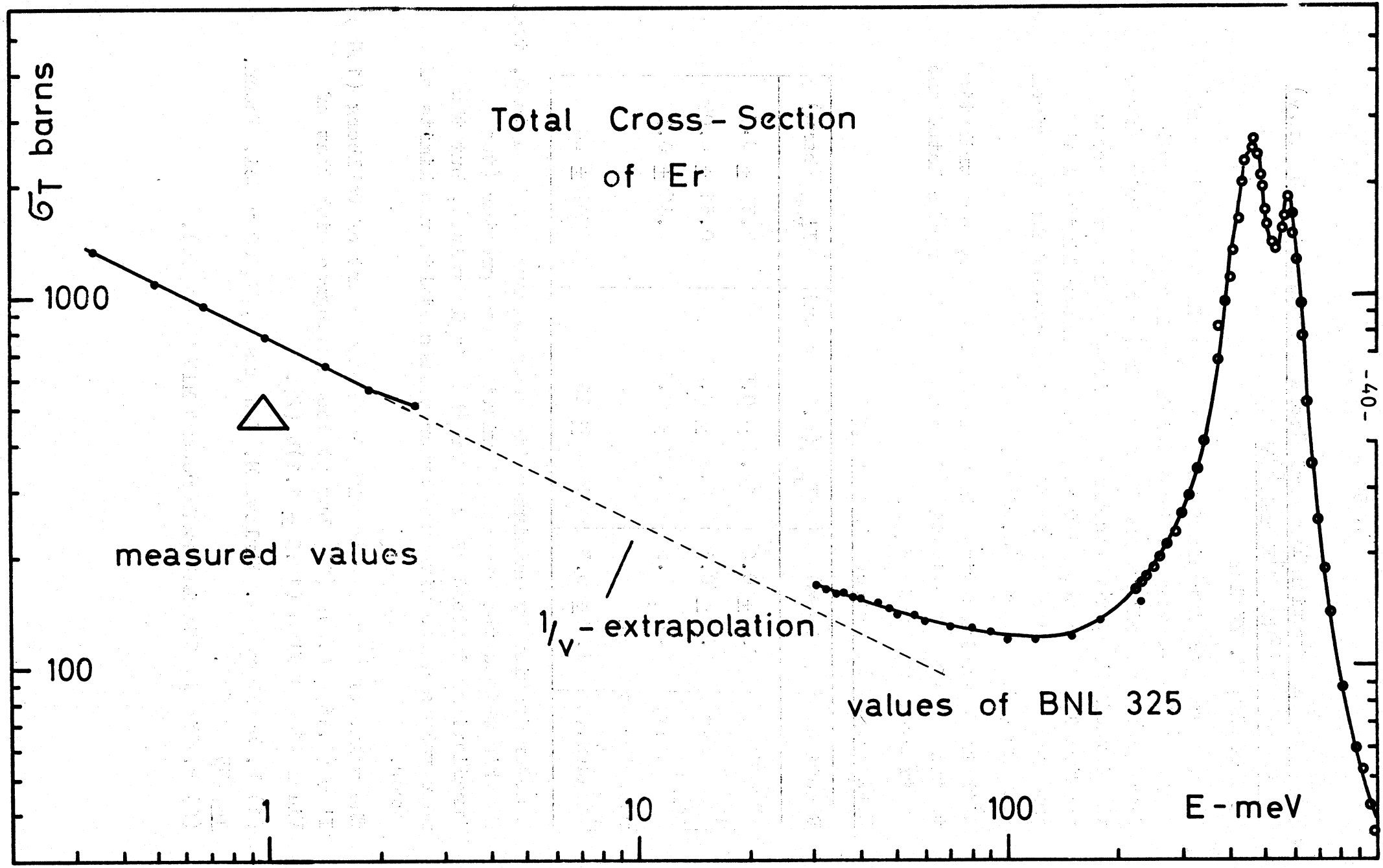
Total Cross-Section
of Er
σT barns
1000
100
measured values
1/v - extrapolation
values of BNL 325
1
10
100
E - meV

Fig. 2.1.

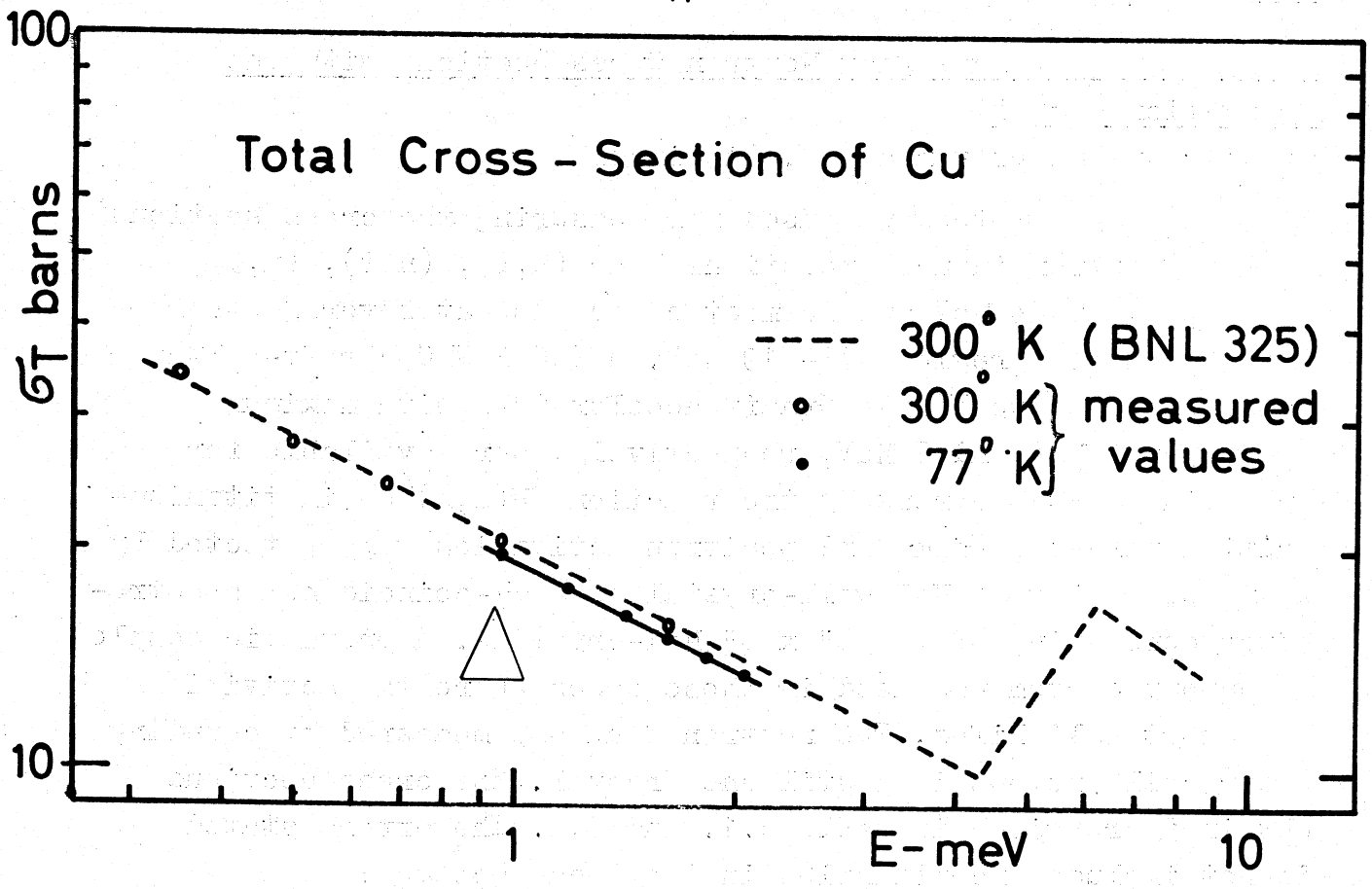
Total Cross - Section of Cu
σT barns
100
10
1
10
E- meV
---- 300° K (BNL 325)
300° K
77° K
measured values

Fig. 2.2.

3. I. INSTITUT FÜR EXPERIMENTAL-PHYSIK, UNIVERSITÄT HAMBURG (GERMANY)

3.1. Measurements of some Fast Neutron Cross Sections with the Activation Method

M. Bormann, F. Dreyer and U. Zielinski

The activation method was used for measuring the cross sections of some neutron induced reactions like (n,p), (n,t), (n,α), and (n,2n) at 14 MeV and in most cases also at several other energies in the region 13 - 19 MeV. A 150 keV Cockroft-Walton generator and two Van de Graaff accelerators with maximum energy of 1 MeV and 3 MeV, respectively, were available for producing fast neutrons by the reaction $^{3}H(d,n)^{4}He$ in titanium-tritium targets. Gamma and positron activities were detected by means of a 3" x 2" NaI well-crystal or a γγ-coincidence spectrometer consisting of two 3" x 3" NaI-crystals. A pneumatic sample transport system was used in those cases where the activities had short half lifes. The neutron flux was measured by counting the recoil protons in a stilbene crystal. The cross sections obtained are given in table 3.1. and 3.2. The errors stated do not include uncertainties in the decay schemes.

Table 3.2.: Cross Sections at 14.10 ± 0.15 MeV

Reaction	σ (mb)
$^{58}Ni(n,p)^{58}Co^{tot}$	532 ± 44
$^{58}Ni(n,p)^{58}Co^{g}$	227 ± 51
$^{58}Ni(n,p)^{58}Co^{m}$	305 ± 26
$^{62}Ni(n,p)^{62}Co^{g}$	14.7 ± 2.2
$^{65}Cu(n,\ )^{62}Co^{g}$	4.8 ± 1.4
$^{75}As(n,p)^{75}Ge^{tot}$	20.3 ± 1.6
$^{75}As(n,p)^{75}Ge^{g}$	1.7 ± 2.2
$^{75}As(n,p)^{75}Ge^{m}$	18.6 ± 1.5
$^{75}As(n,\ )^{72}Ga$	12.5 ± 1.5
$^{75}As(n,\ )^{76}As$	22.2 ± 1.8

Table 3.1 Neutron Cross Sections

$O^{16}(n,p)N^{16}$		$Mg^{25}(n,p)Na^{25}$		$S^{34}(n,p)P^{34}$		$Ni^{58}(n,p)Co^{58}$	
E_n(MeV)	σ (mb)	E_n(MeV)	σ (mb)	E_n(MeV)	σ (mb)	E_n(MeV)	σ (mb)
13,35 ± 0,14	47,0 ± 4,8	13,00 ± 0,16	52,5 ± 5,3	14,00 ± 0,22	78 ± 7,5	12,95 ± 0,20	532 ± 44
13,58 ± 0,14	43,4 ± 4,4	13,25 ± 0,18	50 ± 5,0	14,96 ± 0,23	73 ± 7,0	13,5 ± 0,25	473 ± 39
14,00 ± 0,14	44,0 ± 4,5	13,55 ± 0,14	53 ± 5,3	15,92 ± 0,26	62 ± 6,0	14,1 ± 0,25	411 ± 30
14,10 ± 0,22	40,1 ± 4,1	14,00 ± 0,14	49 ± 4,9	16,17 ± 0,28	58 ± 5,6	14,9 ± 0,30	373 ± 31
14,25 ± 0,14	37,7 ± 3,8	14,28 ± 0,16	43 ± 4,3	16,42 ± 0,30	57 ± 5,5	15,6 + 0,30 − 0,35	317 ± 26
14,53 ± 0,14	38,9 ± 4,0	14,74 ± 0,20	40 ± 4,0	16,65 ± 0,20	53 ± 5,1		
14,82 ± 0,16	35,8 ± 3,7	15,21 ± 0,28	37 ± 3,7			16,3 + 0,30 − 0,35	277 ± 23
15,08 ± 0,17	32,2 ± 3,3	15,68 ± 0,29	36 ± 3,[illegible]				
15,30 ± 0,18	33,2 ± 3,4	15,92 ± 0,23	37,5 ± 3,[illegible]			17,25 + 0,25 − 0,40	246 ± 20
15,54 ± 0,19	34,0 ± 3,5	16,17 ± 0,28	36 ± 3,6				
15,76 ± 0,19	31,8 ± 3,2	16,42 ± 0,30	34 ± 3,4			18,0 + 0,25 − 0,35	221 ± 18
15,93 ± 0,21	31,3 ± 3,2	16,65 ± 0,20	27,5 ± 2,8			18,9 + 0,15 − 0,30	209 ± 17
16,17 ± 0,28	31,0 ± 3,2						
16,50 ± 0,30	29,7 ± 3,0					19,6 + 0,15 − 0,25	215 ± 18
16,65 ± 0,26	26,0 ± 2,7						

Table 3.1.(continued)

$Se^{74}(n,p)As^{74}$		$S^{32}(n,t)P^{30}$		$Ca^{40}(n,t)K^{38g}$		$Mg^{26}(n,\alpha)Ne^{23}$	
E_n(MeV)	σ (mb)	E_n(MeV)	σ (μbarn)	E_n(MeV)	σ (μbarn)	E_n(MeV)	σ (mb)
12,95 ± 0,20	174 ± 52	14,7 ± 0,35	7,5 ± 0,7	14,9 $^{+1,4}_{-1,25}$	31 ± 5	13,00 ± 0,16	90 ± 9,0
13,5 ± 0,25	107 ± 32	16,05 ± 0,95	471 ± 61	16,1 ± 1,4	93 ± 11	13,25 ± 0,18	81 ± 8,1
14,1 ± 0,25	105 ± 20	17,05 ± 0,95	737 ± 96	17,1 $^{+1,3}_{-1,4}$	135 ± 15	13,55 ± 0,14	88,5 ± 8,9
14,9 ± 0,30	111 ± 33	18,0 $^{+0,7}_{-0,9}$	1000 ± 130	17,7 $^{+1,2}_{-1,4}$	157 ± 17	14,00 ± 0,14	84 ± 8,4
15,6 $^{+0,30}_{-0,35}$	73 ± 22	18,7 $^{+0,5}_{-0,75}$	1260 ± 160	18,0 $^{+1,0}_{-1,3}$	158 ± 17	14,28 ± 0,16	77 ± 7,7
16,3 $^{+0,30}_{-0,35}$	81 ± 24	19,6 $^{+0,2}_{-0,3}$	1380 ± 180	18,7 $^{+0,7}_{-1,2}$	188 ± 20	14,74 ± 0,20	66,5 ± 6,7
17,2 $^{+0,25}_{-0,40}$	79 ± 24			19,6 $^{+0,2}_{-0,3}$	169 ± 18	15,21 ± 0,28	61 ± 6,1
18,0 $^{+0,25}_{-0,35}$	70 ± 21					15,68 ± 0,29	59 ± 5,9
18,9 $^{+0,15}_{-0,30}$	72 ± 22					15,92 ± 0,23	64 ± 6,4
19,6 $^{+0,15}_{-0,25}$	69 ± 21					16,17 ± 0,28	61 ± 6,1
						16,42 ± 0,30	59 ± 5,9
						16,65 ± 0,20	53 ± 5,3

Table 3.1.(continued)

$Ce^{140}(n,\alpha)Ba^{137m}$		$S^{32}(n,2n)S^{31}$		$Co^{59}(n,2n)Co^{58tot.}$		$Co^{59}(n,2n)Co^{58g}$	
E_n(MeV)	σ (mb)	E_n(MeV)	σ (mb)	E_n(MeV)	σ_{tot}(mb)	E_n(MeV)	σ_g(mb)
13,35 ± 0,14	13,5 ± 1,30	15,92 ± 0,26	0,145 ± 0,014	12,55 ± 0,15	429 ± 34	12,55 ± 0,15	126 ± 56
13,58 ± 0,14	13,0 ± 1,25	16,17 ± 0,28	0,28 ± 0,027	14,10 ± 0,30	642 ± 32	14,10 ± 0,30	195 ± 53
14,00 ± 0,14	12,1 ± 1,16	16,42 + 0,30	0,58 ± 0,057	15,20 ± 0,30	695 ± 56	15,20 ± 0,30	181 ± 95
14,10 ± 0,22	12,4 ± 1,19			16,70 + 0,30 − 0,40	700 ± 56	16,70 + 0,30 − 0,40	214 ± 92
14,25 ± 0,14	11,4 ± 1,09						
14,53 ± 0,14	11,0 ± 1,06			18,20 + 0,25 − 0,35	761 ± 61	18,20 + 0,25 − 0,35	240 ± 99
14,82 ± 0,16	11,8 ± 1,13						
15,08 ± 0,17	11,6 ± 1,11			19,60 + 0,15 − 0,25	864 ± 69	19,60 + 0,15 − 0,25	227 ± 118
15,30 ± 0,18	12,1 ± 1,16						
15,54 ± 0,19	10,0 ± 9,6						
15,76 ± 0,19	10,8 ± 1,04						
15,93 ± 0,21	8,7 ± 0,84						
16,17 ± 0,28	9,8 ± 0,94						
16,50 ± 0,30	10,1 ± 0,97						
16,65 ± 0,26	8,4 ± 0,76						

Table 3.1.(continued)

$Co^{59}(n,2n)Co^{58m}$		$Ni^{58}(n,2n)Ni^{57}$		$As^{75}(n,2n)As^{74}$		$Se^{74}(n,2n)Se^{73tot}$	
E_n(MeV)	σ_m(mb)	E_n(MeV)	σ (mb)	E_n(MeV)	σ (mb)	E_n(MeV)	σ_{tot}(b)
12,55 ± 0,15	303 ± 45	12,95 ± 0,20	4,7 ± 0,3	12,55 ± 0,15	686 ± 43	12,95 ± 0,20	82,2 ± 6,7
14,10 ± 0,30	447 ± 42	13,5 ± 0,25	11,9 ± 0,8	13,3 ± 0,25	881 ± 56	13,5 ± 0,25	300 ± 2[illegible]
15,20 ± 0,30	514 ± 77	14,1 ± 0,25	22,7 ± 1,4	14,1 ± 0,25	1013 ± 56	14,1 ± 0,25	472 ± 47
16,70 + 0,30 − 0,40	486 ± 73	14,9 ± 0,30	34,6 ± 2,4	14,9 ± 0,30	1101 ± 69	16,3 ± 0,30 0,35	540 ± 45
18,20 + 0,25 − 0,35	521 ± 78	15,6 + 0,30 − 0,35	40,6 ± 2,8	15,6 + 0,30 − 0,35	1120 ± 71	17,2 + 0,25 − 0,40	608 ± 50
19,60 + 0,15 − 0,25	637 ± 96	16,3 + 0,30 − 0,35	44,3 ± 3,0	16,3 + 0,30 − 0,35	1090 ± 69	18,0 + 0,25 − 0,35	639 ± 53
		17,25 + 0,25 − 0,40	48,2 ± 3,3	17,2 + 0,25 − 0,40	1147 ± 72	19,6 + 0,15 − 0,25	662 ± 55
		18,0 + 0,25 − 0,35	51,3 ± 3,5	18,0 + 0,25 − 0,35	1114 ± 70		
		18,9 + 0,15 − 0,30	52,1 ± 3,5	18,9 + 0,15 − 0,30	1099 ± 69		
		19,6 + 0,15 − 0,25	53,5 ± 3,6	19,55 + 0,15 − 0,25	989 ± 62		

Table 3.1.(continued)

$Se^{74}(n,2n)Se^{73g}$		$Se^{74}(n,2n)Se^{73m}$		$Sr^{84}(n,2n)Sr^{83}$		$Ce^{140}(n,2n)Ce^{139}$	
E_n(MeV)	σ_g(mb)	E_n(MeV)	σ_m(mb)	E_n(MeV)	σ (mb)	E_n(MeV)	σ_m(mb)
12,95 ± 0,20	61,9 ± 5,6	12,95 ± 0,20	20,3 ± 3,8	12,95 ± 0,20	310 ± 42	12,88 ± 0,27	1230 ± 118
13,3 ± 0,25	134 ± 12	14,1 ± 0,25	41,7 ± 4,6	13,5 ± 0,25	581 ± 59	13,8 ± 0,25	1390 ± 13
14,1 ± 0,25	258 ± 21	14,9 ± 0,30	78 ± 31	14,1 ± 0,25	917 ± 65	13,48 ± 0,26	1440 ± 138
14,9 ± 0,30	394 ± 35	16,3 + 0,30 − 0,35	60,6 ± 11,3	14,9 ± 0,30	1244 ± 114	13,98 ± 0,27	1230 ± 118
15,6 + 0,30 − 0,35	430 ± 39	17,2 + 0,25 − 0,40	81 ± 16	15,6 + 0,30 − 0,35	1372 ± 123	14,25 ± 0,14	1370 ± 131
16,3 + 0,30 − 0,35	479 ± 43	18,0 + 0,25 − 0,35	73 ± 14	16,3 + 0,30 − 0,35	1409 ± 127	14,33 ± 0,30	1190 ± 114
17,2 + 0,25 − 0,40	527 ± 47	19,6 + 0,15 − 0,25	72,5 ± 13	17,2 + 0,25 − 0,40	1462 ± 129	14,53 ± 0,14	1250 ± 120
18,0 + 0,25 − 0,35	566 ± 51			18,0 + 0,25 − 0,35	1513 ± 133	14,68 ± 0,30	1160 ± 111
18,9 + 0,15 − 0,30	590 ± 53			18,9 + 0,15 − 0,30	1429 ± 124	14,82 ± 0,16	1150 ± 110
19,6 + 0,15 − 0,25	589 ± 53			19,55 + 0,15 − 0,25	1423 ± 122	15,08 ± 0,17	1140 ± 109
						15,17 ± 0,30	1130 ± 108
						15,30 ± 0,18	1180 ± 113
						15,42 ± 0,30	1070 ± 103
						15,54 ± 0,19	1080 ± 104
						15,76 ± 0,19	1100 ± 106
						15,93 ± 0,21	1025 ± 98,3
						16,17 ± 0,28	986 ± 94,7
						16,65 ± 0,20	1015 ± 97,4
						16,90 ± 0,25	938 ± 90,0

3.2. Total Neutron Cross Section of Natural Lithium in the Energy Range 4.2 - 6.1 MeV

M. Bormann und H. Genz

The total neutron cross section of natural lithium was measured in the energy range 4.2 - 6.1 MeV by means of the transmission method. Monoenergetic neutrons were obtained via the reaction $^{2}H(d,n)^{3}He$ using a gas target and the deuteron beam of a 3 MeV Van de Graaff. For neutron detection a Stilbene recoil proton spectrometer was used. Its gamma-sensitivity was reduced by pulse-shape discrimination. The transmission data were corrected for neutrons elastically scattered in forward direction. The results are given in table 3.3. The neutron energy resolution was $\Delta E_n = 40$ keV. The errors of the cross sections amount to $\Delta\sigma_{nT} = {}^{+1\%}_{-2\%}$.

Table 3.3.: Total Cross Section of Natural Lithium in the Emergy Range 4.2 - 6.1 MeV

E_n(MeV)	$_T$(barn)	E_n(MeV)	$_T$(barn)
4.17	2.45	5.08	2.43
4.21	2.44	5.13	2.35
4.25	2.41	5.18	2.17
4.29	2.49	5.23	2.19
4.34	2.47	5.28	2.24
4.38	2.50	5.33	2.24
4.44	2.49	5.38	2.11
4.48	2.43	5.43	2.20
4.53	2.48	5.48	2.18
4.57	2.35	5.54	2.18
4.62	2.44	5.59	2.11
4.66	2.44	5.64	2.21
4.72	2.45	5.69	2.21
4.76	2.41	5.75	2.21
4.81	2.54	5.80	2.20
4.85	2.36	5.85	2.23
4.90	2.48	5.90	2.10
4.95	2.46	5.95	2.23
4.99	2.30	6.01	2.17
5.04	2.39	6.06	2.12

Table 3.4. Cross Sections for (n,α) Reactions in Na^{23}

E_n (MeV)	$\sigma_{tot} \equiv \sigma(n,\alpha\gamma) + \sigma(n,\alpha n') + \sigma(n,n'\alpha)$ from total α-spectrum	$\sigma_I \equiv \sigma(n,\alpha\gamma)$ from activation measurement	$\sigma_{II} \equiv \sigma(n,n'\alpha)$ from statistical theory analysis of α-spectrum	$\sigma(n,\alpha n') \equiv \sigma_{tot} - \sigma_I - \sigma_I$
12.6 ± 0.3	160 ± 11 (mb)	159 ± 15 (mb)		
13.2 ± 0.3	159 ± 11	152 ± 14		
14.1 ± 0.4	154 ± 12	136 ± 14		
15.4 ± 0.4	158 ± 12	126 ± 11	22 ± 3 (mb)	10 ± 18 (mb)
16.4 ± 0.4	168 ± 14	96 ± 10	33 ± 4	39 ± 17
17.6 ± 0.3	196 ± 16	87 ± 8	44 ± 6	65 ± 19
18.7 ± 0.3	217 ± 18	70 ± 6	54 ± 7	93 ± 20

4. INSTITUT FÜR REINE UND ANGEWANDTE KERNPHYSIK, KIEL (GERMANY)

4.1. Fast Chopper

H.H. Jung, W. Biel, W. Komenda

4.1.1. Total neutron cross section measurements on V, Ca, and As have been made with the fast chopper facility at the swimming pool type reactor at Geesthacht (FRG-I). The data are to be published in Atomkernenergie.

4.1.1.1. Vanadium

sample: solid metal
thickness: 0.13 atoms/barn
energy range: 0.5 - 100 eV
resolution: 460 ns/m

4.1.1.2. Calcium

sample: CaO
thickness: 0.125 atoms/barn
energy range: 0.8 - 80 eV
resolution: 370 ns/m

4.1.1.3. Arsenic

sample: As-powder
thickness: 0.0662 atoms/barn
energy range: 0.5 - 40 eV
resolution: 460 ns/m
preliminary results are expected early in 1966.

4.1.2. Measurements on copper single crystals have been performed in order to look for crystal effects on total neutron cross sections in the energy range up to 1 keV. The experiment shows that there are crystal effects as they have been predicted by DRITTLER (Naturwissenschaften 52, 205 (65)); they are smaller than expected but well above the statistical error. Data evaluation will be finished in spring 1966.

4.1.3. The design and construction of a new fast chopper facility (Fe-rotor with U-core, 1 % resolution at 100 eV) have been completed. It will be installed at the FRG-I early in 1966. First runs are expected in summer 1966.

Total neutron cross section measurements on radioactive nuclides are planned.

4.2. Crystal Spectrometer

4.2.1. Total Neutron Cross Section Measurement in Hydrogeneous Compounds

B. Bröcker

Total neutron cross section measurements of hydrogen have been made in the following hydrogeneous compounds: cyclohexane, benzene, paraffin, hexane, glyzerin, methanol, ammoniumchloride, ammoniumbromide, ammoniumiodide, zirconiumhydride and titaniumhydride. The energy range was 0.025 to 0.4 eV and the resolution between 0.5 and 1.5 %.

4.2.1.1. Organic Compounds

The cross section is nearly the same in all organic compounds. Very big molecules and such compounds, which are solid at room temperature show a cross section about 4 b higher than that of little molecules and liquids at the lowest energies. Above 0.1 eV difference completely disappeares. Results are given in fig. 4.1. - 4.2.

4.2.1.2. Ammonium Salts

Results are given in fig. 4.3. - 4.5. The arrows mark the energy of hindered rotation of the NH_4 - ion. It is seen as a soft dip in the total cross section.

4.2.1.3. Metal Hydrides

Zirconium and titanium hydrides show sharp resonance dips at multiples of the vibration energy of the hydrogen atom in the crystal (W.L. Whithemore and A.W. Mc Reynolds, Phys. Rev. 113, 807 (1959)). The vibration energy was determined to be 0.133 eV for $Zr\,H_{1.63}$ and 0.14 eV for $Ti\,H_{1.94}$. Results are given in fig. 4.6. - 4.7.

Further measurements are planned to determine the dependence of the vibration energy from temperature, hydrogen-concentration and deuterium content.

4.2.2. Use of Totally Reflected Cold Neutrons for Measurement of the Temperature Dependence of the (n,p) Cross Section for Chemically Bound Protons

U. Schmidt, M. Saad

A beam of cold neutrons was produced by total reflection from iron plates of a special constructed collimator. The

reflected beam contains all energies up to a limiting energy, which is determined by angular position of the collimator.

This method has been used to determine the total cross sections of the n-p scattering in Cyclohexane, Benzene, Diphenyl, o-Terphenyl and m-Terphenyl in the temperature range between - 50 and + 180° C for a neutron beam with a limiting energy of $1.8 \cdot 10^{-3}$ eV. The cross section increases slightly with temperature and shows a step at the melting point. The results are shown in fig. 4.8.

The measurements are to be published in Atomkernenergie.

4.3. Scattering Cross section of Hydrogen in Water Dioxan Solutions

A. Suszkin

Scattering cross sections of the hydrogen in water-dioxan solutions were calculated from obtained values of the transmissions, which were measured for 13 solutions with varying water concentration for the neutron energies between 0.578 and 0.024 eV.

The measurements were conducted with the following errors: the error of the determination of the thickness of the cuvette: ± 3 %, the error of small-angle scattering: + 0.6 %, statistical error: ± 0.6 %, and the total error of the measurements (without the error of the cuvettes): ± 3.1 %.

As it can be seen from fig. 4.9. the scattering cross section of hydrogen varies for the energy range 0.578 - 0.024 eV in the case of dioxan between 23 and 61 barns and in the case of water between 22 and 52 barns. The observable difference between values of the scattering cross sections for water and dioxan appears at the energy value of 0.17 eV, grows up until energy value of 0.06 eV and remains further approximately constant at the value of 9 barns.
From fig. 4.10. can be concluded that the scattering cross section in the water-dioxan solutions diminishes almost linear with increasing concentration for each value of neutron energy.

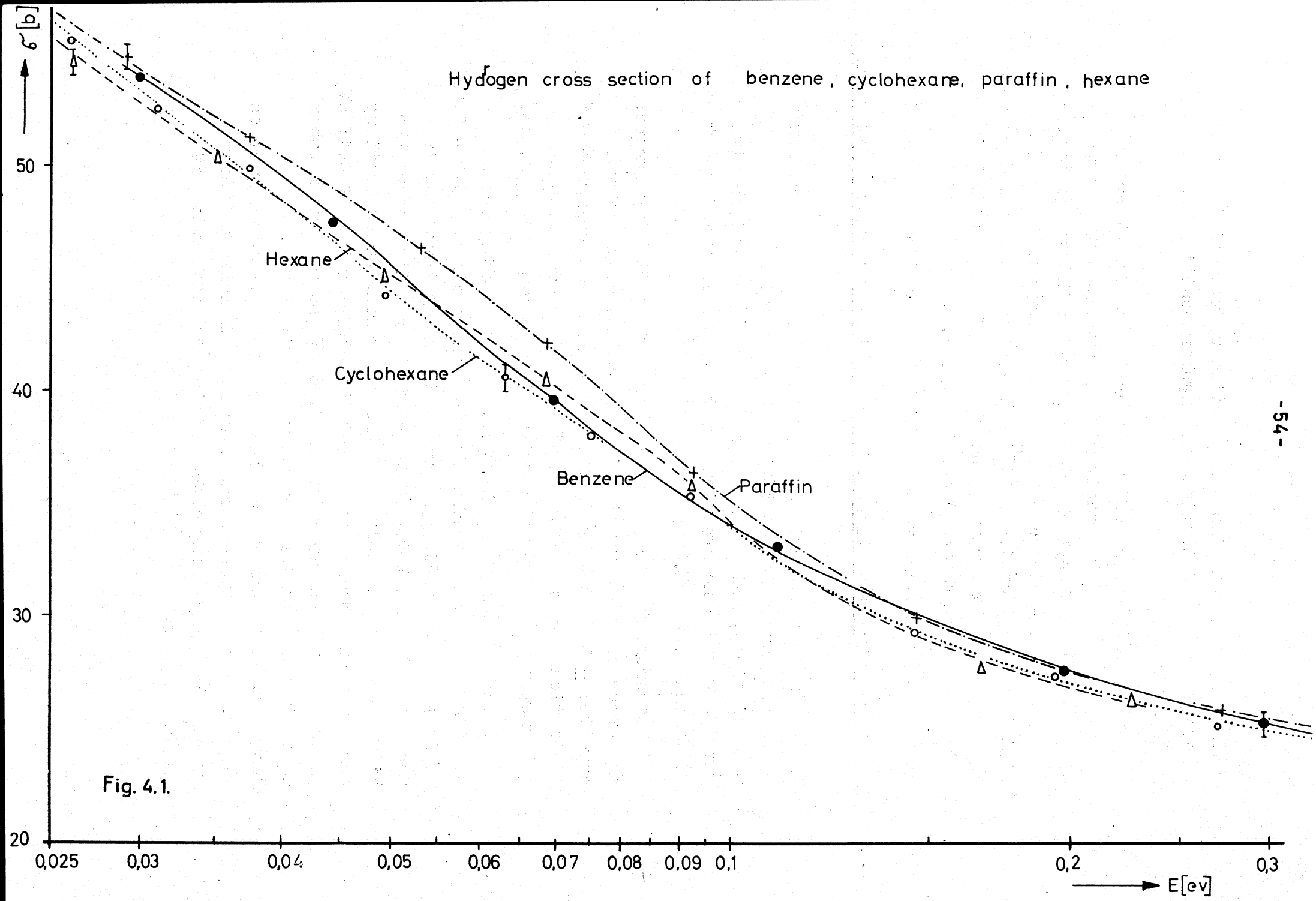
Hydrogen cross section of benzene, cyclohexane, paraffin, hexane
σ [b]
50
40
30
20
Hexane
Cyclohexane
Benzene
Paraffin
0,025
0,03
0,04
0,05
0,06
0,07
0,08
0,09
0,1
0,2
0,3
E[ev]

Fig. 4.1.

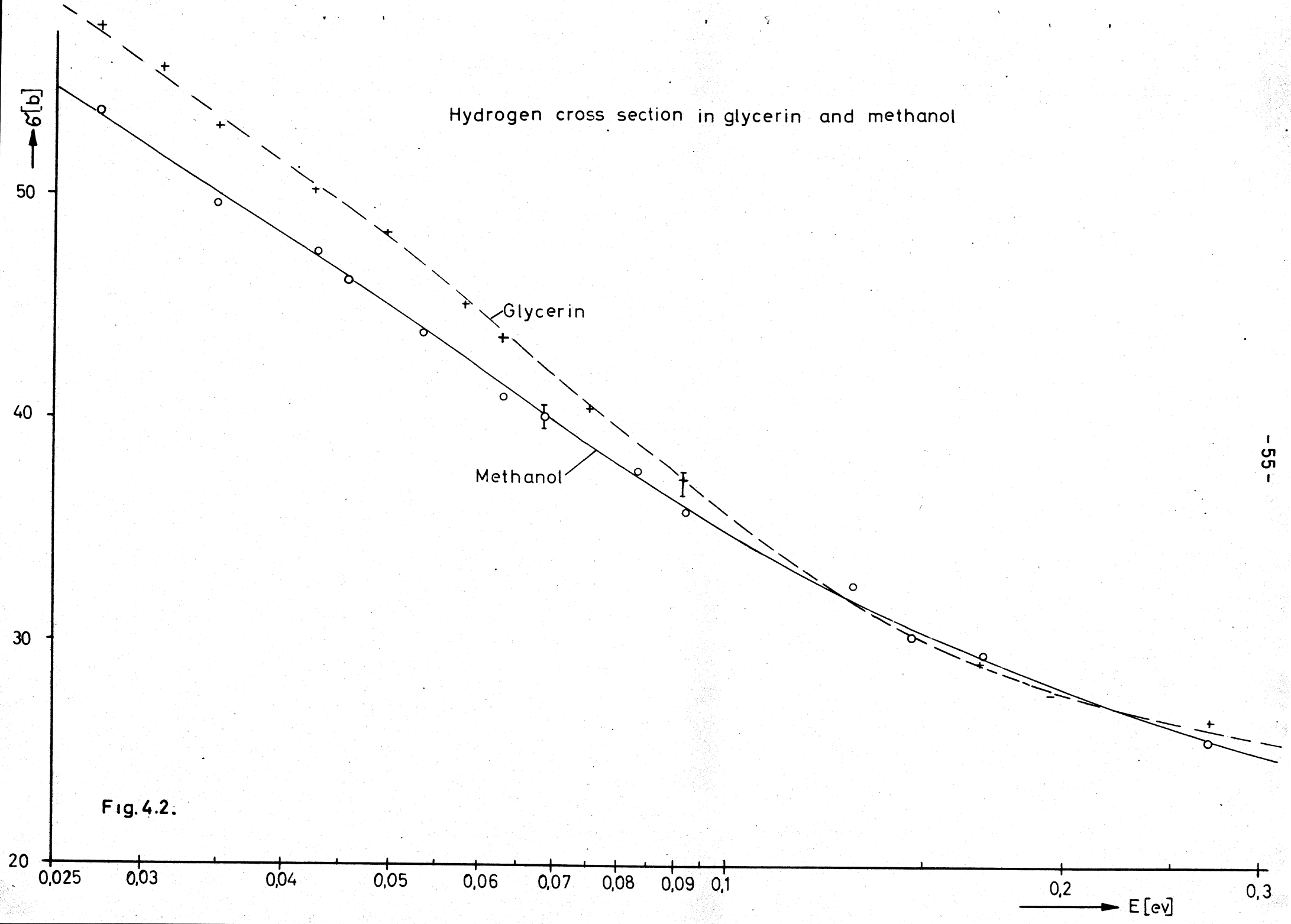
Hydrogen cross section in glycerin and methanol
σ [b]
50
40
30
20
Glycerin
Methanol
0,025
0,03
0,04
0,05
0,06
0,07
0,08
0,09
0,1
0,2
0,3
E [ev]

Fig. 4.2.

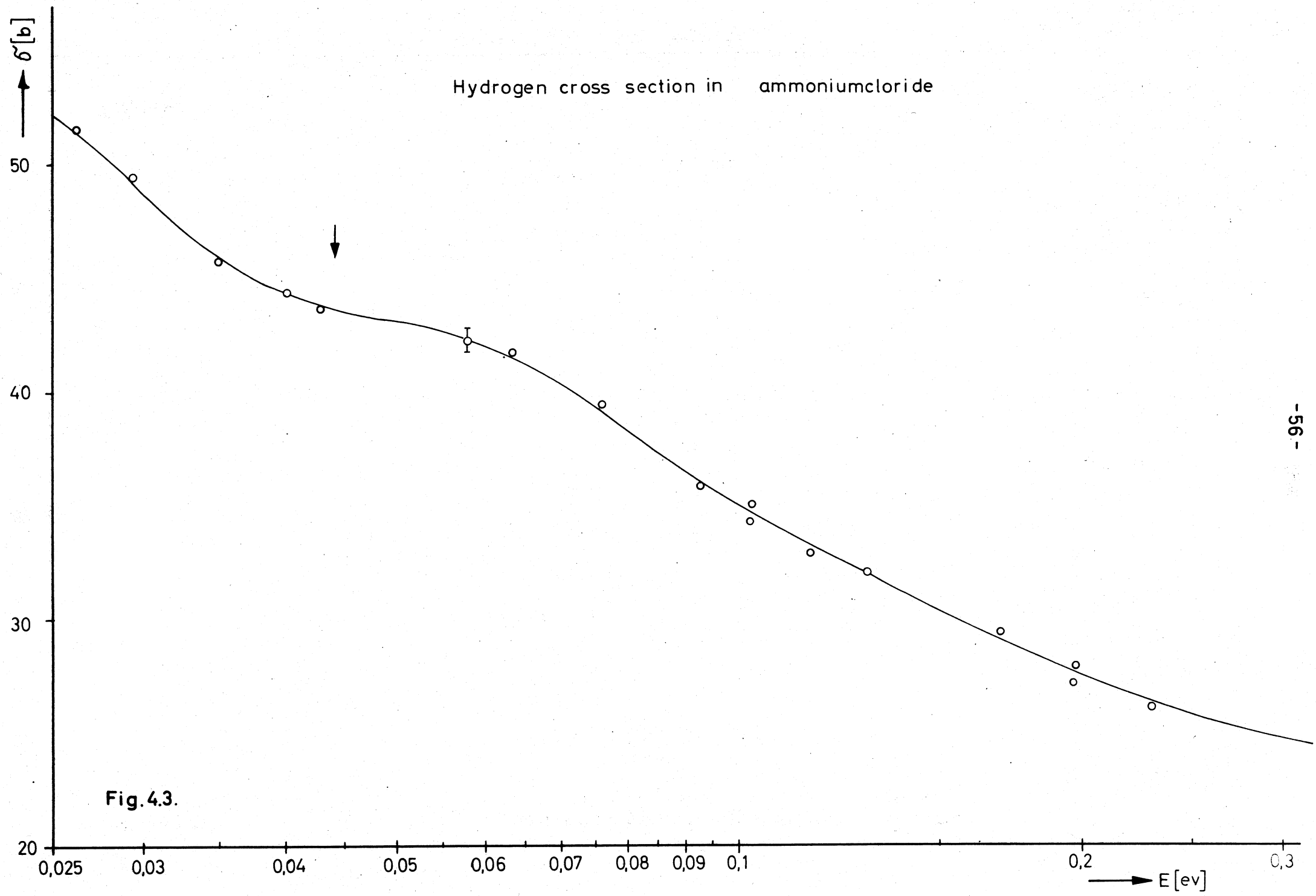
Hydrogen cross section in ammoniumcloride
σ [b]
50
40
30
20
0,025
0,03
0,04
0,05
0,06
0,07
0,08
0,09
0,1
0,2
0,3
E [ev]

Fig. 4.3.

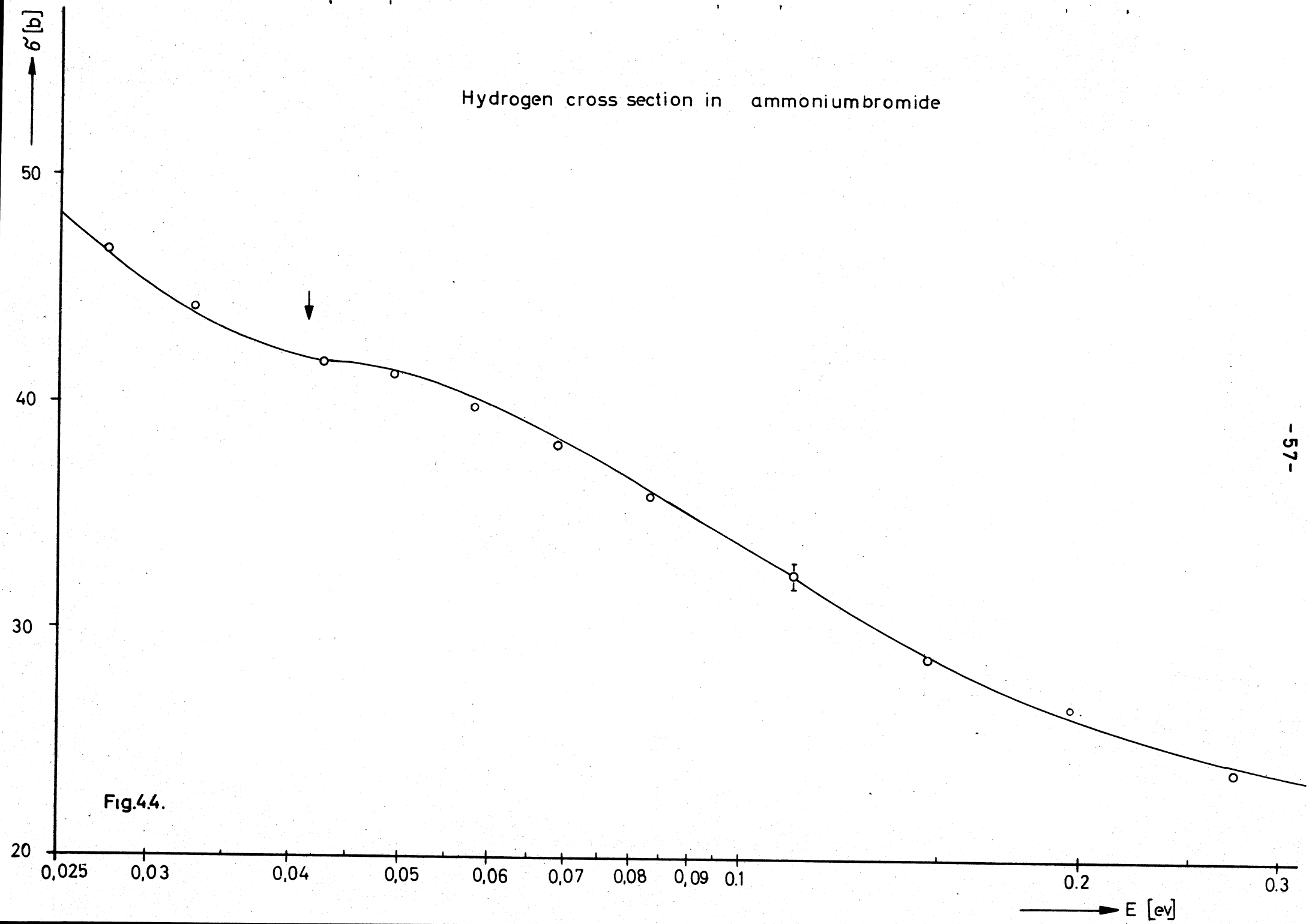
Hydrogen cross section in ammoniumbromide
σ [b]
50
40
30
20
0,025
0,03
0,04
0,05
0,06
0,07
0,08
0,09
0.1
0.2
0.3
E [ev]

Fig.4.4.

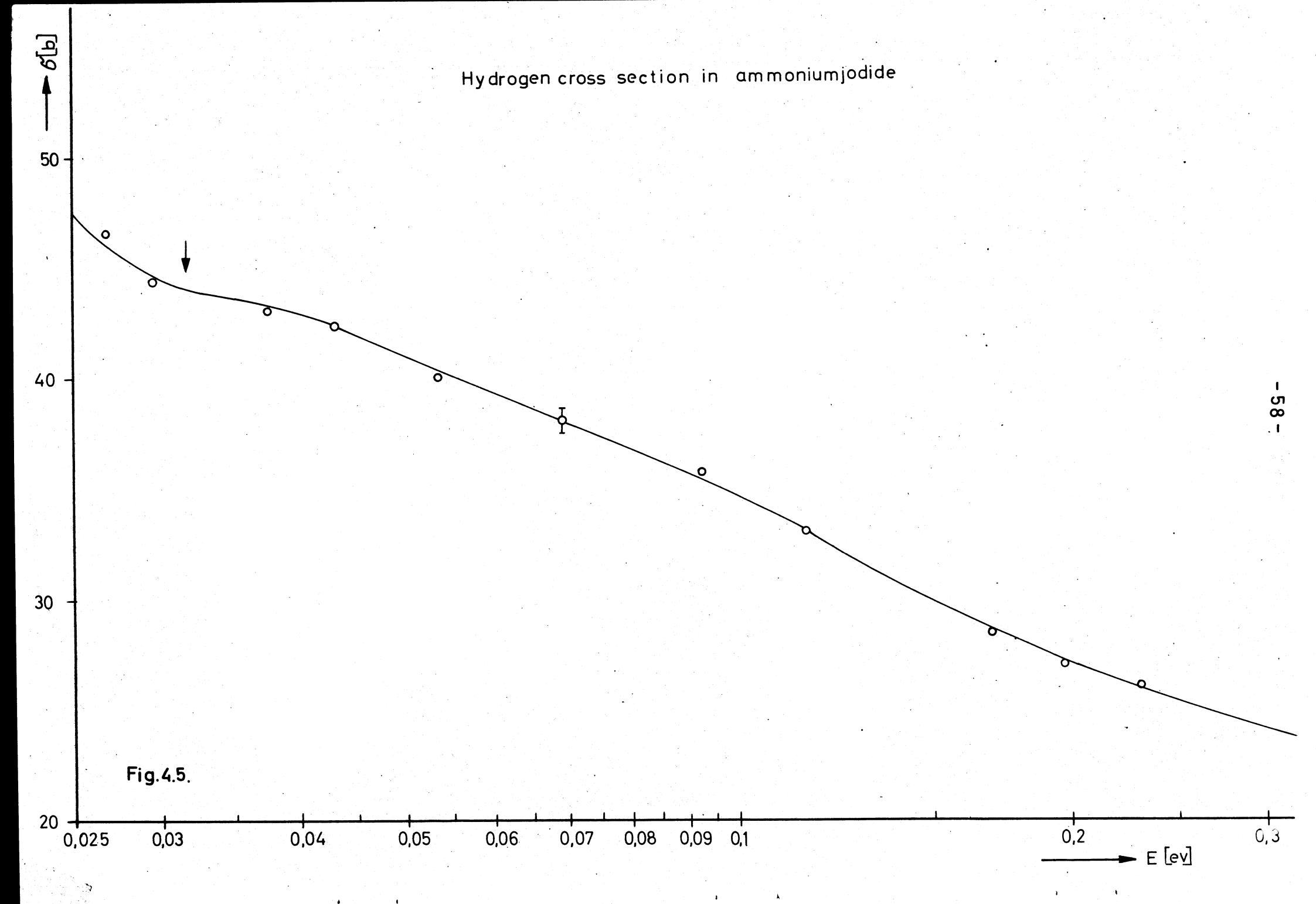
Hydrogen cross section in ammoniumjodide
σ [b]
50
40
30
20
0,025
0,03
0,04
0,05
0,06
0,07
0,08
0,09
0,1
0,2
0,3
E [ev]

Fig. 4.5.

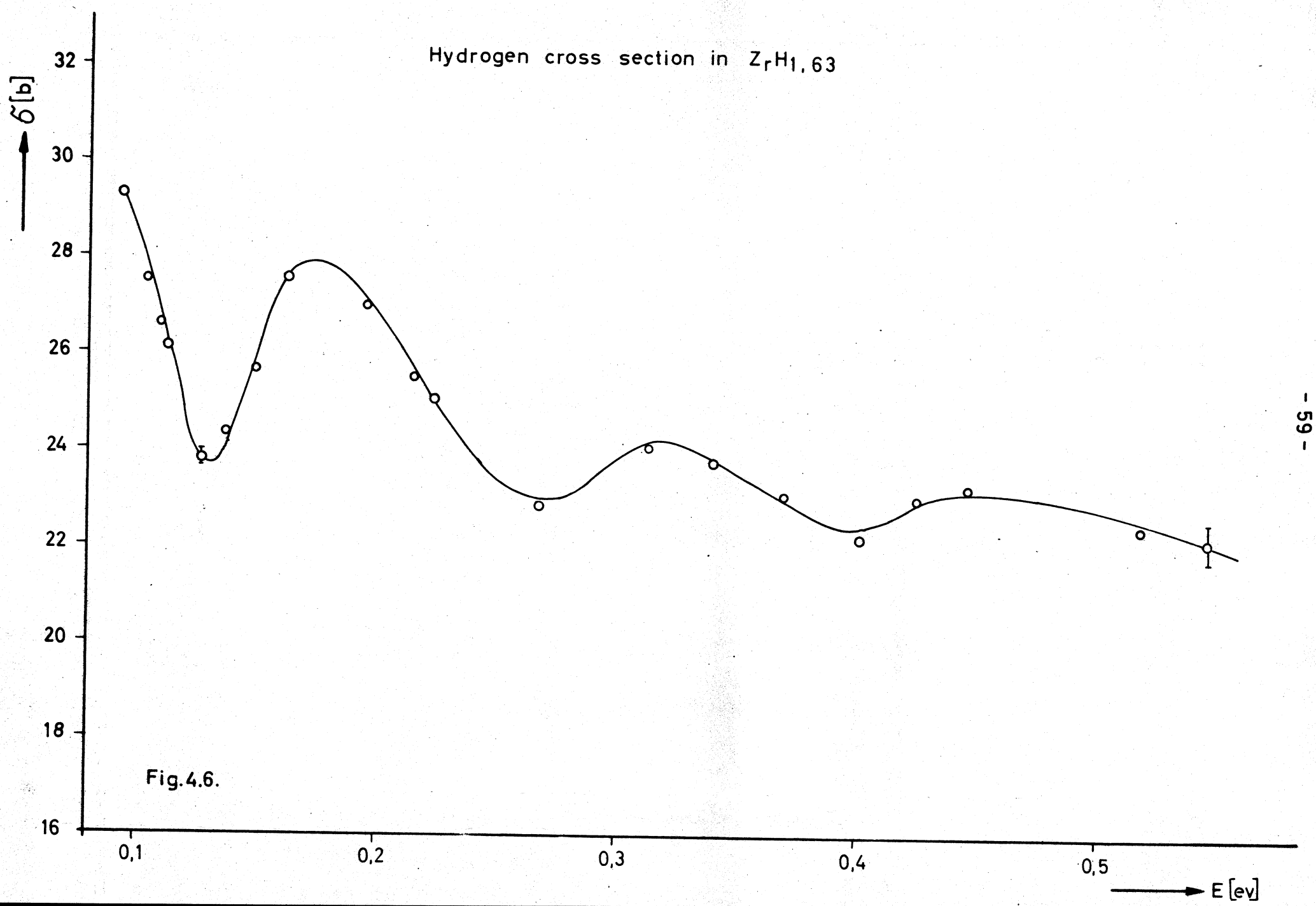
Hydrogen cross section in $Z_rH_{1,63}$
σ [b]
32
30
28
26
24
22
20
18
16
0,1
0,2
0,3
0,4
0,5
E [ev]

Fig.4.6.

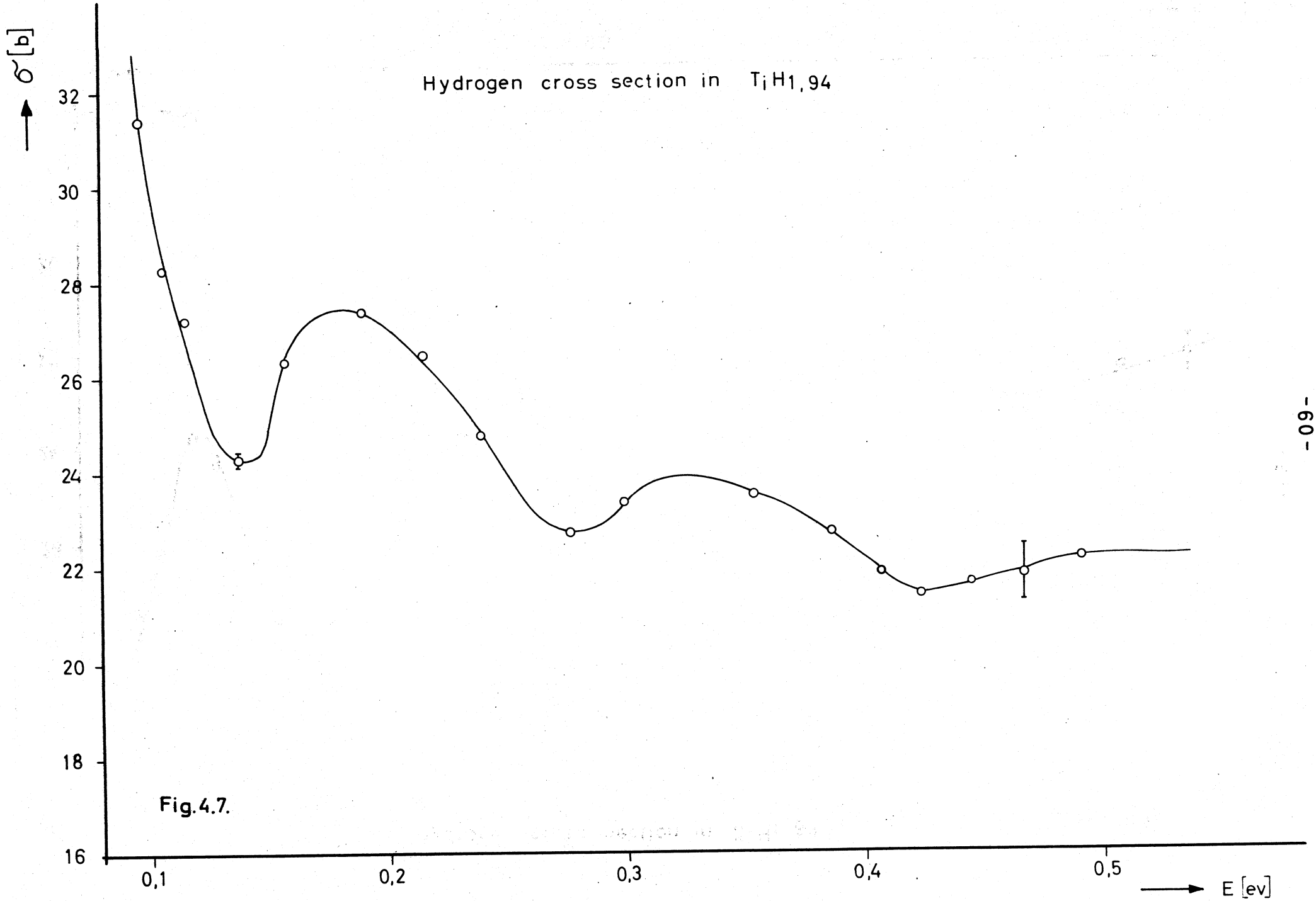
Hydrogen cross section in $T_iH_{1,94}$
σ [b]
32
30
28
26
24
22
20
18
16
0,1
0,2
0,3
0,4
0,5
E [ev]

Fig.4.7.

Total cross section of the (n,p) scattering in organic compounds

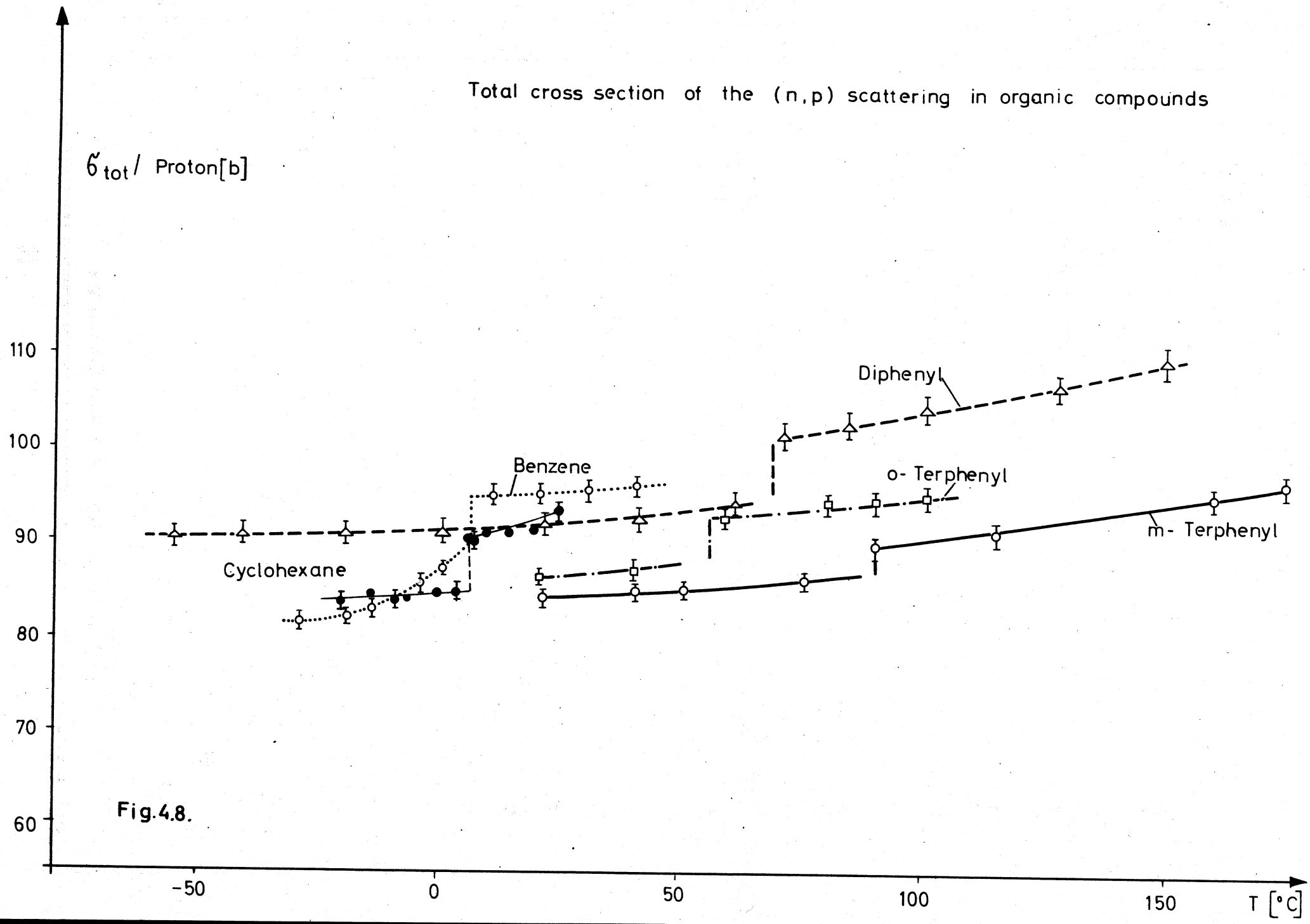

Fig.4.8.

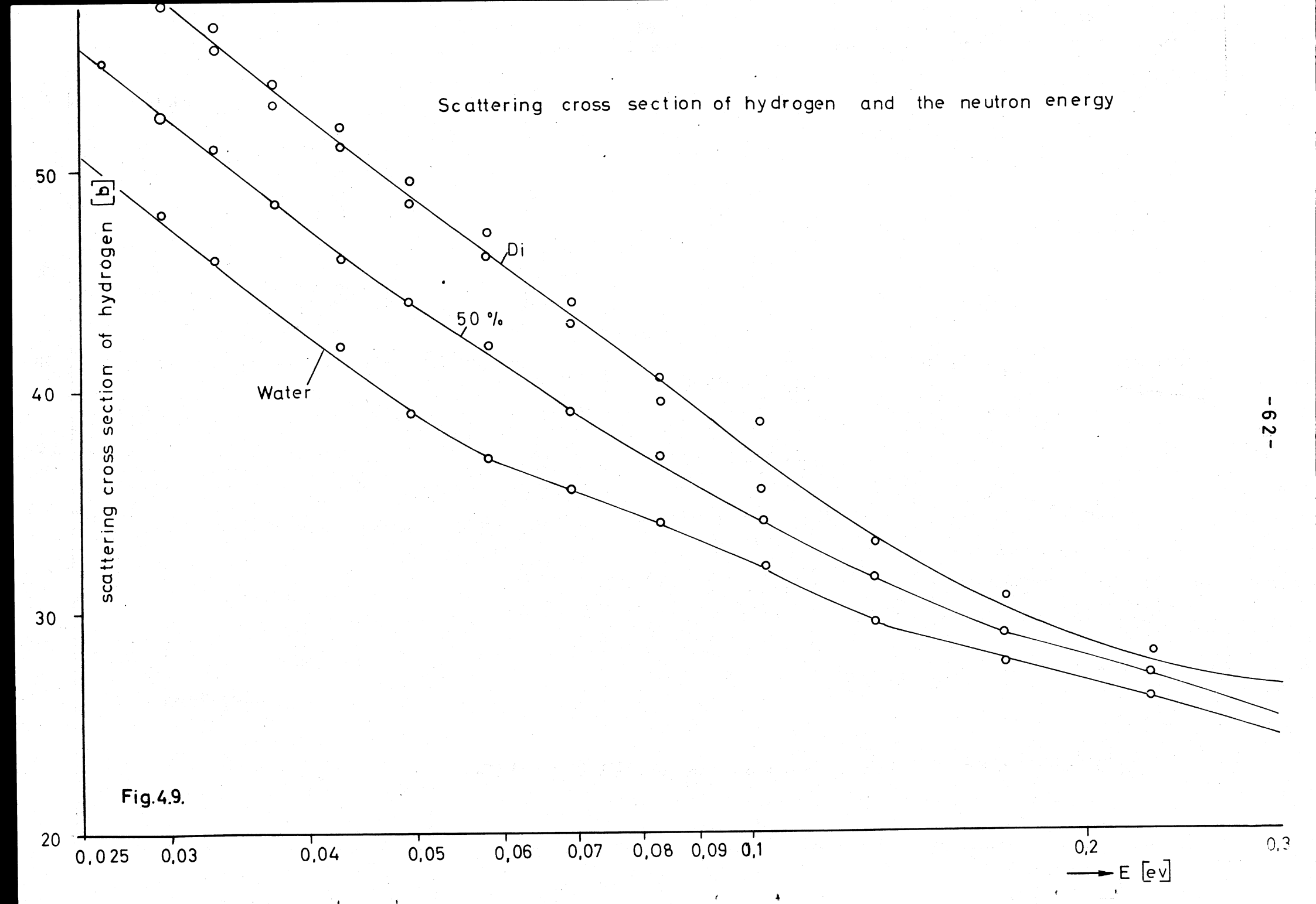
Scattering cross section of hydrogen and the neutron energy
scattering cross section of hydrogen [b]
50
40
30
20
Di
50 %
Water
0,025
0,03
0,04
0,05
0,06
0,07
0,08
0,09
0,1
0,2
0,3
E [ev]

Fig.4.9.

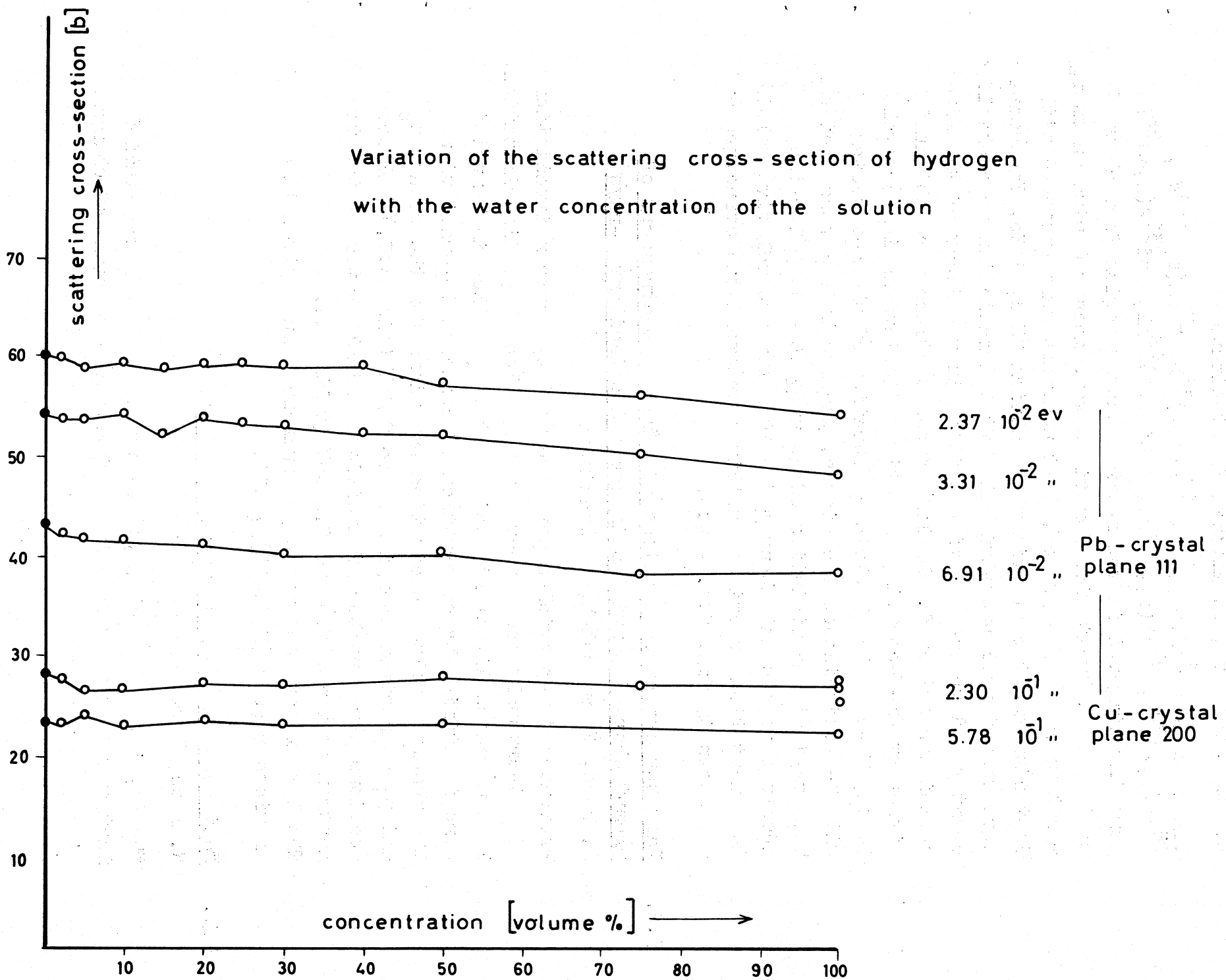
Variation of the scattering cross-section of hydrogen
with the water concentration of the solution
scattering cross-section [b]
70
60
50
40
30
20
10
concentration [volume %]
10
20
30
40
50
60
70
80
90
100
2.37 10^{-2} ev
3.31 10^{-2} "
6.91 10^{-2} "
Pb - crystal plane 111
2.30 10^{-1} "
5.78 10^{-1} "
Cu - crystal plane 200

Fig. 4.10.

5. INSTITUT FÜR KERNPHYSIK DER UNIVERSITÄT FRANKFURT, FRANKFURT (GERMANY)

5.1. Fast neutron excitation functions by activation techniques

R. Bass, P. Haug, K. Krüger, B. Staginnus

The reactions $^{19}F(n,p)^{19}O$, $^{19}F(n,\alpha)^{16}N$, $^{23}Na(n,p)^{23}Ne$, $^{23}Na(n,\alpha)^{20}F$, $^{27}Al(n,p)^{27}Mg$, $^{28}Si(n,p)^{28}Al$, and $^{31}P(n,\alpha)^{28}Al$ were investigated in the neutron energy region from about 5 up to 9 MeV. Excitation functions were measured with an energy resolution of 25 - 30 keV. Fast neutrons were produced with deuterium gas targets via the reaction $^{2}H(d,n)^{3}He$. The samples were transferred pneumatically after irradiation to a shielded counter and the γ-radiation emitted in the decay of the final nuclei was detected. Absolute cross sections were obtained either by 4π-β-counting in activated scintillation crystals (CaF_2, NaJ) or by absolute calibration of the γ-detector with β-γ coincidence techniques. The resulting cross sections have typical uncertainties of about $\pm$ 10 - 15 % for the absolute values and about $\pm$ 5 - 10 % for the relative values. The excitation functions exhibit characteristic structure and are shown in fig. 5.1. - 5.6.

5.2. Fast neutron cross sections of ^{23}Na by spectroscopy of prompt charged particles in NaJ and coincident -rays

R. Bass, Fatma Saleh, B. Staginnus

Protons and α-particles were produced by neutron irradiation of NaJ-crystals and detected using pulse shape discrimination. In some cases different excited states of the final nuclei were identified by observation of coincident γ-radiation. The results include excitation functions for the groups p_0 and p_1 at neutron energies up to 8 MeV (fig. 5.7.) and cross sections for a number of individual final states at the two neutron energies 8.0 and 8.8 MeV (table 5.1.). The latter data supersede preliminary values given in a previous report (EANDC(E)57"U").

5.3. Fast neutron cross sections of ^{40}Ca

R. Bass, Fatma Saleh

The (n,n'), (n,p) and (n,α) reactions of ^{40}Ca were studied further using the following methods: a) Detection of charged

particles in CaF_2(Eu) scintillation crystals; b) Spectroscopy of γ-radiation in coincidence with charged particles; c) Straight γ-ray measurements in ring geometry. The previous energy range (3.7 - 7.5 MeV) was extended down to 2.0 MeV using tritium gas targets and the source reaction $^3H(p,n)^3He$. The data analysis has now been completed and a major portion of the results is shown in fig. 5.8., which supersedes the corresponding figures in a previous report (EANDC(E)57"U"). Typical uncertainties of the cross sections range from ± 10 to ± 25 %, depending on particle group and incident energy.

5.4. Inelastic scattering of neutrons from lithium

R. Bass, G. Presser

The cross section for excitation of the 0.48 MeV state in ^7Li was measured by γ-detection in ring geometry for neutron energies from 1 MeV up to 9 MeV. The incident energy resolution was 50 keV below 4 MeV and 100 keV above 4 MeV. The excitation function shows a broad maximum centered at 3.9 MeV with a width of about 1 MeV. Preliminary results have been presented at the Antwerp conference. Later additional measurements were made in the upper part of the energy range, but have not been evaluated yet. Recently an investigation of inelastic scattering to the 3.56 MeV state in ^6Li has been started using a scatterer highly enriched in ^6Li. A preliminary analysis indicates a cross section of the order of 20 mb at E_n = 5 MeV.

Table 5.1.: Cross sections for the reactions
$^{23}Na(n,p)^{23}Ne$ and $^{23}Na(n,\ )^{20}F$

Group	Excitation energy of final state (MeV)	Cross section (mb) at E_n = 8.0 MeV	Cross section (mb) at E_n = 8.8 MeV
p_0	0	15 ± 2	12 ± 2
p_1	1.02	5.4 ± 1	5.4 ± 1
p_2	1.70	5.75 ± 1.5	12.6 ± 2
p_3	1.83	5.0 ± 1.5	6.0 ± 1.5
p_4	2.31		4.0 ± 2.5
p_5	2.52		4.5 ± 1.5
α_0	0	5 ± 2	13 ± 3
α_1	0.66	9.0 ± 2	19.2 ± 3
α_2	0.83	3.4 ± 1	7.2 ± 2
α_3	0.99	2.55 ± 0.6	4.5 ± 1
α_4	1.06	1.3 ± 0.3	4.5 ± 1
α_5	1.31	1.35 ± 0.3	3.6 ± 0.8

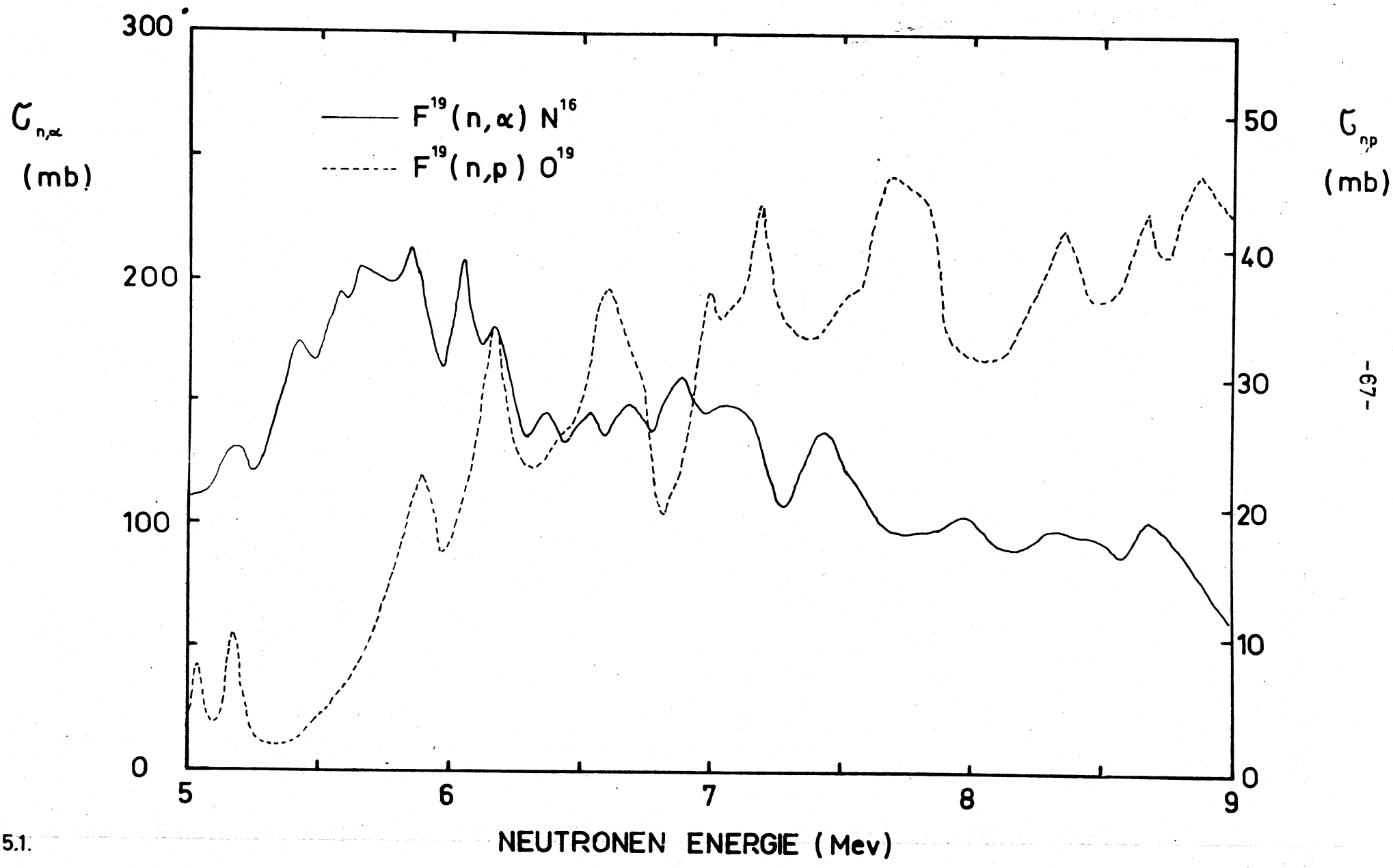
300
200
100
0
$\sigma_{n,\alpha}$
(mb)
$F^{19}(n,\alpha)\,N^{16}$
$F^{19}(n,p)\,O^{19}$
50
40
30
20
10
0
σ_{np}
(mb)
5
6
7
8
9
NEUTRONEN ENERGIE (Mev)

Fig. 5.1.

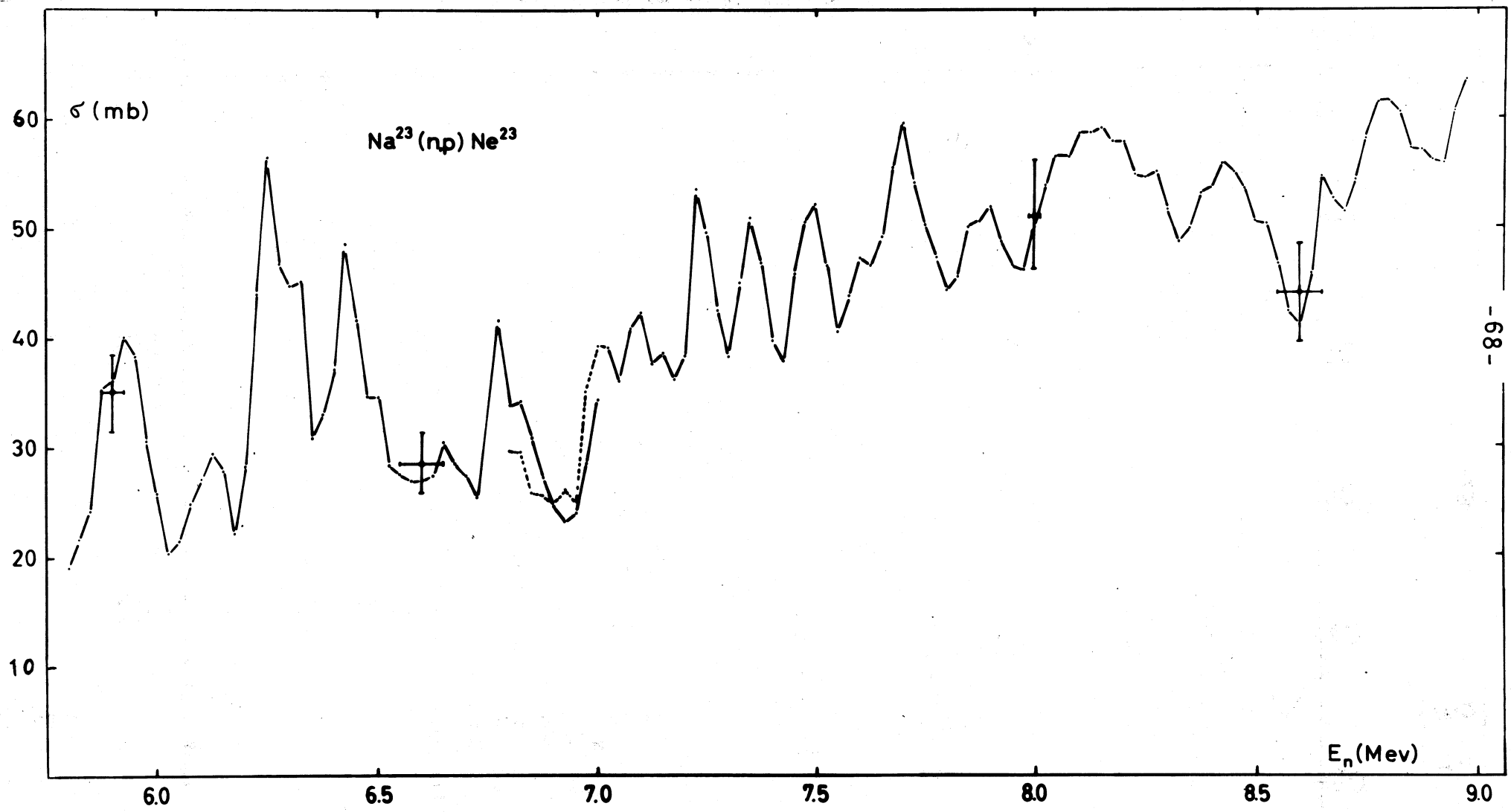

Fig. 5.2.

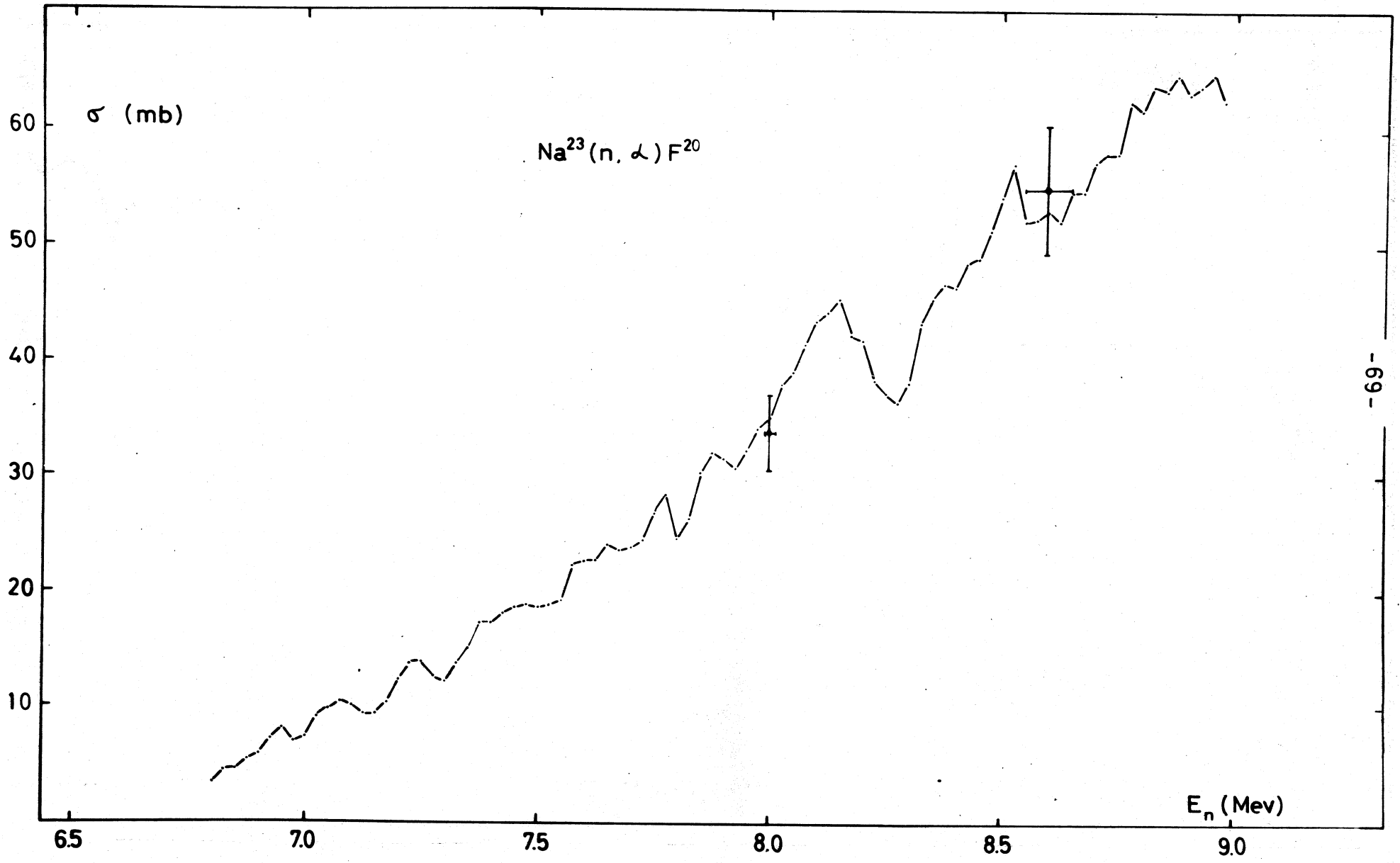

Fig. 5.3.

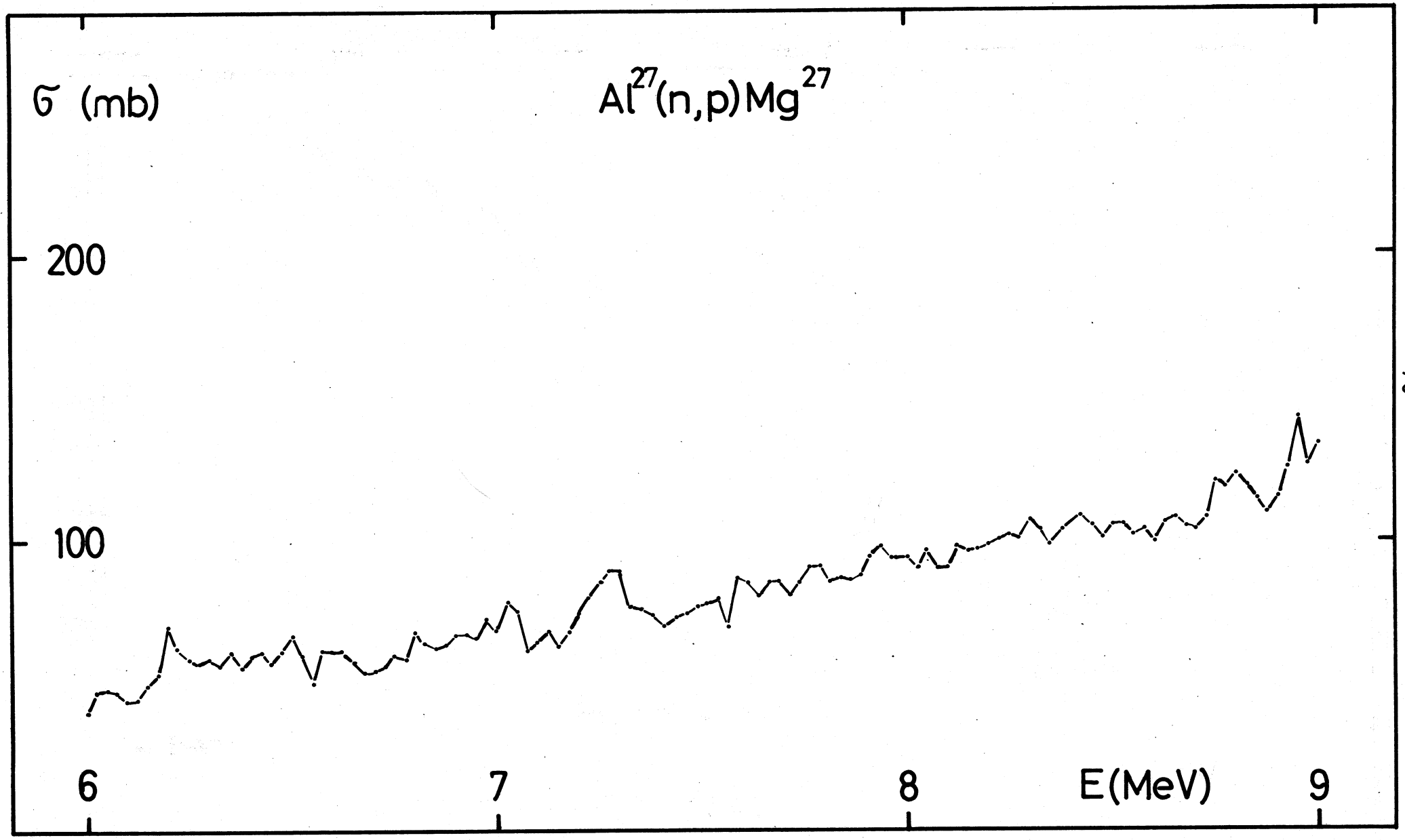

Fig. 5.4.

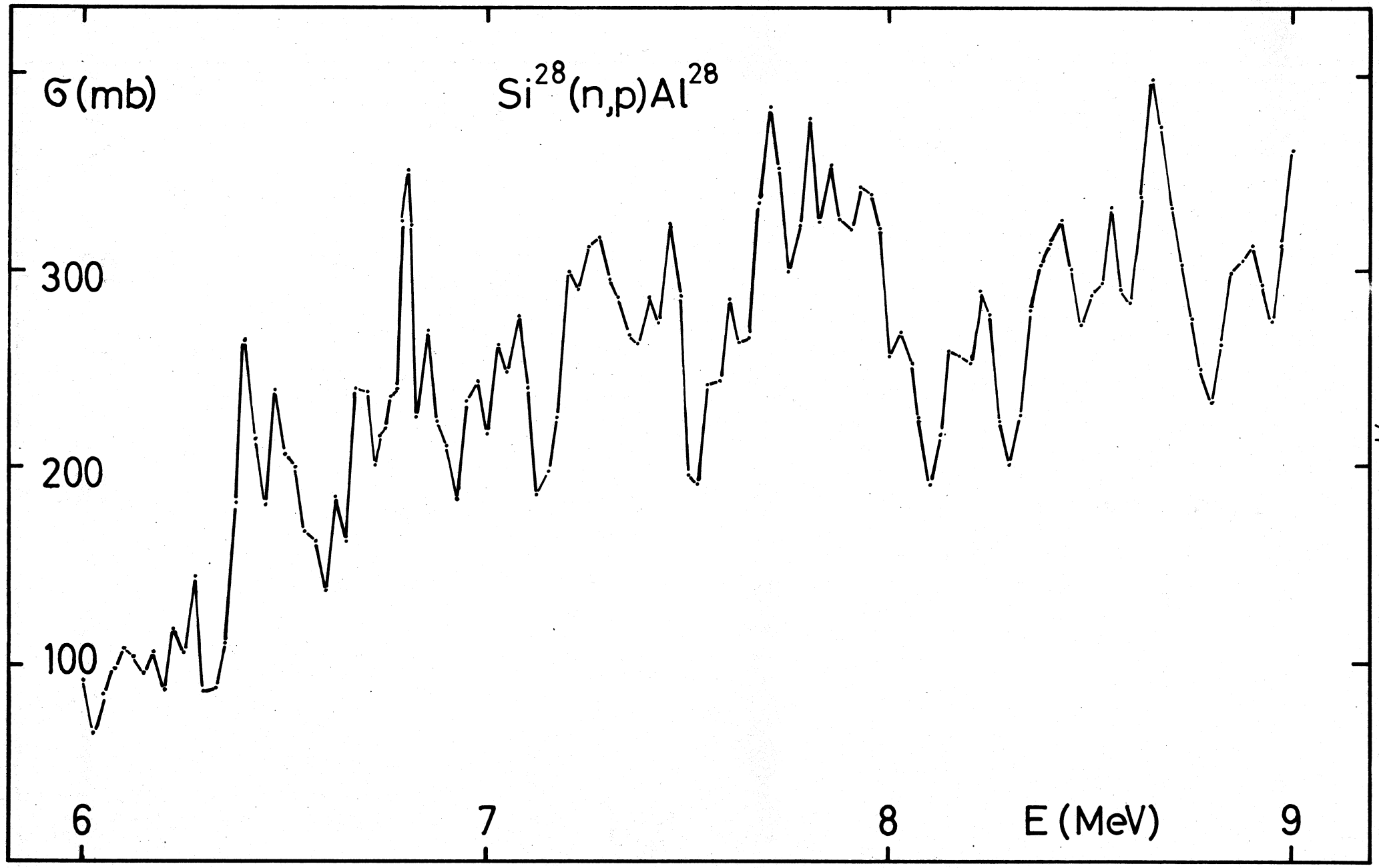

Fig. 5.5.

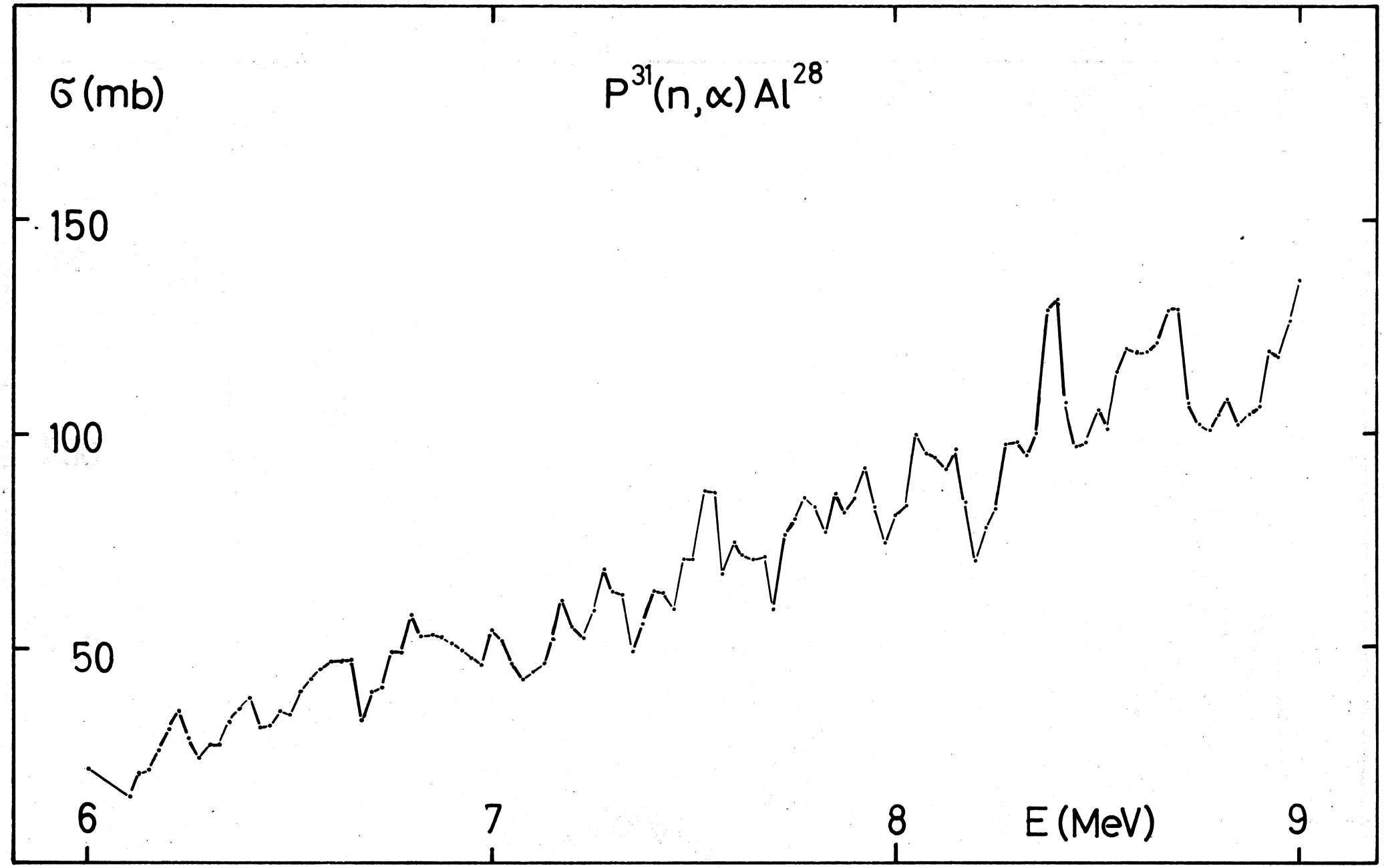

Fig. 5.6.

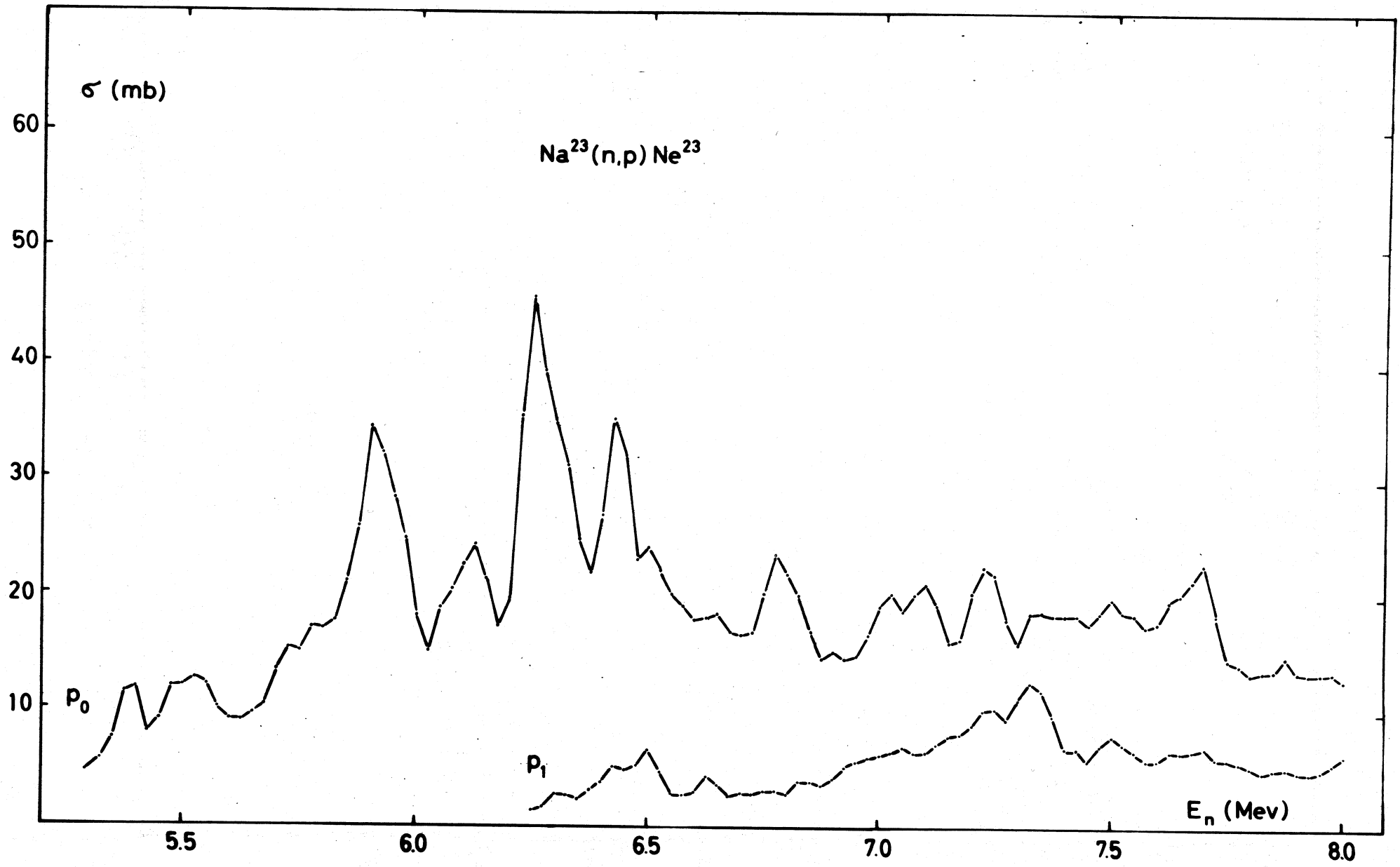

Fig. 5.7.

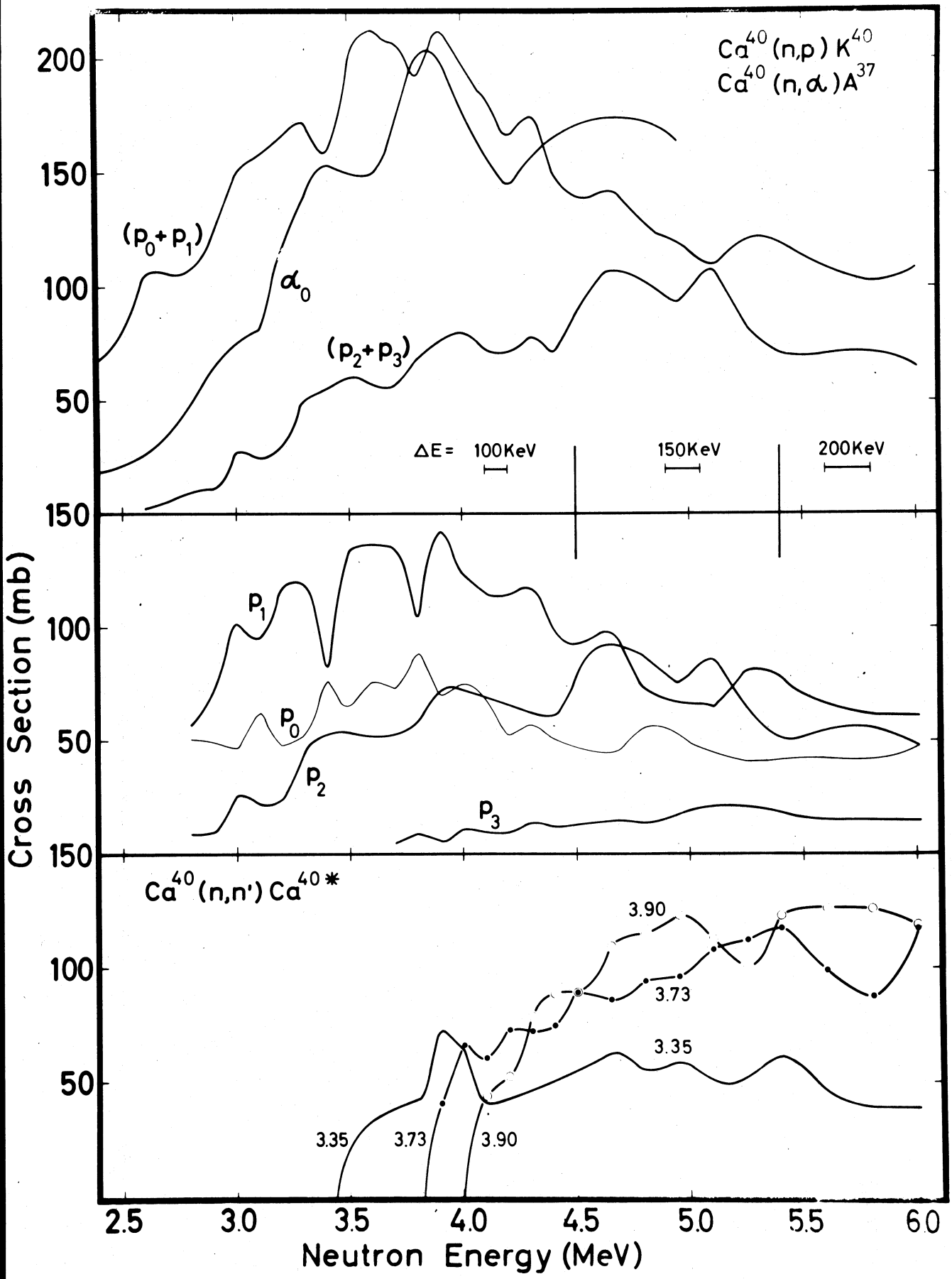
Ca40 (n,p) K40
Ca40 (n,α) A37
(P0+P1)
α0
(P2+P3)
ΔE= 100KeV
150KeV
200KeV
P1
P0
P2
P3
Ca40 (n,n') Ca40*
3.90
3.73
3.35
3.35
3.73
3.90
Cross Section (mb)
Neutron Energy (MeV)
200
150
100
50
2.5
3.0
3.5
4.0
4.5
5.0
5.5
6.0

Fig. 5.8.

6. REACTOR CENTRUM NEDERLAND, PETTEN (NETHERLANDS), PHYSICS DEPARTMENT

6.1. Gamma-gamma angular correlation measurements in (n,) reactions

G. van Middelkoop, P. Spilling, H. Gruppelaar and A.M.F. Op den Kamp.

The γ- γ coincidence and angular correlation spectrometer at the Dutch High Flux Reactor in Petten was used for studying the $^{35}Cl(n,\gamma)^{36}Cl$ and $^{32}S(n,\gamma)^{33}S$ reactions, while measurements in the $^{24,25}Mg(n,\gamma)^{25,26}Mg$ reactions are started, using natural magnesium and enriched isotopes.

The spectrometer, which was completed in 1963, is briefly described in ref. (1), where results of measurements in the $^{31}P(n,\gamma)^{32}P$ reaction are reported. Only a few essential points of the equipment are presented here.

A thermal neutron beam from a horizontal radial beam hole of this reactor is obtained by removing the fast neutrons and radiation from the beam by single crystals of quartz and bismuth. Since this year, the filter is at liquid nitrogen temperature. The flux obtained is $8 \times 10^{6} cm^{-2} s^{-1}$. Two gain-stabilized 12.7 cm x 12.7 cm NaI(Tl) scintillation spectrometers detect the capture γ-radiation. One of these detectors can be rotated in a vertical plane around the target. Both ordinary coincidence and sum-coincidence techniques are applied (resolving time $2\tau = 30$ ns). The equipment is fully automatized, the data are punched on paper tape.

The results from measurements in the $^{35}Cl(n,\gamma)^{36}Cl$ reaction are reported briefly in ref. (2) and in more detail in ref. (3). The $^{32}S(n,\gamma)^{33}S$ reaction is discussed in ref. (4).

This investigation is a part of the programme of the Dutch Foundation for Fundamental Research on Matter (Stichting voor Fundamenteel Onderzoek der Materie, F.O.M.).

References

(1) G. van Middelkoop and P. Spilling, Nuclear Physics 72, 1 (1965).

(2) G. van Middelkoop and P. Spilling, Int. Conf. on the Study of Nuclear Structure with Neutrons, Antwerp, 1965.

(3) G. van Middelkoop and P. Spilling, to be published in Nuclear Physics.
(4) G. van Middelkoop and H. Gruppelaar, to be published in Nuclear Physics.

6.2. Nuclear orientation experiments with reactor neutrons

H. Postma, E.R. Reddingius and J.F.M. Potters.

A nuclear orientation facility has been constructed at the Dutch High Flux Reactor of the Reactor Centre Netherlands (R.C.N.). This project has been undertaken by the Kamerlingh Onnes Laboratory of the Leyden University and is financed by the foundation for Fundamental Research on Matter (F.O.M.). With this facility it is possible to do the following type of experiments:

a) transmission of polarized neutrons through targets of polarized nuclei;
b) the study of anisotropy of capture-gamma-ray emission from aligned nuclei;
c) experiments on beta- and gamma-ray emission from short living nuclei, produced by neutron capture.

The current effort concerns mainly the second type of experiments. Preliminary experiments on some rare-earth isotopes have been done, while rather detailed experiments are carried out with aligned neodynium isotopes. Some spin assignments of levels of ^{144}Nd have been obtained. The high-energy capture gamma rays are detected with a three-crystal pair-spectrometer. Some low-energy lines are detected by a Ge-Li-drifted detector.

7. LABORATORIO DATI E CALCOLI NUCLEARI, CENTRO DI CALCOLO DEL C.N.E.N., BOLOGNA (ITALY)

During 1965 the following theoretical works have been developed at the Computation Centre of C.N.E.N. (located in Bologna, Italy), or by personnel of the Centre.

7.1. Effects of Nonlocality in Off-Diagonal Potentials

The effects of nonlocality in the off-diagonal parts of the optical potental have been studied in distorted-wave Born approximation by using a local energy approximation. The effects were found to be very small in the case of inelastic scattering to low lying collective states because of the small Q value and the approximate equality usually assumed for the distorting potentials in the initial and final channels. For (p,n) reactions to isobaric analog states, because of the large Q value and the differences between distorting potentials, the effects were found to be appreciable but mostly change the magnitude of the cross section.

For details, see Ref. (1).

7.2. 2^+ Level Excitation in Neutron-^{12}C Elastic Scattering

The n-^{12}C elastic scattering below 4 MeV has been analyzed first by a single-particle model and subsequently by a channel coupling model which takes into account the virtual excitation of the 2^+ target level. The spherical potential is able to reproduce the behaviour of the non-resonant phase shifts and the broad single-particle resonances. By introducing a deformed potential the observed spectrum is reproduced and a satisfactory agreement with the experimental phase shifts is obtained.

For details, see Ref. (2).

7.3. Compound Nucleus Radiative Capture Cross Section in the MeV Energy Range and Nuclear Level Density

The neutron radiative cross sections in the MeV region for nuclei with neutron number $40 \leq N \leq 90$ have been examined on the basis of the statistical model. An energy dependence of the level density like $\rho(\bar{U}) \sim (A(\bar{U}+t)^{-2} \exp(2(a\bar{U})^{\frac{1}{2}})$ was assumed. The a-values obtained from the analysis were

compared with those given by the analysis of the level density at binding excitation energy.

For details, see Ref. (3).

7.4. Effect of Nucleon Number Parity on the Magnitude of Radiative Capture Cross Sections

The capture cross sections of even-odd and odd-even nuclei at 25 keV neutron energy have been analyzed in order to investigate the parity effects. It does not seem that there is any definite indication that even-odd cross sections are systematically higher than neighbouring odd-even values, as suggested by Belanova and Kazachkovskii.

For details, see Ref. (4).

7.5. A Rotational Optical Model Analysis of Fast Neutron Scattering by ^{232}Th Nucleus

In order to see the effects of the nuclear deformation, some calculations have been performed by means of a rotational optical model which was used successfully in the analysis of fast neutron scattering by ^{238}U. A very good agreement was found for angular distribution between 0.57 MeV and 15 MeV as well as for the total scattering cross section. This seems to support the faxt that, for strongly deformed nuclei, the direct coupling between the incident particle motion and the nuclear surface rotation cannot be neglected in the analysis of the experimental data.

For details, see Ref. (5).

7.6. Scattering of Neutrons by Nonspherical Nuclei

It is well known that the spherical optical model has been found quite inappropriate to the analysis of strongly deformated nuclei. On the other hand, recent calculations have been successful in predicting the observed angular distributions for neutron scattering by deformed even-even nuclei, assuming a nonspherical potential.

However, to develop such an assumption for odd A as well as for even A nuclei is, in general, very difficult. The problem is greatly simplified if the so-called "adiabatic

approximation" can be considered a satisfactory one. Using this approximation some calculations were developed for ^{181}Ta and ^{165}Ho. A good agreement was found with the results obtained by Barret on the basis of an exact solution of the Schrödinger equation.

For details, see Ref. (6).

References

(1) F.G. Perey and A.M. Saruis - Nuclear Physics, 70, 225 (1965).
(2) G. Pisent and A.M. Saruis - Work partially carried out under Contract Euratom-CNEN-INFN (INFN/BE-65/8 - 1965).
(3) V. Benzi and M.V. Bortolani - Il Nuovo Cimento, Serie X, 38, 216-233 (1965).
(4) Journal of Nuclear Energy, P arts A/B, 19, 364-367 (1965).
(5) B. Baldoni and V. Benzi - Paper presented at International Conference on the Study of Nuclear Structure with Neutrons (Antwerp, Belgium, July 19 to 23, 1965).
(6) N. Janeva and L. Zuffi - Paper presented at International Conference on the Study of Nuclear Structure with Neutrons (Antwerp, Belgium, July 19 to 23, 1965).

8. LABORATORIO DI FISICA NUCLEARE APPLICATA, CENTRO DI STUDI NUCLEARI DEL C.N.E.N., CASACCIA (ROMA) (ITALY)

In the last year the Nuclear Physics group of "Centro di Studi Nucleari della Casaccia", has been employed in the following activities:

1) Resonant scattering of γ-rays produced by (n,γ) reactions.
2) Elastic and inelastic cross sections for neutrons.
3) Statistical calculations of E1 radiative widths.
4) Studies on odd-odd deformed nuclei.

Let us now shortly describe the progress made in the year.

8.1. Resonant scattering of γ-rays produced by (n,γ) reactions

The aim of this experimental work is the determination of radiative widths for single nuclear levels lying near the treshold for particle emission. Monochromatic beams of γ-rays produced by radiative capture of thermal neutrons have been employed. The description of the experimental arrangement and of the first results obtained by us has been published in two previous papers (1).

In the published works we have determined resonant scattering and resonant absorption cross sections by means of separate measurements. We would like to point out that the "scattering-absorption method" employed for the absorption cross sections introduced large statistical errors. The measurements carried out in the present year are grounded on the determination of "the scattering yield" as a function of the thickness of the scattering target. The experimental data have been analyzed by means of a computer IBM 7040.

Further we have also studied in all cases the angular distribution of scattered γ-rays in order to determine the angular momenta of the resonant levels. These data and the energies of anelastic γ-rays allowed us in some cases to recognize the resonant isotopes in the natural targets. The preliminary results of analysis are shown in table 8.1.

Let us finally point out an interesting feature of resonant scattering. The energy of neutrons capture γ-lines can be changed to some extent (1 ÷ 2 keV) by means of resonant

scattering processes. After a resonant process the energy of the γ-rays is lowered of the nuclear recoil energy depending on the scattering angle. Therefore collimated beams of scattered γ-rays can be employed as very narrow monochromatic sources of variable energies in order to find new resonances. Our experimentated arrangement has been modified in order to apply this technique.

8.2. Elastic and inelastic cross sections for neutrons

In order to satisfy the requests which appeared in some EANDC compilations we have set up an apparatus for measurement of cross sections in the energy range 2.7 ÷ 3.4 MeV [2]. The neutron source was a Van de Graaff accelerator. In the measurements spherical scatterers were employed. The scattered neutrons were detected by an ORTEC Neutron Sandwich Spectrometer.

The first measurement has been performed on ^{24}Mg and ^{28}Si with the following preliminary results:

	σ_{el}	σ_{in}
$^{24}_{12}Mg$	1.67 ± 0.18	0.594 ± 0.064
$^{28}_{14}Si$	2.14 ± 0.10	0.458 ± 0.020

8.3. Statistical calculations of E1 radiative widths

Following a recent suggestion by Axel we have applied the principle of detailed balance to the study of radiative widths of nuclear levels in the range 5 ÷ 9 MeV. We have thus been able to connect the probabilities for γ-decay to the ground state with the E1 absorption cross sections, which are described by the well known "giant resonance formula".

It is also possible to evaluate total radiative widths by introducing statistical hypothesis for the level density. We have analysed different experimental results arising both from (n,γ) and (γ,γ) reactions. Our approach reproduces the average of experimental data over intervals of 1 ÷ 2 MeV. The existence of an average theoretical curve allowed a more precise discussion of the fluctuations recently found by Axel [3].

In fig. 8.1. our statistical calculations are compared with

the elastic scattering cross sections of γ rays on Sn natural targets.

8.4. Studies on odd-odd deformed nuclei

The experimental investigation of ^{182}Ta is now over [4]. Our data have been analysed together with already existing ones, with the aim of obtaining a complete scheme of the low lying levels (fig. 8.2. - 8.3.). The data have been compared with the predictions of a theoretical model previously developed by us [5]. The effects of the residual n,p interaction have been calculated by means of Nilsson wave functions. A complete analysis of all data available on odd-odd deformed nuclei is now in progress.

References

(1) M. Giannini, P. Oliva, D. Prosperi, S. Sciuti - Nuovo Cimento, X, 34, 1116 (1964) - Nucl. Phys. 65, 344, (1965).
(2) F. Demanins, V. Rado, F. Vinci - (to be published).
(3) P. Axel, K. Min, N. Stein, D.C. Sutton - Phys. Rev. Letters 10, 299 (1963).
(4) P. Nunberg, D. Prosperi - (to be published)
(5) P. Nunberg, D. Prosperi - Nuovo Cimento B 40, 318 (1965).

TABLE 8.1.

Scatterer	Energy (MeV)	$\bar{\sigma}_{scatt.}$ (b)	$\bar{\sigma}_{abs}$ (b)	Γ_{γ} (eV)	$\Gamma_{\gamma o}$ (eV)	σ (eV)
Bi^{209}	7.00	1.47 ± 0.07	3.8 ± 1.3	0.63 ± 0.31	0.53 ± 0.18	3.2 ± 0.5
Pb^{208}	7.28	5.62 ± 0.15	17.5 ± 1.5	1.2 ± 0.2	0.86 ± 0.06	5.0 ± 0.5
Pb^{208}	6.98	1.29 ± 0.06	22.1 ± 2.7	~ 3.5	0.95 ± 0.10	10 ± 1
Sn^{120}	7.01	4.0 ± 0.1	$\lesssim$ 5.3	~ 0.20	~ 0.08	4.0 ± 0.7
Cd^{114}	7.64	0.287 ± 0.006	4.1 ± 1.8	1.6 ± 0.5	0.22 ± 0.05	$\lesssim$ 1
Cu^{65}	8.50	$(34 \pm 1) \cdot 10^{-3}$	0.66 ± 0.08	2.9 ± 0.5	0.26 ± 0.03	8.8 ± 0.3
Cu^{65}	6.07	.31 ± 0.02	2.0 ± 0.4	1.16 ± 0.36	0.39 ± 0.08	7.5 ± 0.4
Ni^{62}	7.64	0.375 ± 0.006	4.4 ± 2.6	3.0 ± 1.5	0.63 ± 0.17	12.5 ± 0.5

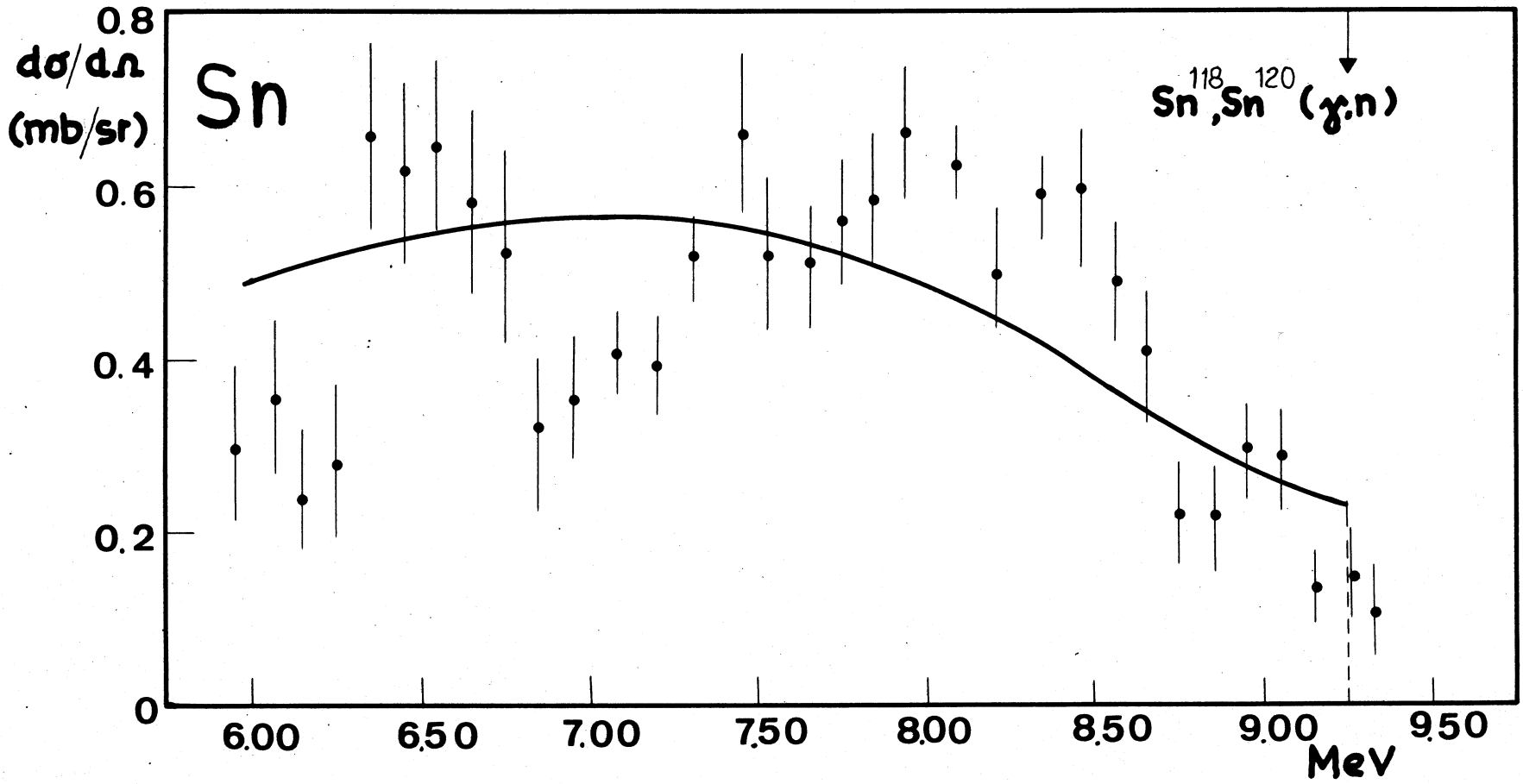
0.8
dσ/dΩ
(mb/sr)
Sn
0.6
0.4
0.2
0
6.00
6.50
7.00
7.50
8.00
8.50
9.00
9.50
MeV
Sn118,Sn120 (γ,n)

Fig. 8.1.

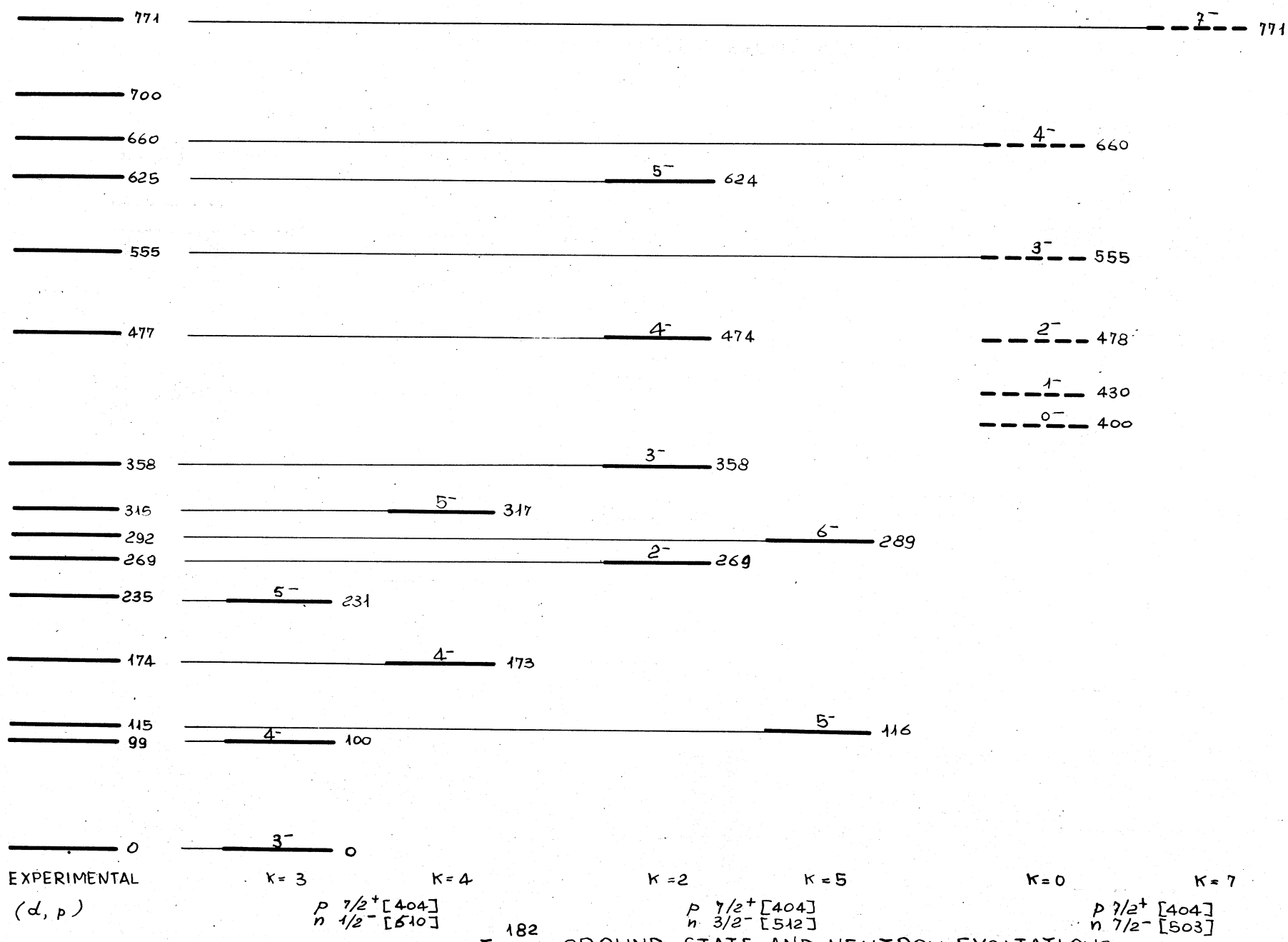

Fig. 8.2. Ta^{182} GROUND STATE AND NEUTRON EXCITATIONS

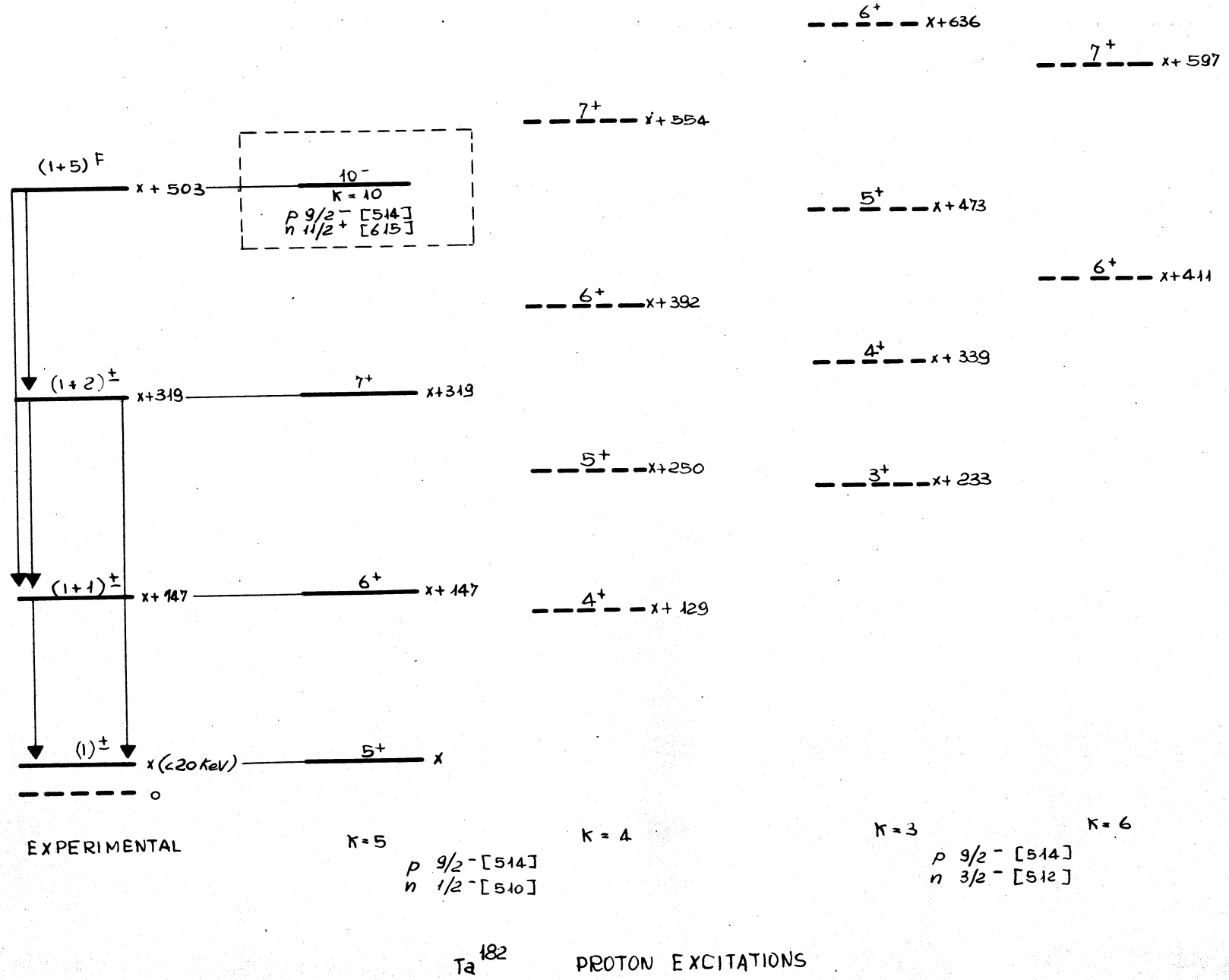

Ta^{182} PROTON EXCITATIONS

Fig. 8.3.

9. ISTITUTO NAZIONALE DI FISICA NUCLEARE, GRUPPO ACCELERATORE DELLA SEZIONE DI TORINO, TORINO (ITALY)

9.1. Scattering of 14.2 MeV neutrons on light and medium nuclei

The scattering of neutrons with energy of 14.2 MeV on light and medium nuclei, has been continued in 1965. The adopted technique is that of time of flight with alpha particle associated. The time resolution of the spectrometer is 1.6 nsec (F W H M), corresponding to an energy resolution of 4% for neutrons of 14.2 MeV and with a flight length of 4 m.

First of all the scattering on ^{27}Al has been examined. Angular distributions of the neutrons scattered elastically and inelastically from the levels at 0.84 MeV; 1.01 MeV; 2.21 MeV; 2.73 MeV; 3.00 MeV ; 4.5 MeV, have been measured. Measurements have been made for angles between 25° and 90° at intervals of about 10°. Neutron peaks due to the levels at 0.84 MeV and 1.01 MeV in the spectra obtained, are not resolved. It is also difficult to ascribe the peak at 4.5 MeV to some known levels of the ^{27}Al.

Measured cross sections have been normalized to the known cross sections of C. Data have not been corrected for multiple scattering and angular resolution. Results are given in table 9.1.

Table 9.1.: Cross sections of ^{27}Al

(C.M)	dσ/dΩ (mb/sr) Q=0	dσ/dΩ (mb/sr) Q=-0.84 -1.01 MeV	dσ/dΩ (mb/sr) Q=-2.21 MeV	dσ/dΩ (mb/sr) Q=-2.73 MeV	dσ/dΩ (mb/sr) Q=-3.00 MeV	dσ/dΩ (mb/sr) Q=-4.5 MeV
26°	290±29	4.4±1.3	7.7±1.7	0.8±0.6	7.7±1.9	2.7±0.7
39°	18±2	4.8±0.3	4.4±1.0	2.3±1.8	5.5±1.3	1.8±0.4
47°	31±3	3.1±0.5	5.6±1.4	0.6±0.5	2.9±0.6	2.7±0.5
57°	63±1	3.9±0.8	4.5±0.8	1.4±1.1	5.0±1.5	1.6±0.9
68°	40±2	2.2±0.7	2.8±1.0	0.6±0.4	1.7±0.5	1.3±0.5
76°30'	25±4	1.4±0.5	1.3±0.5	0.4±0.3	2.0±0.7	1.6±0.2
89°30'	15±2	1.9±0.7	2.3±0.8	0.7±0.5	1.7±0.6	1.4±0.3

The nucleus ^{19}F has been also examined. In order to overcome the difficulties due to the particular nature of this nucleus, a target of Teflon (F_{2n} C_n) has been used. The measurements have

been made alternatively on a target of Teflon and on a target of Carbon in order to subtract the contribution due to the Carbon. Targets mentioned have been used in order to have the same number of neutrons scattered by ^{12}C.

Measurements have been performed for angles between 30° and 140°, at intervals of about 10°. The spectrum of ^{19}F shows inelastic neutron peaks at energies of 1.5 MeV, 2.8 MeV, 4.7 MeV and 5.5 MeV. Among these peaks, only that at 2.8 MeV is due to the excitation of an unique level of the ^{19}F, whereas the others are due to many known levels of the ^{19}F.

The elastic cross section, too, is contamined by the contribution of the two first levels at 0.11 MeV and 0.198 MeV. It is impossible to resolve this contribution with the present experimental techniques.

Measured cross sections have been normalized to the known cross sections on H; the data have not been corrected for multiple scattering and angular resolution.
Measured cross sections are given in table 9.2.

Table 9.2.: Cross sections of ^{19}F

(C.M)	$d\sigma/d\Omega$ (mb/sr) Q=0	$d\sigma/d\Omega$ (mb/sr) Q=-1.5 MeV	$d\sigma/d\Omega$ (mb/sr) Q=-2.8 MeV	$d\sigma/d\Omega$ (mb/sr) Q=-4.7 MeV	$d\sigma/d\Omega$ (mb/sr) Q=-5.5 MeV
27°	210±23	14.0±1.5	3.9±0.4	4.0±2.8	10.6±2.5
40°	70±3	12.3±0.9	3.6±0.9	7.6±2.2	10.1±2.2
51°30'	53±2	9.0±0.6	3.5±0.6	4.2±1.1	10.6±2.7
63°	70±2	10.2±0.8	2.5±0.5	5.4±1.3	8.7±1.9
73°	71±2	9.0±1.2	2.7±0.8	5.6±1.4	10.0±2.2
83°	52±2	5.6±0.9	2.8±0.5	2.9±0.6	7.1±2.0
92°	30±3	6.4±0.8	2.1±0.4	2.6±0.7	7.6±1.9
101°30'	18±3.6				
110°30'	15±1.5	4.4±0.8	1.2±0.6	3.0±1.1	4.0±1.5
126°	7±0.8	7.0±0.8		6.7±1.9	7.0±1.7
136°	12±0.7	4.3±1.6	1.2±1.0	4.9±1.5	7.7±1.3

Measurements on Cl (natural isotopic composition) are on the way. The experiment is performed in the same way as for ^{19}F, using a target of CCl_4. Preliminary data are under examination.

Publications

Evidence for Core Excitation in ^{27}Al - G.C. Bonazzola, E. Chiavassa, T. Bressani - Nuovo Cimento 38, 1444 (1965).

Excited Core Model in ^{27}Al and Inelastic Scattering of 14.2 Neutrons - G.C. Bonazzola, E. Chiavassa, T. Bressani - Physical Review 140, B835 (1965).

Excitation of a 4.5 MeV in ^{27}Al by Inelastic Scattering of 14 MeV neutrons - G.C. Bonazzola, E. Chiavassa, T. Bressani - Nuovo Cimento (in press).

Diffusione di Neutroni di 14.2 MeV sul ^{19}F - (presented at "LI° Congresso Nazionale della Società Italiana di Fisica") Bollettino della S.I.F. 46, 12 (1965).

10. CENTRO DI INFORMAZIONI STUDI ESPERIENZE (CISE), SEGRATE (MILANO) (ITALY)

10.1. Measurements of (d,p) and (d,α) reactions on ^{27}Al and ^{25}Mg

These measurements are performed at deuteron energies between 1.5 and 3 MeV at intervals of 10 keV with an energy resolution of 3 keV. Protons and alpha particles, in correspondence of some well identified levels of the final nucleon, are detected. Measurements are performed at several angles between 0° and 180°.

As it is well known, cross sections corresponding to the different lines of emission exhibit strong fluctuations. The analysis of these fluctuations gives information on the properties of the compound nucleus. In particular, the average lives of the excited nuclei can be studied in this way.

10.2. Analysis of the parameters of the nuclear level densities

A large analysis of the statistical parameters of the nuclear levels densities is on the way. Th ese parameters are obtained from the analysis of the emission spectra, fission of nuclei in the region Bi-Cf as well as from the analysis of the widths of compound nucleus.

In 1966 a table containing the parameters obtained, will be completed. It is well known that the density of the nuclear levels is very important in the calculation of statistical reactions cross sections.

11. CENTRO SICILIANO DI FISICA NUCLEARE, ISTITUTO NAZIONALE DI FISICA NUCLEARE, SEZIONE SICILIANA - ISTITUTO DI FISICA DELL'UNIVERSITA', CATANIA (ITALY)

11.1 Experimental research work on nuclear structure and reactions

11.1.1. Nuclear Fission

We are studying by means of nuclear emulsion, the angular distributions of fission fragments of Th produced by monoenergetic neutrons in the energy range 1.8 ÷ 5.2 MeV. Preliminary results show that the experimental angular distributions are forward peaked and can be fitted by polynomials like $N(\varphi) = \Sigma A_m \cos^{2m} \varphi$. The anisotropy varies with neutron energy and shows a maximum ($R = 1.5 \pm 0.02$) at $E_n \approx 2.4$ MeV [1].

11.1.2. (n,α) Reactions

To study (n,α) reactions with negative Q values by determining the spectra and angular distributions of emitted particles, a counter telescope was realized. It was made up by a silicon junction detector and a gas scintillation counter. Preliminary measurements of the α-particle spectra from the $^{40}Ca(n,\alpha)^{37}A$ and $^{19}F(n,\alpha)^{16}N$ reactions gave satisfactory results [2].

11.1.3. Angular Correlations of the $^{19}F(d,p\gamma)^{20}F$ Reaction [3]

Angular correlation measurements are in progress on the first excited level of the ^{20}F trough the reaction $^{19}F(d,p\gamma)^{20}F$ with a deuteron energy $E_d = 1.6$ MeV. The coincidences between the protons and the related γ-rays are measured by a fast-slow coincidence circuit with $\tau = 35$ ns. The protons are detected by a solid state counter and the γ-rays by a NaI(Tl) scintillation counter 7.5 cm x 7.5 cm.

The data collected till now give the correlation function (p,γ) on the reaction plane for a proton emission angle $\varphi_p = 45°$. Further measurements will be done on the planes ortogonal to the reaction plane and for other proton emission angles.

11.1.4. Resonant Absorption of γ -Rays

Preliminary experiments were performed on resonant absorption of γ-rays produced in (p,γ_o) reactions. The experimental arrangement gave a geometrical resolution width of 400 eV for the γ-rays of 10.786 MeV from the $^{31}P(p,\gamma_o)^{32}S$ reaction. The first results concern the transmission curve of an ^{32}S sample, 37 cm thick, for these γ-rays.

11.1.5. ^{7}Li+d Reactions

An extensive study was performed on the ^{7}Li+d reactions at E_d = 0.8 and 1 MeV. The spectra and angular distribution of the neutrons from $^7Li(d,n)^8Be$ reaction and of the α-particles from the $^7Li(d,\alpha)^5He$ reaction were measured. Furthermore the angular correlation between the α-particles and the bidimensional α-spectra were investigated.

The experimental results on the angular correlation are well fitted assuming $N(\theta) \sim 1+(3\pm0.3)\sin^2\theta$ for the α-particles distribution around the ^{5}He momentum in the system in which this nucleus is at rest. The bidimensional α-spectra do not give evidence of three body breakup. The transitions to the ground state of the ^{5}He nucleus seem to contribute for about 60% to the spectra of the α-particles with energy higher than 2 MeV [4,5].

11.2. Theoretical research work on nuclear structure and reactions

A method has been proposed for the determination of the effective neutron-proton interaction from angular distributions of (n,p) reactions on closed shell nuclei, using the DW Born approximation [6,7].

An extension of the shell model has been studied [8], allowing the treatment of elastic and inelastic scattering amplitudes and taking into account particle-hole residual interactions. The effects of the extension on the energy spectrum of particle-hole excitations have been found to be reasonably small. Calculations are in progress to determinate the electromagnetic form factors and the neutron s and p wave strength functions.

A new approach has been proposed to the problem of taking into account nucleon correlations in the ground state of closed shell nuclei, both in spectroscopic calculations and in the evaluation of transition amplitudes [9].

References

(1) S. Lo Nigro, C. Milone - Comm. at the S.I.F. Annual Meeting - Bologna 1965.
(2) R. Potenza - Comm. at the EURATOM Annual Meeting - Milano 1965.
(3) G. Calvi, S. Cavallaro, A.S. Figuera, M. Sandoli - Comm. at the S.I.F. Annual Meeting - Bologna 1965.
(4) R. Potenza - Seminar at the XXXVI Course of the Intern. School of Physics "E. Fermi" - Varenna 1965 - to be published.
(5) C. Milone, R. Potenza - The ^{7}Li+d reactions - Submitted to Nuclear Physics.
(6) G. Schiffrer - Physics Letters 17, 122 (1965).
(7) G. Schiffrer - Seminar at the Intern. School of Physics "E. Fermi" - Varenna 1965 - to be published.
(8) A. Agodi, F. Catara, M. Di Toro - Comm. at the S.I.F. Annual Meeting - Bologna 1965.
(9) A. Agodi - Seminar at the Intern. School of Physics "E. Fermi" - Varenna 1965 - to be published, Comm. at the S.I.F. Annual Meeting - Bologna 1965.

12. GRUPPO DI RICERCA DEL CONTRATTO EURATOM-CNEN-INFN DELL' UNIVERSITA', MILANO (ITALY)

The Euratom-CNEN-INFN group of the University of Milan has pursued a research program in the interaction of fast neutrons with several nuclei. The 14 MeV neutron source in dotation to the group has been used for this work. The research has been centered on (n,d) pick-up reactions and (n,p) reactions on nuclei in the 2 p 3/2 proton shell.

12.1. The (n,d) reaction on ^{63}Cu and ^{65}Cu

The (n,d) pick-up reaction may give interesting information about the level structure and single-particle strength of the residual nuclei levels. The same information can be obtained through the study of other pick-up reactions such as $(d,{}^3He)$[1-3], but in the latter case the theoretical interpretation is a little more complex because of the absolute normalization factor deriving from the internal wave function of ^3He.

Recently considerable theoretical interest is being directed to the ^{63}Cu[4-6] and ^{62}Ni[7,8] isotopes. These nuclei can be described in terms of a core excitation model in which the first four excited states in ^{63}Cu are the result of the coupling of a proton in a $p_{\frac{1}{2}}$, $p_{3/2}$ or $f_{3/2}$ state to the one-phonon 2^+ excited state of ^{62}Ni. Also the many-particle shell model is in some cases used for the interpretation of experimental results involving these nuclei [9].

The deuterons emitted by the interaction of 14.08 MeV neutrons on the target nuclei were detected by means of a dE/dx and E counter telescope. The dE/dx and E counters were two solid state silicon detectors respectively 80 μm and 1800 μm thick. Additional coincidences with proportional gas counters were required to lower the background. The ^{63}Cu and ^{65}Cu target were 15.65 and 10.56 mg/cm^2 thick; their thickness determines the overall energy resolution of the system, which is however adequate to resolve the ground and first excited state of residual nuclei. The angular acceptance of the counter varies between 11° and 14° FWHM (full width half maximum).

The angular distribution of the deuterons to the ground and the 2^+ first excited state in ^{62}Ni are shown in fig. 12.1. and 12.2. The angular distribution to the ground state has been analysed in terms of DWBA[10] assuming a single-particle pick-up mechanism and has been fitted, as seen from fig. 12.1., with an $l = 1$ momentum transfer. The optical model parameters used are given in table 12.1. This fit is in agreement with the core excitation model which predicts that the transition is a pure $p_{3/2}$ pick-up. If the ^{62}Ni nucleus could be described in terms of a closed $f_{3/2}$ proton shell, one would have from the same model that the f component (in this case $f_{3/2}$) in the transition to the first excited state of ^{62}Ni is negligible. The model also predicts that the ratio of the intensity of the first excited state to that of the ground state should be about 0.11.

In fig. 12.2. the angular distribution to the 1.172 MeV first excited level of ^{62}Ni is compared with two DWBA curves: the full curve corresponds to a $l = 1$ over $l = 3$ ratio given by the core excitation model, the dashed one to a ratio set equal to 0.5. Although the present data do not permit to assess precisely the amount of $l = 3$ present, it seems clear that in order to obtain a fit to the angular distribution a larger amount than predicted is required. The ratio of the cross section of this transition to that of the ground state is about 0.26. This ratio and the strong $l = 3$ component in the transition to the 1.172 MeV excited state can be explained with the hypothesis by Blair[9] that the $f_{3/2}$ proton shell is partially empty in the ^{62}Ni nucleus. Also other possible ways to explain this disagreement exist[3,11].

From our analysis in terms of DWBA it is possible to obtain some information on the single-particle strengths in the ^{62}Ni levels. Since the $p_{\frac{1}{2}}$ strength is in our case negligible, we can attribute all the $l = 1$ component to $p_{3/2}$ pick-up. Although the amount of $l = 3$ present in the first excited state cannot be assessed precisely on the basis of our experimental data, as said before, a calculation shows that the ensuing error on the distribution of the $p_{3/2}$ single-particle strength is negligible. On this basis we obtain

that the $p_{3/2}$ single-particle strength in the first excited state is 0.40 ± 0.05 of that present in the ground state instead of the predicted value of 0.17. If the calculated single-particle strengths are taken into account, that is if we consider that a part of the $p_{3/2}$ strength is found in the first excited level, the absolute value of the DWBA should be multiplied by a factor of about 1.4 to obtain an agreement with the experimental data. Of course this number depends very much on the optical model parameters used. It should be noted that we have neglected any $p_{3/2}$ strength in higher excited states which, however, seems to be rather small [3].

The angular distribution of the deuterons from the reaction $^{65}Cu(n,d)^{64}Ni$ to the ground state of ^{64}Ni (fig. 12.3.) is very similar to that to the ground state of ^{62}Ni. The reduced width is, within 10 %, the same as in ^{63}Cu, indicating that ^{63}Cu and ^{65}Cu have similar ground-state wave functions.

12.2. The (n,d) reaction on Zn^{64}

The reaction $Zn^{64}(n,d)Cu^{63}$ involves, as residual, the same nucleus, ^{63}Cu, as in the previous measurement. In fig. 12.4. the deuteron spectra taken at 9° and integrated between 6° and 48° are shown. It can be seen that no other levels are strongly excited besides the ground state and therefore one can deduce that the l = 1 single particle strength corresponding to the pick-up of one of the two $p_{3/2}$ protons is concentrated mostly in it.

In fig. 12.5. is shown the angular distribution of the deuterons to the ground state of ^{63}Cu. No pronounced minimum is present; its absence cannot be justified by the presence of an l = 3 component of reasonable intensity using Saxon-Wood volume interaction. A calculation of the compound nucleus evaporation cross section for this case has been done, but it results of too low magnitude to explain the absence of the minimum. Also possible interference effects between the evaporated and the direct part have been considered but again their effects should be of low magnitude. Some efforts have then been done to explain the possibility of fitting the experimental angular distribution by a suitable choice

of the optical model well. For the deuteron interaction both a volume and a surface interaction give similar results. In the neutron case different curves are obtained varying the shape of the well. Using a volume interaction (which gives good results for the elastic scattering) for the deuterons and a surface interaction of the gaussian type for the neutrons a curve calculated for l = 1 gives a good fit, to the angular distribution, as shown in fig. 12.5.

The optical wells required to fit deuteron angular distributions on several nuclei measured by other authors and in the present experiments are given in table 12.1. No unique choice seems possible and furthermore parameters found satisfactory for elastic scattering seem to fail in the case of reactions. This may be due, as already noted in proton inelastic scattering [12], to the fact that in the case of deformed nuclei it is necessary to use deformed wells and channel coupling in order that a surface - and a volume - absorbing potential, which gives similar elastic scattering, should also give good reaction angular distributions.

12.3. The (n,p) reaction on Zn isotopes

In fig. 12.6. are given the (n,p) spectra from the isotopes ^{64}Zn, ^{66}Zn, ^{67}Zn in log scale. The (n,np) thresholds for the different isotopes are indicated. The evaporation model analysis gives values for the parameters a which are in agreement with those calculated from other analysis.

References

(1) J.L. Yntema, T.H. Braid, B. Zeidman and H.W. Broek - Rutherford Jubilee Conference - C 5/17 - Manchester 1961, p. 521.
(2) B. Cujec - Phys. Rev. 128, 2303 (1962).
(3) J.C. Hiebert, E. Newmann and R.H. Bassel - Phys. Letters 15, 160 (1965).
(4) M. Bouten and P. Van Leuven - Nucl. Phys. 32, 499 (1965).
(5) V.K. Thankappan and W.W. True - Phys. Rev. 137, B 793 (1965)
(6) W. Beres - Phys. Letters 16, 65 (1965).
(7) L.S. Kisslinger and R.A. Soerensen - Klg. Dansk. Viedenskab. Selskab Mat. Fys. Medd. 32, 9 (1961).
(8) Giu Do Dang and A. Klein - Phys. Rev. 133, B 257 (1964).

(9) A.G. Blair - Phys. Lett. 9, 37 (1964).
(10) R. Cirelli, P. Gulmanelli and A. Marini - ed. Viscontea - Milano (1963).
(11) S.K. Penny and G.R. Satchler - Nucl. Phys. 53, 145 (1964).
(12) M.P. Fricke, G.R. Satchler - Phys. Rev. 139, B 567 (1965).

Figure Captions

Fig. 1 - Angular distribution of the deuterons to the ground state of ^{62}Ni. The full curve is the result of DWBA with l = 1 and is smeared out according to angular acceptance.

Fig. 2 - Angular distribution of the deuterons to the 1172 MeV 2^+ excited state of ^{62}Ni. The full curve is the result of DWBA with a mixture of l = 1 and l = 3 in the ratio given by the unified model. Dashed curve is the same for a ratio l = 1 to l = 3 equal to 0.5.

Fig. 3 - Angular distribution of the deuterons to the ground state of Ni^{64}. The full curve is the result of DWBA with l = 1 and is smeared out according to angular acceptance.

Fig. 4 - Energy spectra of the deuterons from the reaction Zn^{64} (n,d) Cu^{63} at 9° and integrated between 6° and 48°.

Fig. 5 - Angular distribution of the deuterons to the ground state of Cu^{63}. The theoretical curves shown are calculated with the parameters indicated.

Fig. 6 - Proton spectra from Zn isotopes against the square root of the excitation energy.

Table 12.1.: Optical parameter used in the analysis of (n,d) reactions.

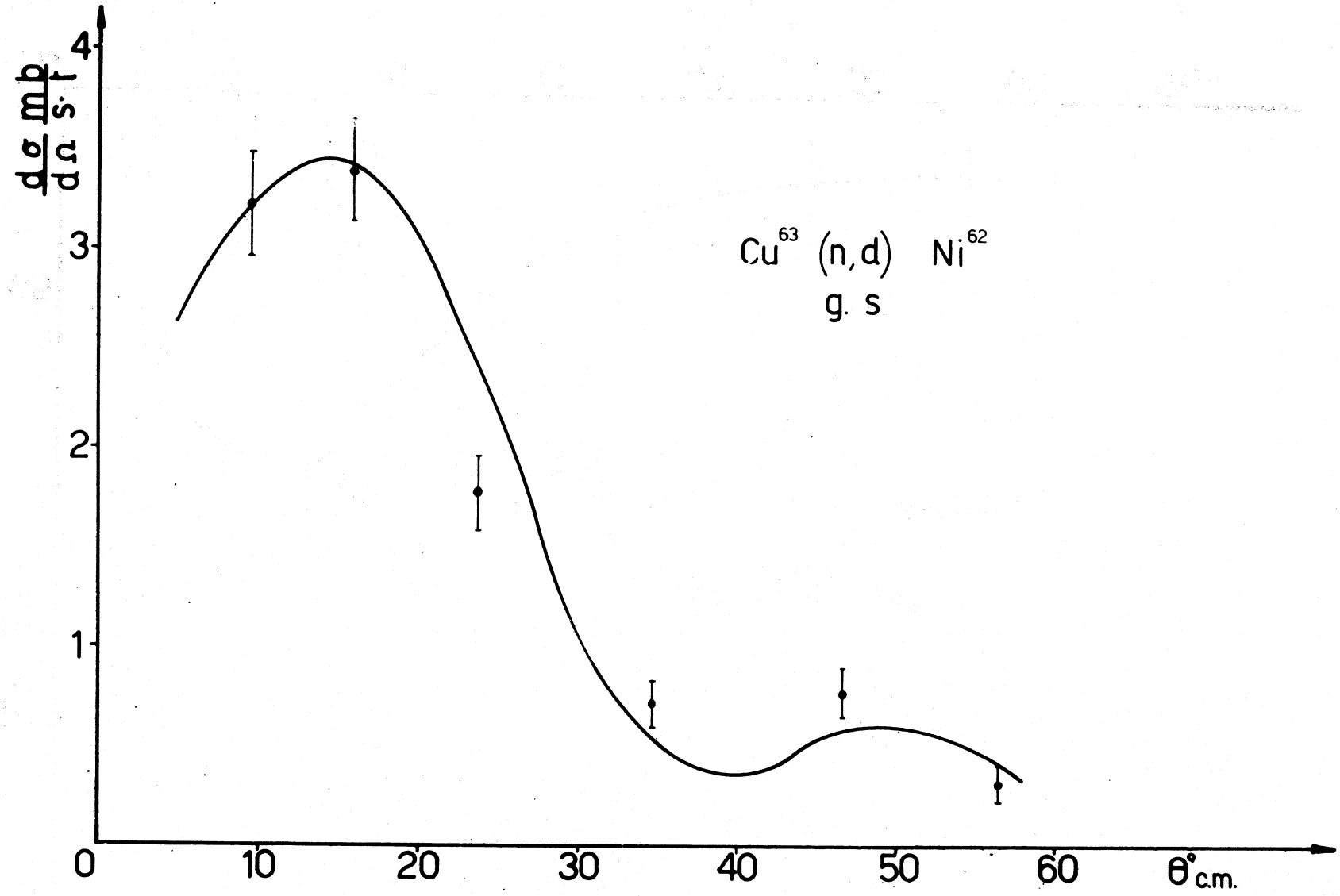
$\frac{d\sigma}{d\Omega}\frac{mb}{sr}$
4
3
2
1
0
10
20
30
40
50
60
$\theta^\circ_{c.m.}$
Cu^{63} (n,d) Ni^{62}
g. s

Fig. 12.1.

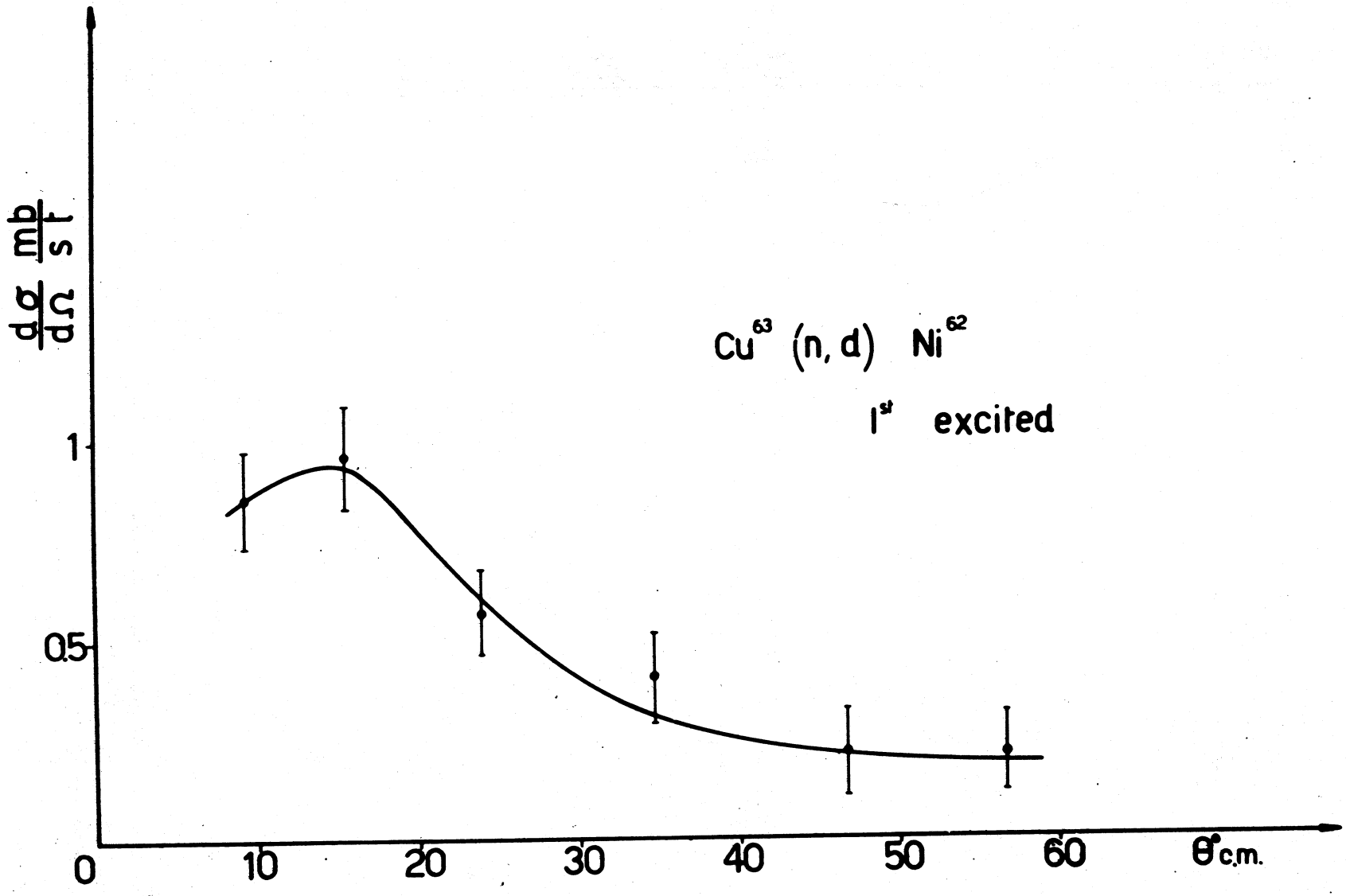
$\frac{d\sigma}{d\Omega}\ \frac{mb}{st}$
Cu^{63} (n, d) Ni^{62}
1st excited
1
0.5
0
10
20
30
40
50
60
$\theta_{c.m.}$

Fig. 12.2.

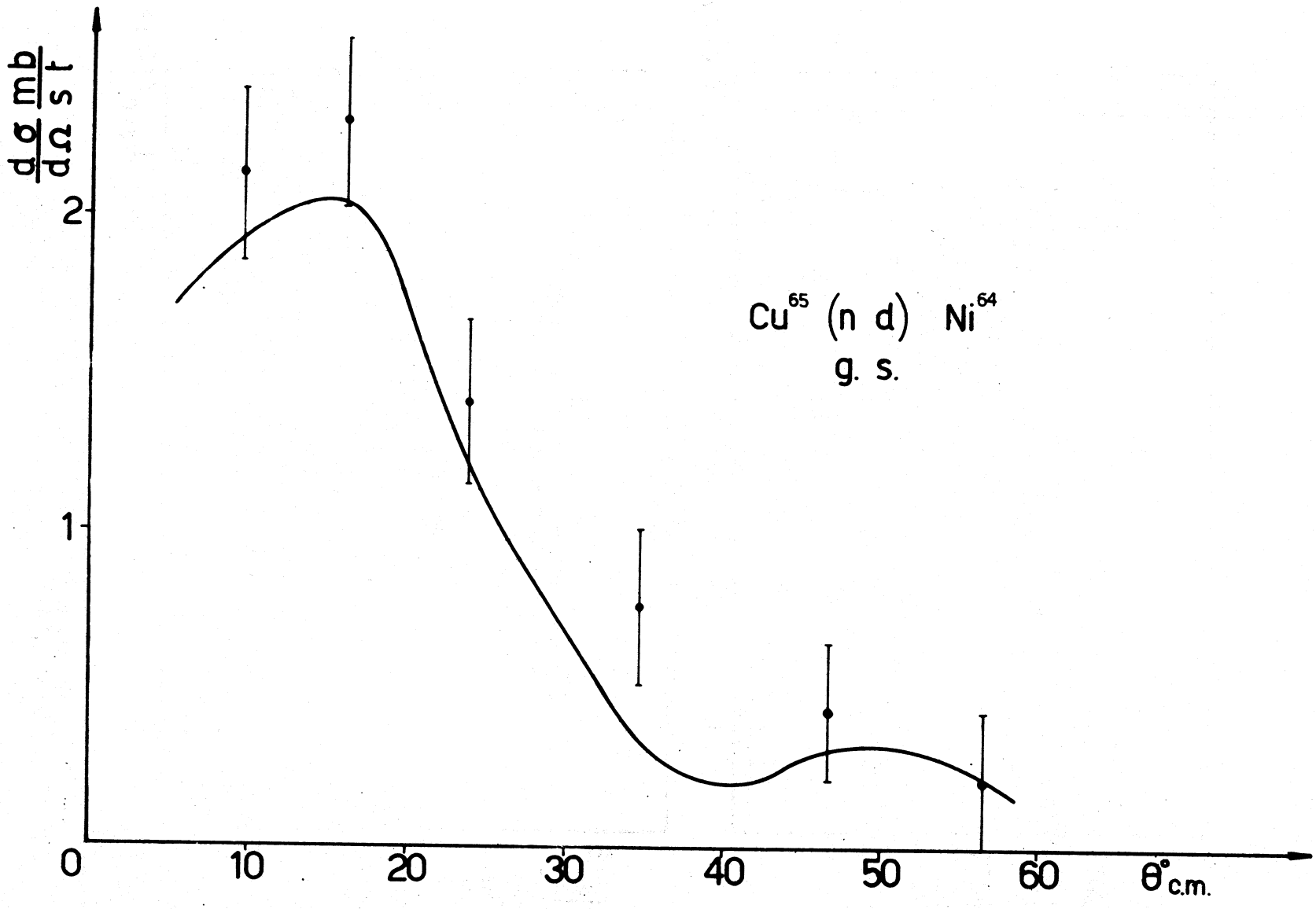
$\frac{d\sigma}{d\Omega}\frac{mb}{st}$
2
1
0
10
20
30
40
50
60
$\theta^\circ_{c.m.}$
Cu^{65} (n d) Ni^{64}
g. s.

Fig. 12.3.

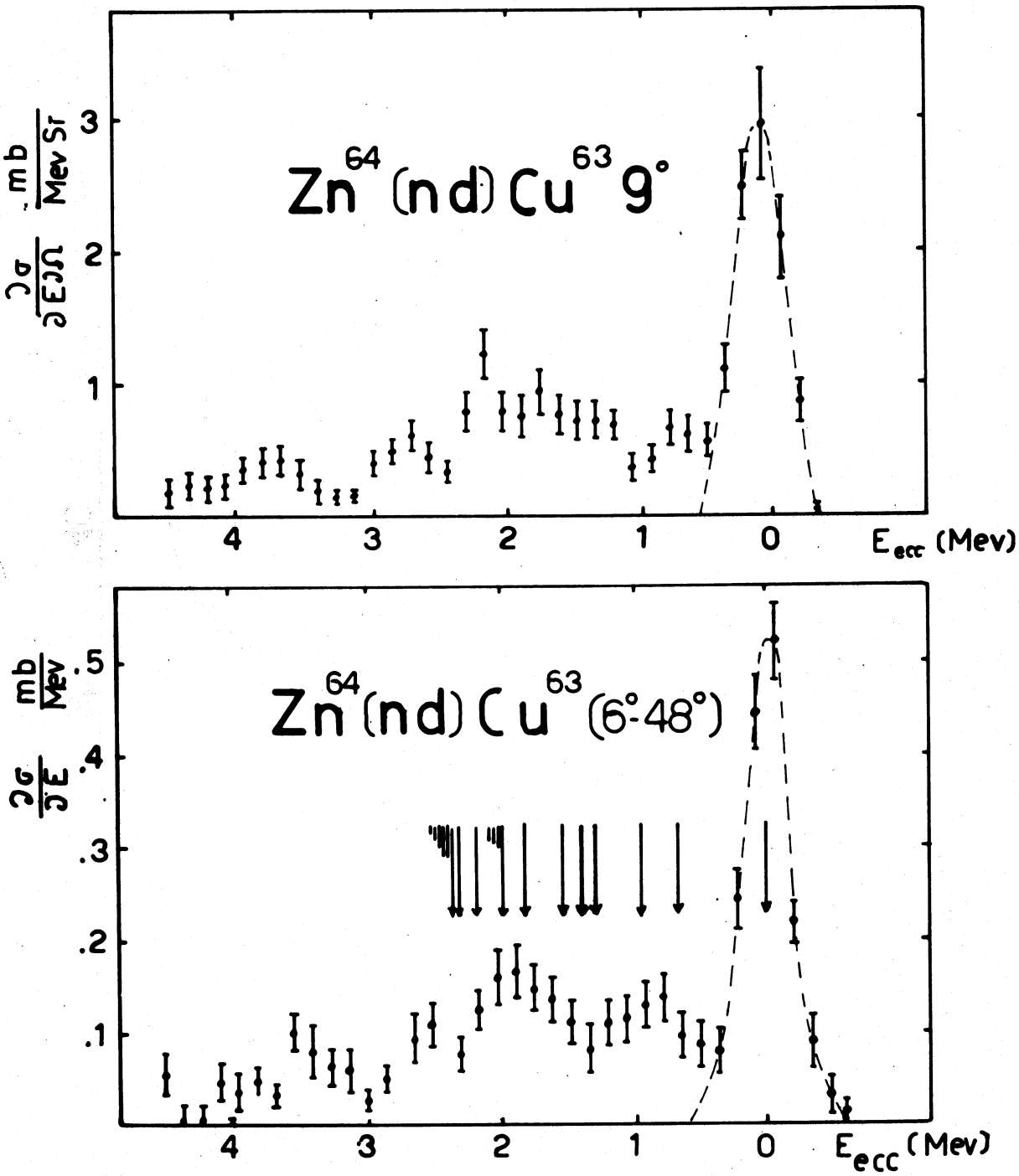
Zn64(nd)Cu63 9°
∂σ/∂EΩ mb/Mev Sr
3
2
1
4
3
2
1
0
Eecc (Mev)
Zn64(nd)Cu63 (6°-48°)
∂σ/∂E mb/Mev
.5
.4
.3
.2
.1
4
3
2
1
0
Eecc (Mev)

Fig. 12.4.

		V	W	r_{0V}	r_{0W}	a_V	a_W	V_{SO}	$R_{coul.}$
d	S-W	60	16	1.50	1.50	0.65	0.65	–	1.3
n	S-W	43	13	1.25	1.25	0.50	0.50	–	–
n	G	31	5.75	1.42	1.42	0.65	0.70	5.5	–

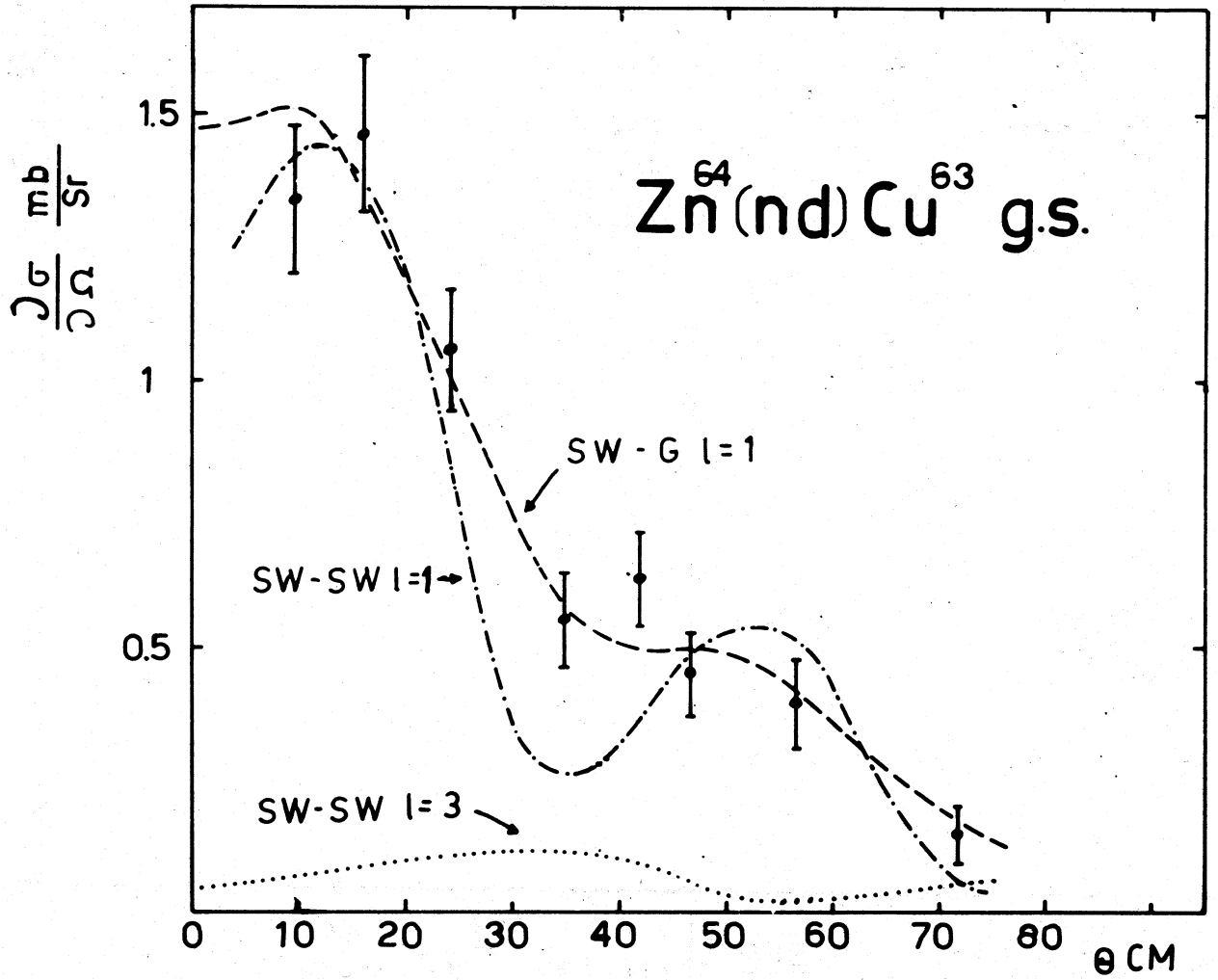

Fig.12.5.

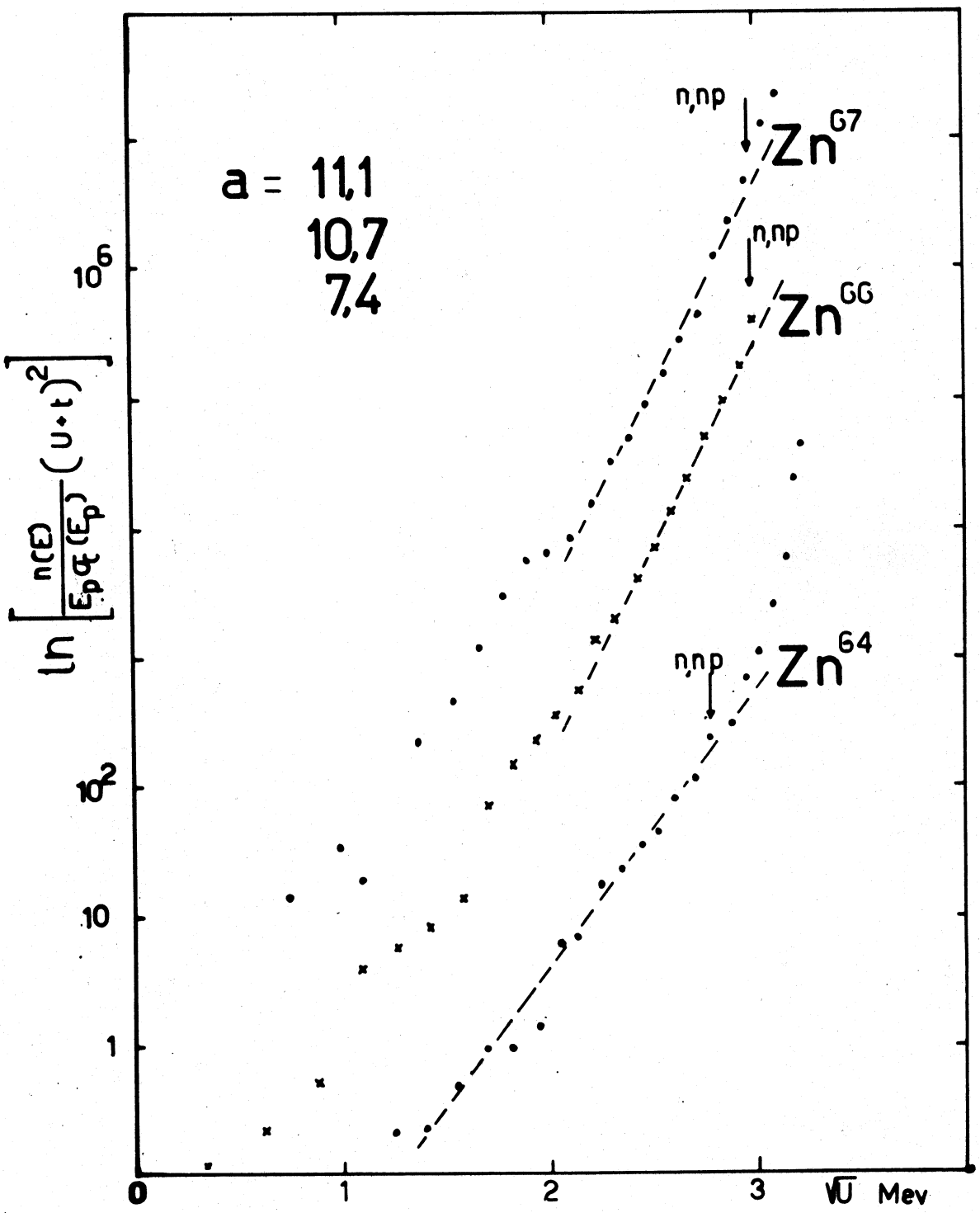
a = 11,1
10,7
7,4
n,np
Zn^{67}
n,np
Zn^{66}
n,np
Zn^{64}
10^6
10^2
10
1
0
1
2
3
$\sqrt{U}$ Mev
$\ln\left[\frac{n(E)}{E_p \sigma_c(E_p)}(U+t)^2\right]$

Fig.12.6.

	TIPO	V	W	V_{so}	r_{ov}	r_{ow}	a_v	a_w	r_c
Ti^{48}	d S	100	17.5	6	1	1.5	0.9	0.6	1.3
	n S	44	9.5	6	1.25	1.25	0.65	0.47	
Fe^{56}	d V	60	20	-	1.5	1.5	0.65	0.65	1.3
	n V	44	10	-	1.25	1.25	0.5	0.5	
V^{51}	d V	55	15	-	1.5	1.5	0.6	0.6	1.3
	n V	44	8.8	-	1.38	1.38	0.36	0.36	
Cu^{63}	d V	60	16	-	1.5	1.5	0.65	0.65	1.3
	n V	43	13	-	1.25	1.25	0.5	0.5	
Zn^{64}	d V	60	16	0	1.5	1.5	0.65	0.65	1.3
	n S	31	5.75	5.5	1.42	1.42	0.65	0.7	

Table 12.1.

13. SOTTOSEZIONE DI FIRENZE DELL'ISTITUTO NAZIONALE DI FISICA NUCLEARE - ISTITUTO DI FISICA DELL' UNIVERSITA', FIRENZE (ITALY)

13.1. $^{28}Si(\gamma,p)$ and $^{28}Si(\gamma,\alpha)$ reactions

Since the last report, the Florence Group has completed the discussion of results on ^{28}Si (γ,p) and $^{28}Si(\gamma,\alpha)$ reactions. Results are published in Nuclear Physics (1). In connection with this work two more studies have been concluded and published: one of technical nature, about the pulse height defect of ^{27}Al and ^{24}Mg ions in a silicon detector (2) and a theoretical study of the effect of the isospin selection rule on the correlation width of Ericson's fluctuations (3).

13.2. $^{20}Ne(n,\alpha)^{17}O$ reactions

In the course of the study of $^{20}Ne(n,\alpha)^{17}O$ reactions with 14 MeV neutron a relatively high number of three prong events have been found. Work is in a progress for interpreting these events. The reaction $^{20}Ne(n,2\alpha)$ ^{13}C seems to fit most of the cases.

13.3. β and γ-spectroscopy

The β and γ-spectroscopy group has completed the construction of a versatile vacuum chamber (4) with facilities for coincidence work in various geometrical arrangements and with the possibility of introducing samples without breaking the vacuum. The effect of backscattering on the efficiency of silicon detectors for β-lines has been studied for the geometries allowed by the above mentioned vacuum chamber and the results are summarized in an INFN internal report (5).

In studying the decay of ^{133}Ba, a Ge detector has been used to determine with better accuracy γ-transition energies in ^{133}Cs and to give an estimate (6) of the relative intensity of the 54 keV transition on which contradictory measurements were reported in the literature. Work is in progress to clarify completely the decay scheme of ^{133}Ba, and the study of decay schemes and production cross sections of ^{143}Sm and ^{164}Ho obtained by (n,2n) processes has been started.

References

(1) P.G. Bizzeti, A.M. Bizzeti Sona, M. Bocciolini, G. Di Caporiacco, T. Fazzini, M. Mando - Ericson fluctuations in the photodisintegration of ^{28}Si, Nuclear Physics 63, 161 (1965).
(2) P.G. Bizzeti, A.M. Bizzeti Sona, G. Di Caporiacco, M. Mando - Pulse height defect for ^{27}Al and ^{24}Mg ions in silicon surface barrier detectors, INFN report TC/64/9, and Nuclear Instruments and Methods 34, 261 (1965).
(3) P.G. Bizzeti - "Cross Section fluctuations in isospin forbidden reactions", Physics Letters 13, 334 (1964).
(4) A. Benvenuti, P. Blasi, P. Maurenzig, P. Sona - A versatile vacuum chamber for semiconductor beta and gamma detectors, INFN report TC/65/12, also Nuclear Instruments and Methods 37, 168 (1965).
(5) A. Benvenuti, P. Blasi, P. Maurenzig, P. Sona - On the backscattering of electrons on silicon detectors, INFN (in press).
(6) A. Benvenuti, P. Blasi, P. Maurenzig, P. Sona - On the gamma spectrum in the decay of ^{133}Ba, INFN report BE-65/2.

14. GRUPPO DI ISPRA PER LE MISURE DI SEZIONI D'URTO DEL C.N.E.N., ISPRA (VARESE) (ITALY)

Fast chopper

14.1. Study of slow neutron resonances in Palladium

Analysis of the data obtained with natural samples has been completed. Parameters of the resonances have been determined up to 63 eV; the spins have been assigned up to 152 eV. A paper on this work has been published in Physics Letters 16, 159 (1965).

Samples of enriched isotopes have been received from Oak Ridge and transmission spectra have been obtained for ^{105}Pd, ^{106}Pd and ^{108}Pd. Preliminary data on the analysis of these samples have been given at the Antwerp Conference (paper n. 72).

14.2. Shape analysis for neutron resonances

A program for the shape analysis of low energy neutron transmission spectra in time-of-flight experiments has been written for the IBM 7090 computer. The experimental transmission is fitted with Breit-Wigner formulae, with interference term between resonant and potential scattering, taking also into account both Doppler and resolution broadenings. New features of this program are:

a) No analytical approximation of the resolution function is made, but its detailed shape is used in order to improve the precision at low energy and extend the range of applicability of the shape analysis to higher energies.

b) The Doppler broadening is made independent of the usual approximation (i.e. to be in the neighbourhood of an isolated resonance) and is applied all over the analysed spectrum.
A CNEN technical report on this work is being published with the title: "Shape analysis program for neutron time-of-flight spectra".

14.3. Interference in the radiative capture in ^{149}Sm

The relative yield of the 7.21 MeV primary gamma transition following neutron capture in ^{149}Sm is measured versus

neutron energy in the range 0.09-2 eV. The partial widths relative to this transition are found to differ strongly for the two lowest resonances at 0.097 and 0.873 eV. Constructive interference is observed between these two resonances, both with spin J=4. However, owing to the very weak intensity of the transition, in these preliminary measurements no quantitative check could be made on the consistency of the results with the hypothesis that the (n,γ_i) reaction may be formally treated as a one-channel process.

15. ISTITUTO DI FISICA DELL'UNIVERSITA', TRIESTE (ITALY)

Neutron spectrum of a ^{241}Am - Be source

Measurements of the neutron spectrum from a ^{241}Am - Be source have been undertaken. The neutron source is a 500 mc source, emitting 1.2 x 10^6 neutrons per sec, obtained from the Radiochemical Center, Amersham.

Two experimental methods have been employed, 1) the activation of threshold detectors and 2) the double crystal or time-of-flight method. In method 1) three reactions have been utilized, i.e., S(n,p), Al (n,p), Al (n,α), and the activation data handled with the known cross section expansion method. Method 2) is sketched in fig. 15.1. Neutrons are elastically scattered by a NE-113 scintillator, mounted on a 56AVP p.m., and the ne utrons scattered at 45° are detected by a NE-102 scintillator, mounted on 58AVP p.m., placed at a known distance from the scatterer. So the t.o.f. of neutrons can be measured. The time resolution of the device for the ^{60}Co gamma radiation turned out to be 1.3 nsec.

Preliminary results of the neutron spectrum measurement performed with the above methods are shown in fig. 15.2. (activation method), and in fig. 15.3. (double crystal method). Further refining work is in progress.

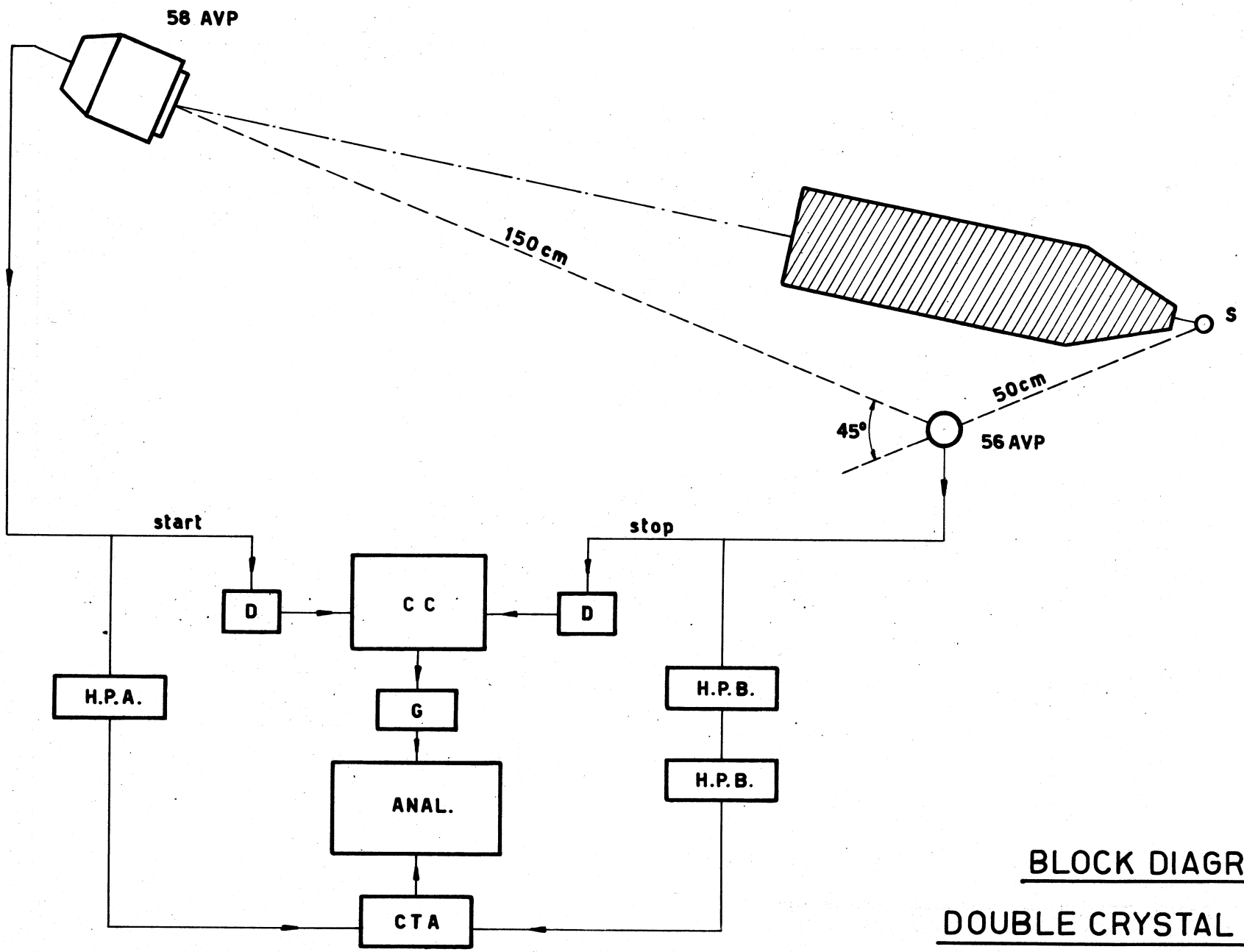

BLOCK DIAGRAM OF THE DOUBLE CRYSTAL SPECTROMETER

Fig.15.1.

NEUTRON SPECTRUM OF THE Am^{241}-Be SOURCE (ACTIVATION METHOD)

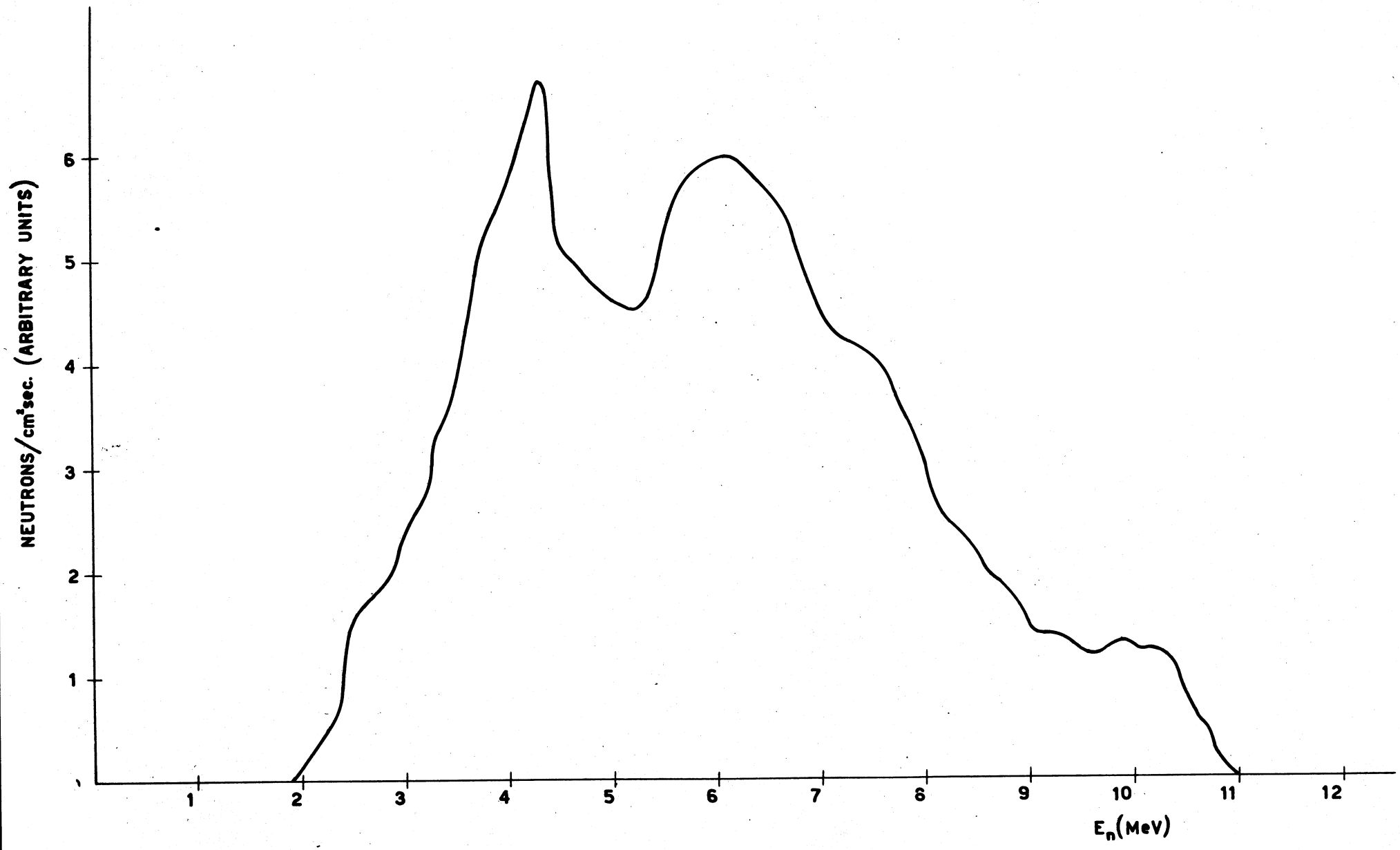

Fig.15.2.

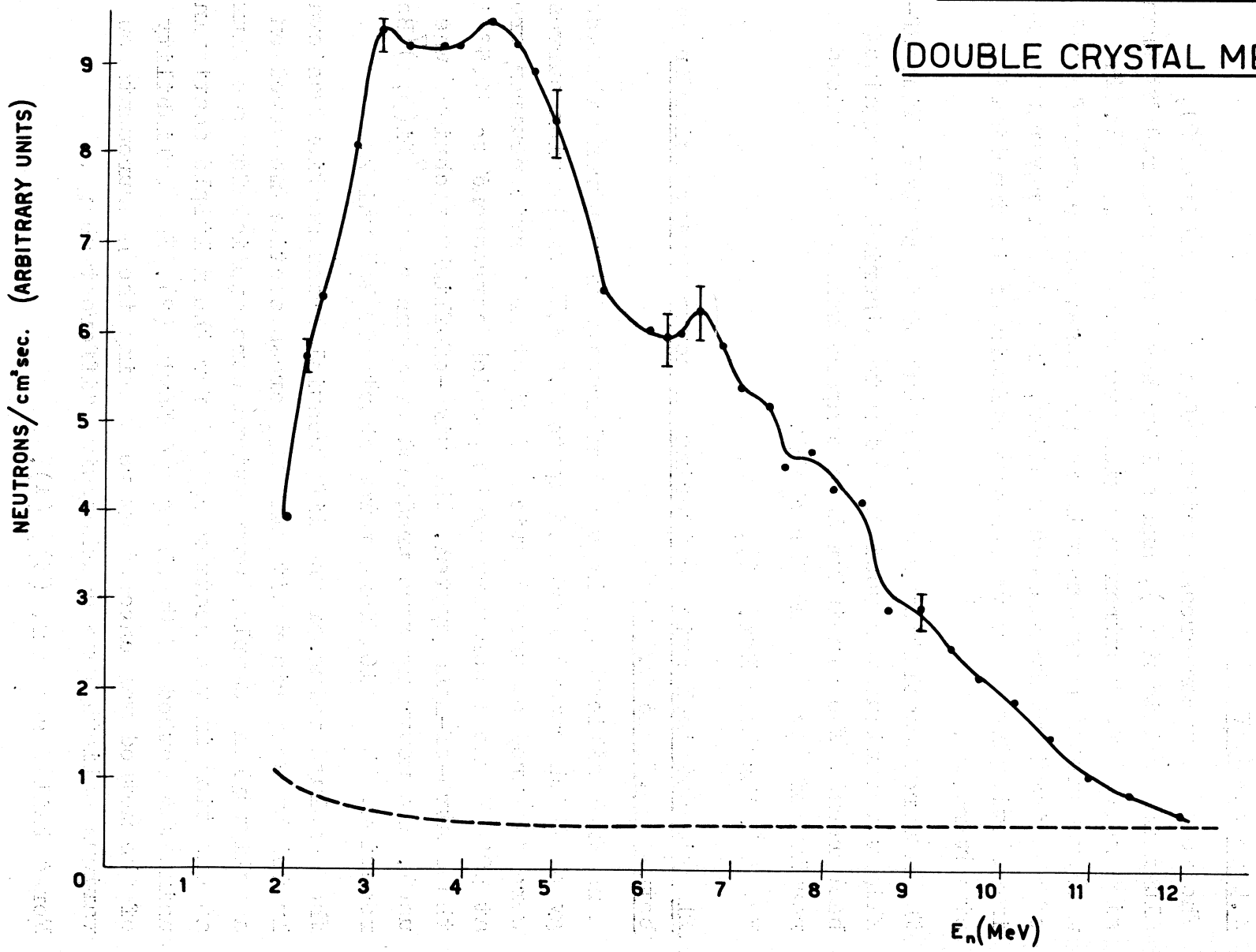
NEUTRON SPECTRUM
OF THE Am^{241}-Be SOURCE
(DOUBLE CRYSTAL METHOD)
NEUTRONS/cm²sec. (ARBITRARY UNITS)
0
1
2
3
4
5
6
7
8
9
1
2
3
4
5
6
7
8
9
10
11
12
E_n(MeV)

16. GRUPPO DI RICERCA DEL CONTRATTO EURATOM-CNEN-INFN - ISTITUTO DI FISICA DELL'UNIVERSITA', PADOVA (ITALY)

16.1. Total neutron cross section of Na, Al, Si, S, and P from 4.5 to 8.5 MeV

The total neutron cross section of natural sodium (2), aluminium, silicon (1), and sulfur has been measured by transmission method for neutron energies from 4.5 to 8.5 MeV. The measurement on phosphorus is in progress. The energy dependence of the total neutron cross section, in this energy range, is interesting in order to observe effects of intermediate structure.

The neutron resolution was from about 30 to 50 keV. Time-of-flight technique was used in order to discriminate against background. The aluminium data compare well with previous results of Carlson and Barschall.

For details, see Ref. (1), (2).

16.2. Elastic and inelastic scattering of neutrons from silicon between 2.3 and 3.8 MeV

A natural silicon sample was bombarded with neutrons the energy of which ranged from 2.3 up to 3.8 MeV. Excitation curves were measured of the elastic and first inelastic neutron group at 50° in the laboratory system, which correspond to 51,5° in the centre-of-mass system. The time-of-flight technique was used. The neutrons were produced by means of the $^{7}Li(p,m)^{7}Be$ reaction. The $^{7}LiO_2$ target was about 100 keV thick.

The absolute value of the differential cross section was evaluated by comparison with the n_{tp} cross section measured on a polietylene sample. Corrections were applied for the flux attenuation in the scatterer, and for the multiple scattering using the method of Cranberg and Levin (2). The reliability of the method was checked by repe ating the measurements on various polietylene samples with different shape.

For details, see Ref. (3), (4).

16.3. The $^{6}Li(^{3}He,n)^{8}B$ reaction

The $^{6}Li(^{3}He,n)^{8}B$ reaction was studied by means of the time-of-flight technique in the energy range of He particles, between 3.4 and 5.5 MeV. The analysis of neutron spectra obtained at various angles between 4.5 and 5.3 MeV showed the existence of one level in the ^{8}B nuclide with (0.67 ± 0.0012) MeV excitation energy, and $Q = -(2.743 \pm 0.012)$ MeV. No other level was observed at excitation energy lower than 1 MeV.

The excitation curve measured between 3.4 and 5.5 MeV increases monotonically. No structures are observed. Three angular distributions taken at 4.3, 5.0, 5.4 MeV, respectively, show that the reaction goes mainly through compound nucleus.

For details, see Ref. (5), (6).

16.4. 2^{+} level excitation in neutron-^{12}C elastic scattering

See Activity Report of "Laboratorio Dati e Calcoli Nucleari-Centro di Calcolo del C.N.E.N. - Bologna.

References

(1) U. Fasoli, D. Toniolo, G. Zago - INFN/BE-65/5, 21/7/65.
(2) F. Fabiani, U. Fasoli, D. Toniolo, G. Zago - INFN/BE-65/9, 20/12/65.
(3) U. Fasoli, D. Toniolo and G. Zago - INFN/BE-65/5, 21/7/65.
(4) Cranberg and Levin - Los Alamos Scientific Lab., LA-2177, 1959.
(5) U. Fasoli, D. Toniolo, G. Zago, Nuovo Cimento 37, 345 (1965).
(6) U. Fasoli, D. Toniolo, G. Zago, International Conference on the study of nuclear structure with neutrons, Antwerp, July 19, 8 (1965).

17. GRUPPO DI RICERCA DEL CONTRATTO EURATOM-CNEN-INFN - ISTITUTO DI FISICA DELL'UNIVERSITA', GENOVA (ITALY)

Light Nuclei Photo Disintegration

17.1. Photoprotons from Mg

Photoprotons from Mg at maximum bremsstrahlung energy 31 MeV have been measured and the results have been compared with particle-hole calculations.
The agreement is rather satisfactory in the lower-energy region of the spectrum, where the structures predicted at Ep = 4.5; 5.5; 6.3; 8.7 MeV are observed in the experiment, but the oscillator strengths appear differently distributed between the resonant levels, than predicted by theory.
There is however no clear evidence of a strong absorption above proton energy 8 MeV, i.e. about 20 MeV of excitation energy in the nucleus; while the calculation predicts two very strong peaks in this interval of energy due to absorption in the k = 1 shell.
The disagreement between the experimental and calculated strengths could be partly explained taking into account the possible transitions to the first excited levels in ^{23}Na.

17.2. Charged photoparticles from Li

The photodisintegration of ^{6}Li has been studied using the 31 MeV bremsstrahlung γ-rays beam of our Betatron. The energy spectra of protons, deuterons and tritons has been measured employing a solid state counter telescope. Triton spectrum shows a large contribution due to the reaction $^{6}Li(\gamma,{}^{3}He)\,{}^{3}H$ (42% of the total number of measured triton events).
From the data the $^{6}Li(\gamma,{}^{3}He)\,{}^{3}H$ cross section, that shows a maximum of 0.5 mb in the energy range between 23 and 26 MeV, has been evaluated.
This value is in disagreement with a peripherical (α,d) model for ^{6}Li. Also the experimental deuteron spectrum seems to disagree with the theoretical spectrum calculated by the periferical model.
These results seem to suggest that a correct calculation should take properly into account appreciable final state interactions between the emitted particles.

17.3. Charged photoparticles from natural lithium

The charged photoparticles from natural lithium were measured using a solid state counter telescope and the bremsstrahlung beam of a 31 MeV Betatron. The ^{7}Li (γ, t) cross section was been directly obtained from the triton spectra.
The most interesting feature of this cross section is the evidence of a large number of sharp resonances corresponding to the ^{7}Li excited levels. A comparison between present results and previously reported measurements exhibits a good agreement. Also the proton spectrum exhibits a complex structure possibly due to ^{7}Li (γ, p) ^{6}He and ^{7}Li (γ, p) ^{6}He reactions.
There is evidence of an high probability of a two-body break up of ^{7}Li also via the reaction ^{7}Li (γ, d) ^{5}He.

17.4. The ^{12}C (γ,n) ^{11}C cross section above giant resonance

The ^{12}C (γ,n) ^{11}C cross section has been measured up to 70 MeV of bremsstrahlung energy. The experiment has been performed revealing in coincidence the β-activity of a liquid scintillator previously exposed to the β^{+}-ray beam of the Synchrotron of the University of Torino.

The Penfold and Leiss analysis of the obtained yields gives a value of the integrated cross section up to 70 MeV of 88$\pm$7 mb MeV in agreement with the classical dipole sum rule; the contribution between 37 and 70 MeV is about 30 mb MeV, i.e. about 34% of the measured integrated (γ,n) cross section.
A wide resonance at about 35 MeV mainly corresponding to $1S^{-1}_{\frac{1}{2}}$ -1 $p_{\frac{1}{2}}$ 1 particle - 1 hole calculated transition has been observed; the strength evaluated as the integrated cross section between 33 and 36 MeV is about 4.1$\pm$1 mb MeV in agreement with (p,γ_o) experiments, well belove the theoretical predictions. There is also some evidence of a wide resonance at 53 MeV.

17.5. Behaviour of positronium in helium

To better understand the behaviour of the positronium formation we selected a very simple material such as helium. We studied the orto-positronium mean life in liquid helium as a function of the density and temperature.

The results are explainable using a model in which we suppose the formation of a bubble around the positronium atom (1) (2).

The same model accounts also for the results in helium gas given by others authors (3).

Measurements in gaseous neon and argon are now in progress to confirm the hypothesis of bubble formation.

Other measurements were also done to study the enhancement of positronium formation in liquid helium due to an applied electric field (4).

The results shows that the lower limit of the Ore's gap in liquid helium is the same as in gaseous helium.

Finally we measured the orto-positronium mean life in solid helium at different densities finding a continuous change of the mean life when going from liquid to solid helium (5).

References

(1) G. Manuzio - Mean life of positronium in liquid helium. Temperature and density effect - to be published in Il Nuovo Cimento.
(2) C.G. Kuper - P.R. 122, 1007.
(3) T. Daniel, R. Stump - P.R. 115, 1599.
(4) G. Manuzio, C. Rizzuto - Effects of an electric field on positronium formation in liquid ^{4}He - to be published in Il Nuovo Cimento.
(5) G. Manuzio, F. Torello - Bollettino della società italiana di fisica 46, 54 (1965).

Publications

G. Manuzio, G. Ricco and M. Sanzone - Photoprotons from Mg - Nuovo Cimento 39, 1057 (1965).

G. Manuzio, R. Malvano, G. Ricco and M. Sanzone - Charged photoparticles from ^{6}Li - Nuovo Cimento, in press.

G. Manuzio, G. Ricco and M. Sanzone - Charged photoparticles from natural lithium - Nuovo Cimento, in press.

N. Fossa, C. Manfredotti and G. Ricco - The ^{12}C (γ,n) ^{11}C cross section above giant resonance - Nuovo Cimento, in press.

18. CENTRE DE PHYSIQUE NUCLEAIRE, UNIVERSITE DE LOUVAIN (BELGIUM)

18.1. Neutron Total Cross Sections between 1 and 6 MeV

G. Deconninck, M. De Vroey

Total cross sections were measured between 1 and 6 MeV neutron energy, using time-of-flight techniques. Typical resolutions ranged from 10 keV (between 1 and 2.5 MeV) to 100 keV (between 2.5 and 6 MeV). The elements studied were Na, K and Ca. Other measurements are underway to search for "doorway states" by means of neutron elastic scattering.

18.2. Pulsed Neutron Research in non-Multiplying Media

G. Deconninck, P. d'Oultremont, M. Stievenart

An experimental and theoretical study of non-multiplying media has been performed; the neutron source was a pulsed Van de Graaff accelerator. The results were presented in:
G. Deconninck, P. d'Oultremont, M. Stievenart, IAEA Symposium on Pulsed Neutron Research, Karlsruhe, May 10-13, 1965.
P. d'Oultremont, Thesis, Université de Louvain (1965).

It is planned to pursue this research activity.

19. LABORATOIRE VAN DE GRAAFF, UNIVERSITE DE LIEGE (BELGIUM)

The essential results obtained in 1965 are found in two contributions to the International Conference on the Study of Nuclear Structure with Neutrons, Antwerp, July 1965.

The abstracts of those contributions are given below.

19.1. Measurement of the Angular Distribution of Tritons from $^6Li(n,t)^4He$ for Neutron Energies in the Range of the 258 keV Resonance

G. Robaye, L. Winand and J.M. Delbrouck-Habaru (paper no. 18).

As a contribution to the measurement of the angular distribution of the tritons from $^6Li(n,t)^4He$ reaction at various neutron energies, we report on the results at E_n = 250 keV, 390 keV and 600 keV. Tritons have been detected with a solid-state detector. The distributions are fitted with a power series of cos θ in the centre-of-mass system.

19.2. Analysis of the $^6Li(n,^3H)^4He$ Reaction in the Frame of the Complex Eigenvalue Theory

C. Mahaux and G. Robaye (paper no. 15).

The integrated and differential cross sections of the $^6Li(n,^3H)^4He$ reaction are analysed in the frame of the complex eigenvalue theory of nuclear reactions (1), for neutron energies less than 600 keV. The cross sections are normalized according to the recent data of Schwarz et al.(2). The experimental results can be satisfactorily accounted for, using a one-level approximation for the $5/2^-$ channel contribution and a constant background approximation in the $1/2^+$ and $3/2^+$ channels. There is no need to include the contribution of a virtual $1/2^+$ state, whose existence was recently suggested by Weidenmüller (3). however, the presence of a virtual $1/2^+$ state cannot be excluded by the present analysis, owing to the experimental uncertainties.

References

(1) J. Humblet and L. Rosenfeld, Nuclear Physics 26, 528 (1961).
(2) S. Schwarz, L.G. Strömberg and A. Bergström, Nuclear Physics 63, 593 (1965).
(3) H.A. Weidenmüller, Nuclear Physics (1965) (in press).

20. CENTRE D'ETUDE DE L'ENERGIE NUCLEAIRE (CEN-SCK), MOL (BELGIUM)

20.1. Slow Neutron Resonances

F. Poortmans, H. Ceulemans

20.1.1. Spin measurements of resonances in stable isotopes

Using the BR2 crystal spectrometer, further measurements of the spin of slow neutron resonances were made by means of the resonant scattering method. By further reduction of the background in the scattering counters, the energy range has been extended to approximately 20 eV. The results obtained are summarized in table 20.1. Most of them have been communicated at the International Conference on the Study of Nuclear Structure with Neutrons, Antwerp, July 1965, contribution 94.

Table 20.1.: Spin determination

Isotope	Resonance Energy(eV)	Spin	
		Mol	Other ref.
^{147}Sm	18.3	4	-
^{149}Sm	0.0976	4	4 (a)
^{157}Gd	17.1	2	-
^{181}Ta	24.1	3	-
^{191}Ir	0.654	2	(2) (b)
	9.07	(2)	(2) (b)
^{193}Ir	9.07	(5)	(2) (b)

(a) H. Marshak, H. Postma, V. Sailor et al., Phys. Rev. 128, 1287 (1962).

(b) A. Stolovy, B.A.P.S. 10, p. 17 (1965).

20.1.2. Resonance scattering measurements in fissile isotopes

A scattering chamber has been constructed for a two-inch diameter, 50 cm active length ^3He counter, with filling pressure of 10 atm. Compared with the BF_3 scattering chamber, the efficiency is the same but the total background is approximately 10 times lower and is now 40 counts per hour. Moreover this counter offers the possibility of pulse-height discrimination between the low energy scattered neutrons and the fission

neutron.

Measurements are underway in the 8.8 eV resonance of ^{235}U ($\Gamma_n/\Gamma = 10^{-2}$).

20.2. Thermal neutron activation cross section of ^{116}Cd

P. Decat and P. del Marmol

As isomeric cross section ratio $\sigma_m/\sigma_g = 0.54 \pm 0.10$ for the formation of the 2.4 h $^{117}Cd^g$ and the 3.4 h $^{117}Cd^m$ by the $^{116}Cd\ (n_{th},\gamma)$ reaction was measured by milking of the 1.92 h $^{117}In^m$ and 39 min $^{117}In^g$ daughters.

An activation cross section of (50 ± 8)mb was obtained for the $^{116}Cd\ (n_{th},\gamma)\ ^{117}Cd^g$ reaction. This result is in complete disagreement with the previous value of 1.4 b quoted by L. Seren et al. (Phys. Rev. 72, 888 (1947)).

A detailed account of this work will be published in Radiochimica Acta.

20.3. Fission Physics

20.3.1. Variation of the binary-to-ternary fission ratio for ^{235}U in the thermal neutron energy region

A.J. Deruytter

A paper on this subject was presented at the IAEA Symposium on the Physics and Chemistry of Fission, Salzburg 22-26 March 1965, and appeared in the Proceedings of this Conference (Vol. II, pg. 429).

Abstract: The slow chopper installed at BR1 was used to make an accurate determination of the binary-to-ternary fission ratio for ^{235}U in the neutron energy-range from 0.005 eV to 0.2 eV. Large gold-silicon surface-barrier detectors are used for the consecutive measurement of long-range α-particles (absorber in) and fission fragments (absorber out). The time analysis is done with a 100 channel time-of-flight analyser. A one-meter flight-path and a rotor speed of 50 rev/s is used.

The B/T ratio was also measured with a high statistical accuracy (about 1 %) in intense beams with well-defined neutron spectra i.e. a "cold-neutron" beam, a beam extracted from a thermal column and beams of 0.066 eV and of 0.137 eV

neutrons produced by crystal diffraction.

The B/T ratio exhibite a small and smooth variation in the energy range considered. This effect seems to be correlated with measurements of some other fission parameters in the same neutron energy range.

20.3.2. Energy balance for spontaneous fission of ^{240}Pu and fission of ($^{239}Pu + n_{th}$)

A.J. Deruytter

Experimentally a small difference $\Delta E_k = (2.2 \pm 0.3)$MeV was found in the sum of the kinetic energies of both fission fragments for the spontaneous fission of ^{240}Pu and the thermal-neutron induced fission of ^{239}Pu (Cfr. EANDC (E) 57 "U").

We plan now a more accurate measurement of the mass distribution of the fission fragments in both fissioning systems to see whether this change in kinetic energy can be attributed to a change in the mass distributions.

For this experiment a two-parameter system was composed, consisting of a double ADC (1024 x 1024 channels) gated by a fast coincidence circuit. Because of the low counting rate a fast paper-tape punch can be used for direct read-out without the use of a buffer memory. The system is now under test with ^{235}U thermal fissions.

20.3.3. Fissioning isomer in ^{242}Am

A.J. Deruytter and C. Wagemans

An experiment is under way to see whether the 13 ms isomer in ^{242}Am decaying by fission, can be formed by neutron irradiation of an ^{241}Am-target in a beam extracted from the tangential beam-hole T7 of BR2.

In this experiment an ^{241}Am-target (1.5 cm^2, 100 $\mu g/cm^2$) placed on the edge of a fast rotating disk passes first in a collimated thermal-neutron beam from T7 and afterwards in front of two detectors located at π from each other with respect to the axis of rotation of the target. The revolution speed of the target is such that there is an elapse of time of 13 ms between the passage of the irradiated target before detectors

1 and 2. So the net counting rates for fission fragments of detectors 1 and 2 should differ by a factor of 2.

In a first run two large gold-silicon surface barrier detectors were used but the α-pile-up from the target was troublesome. So we changed to solid state track detectors (muscovite mica) where a perfect discrimination was reached between fission fragments and α-particles.

Several experiments to detect eventual background were performed and the final experiments are under way.

20.4. Delayed neutron precursors in antimony and arsenic fission products

P. del Marmol and A. Speecke

Preliminary results were published in "Physics and Chemistry of Fission", I.A.E.A., Vienna, 1965, vol. II, pg. 225.

Antimony and arsenic fission products were isolated by a fast radiochemical procedure and their activities measured by neutron counting. The whole process was performed automatically and the time between end of irradiation and beginning of counting was varied between 2 s and 7 s.

A (2.15 ± 0.15)s half-life was observed and attributed to ^{85}As or ^{86}As. This neutron activity contributes to about 1.25 % of known delayed neutron emitters, the yields being measured by comparison with the well known 55 s activity of a ^{235}U source irradiated and counted under the same conditions.

The absence of neutron activity from a ^{87}Br granddaughter product permits to derive a maximum half-life for ^{87}As of . The upper limit one can set to the contribution of 1.9 s ^{135}Sb would be 0.3 % of the total delayed neutron emitters.

A 10 s half-life neutron activity is observed in addition to the 2.2 s activity and is being investigated. It was proved that it did not belong to As.

The Mol results essentially agree with those obtained independently by Tomlinson (Chem. Div., Harwell) and presented at the same IAEA Salzburg Conference.

20.5. Half-life of ^{54}Mn

A. Fabry, J.P. Deworm

Our previous value of (302 ± 6)d reported in EANDC(E) 57"U" must be modified to $T_{1/2}$ (^{54}Mn) = (308 ± 5)d. The 835 keV gamma ray peak of our initial pure ^{54}Mn source has now been followed for decay during more than 760 d (from october 1963 to end 1965) on our calibrated crystal. The new figure results from a least square analysis of all our measurements. The points available at time of EANDC(E) 57"U" have been analyzed again and a numerical error has been found, the corrected result being also 308 d.

20.6. Average fission spectrum cross sections for threshold reactions

A. Fabry, J.P. Deworm

The measurements of average fission spectrum cross sections for threshold reactions of interest in fast neutron dosimetry have been continued (cfr. EANDC(E) 57"U"). Some new results are given in table 20.2.

All these cross sections are relative to 63 mb for $^{32}S(n,p)^{32}P$ and 0.63 mb for $^{27}Al(n,\alpha)^{24}Na$, which are the main basic reactions used for the calibration of the CEN standard fission spectrum facilities (cfr. A. Fabry, EAES symposium on in-pile flux monitors Grenoble, 15-17 November, 1965) into which all the samples were irradiated, with exception of copper. For this last reaction, the determination was done in the intense fission spectrum of BR2 fuel elements relatively to the $^{54}Fe(n,p)^{54}Mn$ and $^{46}Ti(n,p)^{46}Sc$ reactions already studied (cfr. EANDC(E) 57"U").

The $^{56}Fe(n,p)^{56}Mn$ reaction, which was previously considered as a basis for the calibration of fission spectrum facilities, has been studied again. The absolute activation rates have been deduced following different methods. The weighted mean result for the average fission spectrum cross section of $^{56}Fe(n,p)^{56}Mn$ is (0.98 ± 0.04)mb and this includes a comparative determination relatively to the well-known 2200 m/s capture cross section of ^{55}Mn.

TABLE 20.2.: Average cross sections

Reaction	Half life of reaction product	Method for determination of absolute activity	(mb)
$^{27}Al(n,p)^{27}Mg$	9.47 min*)	$4\pi\beta-\gamma$ (Mr. Jacquemin, CEN, absolute measurement group)	3.53
		calibrated NaI(Tl) well crystal**)	3.42
		calibrated 3"x3" NaI(Tl) cylindrical crystal**)	3.56
		mean result	3.5±0.17
$^{92}Mo(n,p)^{92}Nb$	10.15 d	calibrated 3"x3" NaI(Tl) crystal (0.930 MeV γ-ray)	6.1±0.3
$^{64}Zn(n,p)^{64}Cu$	12.84 h	relatively to a ^{22}Na standard source by $\gamma-\gamma$-coincidence counting of β^+-annihilation γ-rays	27.7
		calibrated 3"x3" NaI(Tl) crystal (511 keV annihilation peak after stripping of $^{69}Zn^m$)	28.0
		weighted mean value	28.0±1.5
$^{63}Cu(n,\alpha)^{60}Co$	5.27 y	on 2.5 MeV sum peak in a well crystal relatively to a ^{60}Co standard source supplied by CBNM	0.52±0.04

*) Checked by following the decay for more than 40 min and substracting the $^{27}Al(n,\alpha)^{24}Na$ contribution.

**) Use has been made of the 0.834 and 1.015 MeV γ-rays of ^{27}Mg together; in this way, the error due to the great differences in level schemes (for example Nuclear Data Sheets or CIUFFOLOTTI, Nucl. Phys. 39, 252 (1962)) is reduced to a minimum (≈1 %).

21. CENTRAL BUREAU FOR NUCLEAR MEASUREMENTS, EURATOM, GEEL (Belgium)

21.1. 3 MeV Van de Graaff Accelerator

21.1.1. Activation cross sections

H. Liskien, A. Paulsen

21.1.1.1. Measurement of neutron fluxes and angular distributions

Using a T(d,n) neutron source at E_d = 0.5 MeV, neutron fluxes measured with a proton recoil telescope or obtained by the associate particle method proved an agreement within 1.4 %. The counter has used down to 0.8 MeV neutron energy by replacing the Cs I-detector by a large area semi-conductor detector and using layers of tristearin as radiators. The neutron flux determination with the telescope counter can now be considered to be accurate within 3 % down to 1 MeV.

At E_p = 3 MeV the T(p,n) angular distribution was measured in the range from 0 to 105°. This first recoil proton telescope measurement is in good agreement with two of the three earlier long counter measurements. Two angular distributions of $^9Be(\alpha,n)$neutrons were taken at E_α = (2.50 ± 0.18) MeV and E_α = (2.65 ± 0.27) MeV in the range from 0 to 130°, corresponding to the irradiation conditions mentioned in chapter 21.1.1.2., and showed reasonable agreement with the earlier work of Risser et al.

21.1.1.2. Cross section determinations

With T(d,n) neutrons: Absolute excitation functions have been determined for neutron energies between 12.6 to 19.6 MeV for the reactions $^{24}Mg(n,p)^{24}Na$ and $^{27}Al(n,\alpha)^{24}Na$. The results were published together with those for the reactions $^{55}Mn(n,2n)^{54}Mn$ and $^{59}Co(n,2n)^{58}Co$ (measured in 1964) (1).

With T(p,n) neutrons: Absolute excitation functions for the reactions $^{58}Ni(n,p)^{58}Co$ and $^{64}Zn(n,p)^{64}Cu$ and relative excitation functions for the reactions $^{31}P(n,p)^{31}Si$ and $^{32}S(n,p)^{32}P$ have been measured in the neutron energy range from 1.0 to 2.2 MeV. Normalization to absolute values will be done in the near future

for the latter reactions. For comparison calculations of the corresponding theoretical cross sections following the formalism of Hauser and Feshbach have been prepared.

With $^{9}Be(\alpha,n)$ neutrons: In the neutron energy range from about 6 to 8.2 MeV absolute cross sections have been determined for the reactions $^{24}Mg(n,p)^{24}Na$, $^{27}Al(n,\alpha)^{24}Na$, $^{56}Fe(n,p)^{56}Mn$, $^{59}Co(n,\alpha)^{56}Mn$, $^{60}Ni(n,p)^{60}Co$, and $^{63}Cu(n,\alpha)^{60}Co$. The thresholds of all these reactions are well above the energy of the second neutron group resulting from the reaction $^{9}Be(\alpha,n)^{12}C^{*}$.

The results for the reactions $^{60}Ni(n,p)^{60}Co$ and $^{63}Cu(n,\alpha)^{60}Co$ give a first rough idea of the excitation function (fig. 21.1. and 21.2.). Average cross sections for fission neutron spectra were calculated with errors directly deduced from choosen "maximum" and "minimum" curves. The resulting regions between the error limits are considerably smaller than the spreads of the available experimental results obtained with fission neutron spectra. A paper has been submitted for publication(2).

Statistical model calculations of (n,2n) excitation functions were carried out for comparison with six measurements on nuclei around Z = 28 (3).

References

(1) PAULSEN, A., LISKIEN, H.: Cross sections for the reactions $^{55}Mn(n,2n)^{54}Mn$, $^{59}Co(n,2n)^{58}Co$, $^{24}Mg(n,p)^{24}Na$, and $^{27}Al(n,\alpha)^{24}Na$ in the 12.6 to 19.6 MeV energy region, Journal of Nuclear Energy, Parts A and B, 19, 907 (1965).

(2) LISKIEN, H., PAULSEN, A.: Cross sections for the $^{63}Cu(n,\alpha)^{60}Co$, $^{60}Ni(n,p)^{60}Co$ and some other threshold reaction using neutrons from the $^{9}Be(\alpha,n)^{12}C$ reaction, Nukleonik, in press.

(3) LISKIEN, H., PAULSEN, A.: (n,2n)-excitation functions for nuclei around Z = 28, contribution no. 119 to the Antwerp Conference on Nuclear Structure, 1965; EUR 2456.e (1965).

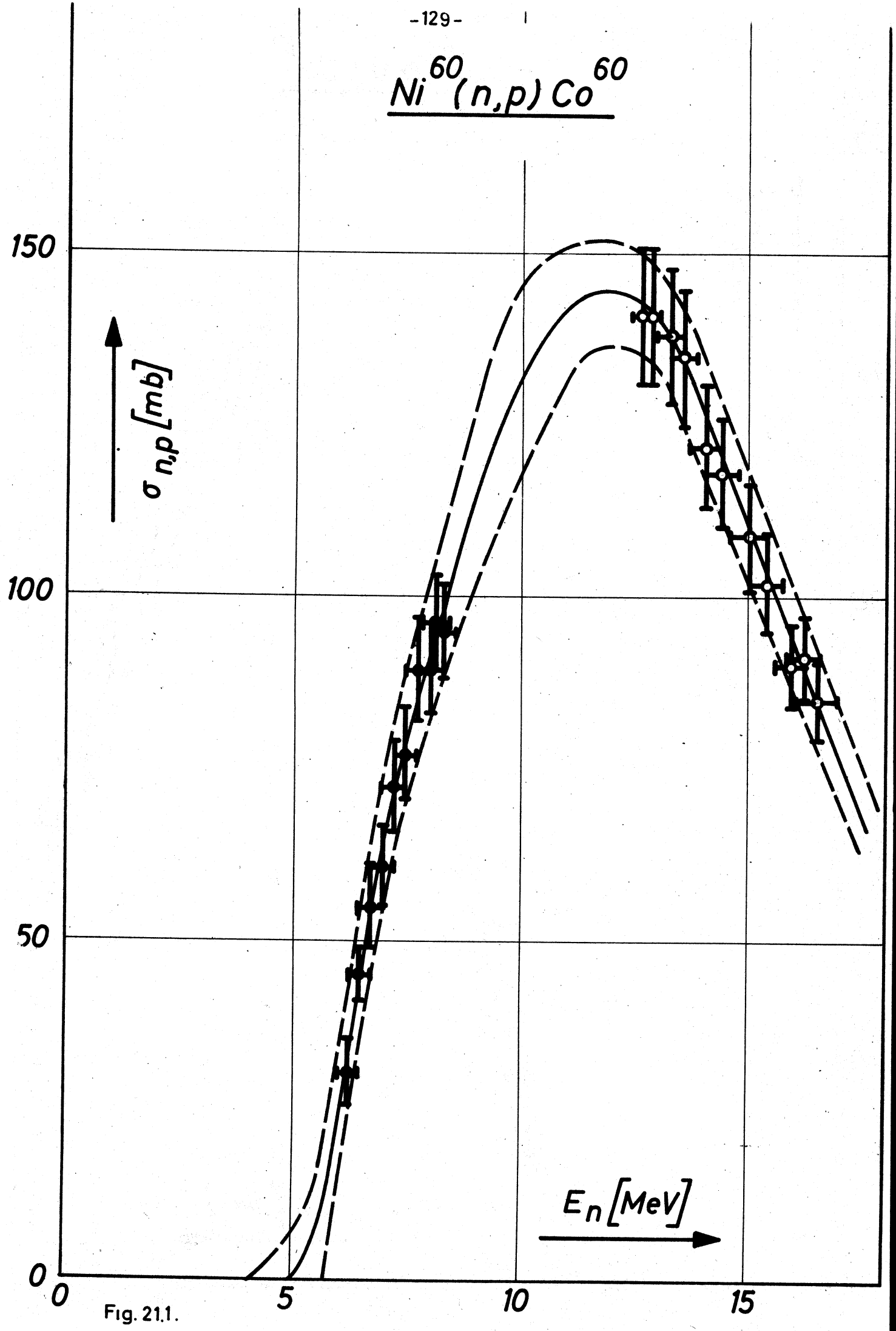

Fig. 21.1.

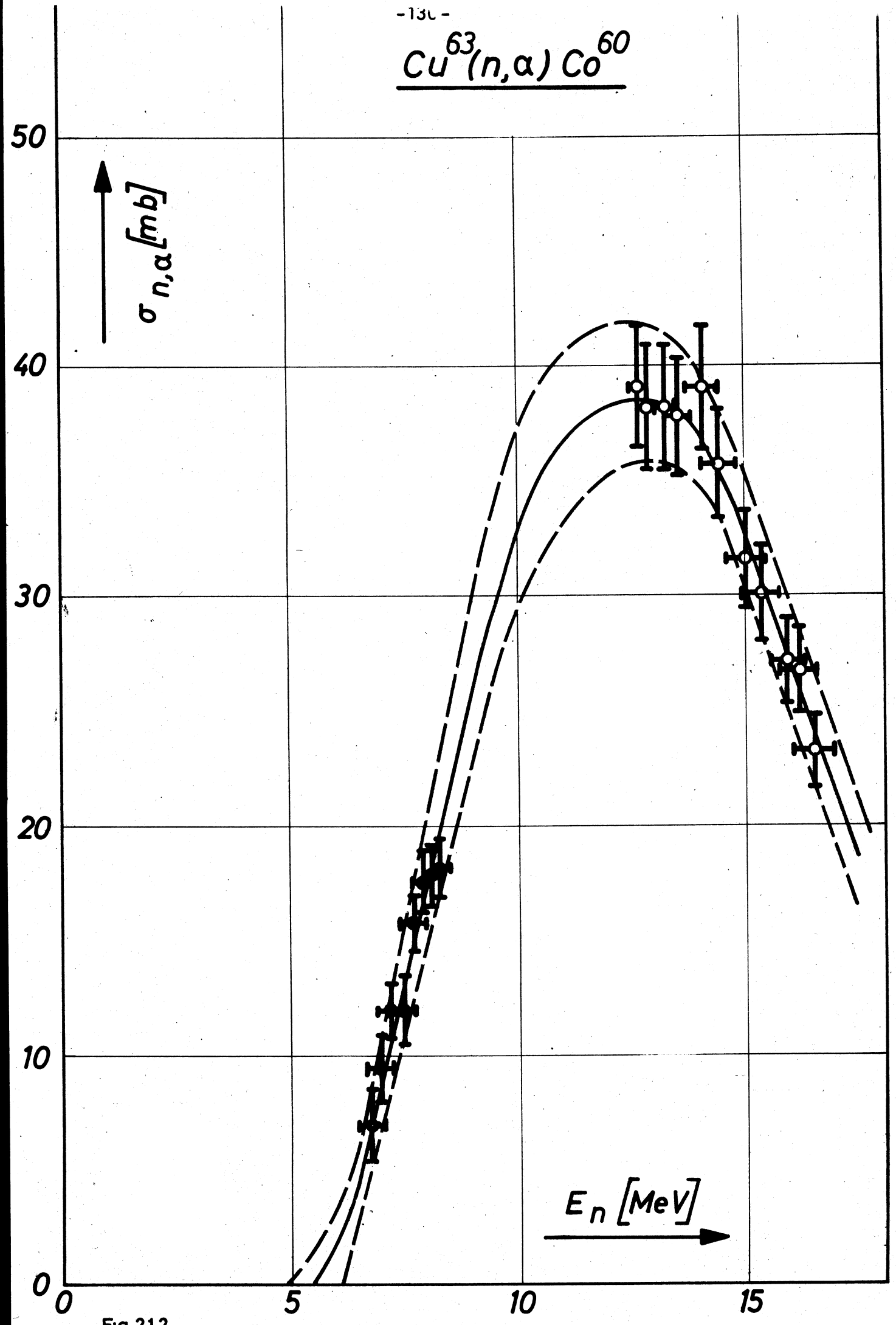

Fig. 21.2.

21.1.2. Scattering cross sections

M. Coppola, H. Knitter

21.1.2.1. Measurements on natural silicon

Seven angular distributions of elastically scattered neutrons were measured at primary neutron energies of 2.28, 1.94, 1.74, 1.41, 1.00, 0.85, and 0.57 MeV, respectively. Differential elastic scattering cross sections were extracted from the experimental results and best fits were obtained with Legendre polynomial expansions. Corrections for beam attenuation were performed using the Cranberg method. Two papers on these measurements have been written (1,2), the results are given in fig. 21.3. and 21.4. In the meantime, more accurate flux attenuation calculations and shape corrections were started with a Monte Carlo program as well as calculations of neutron elastic scattering cross sections in the neighborhood of resonances using the nuclear theory of Blatt and Biedenharn (see 21.3.2.).

21.1.2.2. Measurements on ^{7}Li

Angular distributions of elastically scattered neutrons and inelastically scattered neutrons leaving the ^{7}Li nucleus in the first excited $1/2^{-}$ level were measured at 7 primary neutron energies between 1.10 and 2.28 MeV. Uncorrected cross section data are available, final results will be published.

21.1.2.3. Further scattering experiments

Further nuclides to be investigated are ^{6}Li and ^{239}Pu. The results of earlier measurements on elastic and inelastic scattering cross sections for natural iron have been published (3,4).

References

(1) COPPOLA, M., KNITTER, H.: Measurements of absolute neutron scattering cross sections of natural Si, contribution no. 146 to the Antwerp Conference on Nuclear Structure, 1965.

(2) COPPOLA, M., KNITTER, H.: Elastic scattering of neutrons from natural silicon, to be published as EUR report.

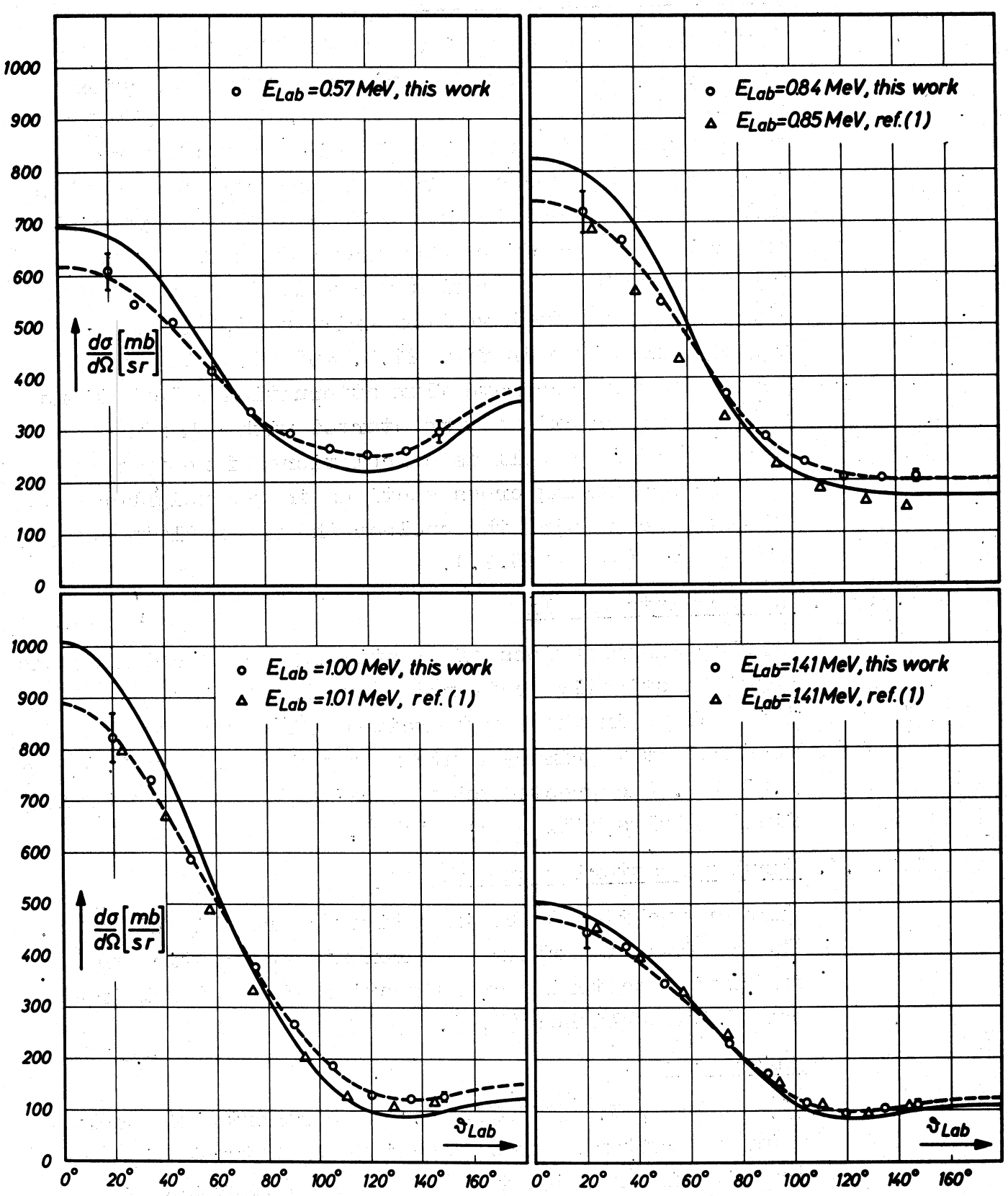

Elastic scattering of neutrons from Si.
--- *Best fits through uncorrected experimental data of this work.*
—— *Angular distributions corrected for multiple scattering.*

Fig. 21.3.

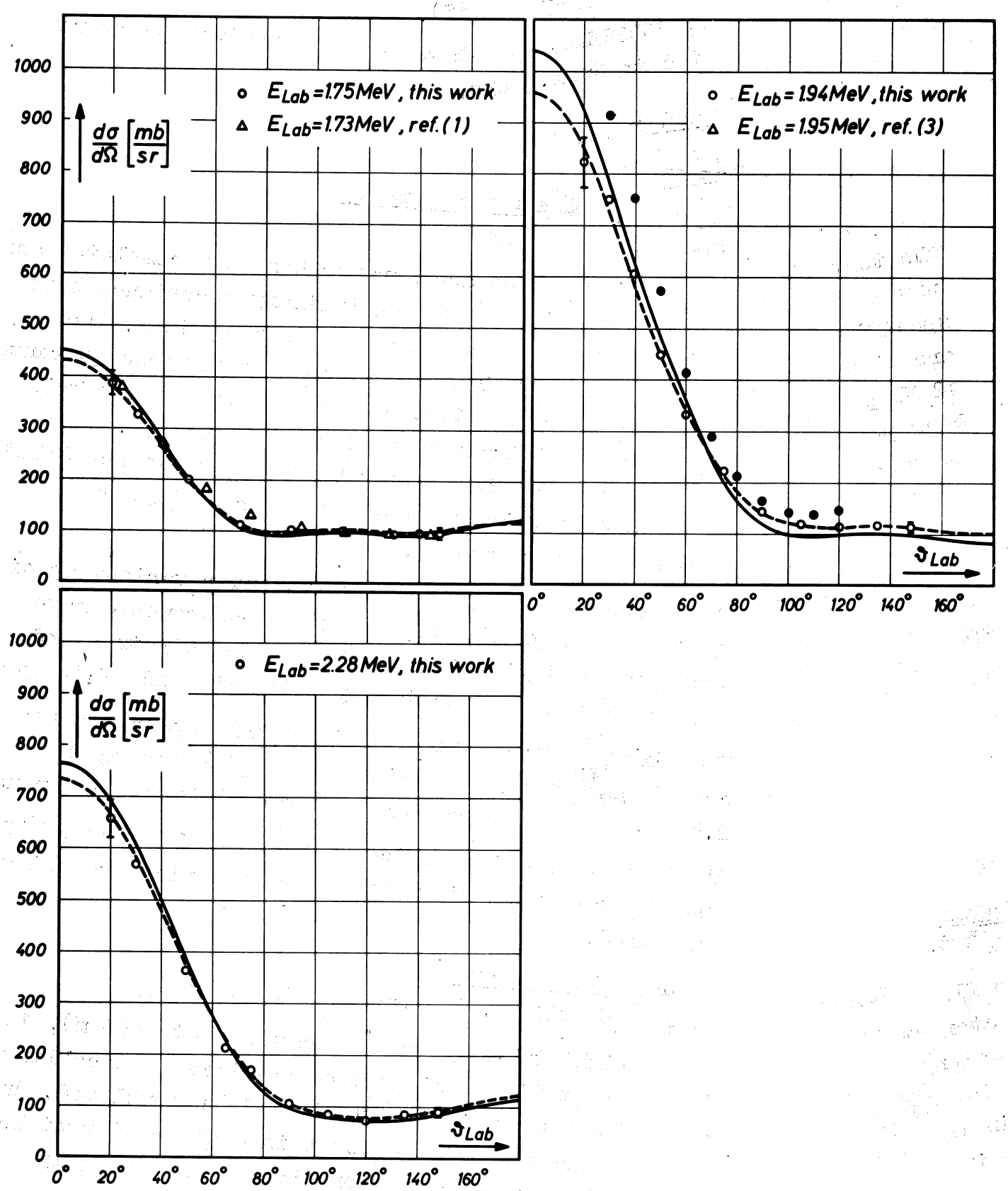

Elastic scattering of neutrons from Si.

--- *Best fits through uncorrected experimental data of this work.*

—— *Angular distributions corrected for multiple scattering.*

Fig. 21.4.

(3) JACQUOT, A., ROUSSEAU, C.: Diffusion elastique et inelastique des neutrons par le fer dans la region du MeV, Internal Report Geel-7 (1965).

(4) JACQUOT, A., ROUSSEAU, C.: Fast neutron scattering on iron, submitted to Nucl. Phys.

21.2. 60 MeV Linear Accelerator

21.2.1. Accelerator and neutron targets

C. Allard, J.M. Salomé

The adjusting of the accelerator has been completed and the tests in view of the preliminary acceptance have been carried out successfully in August, 1965. The specifications obtained as compared with those quaranteed are listed in table 21.1. They correspond to maximal 12 MW peak and 8 kW average klystron power (4.2 kW beam power). For 1966 a stepwise increase is scheduled up to 25-30 MW peak and 16-20 kW average klystron power (15 kW beam power).

After acceptance, endurance tests under various specifications and preliminary neutron measurements have been performed yielding a total of 386 klystron and 344 beam hours, respectivelly, till the end of the year.

The first neutrons were obtained from several water cooled lead targets dissipating beam powers up to 2.5 kW. A natural uranium 4 kW target is ready for use.

The beam deflection device as well as the target lift and the target carriage and storage device are being installed.

21.2.2. Neutron flight paths

K.H. Böckhoff, K. Gubernator, H. Moret

Nine flight tubes (nominal lengths 30 to 400 m), 16 detector stations, eight beam catchers, and cabling work along the flight paths have been completed. Angles and distances between check points at the target bunker and in the detector stations have been precisely determined.

TABLE 21.1.: Linac specifications

Pulse width (μs)	Specification	Repetition frequency (Hz)	Max. energy at zero current (MeV)	Energy range at nominal current (MeV)	Max. peak current (A)	FWHM of energy spectrum (%)	Fraction of current at $E_{nom} \pm 5$ % (%)	Fraction of current after deflection (%)
0.01	guaranteed	1000	57.5	53 - 57.5	3		-	-
	obtained	1000	66	46 - 64	3.6	13	50	98
0.1	guaranteed	880	57.5	41.5 -57.5	1		-	-
	obtained	880	62	26 - 59	1.2	26	28	64
1	guaranteed	380	57.5	41.5	0.2	10	-	-
	obtained	380	62	42.5	0.35	3.8	53	80
2	guaranteed	250	57.5	41.5	0.2	10	50	-
	obtained	250	62	43	0.35	4.4	75	95

21.2.3. Total cross sections

K.H. Böckhoff, G. Cardinael*, A. De Keyser, W. Kolar, H. Martin

The gross equipment for total cross section measurements on ^{240}Pu has been mounted and aligned at 50 and 100 m stations. It consists of four collimators, an automatic remote-controlled 4-position sample changer, a heavy γ-shield, and a lead shielded detector (^{10}B slab viewed by NaI crystals). The electronic equipment for the time-of-flight measurements has been completed and tested. For photomultiplier gain stabilisation, special units have been developed using gallium phosphide diodes as reference light sources.

The Linac has been operated for testing the total experimental set up including the 4096 channel time-of-flight analyser, and for obtaining preliminary information on background under different frequency and overlap filter conditions. With a typical collimator and detector arrangement and negligible overlap neutron intensity, the following background values were obtained with the black resonance technique (detector at 100 m): 7 % at 35 keV; 8 % at 132 eV; 22 % at 4.9 eV.

A transmission measurement has been performed on carbon. Evaluation of the results via the known carbon cross section confirmed within the statistical error the background values obtained by the black resonance technique down to 132 eV.

The fast neutrons from a bare lead target have been time-analysed with a plastic scintillator (thickness 1 cm) at the end of the 400 m flight path. Linac burst width and analyser channel width were 10 ns, several thin aluminium windows were inserted in the beam. The resulting time-of-flight spectrum is shown in fig. 21.5.

---

* Now at Louvain University

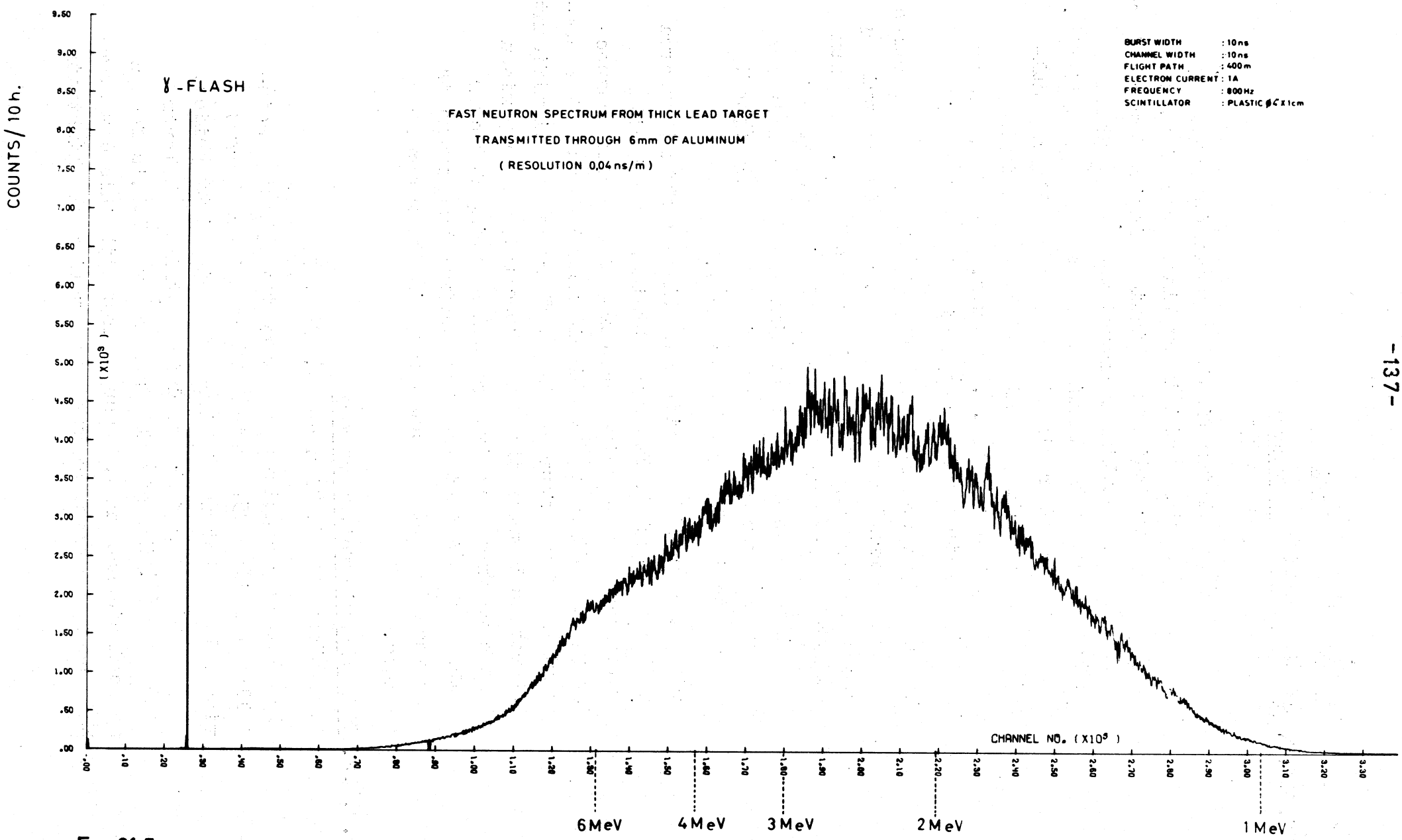
FAST NEUTRON SPECTRUM FROM THICK LEAD TARGET
TRANSMITTED THROUGH 6mm OF ALUMINUM
(RESOLUTION 0,04 ns/m)
BURST WIDTH : 10 ns
CHANNEL WIDTH : 10 ns
FLIGHT PATH : 400 m
ELECTRON CURRENT : 1A
FREQUENCY : 800 Hz
SCINTILLATOR : PLASTIC ØC x 1cm
γ-FLASH
COUNTS/10 h.
(X10³)
CHANNEL NO. (X10³)
6MeV
4MeV
3MeV
2MeV
1MeV

Fig. 21.5.

21.2.4. Fission cross sections

21.2.4.1. Fission neutron detector

E. Migneco, J. Theobald

A liquid scintillator fission neutron detector has been tested during preliminary Linac operation. It consists of four individual liquid scintillator chambers forming a hollow cylinder around the sample which is shielded towards the liquid by means of a ^{6}Li cylinder. Each of the chambers is viewed by a 58 AVP photomultiplier. 6 coincidence units link, respectively, 2 combinations of the 4 P.M. outputs. Each P.M. output is equiped with a pulse shape discrimination unit.

Time-of-flight measurements on preliminary ^{235}U samples have been carried out at 100 resp. 60 m in the primary neutron energy range between 4 eV and 30 eV. In a run of about 40 hours the number of fission events has been time-analysed with a preliminary time resolution of about 20 ns/m and low counting statistics (about 2500 counts in the 19 eV resonance).

During this run three different time-of-flight spectra have been recorded. Two were obtained by coincidences between the two opposite chambers of the tank, respectively, the other one by coincidences between all 6 combinations of the four chambers. There are no significant differences between the three spectra. The comparison of spectra from opposite and neighbouring detector chambers showed that the fast neutron background is less than 10 % of the count rate in the resonance valleys.

21.2.4.2. Thin plastic foil detector

K.H. Böckhoff, E. Migneco, J. Theobald

This detector consists of 2 very thin plastic scintillator foils (25μm thick, 16 cm x 16 cm large) viewed by 2 photomultipliers via thin light guides. The scintillator foils sandwich a thin ^{235}U layer (400 $\mu g/cm^2$). The signals from the two P.M.'s feed a sum coincidence unit. Measurements with this detector have been performed at the 30 m station of flightpath

no. 16 simultaneously with the fission neutron detection studies described before. The energy range extended from 6 to 300 eV. In the comparable energy range (4 to 30 eV) the time-of-flight spectra of fragment and neutron detection show the same shape (see fig. 21.6.).

The efficiency for fission event detection was determined by comparison with a BF_3 counter using known cross section data of the $^{10}B(n,\alpha)$ and $^{235}U(n,f)$ processes. It turned out to be about 50 %. A mapping of this efficiency over the sensitive area of the detector is performed.

21.2.4.3. Ionisation chamber

E. Migneco, J. Theobald, J. Winter

A large area multiplate ionisation chamber (8 partial chambers) has been constructed and studied with an $^{241}Am-\alpha$ and a ^{252}Cf fission source. Moreover its behaviour in the γ -flash of the Linac has been investigated. The chamber will be used for cross section measurements on ^{235}U.

21.2.4.4. Spark chamber

E. Migneco, J. Theobald

This detector is being studied and developed for fission cross section measurements on highly α -active nuclides. A test chamber has been constructed which allows easy variation of essential parameters (gas pressure, humidity, electrode shape, geometry) in order to determine optimum operation conditions. The reasons for fluctuations and non-reproducibility of count rates are not yet understood.

21.2.4.5. Surface barrier detectors

H. Meyer

Fast amplifiers with a risetime of $\tau(0-63\%) = 0.5$ ns were developed for use with Si surface barrier detectors. The charge collection time in self-produced detectors of 250 Ω cm to 10 k Ω cm resistivity was measured vs. bias voltage for α-particles and fission fragments (1). Comparison of experimental results with calculations

235 U fission rates vs. neutron time of flight

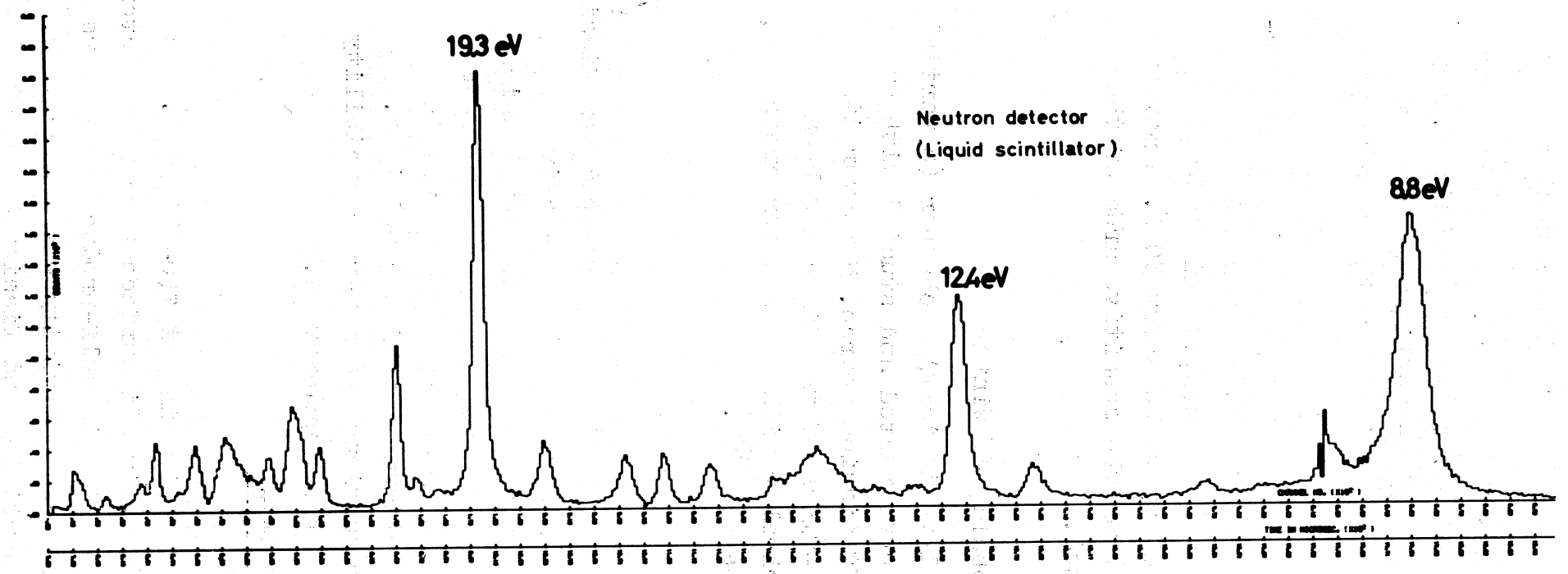

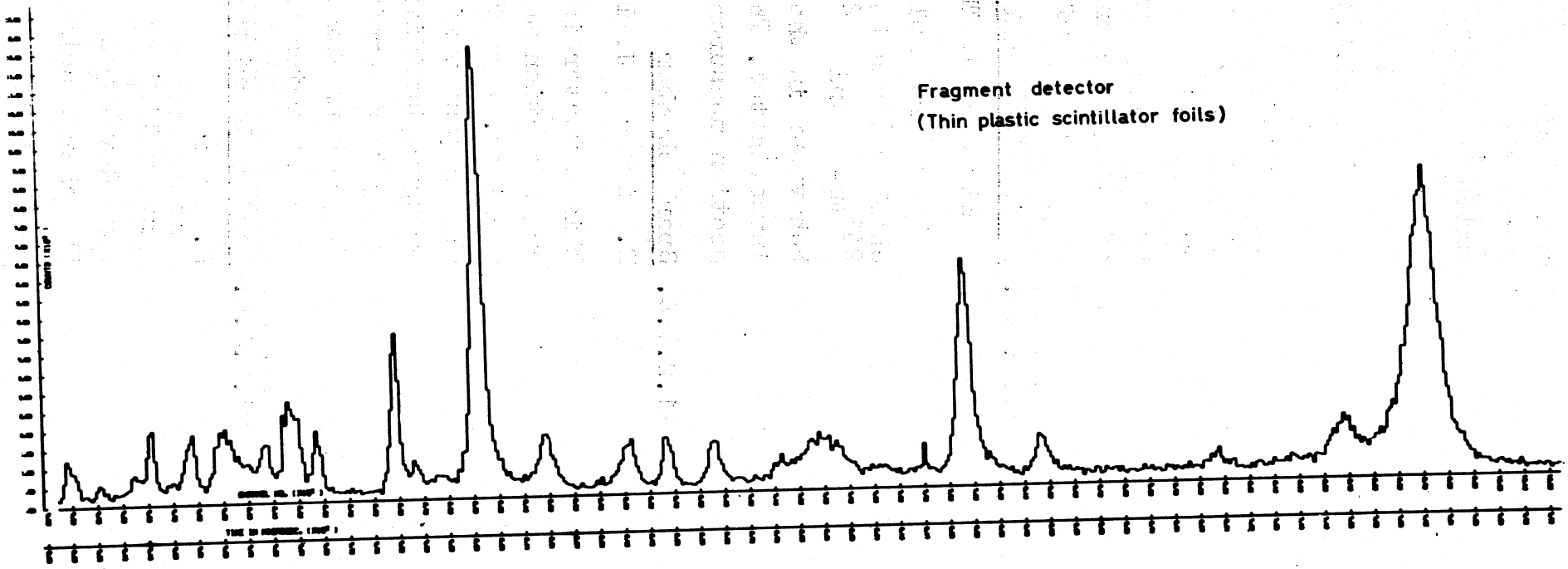

Fig. 21.6.

showed the important influence of the carrier density in ionization tracks on the charge collection time.

Reference

(1) MEYER, H.: Studies of the response speed of silicon surface barrier detectors, when irradiated with different particles, Proceedings of the 10th Scintillator and Semiconductor Counter Symposium, Washington, March 1966, in press.

21.2.5. Capture cross sections

G. Carraro, H. Weigmann

A first specimen of an improved version of the Moxon-Rae detector, consisting of six sheets of plastic scintillator alternatively connected to two photomultipliers operating in coincidence, has been constructed and tested with respect to its efficiency as a function of γ-ray energy.

21.3. Data Handling and Evaluation

21.3.1. Data handling equipment

21.3.1.1. Tele-processing equipment

A. De Keyser, H. Horstmann

The tele-processing machines IBM 1050 and IBM 7702 have been installed in March, 1965. The IBM 7702 magnetic tape transmission terminal has been operating satisfactorily, whereas the IBM 1050 data communication system showed a very low efficiency. Due to this fact and many other drawbacks the present data handling system turned out to be very slow. An improved system has been studied.

21.3.1.2. Improvement of data acquisition

A. De Keyser, H. Horstmann

Electronic work is being done to record the data of simultaneously operating multi-channel analysers on magnetic tape in order to speed up the output rate of the data acquisition system as well as the input rate for the data handling equipment. Several code and data format problems have been solved in order to improve the compatibility between data acquisition and data handling equipment.

21.3.1.3. Nanosecond time coder

H. Meyer, H. Verelst

The first final version of a one-nanosecond digital time coder (1) has been put into operation. Also a channel width equalizing system has been developed (2,3) to reduce the differential nonlinearity down to 1 ns channel width from 10 % to< 0.3 %. A second final version is under development. Maximum analysis range ≈ 3 ms; maximum channel number 130.000; channel width 1 ns to 256 ns in digital steps; more than one measurement per analysis cycle; minimum distance between two measurements 256 ns.

References

(1) MEYER, H., VERELST, H.: Test equipment for accurate determination of time relations and its use for the measurement of the timing accuracy and the calibration of fast photomultipliers, EUR 2247.e (1965).

(2) STÜBER, W.: Subtractor circuit with integrated logic elements, Nucl. Instr. and Meth., in press.

(3) MEYER, H.: A simple equalizing system for small differential nonlinearity with a one nanosecond digital time coder, Nucl. Instr. and Meth., in press.

21.3.1.4. Data storage systems

F. Colling, B. Idzerda, W. Stüber

Data from coders with up to 17 bit word length can be stored on a 1" magnetic tape. The stored information can be read out for selective sorting and integration into a 12 bit address core memory or a computer. The system includes a 10 word / 20 bit buffer store (resolution 1 μs), a programming unit and magnetic tape device. Data rates may range from 0.3 words/s to 3000 words/s.

A buffer store with a capacity of 16 words/20 bits or 8 words/40 bits, respectively, is under development.

Maximum word density on continuously running magnetic tape is now 500 words/inch and for stepwise recording 250 words/inch, for data rates from almost 0 to 7500 words/s.

A storage display system with a storage tube has been developed. The equivalent word capacity will be finally about 500.000.

21.3.2. Computer programming and data analysis

M.G. Cao, H. Horstmann, H. Schmid

The following computer programs have been written:

A Monte Carlo program for calculating energy, time, and space dependence of neutron capture in homogeneous B_4C and heterogeneous B_4C and CH_2 slabs or cylinders. Impurity effects are considered for all parameters.

Calculations of pulse shape discrimination have been done with two programs, the first one performing the selection of the number of RC blocks and RC values providing the optimum figure of merit, the second one computing the statistical fluctuation effect on the zero-crossing time and on the figure of merit.

IBM 7090 program for Racah, Clebsch-Gordan and Z coefficients (1).

A least squares fit program with the general formula of Blatt and Biedenharn for the differential elastic neutron cross section.

An IBM 7090 program for the kinematic parameters of non-relativistic particles for two-body reactions.

An IBM 7090 program for the kinematic parameters of the $^9Be(n,2n)^8Be$ reaction.

An IBM 7090 program tabulates kinematic parameters for (p,n),(d,n), and (α,n) reactions. Relativistic effects are considered.

In cooperation with CETIS, Ispra, and the ENEA Computer Programme Library, the Stretch version of the Monte Carlo program MAGGIE (Aldermaston) has been corrected and modified for the IBM 7090 computer. The program has been used to calculate flux attenuation factors and multiple scattering corrections for angular distributions of elastic neutron scattering cross sections of Si and Fe.

A program for the interpretation of activation cross section measurements calculates cross sections for two-particle emission according to the statistical theory.

The Calcomp plotter subroutine package of CETIS has been adapted to the CBNM Calcomp plotter model 506/570.

An IBM 7090 program processes and reduces the raw data of total cross section experiments. The program includes routines for dead-time and background corrections, data smoothing and plotting.

Programs for neutron flux corrections, decay time corrections, Hauser-Feshbach calculations, and for the analysis of Van de Graaff total cross section data.

Reference

(1) CAO, M.G.: Calcul des coefficients de Racah, Clebsch-Gordan et Z, EUR 2639.f (1965).

21.4. Radionuclides

21.4.1. Standardization of sources, development of counting methods

W. Bambynek, A. Spernol, W. van der Eijk, R. Vaninbroukx

Standard sources of ^{22}Na, ^{24}Na, ^{46}Sc, ^{51}Cr, ^{54}Mn, ^{56}Mn, ^{58}Co, ^{60}Co, ^{65}Zn, ^{137}Cs, ^{241}Am, and ^{252}Cf have been prepared with accuracies of generally a few tenths of a percent. Extended sources of ^{32}P and ^{31}Si have been calibrated with good precision using a bremsstrahlung method.

Older investigations on high precision alpha counting with solid angle devices (1) have been extended to X-rays with energies of 4 - 20 keV. 1 % accuracy has been reached using Xe-filled proportional counters with thin windows of Be or plastic (2). The results of our γ-spectrometer measurements of the last 5 years have been collected in a report (3). The previously reported (4) investigations on high precision liquid scintillation counting have been extended to other nuclides (especially U) and to low energies. The thin foil β-absorption investigations in 4π-geometry (5)

have been continued using the sandwich method. The comparison with the backing method used previously (5) allowed to confirm that the linear extrapolation used is correct.

21.4.2. Determination of nuclear constants

W. Bambynek, H. Hansen, A. Spernol, R. Vaninbroukx

The fluorescence yield of Cr has been determined with 1.5 % precision to 0.277 (6), which is not at all in agreement with the presently accepted value of 0.229. The thermal cross section of ^{59}Co has been determined to (37.4 ± 0.3) barns (7). The intensities of some conversion electrons after ^{241}Am decay have been determined and the decay scheme of this nuclide has been reexamined (8). The γ-branching in the decay scheme of ^{65}Zn has been determined to (50.9 ± 0.3)%. New measurements on this nuclide which are under evaluation will deliver all branching ratios in the ^{65}Zn decay with 0.1 % accuracy. The γ -branching in the ^{85}Kr decay has been determined to 0.438 % by gas- and γ -counting with 1 % accuracy.

References

(1) SPERNOL, A., LERCH, O.: Eine auf 0,2% genaue Zählung von Alphateilchen mit Plastikdetektoren, Nucl. Instr. Meth. 32, 293 (1965); EUR 1105.d (1965).

(2) BAMBYNEK, W., LERCH, O., SPERNOL, A.: Eine auf 1 % genaue absolute Zählung von X-Strahlen geringer Energie, Nucl. Instr. Methods, 39, 104 (1966).

(3) VANINBROUKX, R., GROSSE, G.: The use of a calibrated γ-spectrometer for precise activity measurements of γ-emitters and EC-nuclides and for purity and sorption tests of solutions of radionuclides, I.J.A.R.I. 17, 41, (1966).

(4) VANINBROUKX, R., SPERNOL, A.: High precision 4π-liquid scintillation counting, I.J.A.R.I. 16, 289. (1965).

(5) VAN DER EIJK, W.: The correction of foil absorption in 4π -counting, EUR 2248.e (1965).

(6) BAMBYNEK, W., DE ROOST, E., SPERNOL, A., VAN DER EIJK, W., VANINBROUKX, R.: Precise determination of the

$p_k \omega_k$ value and the fluorescence yield of Cr, EUR 2524.e (1965).

(7) VANINBROUKX, R.: The thermal-neutron cross section of ^{59}Co, Nucl. Sc. Eng. 24, 87 (1966).

(8) BAMBYNEK, W.: Zum Zerfall des ^{241}Am, EUR 2632.d (1965).

21.5. Isotopic Standards of Stable and Fissile Nuclides

21.5.1. Boron

P. De Bièvre, G.H. Debus

Instrumental development led to a considerable increase of precision by a factor of four on isotope ratio measurements of boron. $^{10}B/^{11}B$ ratios are now measured with a precision of 0.1% or better. The CBNM boron standard has been recalibrated, using the new tandem mass spectrometer. Measurements were also performed at the National Bureau of Standards (Washington) and New Brunswick Laboratory (U.S.). As shown in table 21.2., all figures agree and confirm the earlier measurements of CBNM (19.81 % ^{10}B).

TABLE 21.2.: The CBNM Boron Standard

Laboratory and Mass spectrometer	Atomic concentration of ^{10}B (%)	Remark
CBNM Tandem	19.80	Corrected for bias by means of CBNM synthetic mixtures; the statistical error will be improved by further measurements.
NBS	19.82	Corrected for bias by means of american synthetic mixtures.
NBL	19.82	Corrected for bias by means of CBNM mixtures.
CBNM M.S.5	19.82	Mean of a very large number of uncalibrated measurements (no bias correction).
CBNM C.E.C.21-702	19.82	Mean of a very large number of uncalibrated measurements (no bias correction).

21.5.2. Lithium

P. De Bièvre, G.H. Debus

A lithium standard programme started and is expected to be completed by the end of 1967. The isotopic quality of the enriched and depleted materials needed have been computed (99.9 % ^{7}Li and 99 % ^{6}Li) and necessary blending precisions determined (0.015 %).

21.5.3. Deuterium

T. Babeliowsky, G.H. Debus

In the framework of the heavy water standard programme, normalization of ^{18}O in D_2O, investigation of the decomposition of D_2O in connection to D/H analysis (precision 0.003 mol % D_2O), and density measurements of D_2O with the float method (standard deviation 0.02 mol % D_2O) have been performed.

Eight institutes are participating in a programme on absolute determination of heavy water isotopic concentration. A sample of 200 ml D_2O was sent to each of the laboratories.

21.5.4. Fissile nuclides

P. De Bièvre, G.H. Debus

Some papers and reports on isotope dilution and isotopic standards were presented or appeared in the open literature (1-4).

References

(1) DE BIEVRE, P.J., DEBUS, G.H.: Precision and accuracy in quantitative determinations of U and Pu by mass spectrometric isotope dilution - 2 issues - ENDC working paper.

(2) DE BIEVRE, P.J., DEBUS, G.H.: Optimal conditions for mass spectrometric quantitative determinations by isotope dilution, EUR 2219.e (1965).

(3) DE BIEVRE, P.J., DEBUS, G.H.: Precision mass spectrometric isotope dilution analysis, Nucl. Instr. Method. 32, 224 (1965).

(4) DE BIEVRE, P.J., SPAEPEN, J.: Isotopic standards and reference substances for nuclear measurements - working paper for EANDC subcommittee on standards.

21.6. Sample Preparation and Assaying

G.H. Debus, H.L. Eschbach, K.F. Lauer, H. Moret, G. Müschenborn, J. Van Audenhove, V . Verdingh

A total of 129 different applications (covering 2506 samples) was carried out in 1965 which is an increase of 46.5% with respect to 1964. The majority of these demands stem from Euratom institutes and national nuclear energy laboratories of the Community, but substantial help was also provided to universities in Belgium, Germany, Italy, and the Netherlands. A limited support was given to laboratories outside the Community.

During fabrication and assaying of samples the main effort consists in studying the new problem and setting up the experiment. The additional effort to make a large series of samples is often less important.

2251 samples of 34 different metals and alloys have been prepared by metallurgical methods such as melting (by induction, levitation, resistance, electron bombardment heating), rolling, punching, machining, powder metallurgy, and electrolyses (1-3).

129 samples were prepared by chemical methods, mostly by electrospraying techniques (4,5). 126 samples were prepared by evaporation techniques, each requiring a special study about adherence, layer thickness, uniformity etc.

Most of the samples have been precisely defined with respect to their isotopic and chemical composition and their physical properties as mass, homogeneity, thickness, and size. In connection herewith, several existing techniques could be considerably improved and new methods have been developed, e.g. a mechanical-capacitive layer thickness meter providing an accuracy of $\pm$ 0.1 μm, an α-absorption and an X-ray absorption device.

Preparation of very precise B and U reference samples for neutron measurements by means of ultra-high vacuum evaporation techniques is being further refined.

References

(1) VAN AUDENHOVE, J., JOYEUX, J.: The preparation by levitation melting in argon of homogeneous aluminium alloys for neutron measurements, Journal of Nuclear Materials, in press.

(2) VAN AUDENHOVE, J., GEORIS, J.P.: The preparation of pure and ductile manganese foils by electrodeposition, technical note to be submitted to Nuclear Instruments and Methods.

(3) VAN AUDENHOVE, J.: Vacuum evaporation of metals by high frequency levitation heating, Rev. Sci. Instr. 36, 383 (1965).

(4) VERDINGH, V., LAUER, K.F.: Equipment for electro-spraying, Nucl. Instr. Meth. 31, 355 (1964).

(5) VERDINGH, V., LAUER, K.F.: The preparation of sodium samples for neutron scattering experiments, EUR 2242.e (1965).

CBNM contributions to special seminars are published in the proceedings concerned:

EANDC Colloquium on High Precision Chemical Analysis of Substances of Interest to Nuclear Energy, Brussels, January, 1965 (organized by CBNM), EANDC-42 "S" (1965).

EANDC Colloquium on Mass Spectrometry and α-Counting Techniques, Brussels, November, 1965 (organized by CBNM), EANDC-53 "S" (1966).

AERE Seminar on Preparation and Standardization of Isotopic Targets and Foils, Harwell, May, 1965, AERE report in press.

22. DEPARTEMENT DE RECHERCHE PHYSIQUE, SECTION DES MESURES NEUTRONIQUES FONDAMENTALES, C.E.A. SACLAY (FRANCE)

R. Joly

22.1. Groupe des neutrons thermiques

H. Nifenecker

Ces expériences ont été effectuées auprès de la pile EL-3 de Saclay par A. Audias, P. Carlos, H. Nifenecker, R. Samama et C. Signarbieux.

22.1.1. Etude des rayonnements γ émis après capture des neutrons thermiques

22.1.1.1. Appareillage

L'installation a été améliorée sur les points suivants:
Un ensemble comportant un cristal central Na I et un anneau anticompton a été installé.
Le bruit de fond a été réduit (gain d'un facteur 3) en entourant la cible d'un cylindre de ^{6}Li (fabriqué par le BCMN-GEEL) destiné à capturer les neutrons diffusés par la cible.
La géométrie de l'expérience de corrélation angulaire et son monitorage ont été améliorés de telle sorte que les enregistrements aux différents angles soient en valeur relative, précis à 1 %.

22.1.1.2. Mesures de corrélation angulaire

Une première mesure sur la corrélation angulaire des cascades du ^{52}V (^{51}V + n) a été effectuée à l'aide d'un ensemble multiparamétrique, permettant l'enregistrement simultané sur bande magnétique des deux énergies, de leur somme (la non linéarité des convertisseurs analogiques digitaux empêche de faire valablement une somme digitale) et d'un spectre de temps obtenu en appliquant les impulsions des deux photomultiplicateurs à un convertisseur temps-amplitude. Cette dernière technique présente de grands avantages sur celle plus courante des coincidences rapides.

Une expérience préliminaire a donné les résultats suivants:
$W(\theta) = 1 + (0.085 \pm 0.047)\ P_2\ (\cos\theta)$ pour la cascade
6.485 MeV - 0.820 MeV,

$W(\theta) = 1 + (0.058 \pm 0.049)\ P_2\ (\cos\theta)$ pour les cascades 5.75 MeV - 1.55 MeV et 5.15 MeV - 2.15 MeV. Une mesure d'une précision bien meilleure est en cours. L'étude du Titane est envisagée.

22.1.1.3. Nouveaux détecteurs

En liaison avec le Service d'Electronique Physique, la fabrication de diodes n-i-p au Germanium a été entreprise. Un détecteur de 1 cm^3 fonctionne depuis 6 mois. On essaye actuellement de déterminer les paramètres permettant d'entreprendre la fabrication de diodes de plus grand volume.

22.1.2. Etudes sur la fission

22.1.2.1. Etude de la distribution des masses des fragments après émission neutronique prompte

Une communication sur ce sujet a été faite au Colloque sur la fission de Salzbourg (1).

22.1.2.2. Etude du mode symétrique dans le cas de la fission thermique

L'étude de la fission symétrique par des moyens physiques (mesure simultanée des deux énergies ou des deux vitesses) est rendue difficile par la présence d'évènements aberrants. Nous essayons actuellement de surmonter cette difficulté par la mesure simultanée des deux énergies et de la différence de temps de vol des deux fragments. La mesure de ces trois quantités permet en principe de définir un critère de cohérence que seuls les évènements non aberrants peuvent remplir.

22.1.2.3. Mesure simultanée de la masse et de la charge des fragments

Les rayons X associés aux déséxcitations des fragments par conversion interne permettent de mesurer leur charge. D'autre part l'énergie libérée sous forme d'énergie cinétique dans le phénomène de fission est donnée par: $E_T = K(Q_1(Q - Q_1))/D$
ou D est la distance des centres de charges au moment de la scission si l'on admet que l'énergie cinétique

de translation à ce moment est négligeable. La mesure simultanée de Q_1, E_1, E_2 permet donc en principe d'étudier le processus de fission en fonction du paramètre D. Nous avons tenté cette étude sur la fission par neutrons thermiques de ^{235}U. Dans l'état actuel des choses le bruit de fond de notre installation est trop important pour nous permettre d'obtenir des résultats valables.

22.1.3. Mesures de temps de vie

Une expérience visant à mesurer le temps de vie du niveau intermédiaire dans une cascade d'électrons de conversion par la méthode du champ hyperfréquence est en cours de montage.

22.1.4. Dépouillement des mesures de sections efficaces de fission (10)

Il semble qu'on ait réussi à rendre compte de l'effet de non détection de résonance sur la distribution des espacements observée. Si q(D) est la probabilité d'observer un espacement D, p(D) la probabilité théorique d'existence d'un tel espacement, E(D) l'efficacité de détection d'une résonance située à la distance D d'un niveau déjà observé, on aurait:

$$q(D) = \left[E(D)\right]^2 \left[p(D) + \int_0^D p(D')\,(1 - E(D')\,E\,(D - D'))\,dD'\right.$$

$$+ \int_0^D p(D')\,(1 - E(D')\,E(D - D'))\int_0^{D-D'} p(D'')(1-E(D'+D'')\cdot$$

$$\left.E(D-D'-D'')\right]\; p\,(D-D'-D'')\,dD\;1 + \text{etc.....}$$

Nous cherchons actuellement à remplacer cette formule par une formule plus compacte.

D'autre part nous avons simulé la courbe de section efficace de fission de ^{233}U par une méthode de Monte-Carlo en utilisant des formules à un niveau. Il apparait qu'on perd environ 50 % des niveaux et que la loi de distribution des espacements observée correspond bien à celle observée sur la courbe de section efficace expérimentale de l'^{233}U et correspond à un rapport des populations

des deux familles de résonances d'environ 1.
L'impossibilité dans laquelle nous avions été jusqu'ici de rendre compte avec un tel rapport de population de la distribution des espacements observés provenait d'une mauvaise méthode de correction pour les niveaux non détectés.

22.2. Groupe des neutrons intermédiaires

A. Michaudon

Ces expériences ont été effectuées auprès de l'Accélérateur Linéaire de Saclay par MM. R. Bayer (stagiaire du Centre d'Etudes Nucléaires de Prague), J. Blons, B. Cauvin, H. Derrien, C. Eggermann, A. Lottin (actuellement détaché à Oak Ridge Nat. Lab., USA), D. Paya, P. Ribon, Melle M. Sanche, MM. E. Silver (détaché à Saclay par ORNL, USA), J. Trochon, A. Michaudon (détaché à MIT jusqu'à Août 1965).

En 1965, l'accélérateur a été utilisé pendant 25 semaines pour ces expériences qui ont été effectuées sur 3 bases de vol:
1 base de longueur maximum 200 mètres, affectée aux mesures de transmission,
1 base de longueur maximum 120 mètres, affectée aux mesures de fission,
1 base de longueur maximum 14 mètres, affectée aux mesures de diffusion.

22.2.1. Appareillage

22.2.1.1. Implantation

Les améliorations suivantes ont été apportées:
Obturation des bases de vol par bouchons d'eau dans le massif de protection.
Remplissage d'Hélium pour la base transmission et remplacement des parois d'Aluminium par des parois minces en mylar.

22.2.1.2. Electronique

Nous avons actuellement à notre disposition:
5 codeurs de temps de vol Intertechnique HC 25, de largeur minimum de canal 50 ns ayant 65.536 canaux, et

dont il est possible de changer la largeur de canal en cours de cycle par programmation.
1 codeur de temps de vol Intertechnique HC 50 de caractéristiques voisines du HC 25 mais dont la largeur de canal minimum est de 10 ns.
4 blocs mémoires BM 96 à 4096 canaux.
2 appareils à bande magnétique de 1" à 16 pistes; à chacun de ces appareils est affectée une unité de lecture permettant de dépouiller les résultats enregistrés.

22.2.1.3. Calculateur électronique et programme

Un calculateur électronique CAE 510, ayant une capacité de mémoire de 24000 mots vient d'être installé.
Un programme d'acquisition en ligne sur ce calculateur a été écrit et des essais en vraie grandeur sont en cours.

22.2.2. Expériences effectuées

22.2.2.1. Mesures de sections efficaces totales

Plutonium-239

La mesure a été effectuée jusqu'à 1200 eV et dans des conditions expérimentales que résume le tableau 22.1. et la fig. 22.1. Pour mieux connaitre la valeur de l'effet Doppler à 77°K, qui dépend beaucoup de la température de Debye, une mesure spéciale a été faite pour des résonances dont le rapport Δ/Γ est le plus grand à la température ambiante et à 77°K. Par une analyse de forme de ces résonances à deux températures différentes, on peut en déduire une valeur de Δ égale à $0.0126 \sqrt{E_{(eV)}}$, un peu plus élevée que celle de $0.0121 \sqrt{E_{(eV)}}$ qui nous avait servi précédemment (2)(3).
L'importance de l'effet Doppler illustré sur la fig. 22.2. où un groupe de résonances est bien résolu à 77°K, mais il ne le serait pas à la température ambiante, ni en transmission ni en fission.
Les résonances parasites du ^{240}Pu vont être éliminées par une mesure de la transmission d'un échantillon de Pu contenant 10 % environ de ^{240}Pu.

Iode

Une mesure à haute énergie (jusqu'à 400 keV) a été entreprise en vue de déterminer σ_p, S_0, S_1.

Neptunium-237

Cette mesure est en cours: la fig. 22.3. présente un résultat préliminaire dont nous indiquons les conditions afin de situer les possibilités d'un Accélérateur Linéaire pour des mesures de transmission sur de petits échantillons (isotopes séparés).

Longueur de vol ..... 16,7 m
Accélérateur ..... f = 500 Hz, t = 60 ns
Sélecteur ..... t = 50 ns
Collimation ..... Ø = 26 mm
Quantité de Neptunium ..... 25 gr sous forme de NpO_2
Durée d'accumulation ..... 1 h 10 min
Taux de comptage par heure et par
canal de 50 ns ..... 1100 coups à 40 eV.

22.2.2.2. Mesures de sections efficaces de fission

Plutonium-239

Une mesure complémentaire de fission du ^{239}Pu, en dessous de 200 eV a été faite, avec le même scintillateur gazeux (4)(5) mais en utilisant comme gaz scintillant un mélange argon-azote à la pression de 300 g/cm^2; ceci afin d'évaluer avec précision les scintillations parasites dans les résonances du Xénon qui avaient été observées dans les mesures précédentes (4)(5). Cette mesure va être reprise dans de meilleures conditions.

Neptunium-237

Un scintillateur gazeux à 12 cellules a été construit pour la mesure de la section efficace de fission du ^{237}Np en dessous du seuil pour des neutrons de résonances. Nous présentons sur les fig. 22.4. et 22.5. un essai préliminaire avec un nombre limité de cellules, à une distance de vol de 16 et 7 m. Le gaz scintillant est du Xénon, utilisé au début des mesures pour ses qualités de scintillation, mais qui sera remplacé ultérieurement par un autre gaz scintillant.

Autres études

Une chambre à étincelles a été essayée pour la mesure

de fission de noyaux à forte radioactivité α comme le ^{241}Am. Un tel détecteur fonctionne bien en laboratoire, mais il est nécessaire d'éliminer les dérives et le manque de reproductibilité dans les résultats, avant de l'employer dans des mesures par temps de vol.

22.2.2.3. Mesures de diffusion

Après des essais préliminaires à 7 mètres, sur l'argent, ces mesures ont été poursuivies à une distance de vol de 14 mètres sur l'or, le Rhodium et récemment sur le Xénon et le Gadolinium.

Le détecteur consiste en une couronne de 16 compteurs à BF_3 à faible "jitter". Il est actuellement en cours de modification pour doubler le nombre de compteurs et donc accroitre l'efficacité de détection.

Parallèlement à ces travaux, d'autres détecteurs sont étudiés en laboratoire.

22.2.3. Analyse des résultats expérimentaux

22.2.3.1. Plutonium-239: quelques données ont déjà été publiées (2)(3) mais l'analyse des résultats se poursuit encore: l'analyse des résonances individuelles parait possible jusqu'à 200 eV pour la fission et 400 eV pour la transmission. D'une façon générale, la réévaluation de l'effet Doppler signalée plus haut conduit à une légère réduction de la largeur naturelle des résonances. De cette analyse, qui pour le moment reste encore assez partielle, il résulte que:
Les effets expérimentaux ont peu d'effet sur la perte des niveaux jusqu'à 200 eV (fig. 22.6.).
La loi de distribution des espacements et celle des largeurs neutroniques réduites sont en bon accord avec les loi théoriques (fig. 22.7. et 22.8.) ce qui semble montrer que la perte de petits espacements et de petits niveaux est beaucoup plus faible que dans l'^{235}U.
La fonction densité, mesurée entre 0 et 200 eV est de:

$$S_o = (1.3 \pm 0.2).10^{-4}$$

Elle est plus élevée que celle déduite de 0 à 50 eV

($So = 1.10^{-4}$) ou de 100 à 200 eV ($So = 1.10^{-4}$).
L'histogramme $\Sigma \quad 2g\Gamma_{n^o}$ pour les résonances situées à une énergie plus basse que E, en fonction de E suggère une variation de la valeur locale de la fonction densité So (fig. 22.9.).
La distribution des largeurs de fission Γ_f (fig. 22.10.) est incompatible avec une famille unique. Au contraire elle suggère l'existence de deux familles ayant des valeurs moyennes très différentes ($< \Gamma_f >= 45$ MeV et $< \Gamma_f > = 750$ MeV). Un classement des résonances suivant leur largeur de fission serait en très bon accord avec les mesures de spins faites à Livermore et la distribution en masse des produits de fission dans les résonances étudiées à Los Alamos. Ces trois mesures justifient la théorie de Bohr, dans le sens que les résonances de spin 0 sont larges et de fission plus symétrique que les résonances de spin 1 qui sont plus étroites.

22.2.3.2. <u>Détermination du spin des résonances du ^{103}Rh et de l'^{197}Au</u> (6)(7)

Par la mesure de diffusion, on mesure la surface A en dessous du pic de résonance pour plusieurs épaisseurs d'échantillons et on en déduit la surface Ao extrapolée à l'épaisseur nulle des échantillons, soit graphiquement, soit par un programme de correction de la diffusion multiple.

Pour l'or et le Rhodium les résultats obtenus sont consignés dans le tableau 22.2.

Il semble que les fonctions densités So soient différentes pour les deux états de spin du ^{103}Rh;
$So = (0.6 \pm 0.27)10^{-4}$ pour les résonances de spin 1 et
$So = (0.22 \pm 0.20)10^{-4}$ pour les résonances de spin 0.
La probabilité qu'elles soient égales est de 11 % seulement. La fonction densité moyenne pour l'ensemble des résonances est:

$$So = (0.52 \pm 0.18).10^{-4}$$

La détermination du spin des résonances de l'^{197}Au (de spin 3/2) bien que plus difficile à cause de la

valeur plus élevée du spin du noyau cible, est en accord avec d'autres mesures publiées récemment.

22.2.3.3. Neptunium-237

Une analyse de la section efficace totale est en cours.

22.2.3.4. Thorium-232

Les résultats sont présentés dans la référence (8).
Les principaux résultats sont les suivants:
265 niveaux ont été identifiés avec certitude au-dessous de 3 KeV ($\overline{D}$ = 11.3 eV) mais il semble que beaucoup de niveaux ne sont pas détectés.
En séparant les ondes "s" et "p" par comparaison de la distribution expérimentale des Γ n° avec une loi de Porter-Thomas à un degré de liberté, on trouve:
$S_o = (0.90 \pm 0.08).10^{-4}$
$S_1 = (3.8 \pm 1.5).10^{-4}$
$\Gamma\gamma$ a été obtenu pour 14 niveaux conduisant à $\langle\Gamma\gamma\rangle$ = 21.9 MeV.

22.3. Groupe des neutrons rapides

J.L. Leroy

Ces expériences ont été effectuées auprès du Van de Graaff 5 MeV par D. Abramson, A. Arnaud, J.C. Bluet, E. Fort, J. Gentil, D. Hebert, C. Le Rigoleur, J.L. Leroy, I. Szabo.

22.3.1. Mesure absolue de flux de neutrons rapides par la méthode de la particule associée

Le principe de cette méthode a déjà été décrit (EANDC(E)33). En utilisant le faisceau pulsé, la particule ^{3}He associée aux neutrons dans la réaction (p,t) a pu être séparée des protons et des tritons parasites. De cette façon une mesure préliminaire de l'efficacité du scintillateur détectant les neutrons par la réaction ^{6}Li(n,α)T a été faite pour une énergie de 250 keV. Toutefois les règlages à faire sont extrêmement délicats et on est obligé de limiter sévèrement l'intensité du faisceau pour éviter les empilements des particules parasites. Pour rendre la méthode tout à fait opérationnelle, on envisage maintenant de construire

un analyseur électro-statique rudimentaire qui permettrait de séparer les particules ^{3}He du bruit de fond constitué par les protons et les tritons.

22.3.2. Section efficace d'activation du Rhodium

La section efficace d'excitation du Rhodium par diffusion inélastique d'un état isomérique produisant un rayon X de 20 keV, a été mesurée pour les énergies de neutrons suivantes: 125 keV, 250 keV, 500 keV, 105 MeV et 2 MeV. Le flux neutronique a été déterminé pendant l'irradiation de l'échantillon de Rhodium, au moyen d'un scintillateur de verre au Lithium.
La mesure absolue de l'activité prise par l'échantillon a été faite par MM. Campan et Despretz du S.E.C.N.R.: les résultats sont en cours d'analyse.

22.3.3. Etudes de distributions angulaires de neutrons diffusés

On a terminé le dépouillement des clichés de la chambre à brouillard concernant la distribution angulaire des neutrons de 1 MeV sur l'hydrogène. Cette expérience avait pour but de contrôler la technique de mesure sur une distribution parfaitement isotrope. On a trouvé un résultat isotrope, à l'erreur statistique près lorsque cos x est compris entre 0.2 et - 1 (x angle de diffusion dans le système du centre de masse). Lorsque cos x est plus grand que 0.2, les traces deviennent peu visibles et ne sont pas toutes mesurées. La méthode semble donc correcte pour les grands angles.
La distribution angulaire des neutrons de 14 MeV par ^{4}He, mesurée au moyen de cette technique (fig. 22.11.) n'est pas en bon accord avec le résultat obtenu précédemment par Seagrave (Phys. Rev. 92, 1222, 1953). L'ensemble des résultats obtenus sera publié prochainement.

22.3.4. Pulsation du faisceau du Van de Graaff

La pulsation de la source d'ions fonctionne de façon satisfaisante. Un dispositif de regroupement magnétique permettant de comprimer les bouffées délivrées par la source jusqu'à 1,5 ns est en cours de mise au point

et devrait pouvoir être utilisé dès Mars 1966.

22.3.5. Mesure du temps de ralentissement des neutrons rapides dans une plaque de matière hydrogénée

Cette mesure a été conduite par le "Groupe des neutrons intermédiaires" (R. Bayer) afin de vérifier les calculs, effectués par une méthode de Monte-Carlo, sur le temps de ralentissement des neutrons dans le modérateur entourant la cible de l'Accélérateur Linéaire d'électrons. La mesure consiste à injecter, dans une plaque de modérateur, un faisceau pulsé (10 ns) de neutrons monoénergétiques. Sur la face opposée, un corps présentant une importante résonance de capture à basse énergie permet, par détection des γ de capture, l'analyse de la distribution en temps des neutrons sortant ayant l'énergie de la résonance. Des résultats préliminaires ont été obtenus.

LISTE DES PUBLICATIONS

(1) C. SIGNARBIEUX, M. RIBRAG, Physics and Chemistry of Fission, Conférence AIEA (1965), Vol. I, 561

(2) J. BLONS, H. DERRIEN, A. MICHAUDON, P. RIBON, International Conference on the study of nuclear structure with neutrons, P/163, Anvers (1965)

(3) J. BLONS, H. DERRIEN, A. MICHAUDON, P. RIBON, G. DE SAUSSURE, C.R. Ac. des Sciences, à paraitre

(4) G. DE SAUSSURE, J. BLONS, C. JOUSSEAUME, A. MICHAUDON, Y. PRANAL, Physics and Chemistry of Fission, Conférence AIEA (1965), Vol. I, 205

(5) G. DE SAUSSURE, J. BLONS, C. JOUSSEAUME, A. MICHAUDON, Y. PRANAL, C.R. Ac. des Sciences, 259, 3498 (1964)

(6) P. RIBON, A. LOTTIN, A. MICHAUDON, J. TROCHON, International Conference on the study of nuclear structure with neutrons, P/165, Anvers (1965)

(7) J. TROCHON, A. LOTTIN, P. RIBON, C.R. Ac. des Sciences, à paraitre

(8) P. RIBON, M. SANCHE, H. DERRIEN, A. MICHAUDON, International Conference on the study of nuclear structure with neutrons, P/166, Anvers (1965)

(9) A. MICHAUDON, Some statistical properties of the interaction of resonance neutrons with U-235, A.P.S. meeting, Washington (Avril 1965), invited paper

(10) H. NIFENECKER, G. PERRIN, Physics and Chemistry of Fission, Conférence AIEA (1965), Vol. 1, 245

(11) C. LE RIGOLEUR, J.C. BLUET, J.L. LEROY, International Conference on the study of nuclear structure with neutrons, P/167, Anvers (1965)

(12) J.C. BLUET, J.L. LEROY, International Conference on the study of nuclear structure with neutrons, P/168, Anvers (1965).

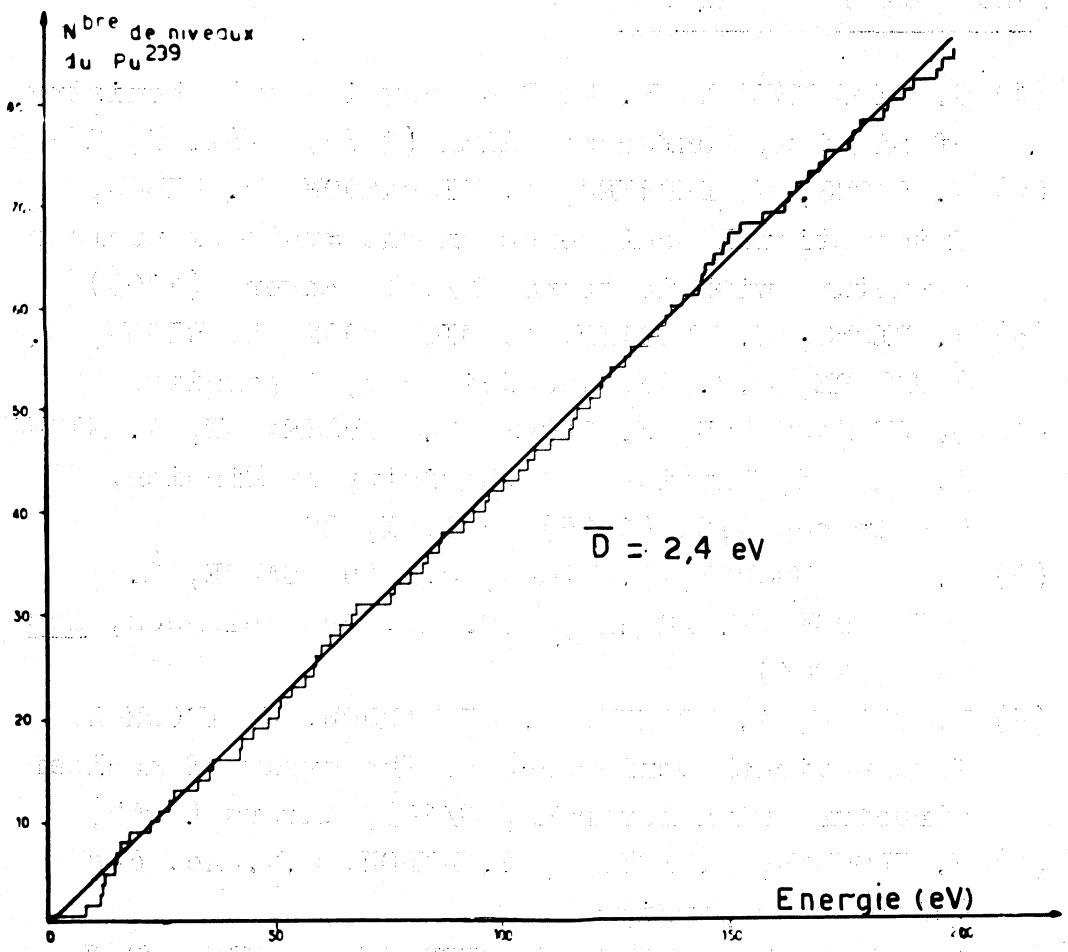

Fig. 22.6.

TRANSMISSION DU Pu-239

Conditions Expérimentales

Gamme d'énergie (en eV)	de 4 à 80	de 70 à 200	de 150 à 1.200
Longueur de vol (en mètres)	53,7	53,7	103,7
Accélérateur : f = 500c/s Δt (μsec)	0,11 ou 0,2	0,065 ou 0,11	0,065
Largeur de canal du sélecteur de temps de vol Δt (μsec)	variable de 0,1 à 0,8	0,05	0,05
Résolution (compte tenu du temps de ralentissement)	4,3 ns/m à 50 eV	2,8 ns/m à 100 eV	0,78 ns/m à 500 eV
Taux de comptage par canal et par heure	800 par canal de 0,1 μs à 50 eV	90 par canal de 0,05 μs à 100 eV	110 par canal de 0,05 μs à 500 eV
Température de l'échantillon	T = 77°K	T = 77°K	T = 77° K

Tableau 22.1.

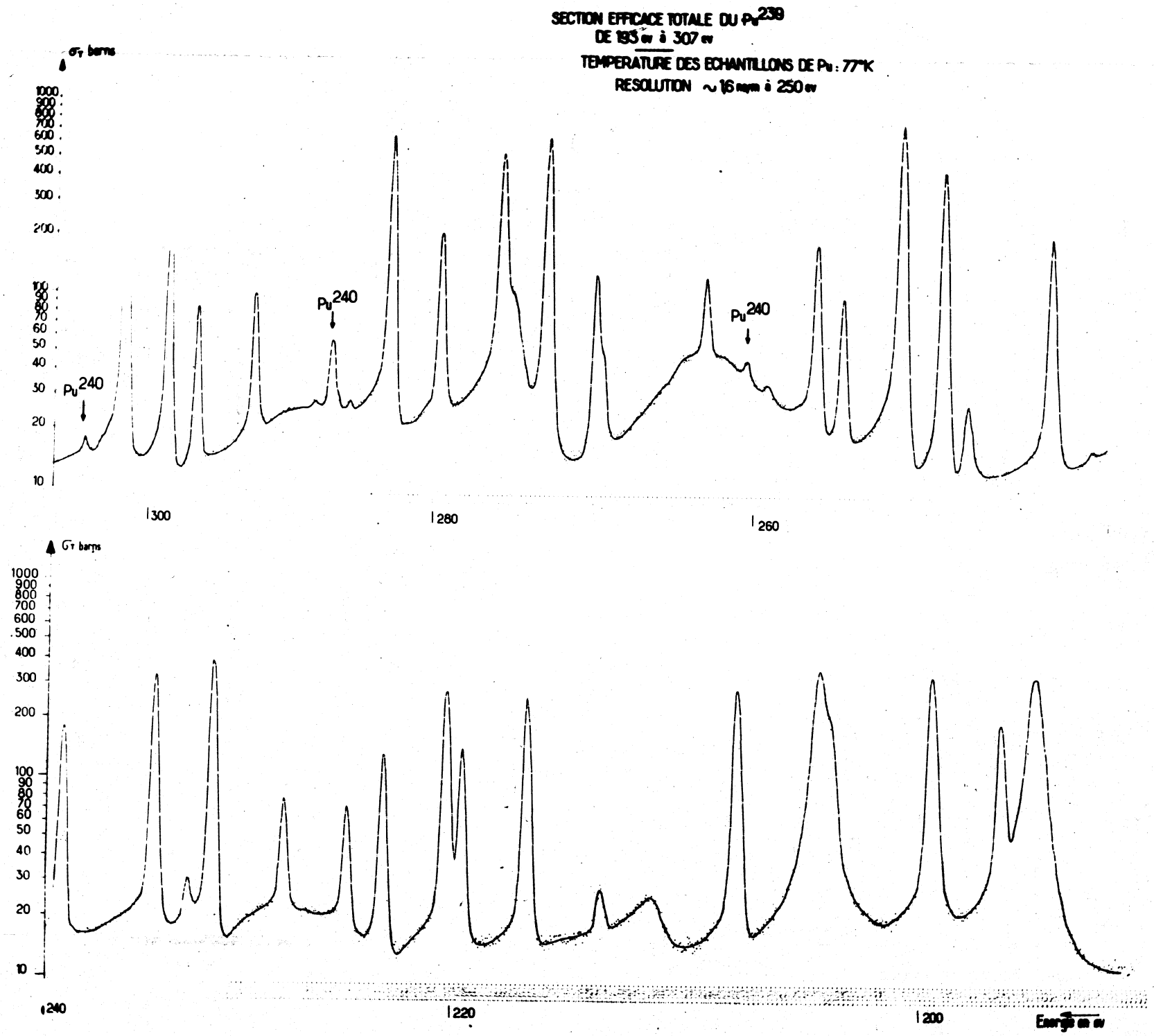
SECTION EFFICACE TOTALE DU Pu239
DE 195 ev à 307 ev
TEMPERATURE DES ECHANTILLONS DE Pu : 77°K
RESOLUTION ~16 mm à 250 ev
σT barns
Pu240
Pu240
Pu240
1300
1280
1260
σT barns
1240
1220
1200
Energie en ev

Fig. 22.1.

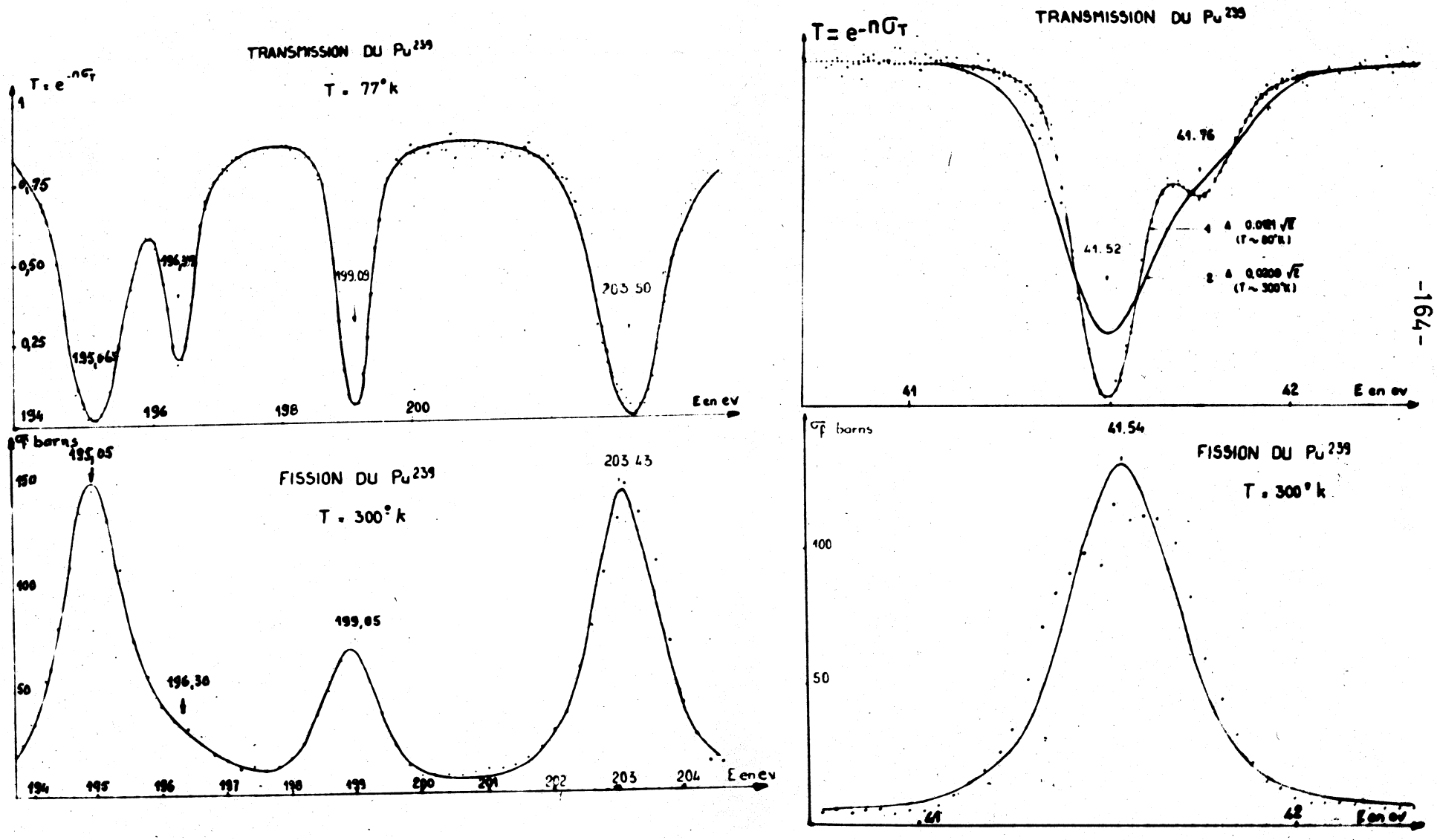
TRANSMISSION DU Pu239
T = 77°k
T = e-nσT
1
0,75
0,50
0,25
195,065
196,375
199.09
203 50
194
196
198
200
E en ev
σf barns
195,05
150
100
50
FISSION DU Pu239
T = 300° k
196,30
199,05
203 43
194
195
196
197
198
199
200
201
202
203
204
E en ev
TRANSMISSION DU Pu239
T = e-nσT
41.76
41.52
41
42
E en ev
σf barns
41.54
FISSION DU Pu239
T = 300° k
100
50
41
42
E en ev

Fig. 22.2.

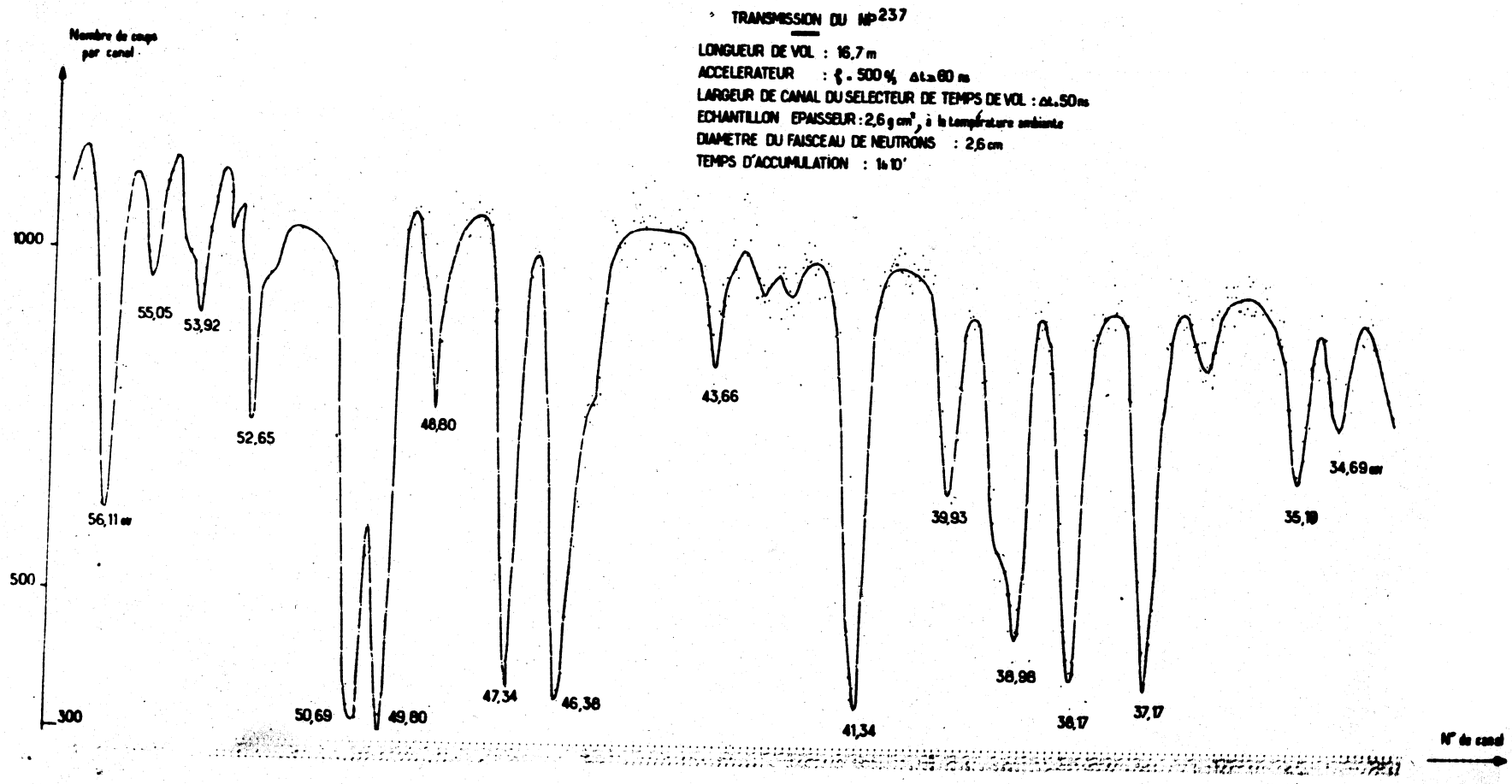
TRANSMISSION DU Np237
LONGUEUR DE VOL : 16,7 m
ACCELERATEUR : ξ = 500 % Δt = 60 ns
LARGEUR DE CANAL DU SELECTEUR DE TEMPS DE VOL : Δt = 50 ns
ECHANTILLON EPAISSEUR : 2,6 g cm², à la température ambiante
DIAMETRE DU FAISCEAU DE NEUTRONS : 2,6 cm
TEMPS D'ACCUMULATION : 1h 10'
Nombre de coups par canal
1000
500
300
56,11 ev
55,05
53,92
52,65
50,69
49,80
48,80
47,34
46,38
43,66
41,34
39,93
38,98
38,17
37,17
35,19
34,69 ev
N° de canal

Fig. 22.3.

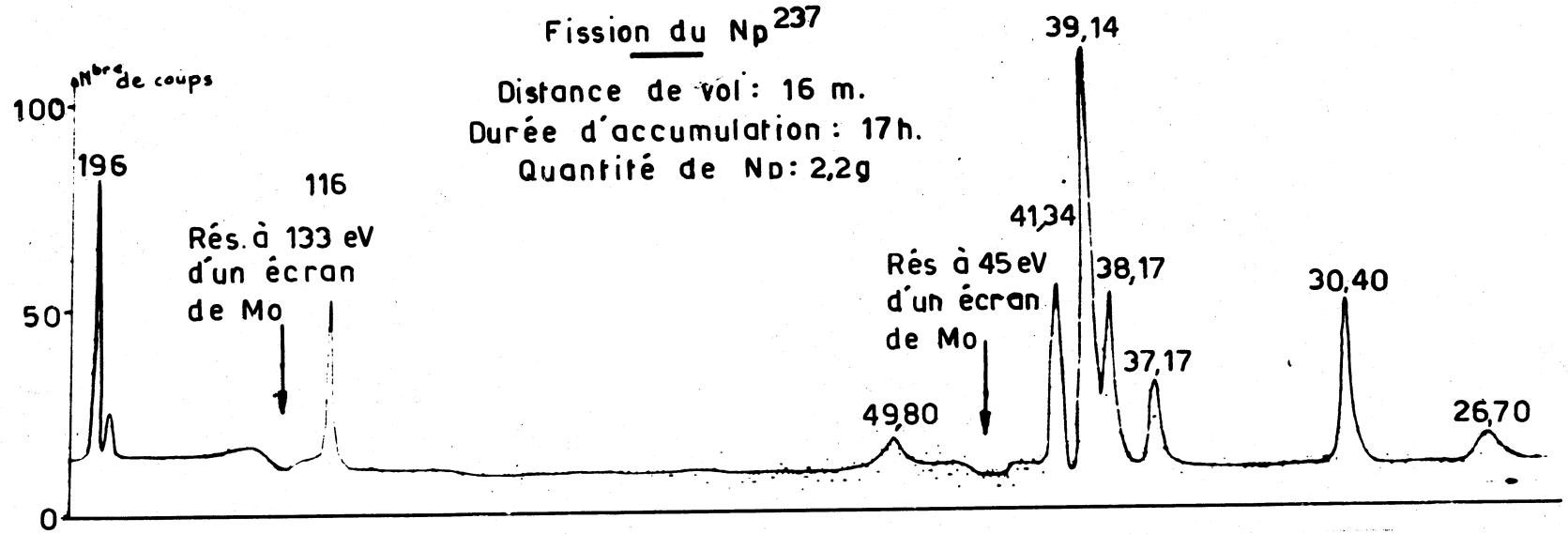

Fig. 22.4.

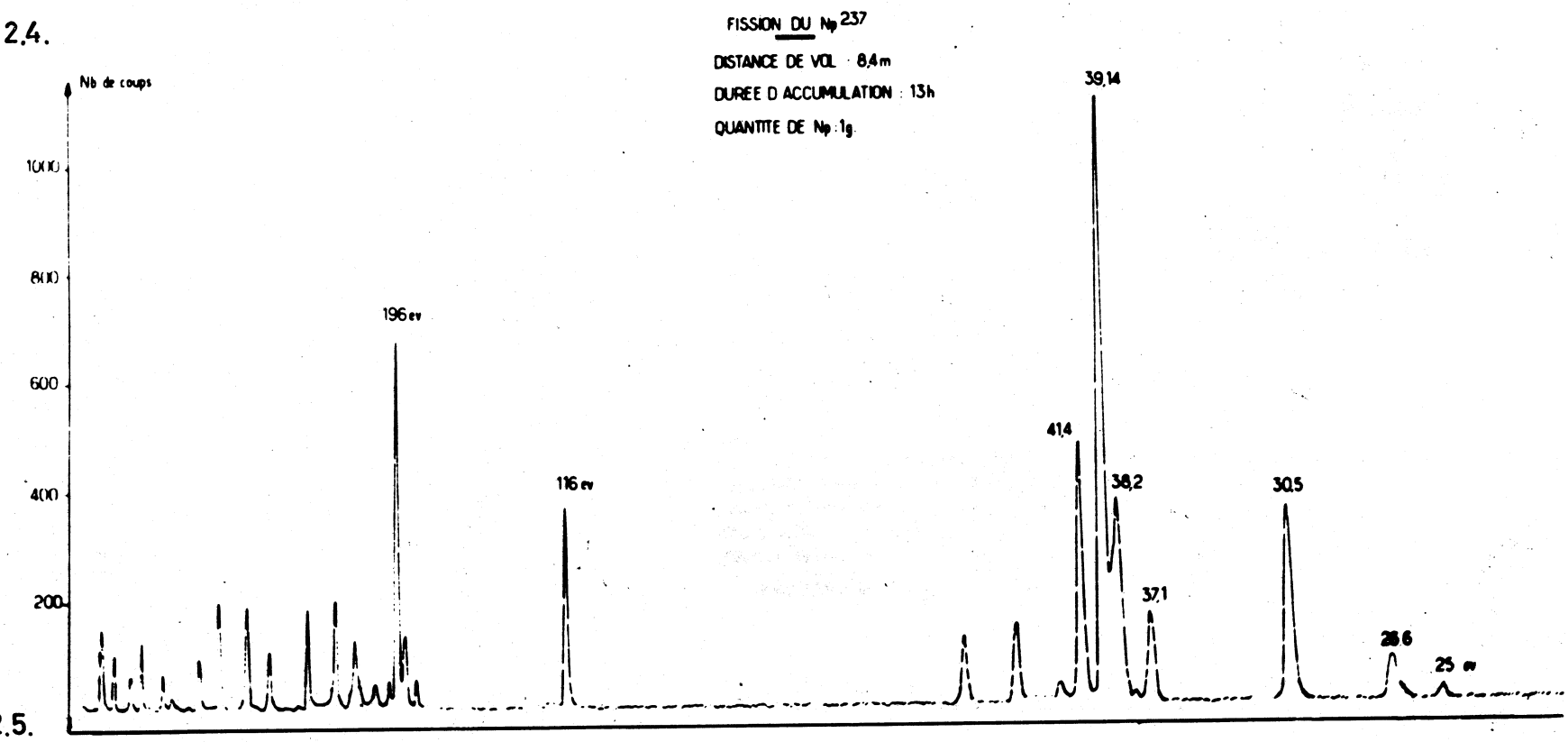

Fig. 22.5.

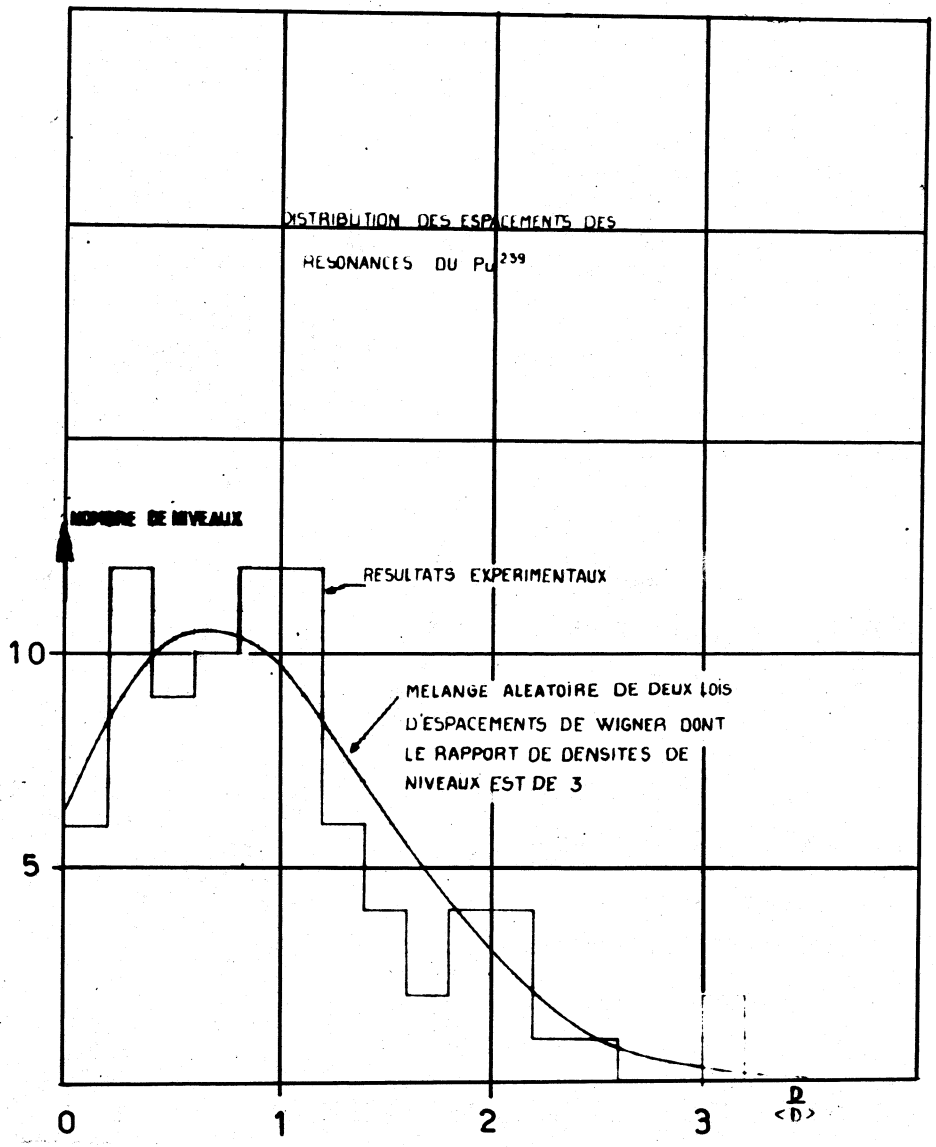

Fig. 22.7.

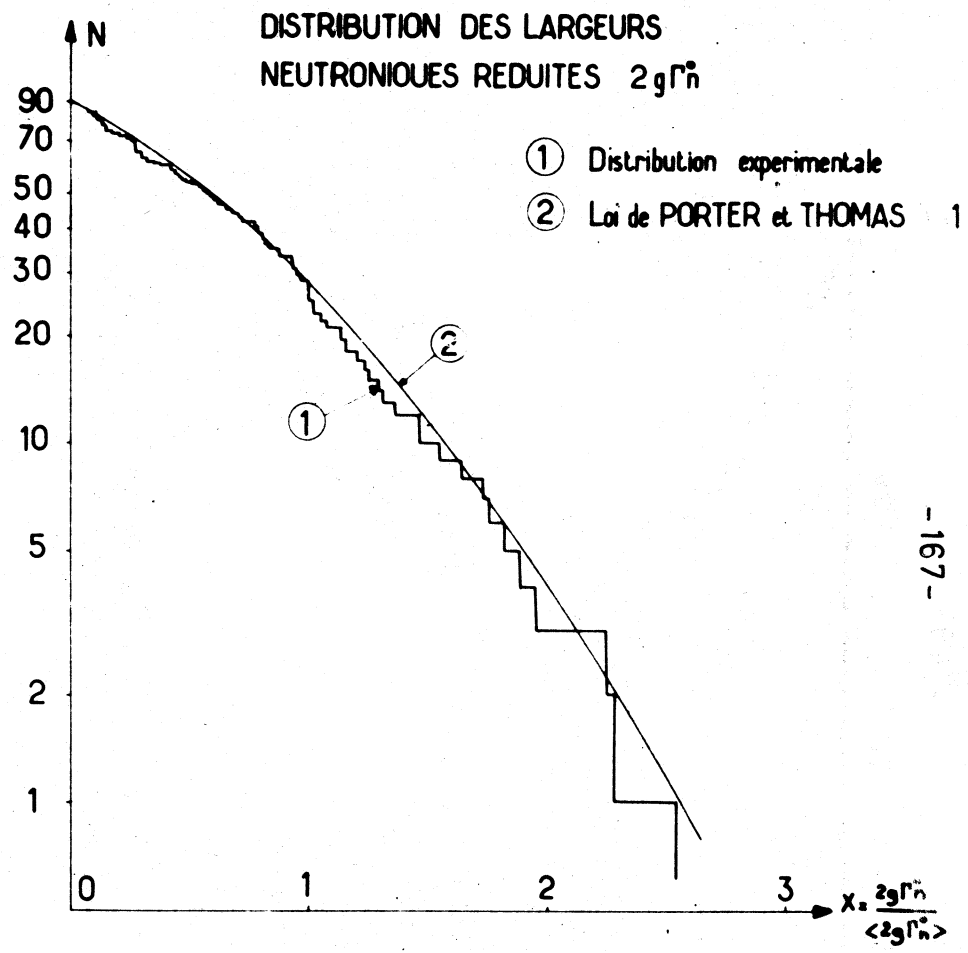

Fig. 22.8.

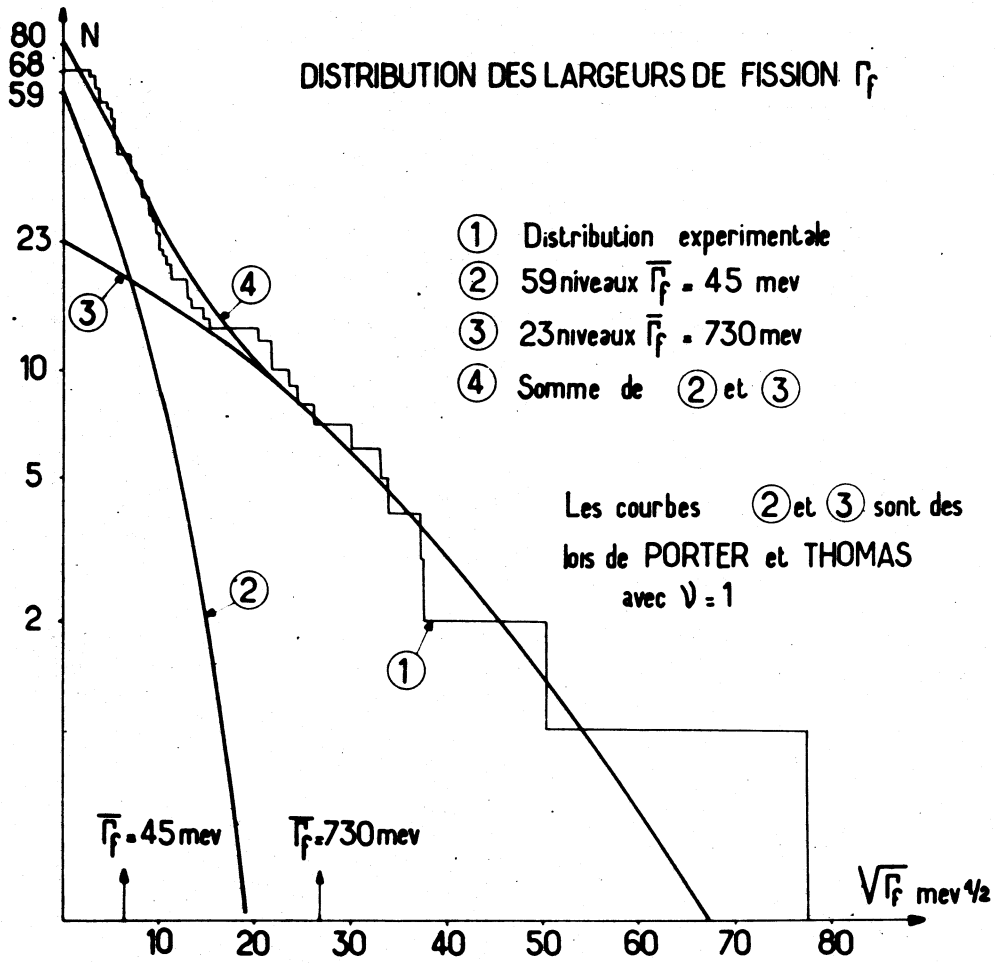

Fig. 22.10.

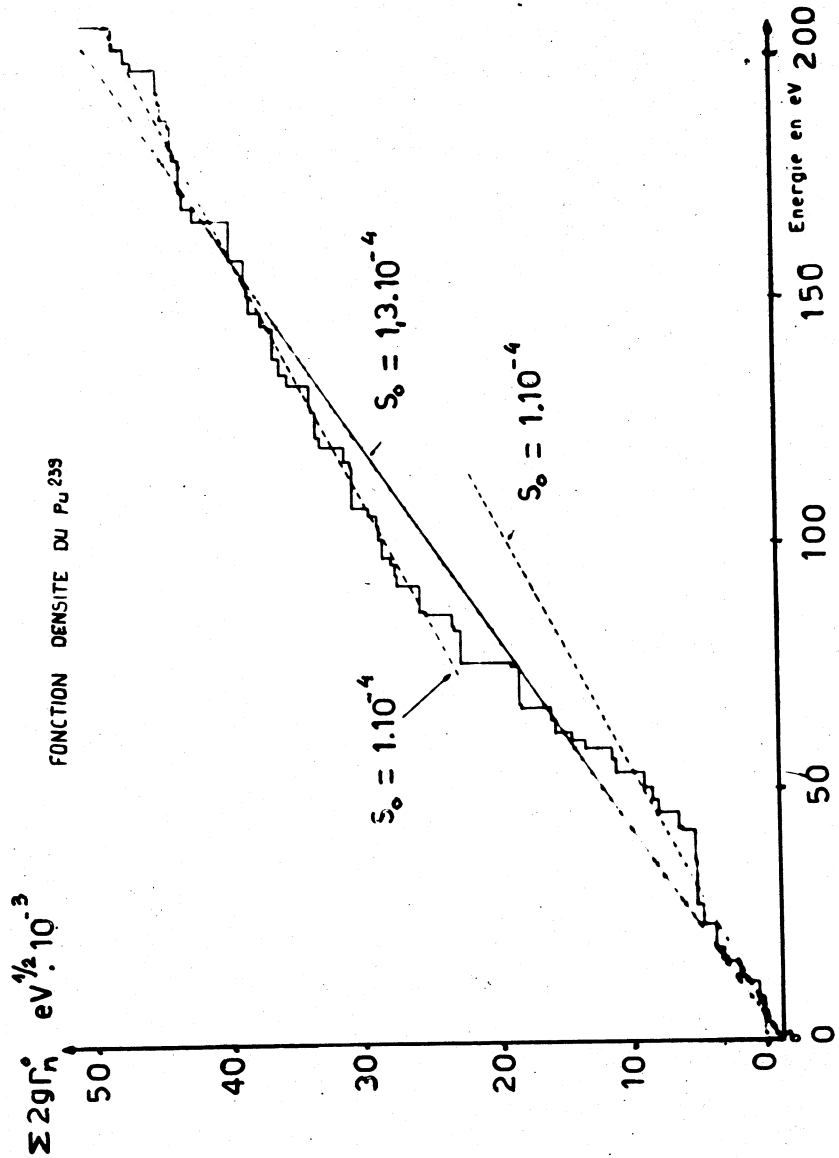

Fig. 22.9.

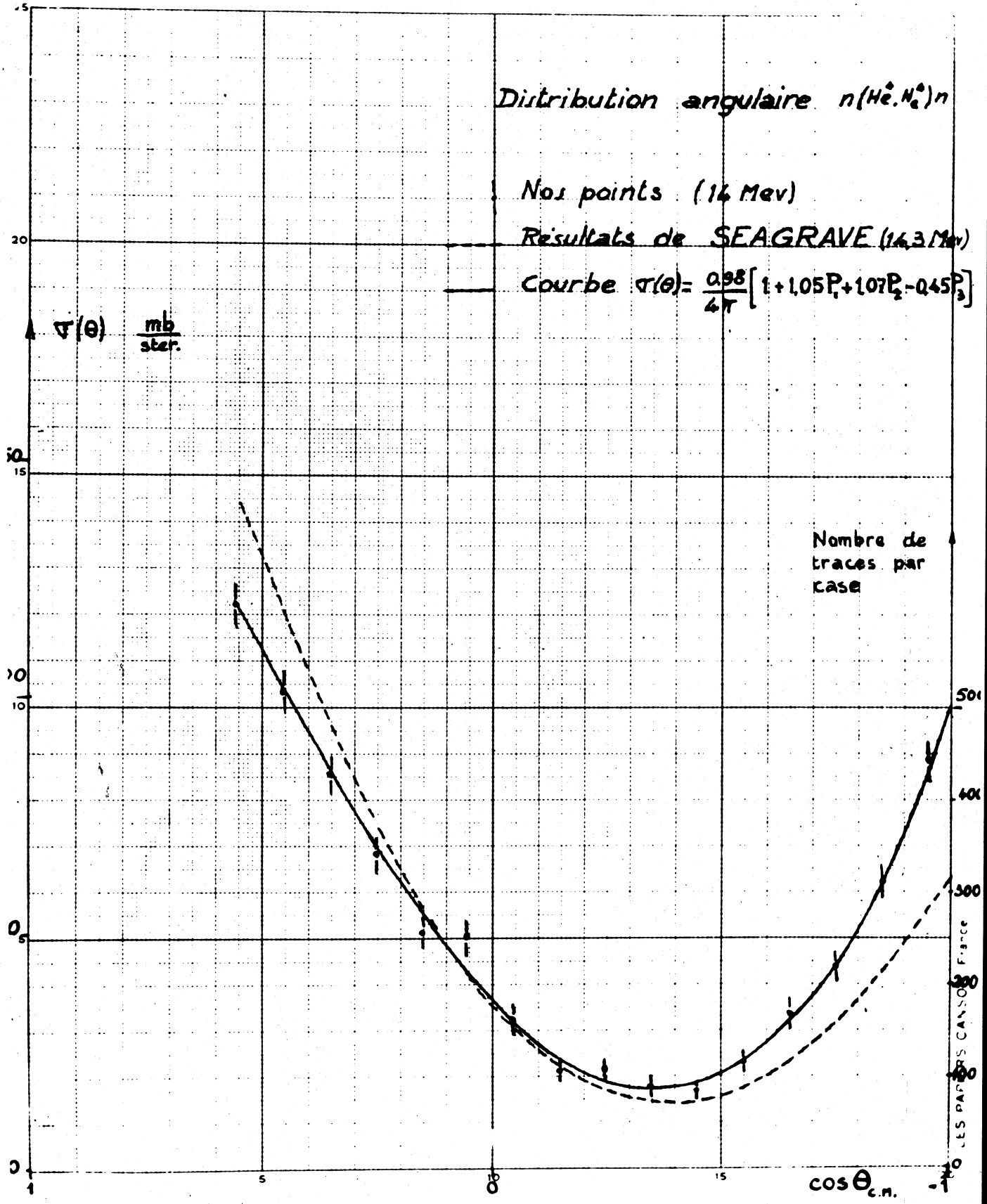
Distribution angulaire n(He4.He4)n
Nos points (14 Mev)
Résultats de SEAGRAVE (14,3 Mev)
Courbe σ(θ)= 0,98/4π [1+1,05P1+1,07P2-0,45P3]
σ(θ) mb/ster.
Nombre de traces par case
cos θc.m.
20
15
10
5
0
1
5
10
15
20
-1
500
400
300
200
100
0

Fig. 22.11.

Paramètres des résonances du Rh-103

E eV	Γ MeV	2gΓn/MeV	Ao expérimental Ao	Ao expérimental ΔAo	Ao théorique g=1/4	Ao théorique g= 3/4	J trouv.
1,25	156	0,78					1*
46	177	0,76	0,35	0,15	0,3	0,1	(0)
95	170	3,8	3	1	3,6	1,2	0
125	186	13	7	3	29,7	8,8	1
154	388	96	700	80	640	213	0
186	213	56	130	25	322	107	1
253	222	52	70	20	190	63	1
272	220	91,6	170	25	574	192	1
289	177	28,7	24	3	65	22	1
319	273	146,5	314	35	1040	347	1
406	213	22	5	1,5	24	8	1
435	431	309	780	100	2090	697	1
565	275	100	204	60	516	172	1
645	294	97	63	20	203	68	1
691	218	125	non résolues				
701	611	400					

Paramètres des résonances de Au-197

E eV	e = 0,05mm $A_N 10^2$	Ao	aire b/eV J = 1	aire b/eV J = 2	J
60,25	504	840	1420	850	2
78,4	27	33	33	20	1
151,2	46,7	57	97,3	58,2	2
162,9	132	162	126	76	1
190	85	104	108	65	1
240,3	215	272	520	310	2

Tableau 22.2.

23. DEPARTEMENT DE PHYSIQUE NUCLEAIRE, SERVICE DE PHYSIQUE NUCLEAIRE A BASSE ENERGIE, CEA, SACLAY (FRANCE)

E. Cotton

Les expériences décrites ici ont été effectuées auprès de l'Accélérateur Linéaire de 45 MeV par Mme S. de Baros MM. P. Chevillon, V.D. Huynh, J. Julien, G. Le Poitevin, J. Morgenstern, F. Netter, et C. Samour.

Les résultats obtenus proviennent de trois types d'expériences; transmission, capture totale, capture partielle. Les expériences de capture totale étant associées aux mesures de transmission pour la détermination du spin ne seront pas décrites.

23.1. Expérience de transmission

Trois longueurs de base de temps de vol sont utilisées suivant le domaine d'énergie étudié (53, 103 et 200 mètres). Les résolutions sont de l'ordre de 0.3 ns/m. Des expériences, avec l'excellente résolution de 0.1 ns/m, ont été réalisées pour étudier la structure de certains éléments ($A < 60$) dans un domaine d'énergie 100 - 400 keV. Les résultats obtenus peuvent se classer ainsi:

23.1.1. Variation de la fonction densité S_o des neutrons "s" en fonction du nombre de masse A et plus particulièrement au voisinage des valeurs $A \approx 55$, $A \approx 95$, $A \approx 140$, $A \approx 180$. La table 23.1. donne les valeurs S_o et la valeur de R' calculées à partir des paramètres des résonances individuelles. Les fig. 23.1. et 23.2. représentent les valeurs expérimentales comparées aux prédictions théoriques des différents modèles. A ces valeurs s'ajouteront les analyses des résultats (celles des éléments suivants: Al, K, Cl, Va, Cr, Ni, Sr, Mo, I, Sb, La, Gd, Tb, Tm). Les données expérimentales paraissent en accord avec les prédictions théoriques du modèle déformé.

23.1.2. Détermination de la fonction densité "p" S_1 déduite à partir des paramètres des résonances individuelles. La manière d'identifier les résonances "p" et "s" a déjà été décrite (1). Les noyaux étudiés ont été Sr, Y, Nb, Zr, Mo. La table 23.2. donne les valeurs des paramètres des résonances pour Nb.

23.1.3. Dépendance de la fonction densité en fonction du spin. Cet effet déjà mis en évidence (2,3,4,5) a été systématiquement étudié pour d'autres noyaux de spin I = 3/2 (6) tels que Cl, K, Cu, Rb, Ba, Gd, Tb. Les tables 23.3. et 23.4. donnent les résultats des paramètres non encore publiés pour Cu et Ba. La table 23.5. résume les résultats connus. Il serait intéressant que les équipes réalisant des expériences de diffusion déterminent les spins des résonances dans le domaine de faible énergie de noyaux tels que Ir, Tb, Gd. Les méthodes de capture totale ne permettant pas toujours, quand $g\Gamma_n$ est faible, de trouver la valeur correcte du spin J. Pour les noyaux cibles étudiés avec I = 1/2, on ne constate aucune dépendance (Y, Tm, ^{195}Pt, ^{183}W) (7,8).

23.1.4. Etude des fluctuations de la fonction densité S_o en fonction de l'énergie des neutrons. Une telle fluctuation, explicable peut-être en termes de structure intermédiaire, a été mise en évidence pour le cobalt dans le domaine 0 à 80 keV. La table 23.6. donne les paramètres des résonances de Co et sur la fig. 23.3. (10) est tracée la quantité $\Sigma\Gamma_n^o$ en fonction de l'énergie des neutrons pour les deux états de spin. On trouvera, dans la référence (9), des valeurs de paramètres de noyaux situés dans la même région de nombre de masse.

De nouvelles expériences avec une base de temps de vol de longueur 200 mètres, des impulsions de neutrons de 20 ns et des canaux de temps de 10 ns ont été réalisées pour préciser de telles fluctuations sur un plus grand domaine d'énergie (30 à 400 keV). Pour les éléments de nombre de masse $A \leq 70$, les effets de structure sont étudiés à partir des résonances individuelles et, pour les éléments plus lourds $A \geq 100$, ces effets sont étudiés en fonction des valeurs de la section efficace totale $\langle\sigma_t\rangle$.

23.1.5. Les différents types d'expériences réalisées, associés à des méthodes d'analyse très sensibles, permettent de déterminer la valeur du spin pour un grand nombre de résonances et de n'omettre qu'une très faible quantité de niveaux.

Il est donc possible de comparer le rapport du nombre de niveaux de spin I + 1/2 et I - 1/2. Pour des noyaux-cibles I = 1/2 (^{195}Pt, ^{183}W, Tm, Ag) la valeur du spin a été trouvée pour 120 résonances. Les résultats trouvés sont en accord avec la loi 1/(2J + 1). On a vérifié aussi un tel accord pour les noyaux I = 3/2 et I = 5/2. Deux noyaux de spin I = 9/2 ont été étudiés (In et Bi) pour déterminer l'importance du terme exponentiel, mais nos résultats ne sont pas encore définitifs pour être publiés ici.

23.1.6. Le faible nombre de résonances omises permet de tracer des courbes d'espacement de niveaux à peu près correctes et de pouvoir les comparer aux prédictions théoriques. Aussi, le manque de faibles espacements signalé par l'équipe de Columbia n'apparaît pas pour les noyaux étudiés ici avec une excellente résolution. La fig. 23.4. représente une telle distribution pour le thulium. 90 résonances ont été observées pour ce noyau entre 2 et 800 eV et le nombre de résonances omises est évalué à 2 ou 3 %. Un tel effet avait été trouvé pour l'or (5). Pour un noyau tel que Pr, nous trouvons dans le domaine d'énergie 500-4000 eV 17 résonances de plus que l'équipe de Columbia pour un espacement moyen D ≈ 70 eV. La distribution est naturellement fort différente. Un papier sur l'ensemble des résultats obtenus dans ce domaine sera prochainement publié.

23.1.7. Variation de la largeur radiative totale en fonction du nombre de masse A. On trouvera ces résultats dans la référence (11). D'autres noyaux tels que Pd, In, I, Sb, Gd, Sm, Tb ... ont été étudiés pour obtenir un tracé plus continu de la courbe (fig. 23.5.) (13).

23.2. <u>Expériences de capture radiative</u>

Ces expériences sont réalisées soit avec des détecteurs conventionnels (cristaux NaI(Tl)), soit avec des diodes de germanium.

23.2.1. Un détecteur à état solide (jonction au germanium) de volume sensible 7 cm^3, fait à Argonne National Laboratory, est utilisé conjointement par notre groupe et H. Jackson

(ANL) en visite pour une durée d'un an à Saclay. La première expérience consiste à étudier la distribution des largeurs radiatives partielles pour une vingtaine de résonances de ^{195}Pt. La fig. 23.6. représente la courbe de temps de vol de capture, la résolution étant de 10 ns/m à 100 eV. Les fig. 23.7. et 23.8. représentent respectivement les spectres de gamma de capture pour la résonance 12 eV de ^{195}Pt (J = 1) et la résonance 96 eV de ^{198}Pt (J = 1/2).

23.2.2. Expériences de multiplicité V (nombre de rayons gamma émis par capture) pour déterminer la valeur du spin quand les méthodes classiques apparaissent insuffisantes. In, Ba, Sm ont été en particulier étudiés. La variation de V en fonction du nombre de masse est entreprise ainsi que l'obtention de quelques valeurs absolues.

23.2.3. Un effet de capture directe a été trouvé en étudiant le spectre de la résonance 4.8 eV de l'or. Les détails sont décrits dans les références (12) et (13). La fig. 23.9. représente l'effet obtenu. Une valeur de la section efficace potentielle de capture inférieure à 0.23 mb est obtenue de cette mesure.

23.2.4. Les spectres de nombreuses résonances dans ^{195}Pt ont été étudiés. Ainsi, il apparaît que le degré de liberté des distributions des largeurs radiatives partielles serait plus près de la valeur 2 que 1 (14, 13).

23.2.5. Effets de corrélations ou non dans la distribution des largeurs radiatives partielles de ^{183}W et ^{238}U (15, 13). Ces expériences seront reprises avec la jonction au germanium.

23.2.6. L'étude du spectre de nombreuses résonances dans Hg, Sn et Nb a été faite pour essayer d'expliquer les fluctuations de la largeur radiative totale de résonance à résonance ou en fonction du moment orbital du neutron. Il a été montré que des transitions dipolaires électriques favorisées pouvaient parfois expliquer ces fluctuations mais non systématiquement (13).

23.2.7. L'étude des spectres des rayons gamma de faible énergie a été faite pour l'attribution des isotopes responsables des résonances trouvées dans les expériences de transmission.

Citons les plus notables : Ag, In, Nd, Gd, Pt.

23.2.8. Conclusion

Les expériences de capture mettent en oeuvre un appareillage assez délicat. Un analyseur multidimensionnel ayant une capacité de 28 digits est utilisé dans ces expériences de capture, ainsi que divers circuits de stabilisation.

L'analyse des données expérimentales est un problème difficile à résoudre. Pour les expériences de transmission, outre les programmes déjà décrits dans les précédents rapports E.A.N.D.C., un programme écrit par G. Bianchi et C. Corge nous permet de traiter les résonances de haute énergie à l'aide du formalisme de la matrice R. La référence (16) expose les méthodes utilisées pour l'analyse des expériences de capture. On peut trouver des compléments plus détaillés dans les références (13, 17 et 18).

REFERENCES

(1) G. LE POITTEVIN et al, Nucl. Phys. 70, 497, 1965.
(2) J. JULIEN et al, Phys. Letters 3, 67, 1962.
(3) J. JULIEN et al, Phys. Letters 10, 86, 1964.
(4) J. JULIEN et al, Nucl. Phys. 66, 433, 1965.
(5) J. JULIEN et al, Nucl. Phys., in press.
(6) A publier.
(7) S. DE BARROS, Thèse de Doctorat d'Université.
(8) A publier.
(9) J. MORGENSTERN et al, Intern. Conf. Antwerpen, 19-23 July 1965.
(10) J. MORGENSTERN et al, Nucl. Phys. 62, 529, 1965.
(11) S. DE BARROS et al, Intern. Conf. Antwerpen, 19-23 July 1965.
(12) V.D. HUYNH et al.
(13) V.D. HUYNH, Thèse de Doctorat d'Etat, Université de Paris, Rapport C.E.A. n° 2810.
(14) V.D. HUYNH, Intern. Conf. Antwerpen, 19-23 July 1965.
(15) C. SAMOUR
(16) V.D. HUYNH et al, Nucl. Instr. Methods 36, 29, 1965.
(17) G. LE POITTEVIN, Thèse de 3ème cycle, Université de Paris, 1965.
(18) M. VASTEL.

LEGENDES DES FIGURES

23.1. Variation de la fonction densité S_o en fonction du nombre de masse et comparaison avec les différents modèles théoriques.

23.2. Variation de la longueur de diffusion R' en fonction du nombre de masse.

23.3. Variation de la quantité $\Sigma_o g \Gamma_n^o$ en fonction de l'énergie pour le cobalt (^{59}Co + n).

23.4. Histogramme de la distribution des espacements pour le thullium.

23.5. Variation de Γ_γ en fonction du nombre de masse.

23.6. Spectre de temps de vol obtenu dans des expériences de capture avec une diode au germanium. Noyau étudié Pt (10 à 500 eV).

23.7. Spectre de rayonnement de capture de la résonance 12 eV de ^{195}Pt obtenu avec une diode au germanium.

23.8. Spectre de rayonnement de capture de la résonance 96 eV de ^{198}Pt obtenu avec une diode au germanium.

23.9. Détermination de la section efficace potentielle de capture dans le cas de l'or par comparaison de l'intensité de rayonnement de capture en fonction de l'énergie.

TABLE 23.1.

Valeurs de la fonction densité S_o et de la longueur de diffusion R' en fonction du nombre de masse

Element	Strength function S_o (in 10^{-4} $eV^{-1/2}$ unit)	Scattering length R' (in 10^{-13} cm unit)
Mn^{55} (4)	4 ± 0.9	3.6 ± 0.4
Co^{59} (4,5)	$3^{+0.8}_{-0.7}$	5.4 ± 0.5
Cu^{63} (6)	$2^{+0.7}_{-0.5}$	7 ± 0.8
Cu^{65} (6)	$1.3^{+0.7}_{-0.5}$	7 ± 0.8
Ga^{69} (7)	1,2 ± 0.45	6.3 ± 1
As^{75} (7)	1.75 ± 0.35	7 ± 0.8
$Br^{79,81}$ (8)	1.5 ± 0.3	7 ± 0.8
Se^{77} (9)	1.5 ± 0.5	
Y^{89} (10)	0.6 ± 0.25	6.6 ± 0.7
Zr^{91} (11)	0.45 ± 0.2	7 ± 1
Nb^{93} (12)	0.35 ± 0.1	7.1 ± 0.3
Ba^{135} (13)	$1.1^{+0.8}_{-0.45}$	
Ba^{137} (13)	$0.9^{+0.8}_{-0.45}$	
Pr^{141} (11)	3.9 ± 0.8	5.6 ± 1.5
Nd^{143} (14)	5 ± 2	
Nd^{145} (14)	4.5 ± 1.5	10 ± 1.5
W^{183} (15)	1.8 ± 0.4	
Pt^{195} (9)	2.2 ± 0.45	9.3 ± 0.8
Au^{197} (16)	1.8 ± 0.3	8.7 ± 0.4
Hg^{199} (17)	1.9 ± 0.5	9.8 ± 0.7
Hg^{201} (17)	1.5 ± 0.5	9.8 ± 0.7

TABLE 23.2.

Valeurs des paramètres des résonances de Nb pour les moments angulaires I = 0 et I = 1.

E (eV)	$g\Gamma_n$ (meV)	$g\Gamma_n^0$ (meV)	ℓ
105,8	0,228	0,022	0
119	2	0,183	0
193	15,3	1,1	0
335,4	8,33	0,46	0
378,3	53,5	2,75	0
460,3	3,9	0,18	0
604,1	1,72	0,07	0
641,1	2,74	0,11	0
741,6	95,6	3,51	0
912,8	1,98	0,06	0
935,4	189,5	6,19	0
1009,6	243	7,64	0
1149,2	90,5	2,67	0
1175,7	151,5	4,41	0
1194,9	19,1	0,55	0
1229,8	20,3	0,58	0
1393,2	89,5	2,38	0
1452,5	443	11,6	0
1576,9	84	2,11	0
1654,6	29	0,71	0
1812,7	54,9	1,29	0
1834,1	354	8,26	0
1992,4	14,8	0,33	0
2023,7	378	8,4	0
2076,1	95	2,09	0
2158,7	166	3,57	0
2231,8	91	1,93	0
2421	1250	25,4	0
2637	1197	23,3	0
2923	144	2,66	0
2948	231	4,25	0
3352	143	2,46	0
3391	400	6,86	0
3520	499	8,41	0
3759	358	5,84	0
3973	454	7,3	0
4066	766	12	0

E (eV)	$g\Gamma_n$ (meV)	$g\Gamma_n^1$ (meV)	ℓ
35,9	0,054	109	1
42,2	0,044	72	1
94,3	0,180	87	1
184,3	0,1	16,5	1
244	1,2	137	1
319	1	76	1
392,6	1,25	66	1
500,9	2,65	104	1
672,3	4,42	109	1
678,3	1,1	26	1
721,5	8	180	1
757,7	1,33	29	1
953,4	6,38	96	1
1016,8	13,3	176	1
1127,9	8,8	100	1
1243,7	7,2	70	1
1283,7	6	58	1
1351,3	16,8	148	1
1355,3	6,5	55	1
1467,9	21,3	163	1
1530	7,7	57	1
1541,3	15	108	1
1557	8,3	59	1
1617	16,7	113	1
1678,5	2,3	15,6	1
1714	15,8	97	1
1768,5	15,0	91	1
1946	27	13,4	1
1982,4	4,7	22	1
2070,2	33	154	1
2118,8	27	121	1
2149,4	40	175	1
2186,4	11	48	1
2462	62,5	222	1
4019	46	80	1

TABLE 23.3.

Paramètres des résonances du cuivre pour des énergies inférieures à 15 keV.

E_0 eV	A	$g\Gamma_n$ (eV)	J	Γ (eV)	$g\Gamma_n^0$ (meV $^{1/2}$)	Γ_n^0 (meV $^{1/2}$)	Γ_γ meV
230	65	0,10±0,0005		0,260±0,02			240± 20
578	63	0,54±0,02	2	1,41±0,05	22,4	36	550±65
2 072	63	16,36	1	43,8	360	960	
2 565	65	10,5	2	16,6	207	328	
2 653	63	2,6	2	4,7	54	88	
3 984	65	8,8	1	25	139	400	
4 473	65	3,6	2	6,05	54	90	
4 564	69	5,96	1	17,7	88	250	
4 942	63	5,47	1	16	78	228	
5 489	63	24,5	2	41	330	555	
6 026	63	6,58	2	10,7	85	138	
6 577	65	17,1	2	28,6	210	352	
7 000							
7 236	63	0,37					
7 732	65	14,23	2	24	162	270	
7795	65	12,55	1	35	141	396	
8 092	63	56,6	2	96	618	1 060	
8 123	65	29,6	2	50	328	555	
8 549	65	3,78	1	10,5	41	114	
9422	63	23,4	2	40	240	412	
10 003							
10 016	63	33,3	1	95	330	932	
11 122	63	37,2	2	64	352	606	
12 891	63	9,3	1	25	82	220	
13 515	63	43,5	2	75	374	645	
13 614	65	50,9	2	87	437	748	

^{63}Cu + n — 13 résonances

$\sum \Gamma_n^0 (J=1) = 2.12$ (eV 1/2) ; $\sum \Gamma_n^0 (J=2) = 3.54$ (eV 1/2)

^{65}Cu + n — 12 résonances

$\sum \Gamma_n^0 (J=1) = 1.38$ (eV 1/2) ; $\sum \Gamma_n^0 (J=2) = 2.34$ (eV 1/2)

TABLE 23.4.

Paramètres des résonances du barium pour des énergies inférieures à 1 keV.

E(eV)	A	J	$g\Gamma_n$ MeV	Γ_n MeV	Γ MeV	Γ_γ MeV
24,27	135	1	5,89	16	120	104 ± 7
46,2						
57,2	134		24	24		
80	135	2	97,3	156	260	104 ± 7
86	135	2	40,5	65	172	107 ± 7
101	136	1/2	50	50	230	180 ± 15
103,97	135	1	61	162		
104,18	135	2	7	11		
220	135	2	45	72		
282	135	2	201	32	410 = 20	86 ± 30
314,9	135	2	20,8	33,3		
315,18	135	1	31,7	85		
375,5	135	2	14,1	22,5		
376	135	1	55	146		
378	130	1/2	1390	1390		
405	135	2	329	525	630	105 ± 20
418	137	2	410,6	656	740	84 ± 20
433	135	2	11,5	18,5		
447	130	1/2	310	310		
464	135	2	45	72		
499	134	1/2	58	58		
510	136	1/2	151	151		
525	130	1/2	300	300		
576	131	1	213	567	675	106 ± 20
580	130	1/2	2531	2531		
649	135	1	61,5	97		
651	135	2	66	105		
666						
669						
676						
721	135	2	47	75		
744	130					
831	134					
836	130					
880	135	2	740	1175		
891	130	1/2	1989	1989		
896	130	1/2	603	603		
940	135	1	169	467		

TABLE 23.5.

Valeurs de la fonction densité S_o en fonction du spin J pour quelques noyaux de spin I = 1/2 et probabilité d'obtenir un tel rapport entre elles en supposant la fonction densité indépendante du spin

Nuclei with $I = \frac{3}{2}$.

Nuclei. Number of detected levels and number of spin assignment.	Value of the strength function $eV^{-1/2}$ with spin assignment.	Probability of finding $S_o(J=1) = a\, S_o(J=2)$ when a is assumed to be equal to 1
$^{75}As + n$ { J = 2, J = 1 } 50 levels with 27 assignments.	$S_o = 2.5 \pm 0.6 \,.\, 10^{-4}$ $S_o = 1 \pm 0.3 \,.\, 10^{-4}$	∼ 0.01
$^{69}Ga + n$ { J = 2, J = 1 } 12 levels with 7 assignments.	$S_o = 1.8 \pm 0.9 \,.\, 10^{-4}$ $S_o < 0.4 \,.\, 10^{-4}$	
$^{79-81}Br + n$ { J = 2, J = 1 } 80 levels with 25 assignments.	$S_{o_{J=2}} / S_{o_{J=1}} \sim 2$	∼ 0.07 for both isotopes.
$^{197}Au + n$ { J = 2, J = 1 } 63 levels with 44 assignments.	$S_o = 2.46 \pm 0.53 \,.\, 10^{-4}$ $S_o = 1.17 \pm 0.3 \,.\, 10^{-4}$	∼ 0.02
$^{63}Cu + n$ { J = 2, J = 1 } 13 levels with 12 assignments.	$S_o = 2.6 \pm 1 \,.\, 10^{-4}$ $S_o = 1.56 \pm 0.8 \,.\, 10^{-4}$	
$^{66}Cu + n$ { J = 2, J = 1 } 12 levels with 11 assignments.	$S_o = 1.72 \pm 0.7 \,.\, 10^{-4}$ $S_o = 1 \pm 0.5 \,.\, 10^{-4}$	

For each presented nuclei the quantity $\Sigma\, g\Gamma^o_n$ for both spin assigments is equal to, or greater than 90 per cent of the quantity $\Sigma\, g\Gamma^o_n$ for all the detected levels.

Calculated probability assumes that the scattering reduced widths Γ^o_n has a χ^2 distribution with one degree of freedom.

TABLE 23.6.

Paramètres des résonances du cobalt pour des énergies inférieures à 80 keV

E_o (keV)	J	$g\Gamma_n$ (eV)	Γ_n (eV)	$g\Gamma^o_n$ (eV $^{1/2}$)	Γ^o_n (eV $^{1/2}$)
0,132	4	2,88	5,13	0,250	0,445
1,38					
2,85					
3,98		0,06 ± 0,04	-	0,001	
4,32	4	59 ± 5	105	0,90	1,60
5,00	3	290 ± 14	660	4,10	9,36
6,38		0,95 ± 0,30		0,012	
8,05	3	16,6 ± 1,2	38	0,185	0,423
8,75		0,36 ± 0,20		0,004	
9,09		1,05 ± 0,30		0,011	
10,70	4	36,5 ± 4	65	0,353	0,628
11,53		1,1 ± 0,30		0,010	
13,29	4	11,2 ± 1,5	20	0,097	0,172
15,65	3	30,7 ± 4	70	0,245	0,560
16,43	4	94,5 ± 7	168	0,728	1,30
19,75		1,15 ± 0,40		0,008	
21,96	3	306 ± 20	700	2,06	4,71
22,53	4	152 ± 16	270	1,01	1,80
24,44	3	145 ± 16	330	0,93	2,12
25,16	4	101 ± 20	180	0,64	1,12
25,95	4	11,2 ± 3	20	0,070	0,125
27,35	4	95,5 ± 0	170	0,58	1,03
29,43		5,0 ± 1		0,03	
30,10	4	180 ± 20	320	1,04	1,85
31,31	3	65,6 ± 10	150	0,37	0,845
31,76		4,25 ± 1,2		0,024	
32,67	3	57 ± 6	130	0,315	0,720
32,97	4	22,5 ± 4	40	0,124	0,220
34,51		2,5 ± 1		0,013	
34,82	4	141 ± 14	250	0,755	1,34
35,42		2,2 ± 1		0,012	
35,75		9,5 ± 2		0,050	
40,23		10 ± 2		0,050	
40,61		1,5 ± 1		0,007	
41,33		17 ± 3		0,084	
42,07		1,0 ± 0,5		0,005	
43,62		1,2 ± 0,5		0,006	
45,02	3 or 4	21,9 or 33,7	50 or 60	0,10 or 0,16	0,228 or 0,317
45,04	4 3	157 144,5	280 330	0,74 0,68	1,32 1,55
45,83	3 4	135 ± 15	310 240	0,63	1,44 1,12
46,63					
47,12	4	22,5 ± 4	40	0,10	
50,31	3	43,8 ± 7	100	0,20	0,457
51,96	4	270 ± 20	480	1,19	2,12
52,65	4	29,2 ± 4	52	0,127	0,228
53,53	3	219 ± 15	500	0,945	2,16
56,24	3	92 ± 9	210	0,390	0,89
57,74		10 ± 2		0,042	
58,94	3	149 ± 16	340	0,615	1,40
59,76	4	56,2 ± 9	100	0,230	0,408
61,08		40 ± 8		0,162	
62,80		22 ± 8		0,088	
66,04		37,5 ± 7		0,146	
68,58					
69,93	4	118 ± 12	210	0,447	0,795
71,36		25 ± 5		0,094	
71,72	3	157 ± 20	360	0,59	1,35
72,33	4	73 ± 10	130	0,27	0,48
74,57		20 ± 5		0,07	
76,95		170 ± 25		0,61	

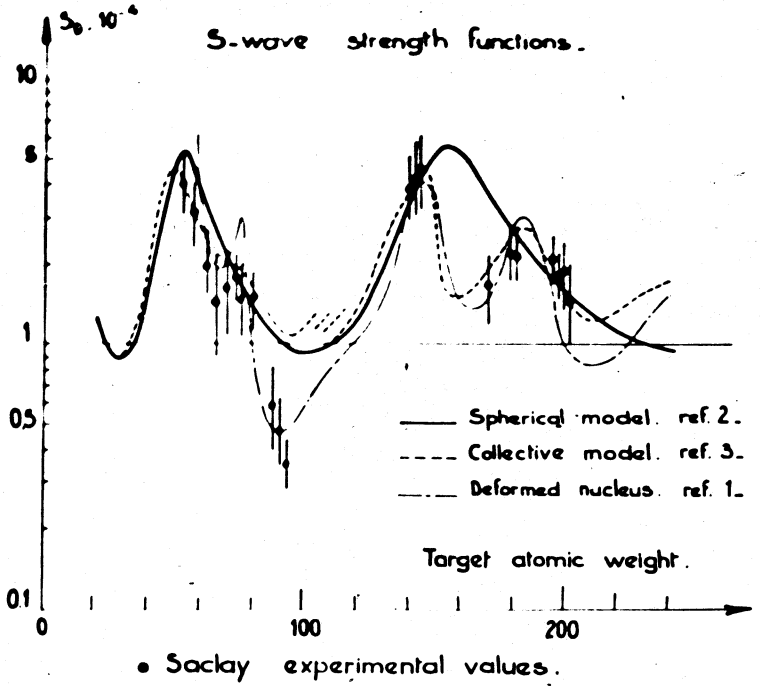

Fig. 23.1.

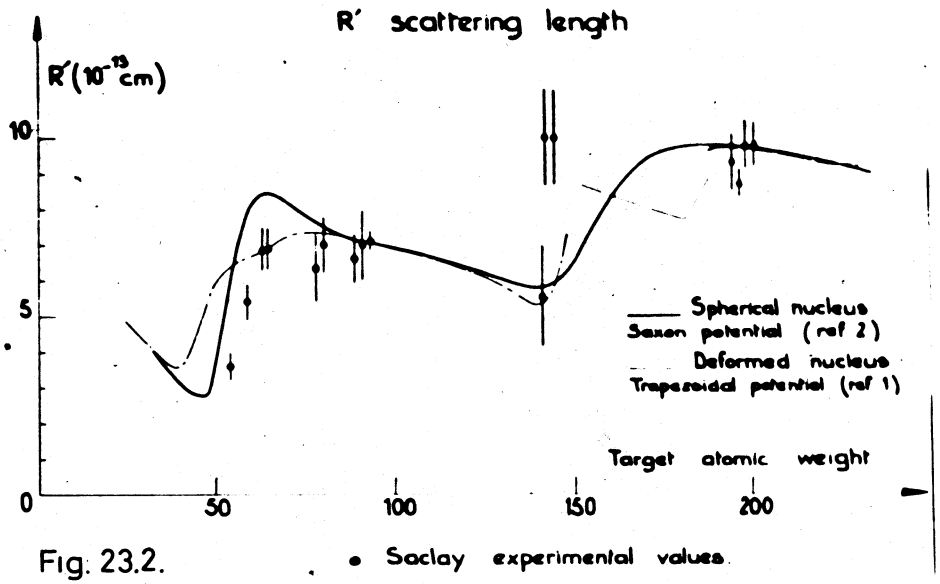

Fig. 23.2.

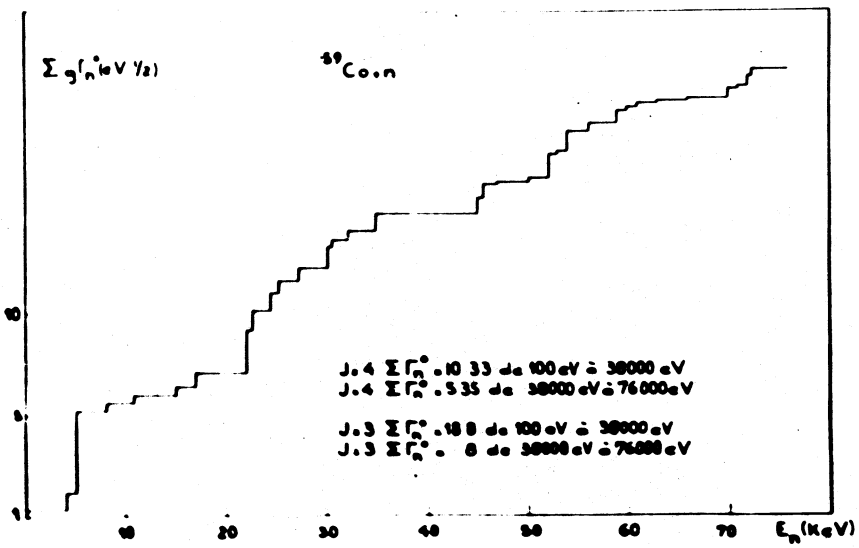

Fig. 23.3.

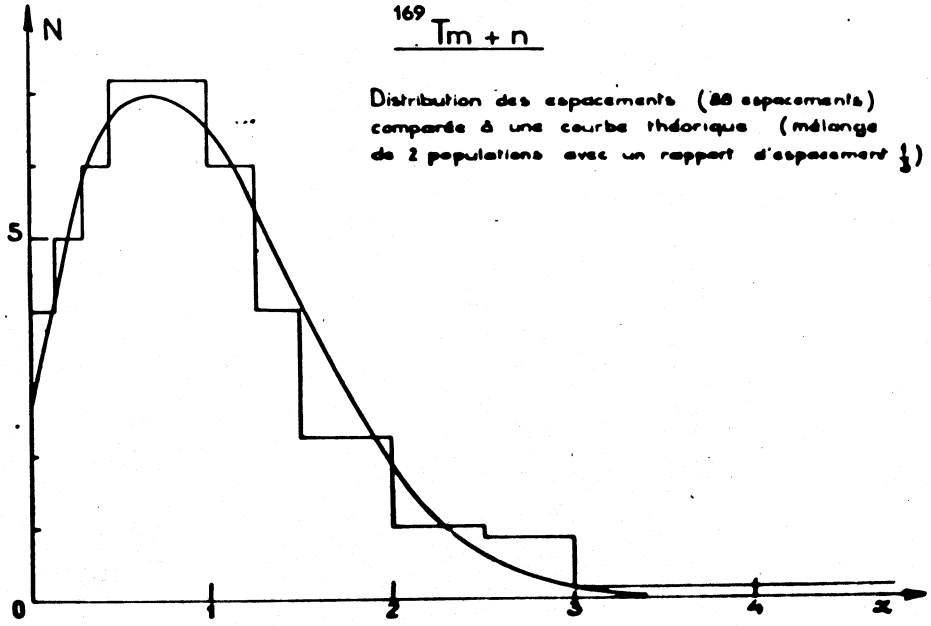

Fig.23.4.

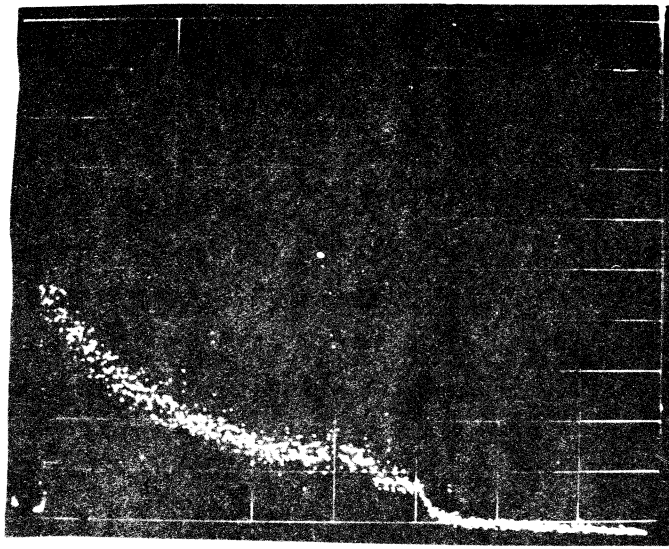

Fig. 23.7.

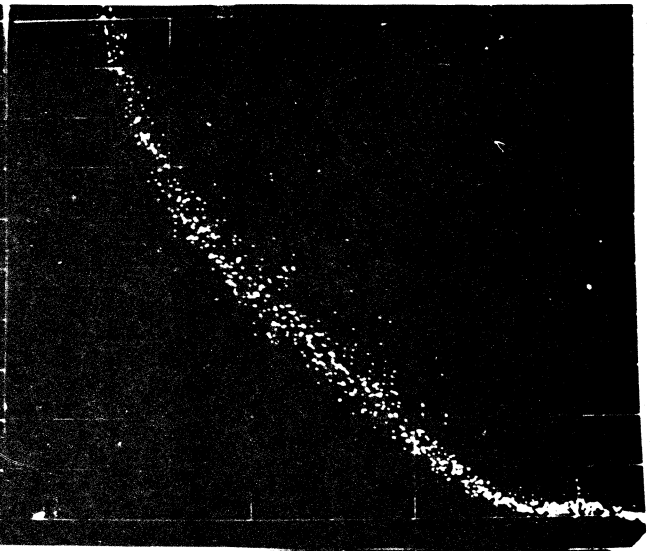

Fig.23.8.

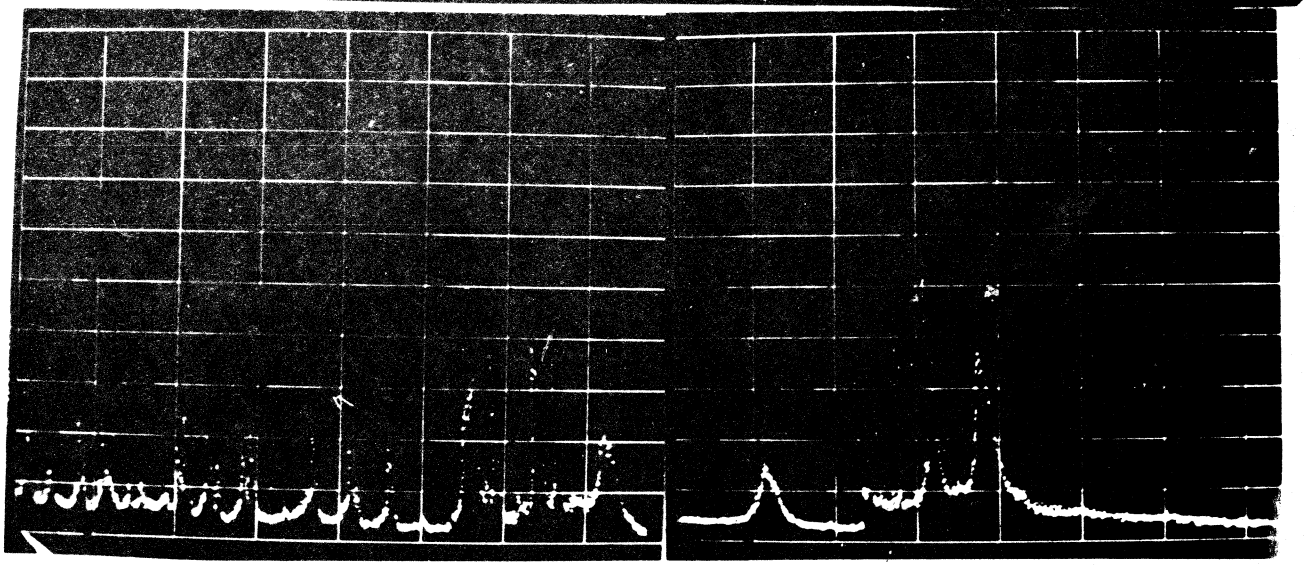

Fig. 23.6.

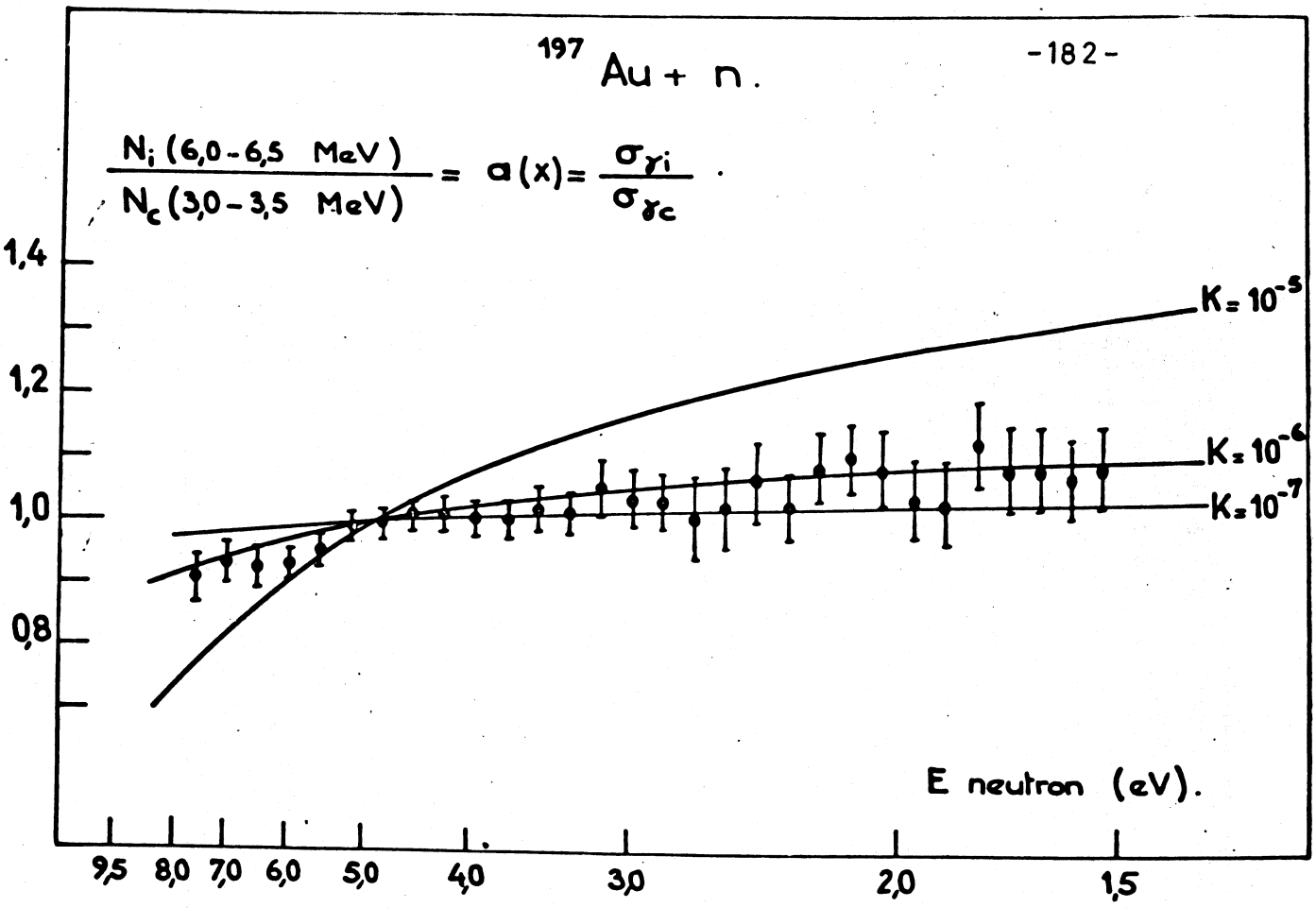

Fig.23,9.

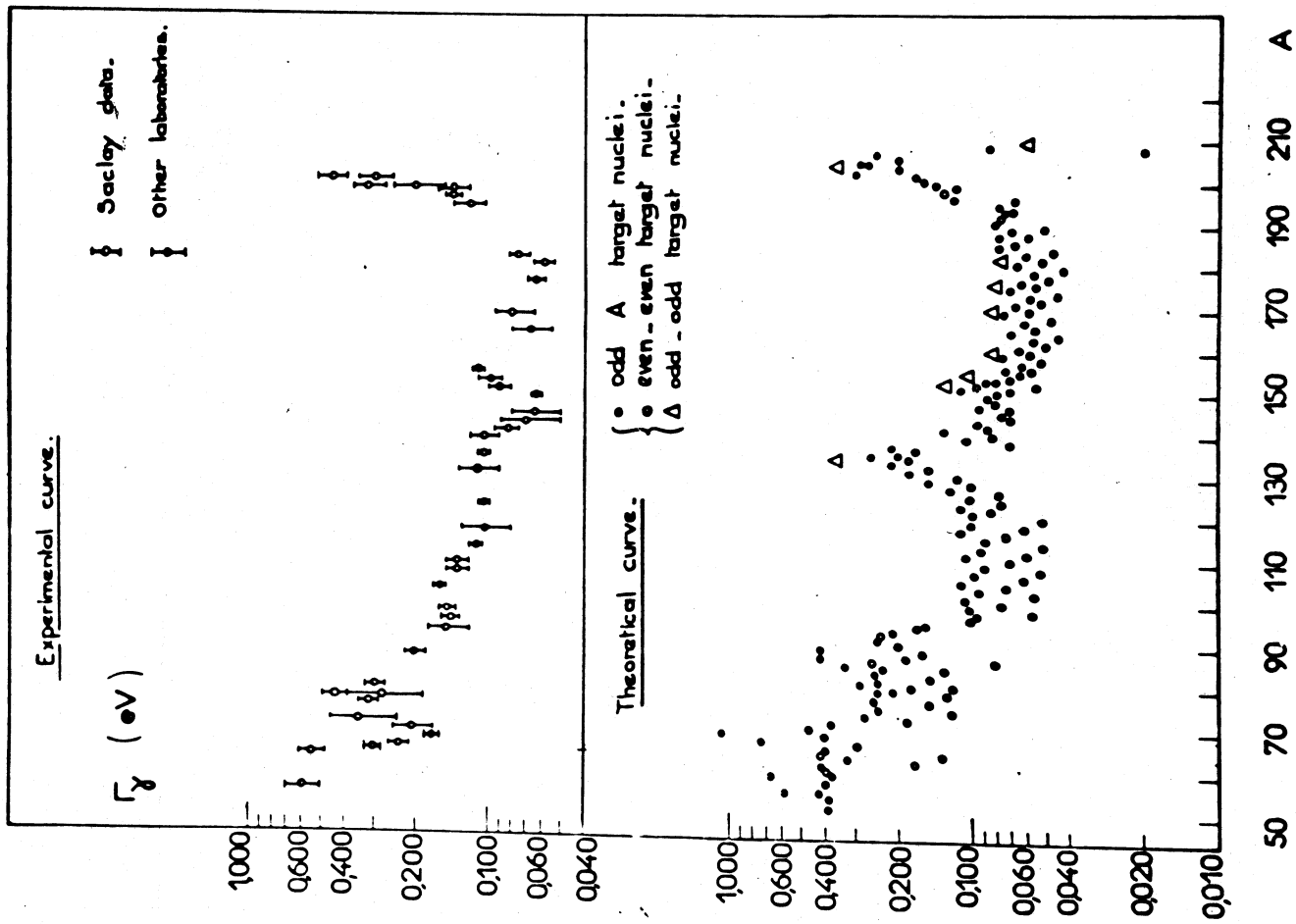

Fig.23.5.

24. SERVICE DE PHYSIQUE EXPERIMENTALE DU COMMISSARIAT A L'ENERGIE ATOMIQUE (FRANCE)

M. J. Jacquesson

24.1. Courbe d'excitation de la réaction (n,2n) sur le ^{63}Cu de 16,59 MeV à 17,71 MeV

G. Bordolle, J. Cabe, M. Laurat

La section efficace (n,2n) du ^{63}Cu a été mesurée en valeur relative pour des neutrons d'énergie comprise entre 16,59 et 17,71 MeV avec des intervalles de 25 keV environ. Les neutrons étaient obtenus par la réaction $T(d,n)^4He$, les deutérons étant accélérés par un Van de Graaff 2 MeV.

La mesure a été faite par une méthode d'activation, le flux de neutrons étant mesuré par un spectromètre à protons de recul, et l'activité β^+ de l'échantillon par la détection en coincidence des deux γ d'annihilation du β^+.

L'erreur sur la valeur relative de la section efficace est inférieure à 2.5 %. La courbe obtenue (fig. 24.1.) montre l'existence d'une structure d'assez faible amplitude et d'une largeur de l'ordre de 50 keV. La mesure de la courbe d'excitation de la réaction $^{63}Cu\ (n,p)^{63}Ni$ est entreprise dans la même gamme d'énergie, les protons étant détectés par un télescope constitué de détecteurs (dE/dx, E).

24.2. Réaction D + n → p + n + n à 13.9 MeV

D. Didier, G. Mouilhayrat, F. Perrault, P. Thouvenin

24.2.1. Etude du spectre en énergie des protons de la réaction D(n,p) 2n

Ce spectre a été mesuré à l'aide d'un télescope à détecteurs semiconducteurs refroidis (J. de Phys. 26, 49A, 1965). On analyse d'une part, l'énergie totale des particules et d'autre part l'énergie qu'elles ont perdue dans les détecteurs $\Delta E/\Delta X$. Ceci permet de séparer protons et deutérons et de tracer les spectres des protons d'énergie supérieure à 4 MeV (fig. 24.2.). Le pic situé au voisinage de 11 MeV sur la fig. 24.2., s'interprète comme traduisant un état final dans lequel les deux neutrons ont un moment re latif faible et sont projetés sensiblement dans la même direction.

Grâce à la bonne résolution du télescope (2.8% à 14 MeV) on peut penser que l'analyse théorique, en cours, fournira des résultats précis sur l'interaction n-n.
Une étude du spectre des protons émis à 50° dans le laboratoire est en cours.

24.2.2. Etude des réactions ^{9}Be (^{3}He,α) ^{8}Be et ^{10}Be(d,α) ^{8}Be

L'étude de ces réactions a été poursuivie, à 1.5 MeV pour ^{3}He et à 1.5 MeV et 9 MeV pour le deutérium, par la technique des deux détecteurs en coincidence. Les résultats obtenus montrent que nous avons affaire à des réactions séquentielles. Une interprétation des spectres obtenus est en cours à l'aide du modèle des agrégats.

24.2.3. Spectrométrie des neutrons par temps de vol

Un nouveau spectromètre à faible seuil a été mis au point. Le détecteur de neutrons est un scintillateur liquide vu par deux photomultiplicateurs 56 AVP. Il est destiné aux mesures de temps de vol des neutrons rapides.

24.3. Mesure de la diffusion élastique et inélastique des protons par le ^{7}Li entre 0.9 et 2 MeV

G. Bardolle, J. Cabe, J.F. Chrétien, M. Laurat

Les sections efficaces différentielles de diffusion élastique et inélastique des protons de 0.9 à 2 MeV par le ^{7}Li ont été mesurées au cours d'une même série d'expériences. Les protons étaient accélérés par un Van de Graaff 2 MeV. Le faisceau d'une dispersion en énergie de 1 keV était collecté dans une cage de Faraday pour la mesure du courant. Les protons diffusés étaient détectés par des diodes RCA du type A 4 75 0.2 auxquelles étaient associées des chaines de spectrométrie ORTEC. Les cibles étaient constituées d'un dépôt métallique de 10 à 20 $\mu g/cm^2$ de ^{7}Li (enrichi à 99.3%) sur un support de carbone.

24.3.1. Diffusion élastique

On a tracé les distributions angulaires entre 0.950 et 1.975 MeV, et les fonctions d'excitation pour des angles de 135°, 150° et 165° dans le système du laboratoire de 50 keV en 50 keV (fig. 24.3. à 24.6.). Les sections efficaces ont été obtenues en valeur absolue avec une

erreur inférieure à 5 %. Les résultats montrent une forte interférence entre les diffusions potentielle et coulombienne, l'existence d'un niveau de spin 1^+ à 1.050 MeV, et la présence d'une diminution de la section efficace au voisinage du seuil de la réaction $^7Li(p,n)^7Be$ à 1.881 MeV.

24.3.2. Diffusion inélastique

On a étudié les mêmes distributions angulaires et tracé les mêmes courbes d'excitation que pour la diffusion élastique (fig. 24.7. et 24.8.). Les résultats indiquent une diminution de la section efficace au voisinage du seuil de la réaction $^7Li(p,n)^7Be$. L'erreur commise sur la valeur absolue de la section efficace varie de 6 à 13%, l'erreur sur la valeur relative pour les courbes d'excitations étant inférieure à 5%.

24.4. Mesure de la diffusion élastique des protons de 1 MeV à 10 MeV par le ^6Li

G. Bardolle, J. Cabe, J.F. Chrétien, M. Laura

Pour mesurer la section efficace différentielle de diffusion des protons par le ^6Li, les protons étaient accélérés suivant l'énergie, soit par un Van de Graaff 2 MeV, soit par un Van de Graaff Tandem 12 MeV; le faisceau était collecté dans une cage de Faraday pour la mesure du courant. Les protons étaient détectés par des diodes au Solicium du type D-4 75 0;2 auxquelles étaient associées des chaines de spectrométrie ORTEC. Les cibles étaient constituées d'un dépôt métallique de 10 à 20 $\mu g/cm^2$ de ^6Li enrichi à 99% sur support de carbone.

Résultats

On a tracé les distributions angulaires (fig. 24.10. à 24.12.) de 1 à 10 MeV pour des angles variant entre 45° et 170° et une courbe d'excitation (fig. 24.9.) correspondant à l'angle de 135° dans le système du laboratoire. Les résultats obtenus font apparaitre l'existence d'un niveau de spin 5/2 (-) au voisinage de 1.780 MeV, ainsi qu'un large maximum attribué à un niveau très large du ^7Be aux environs de 4.6 MeV, dont le spin n'a pu être déterminé d'une façon précise. Ces résultats sont en très bon accord avec ceux obtenus par J.A. Mc Cray (jusqu'à 2.8 MeV)

ainsi que ceux de W.D. Harrison et A.B. Whitehead (de 2.4 MeV à 12 MeV). Ce travail sera complété par l'étude en cours de la diffusion inélastique des protons sur le ^{6}Li (niveaux de 2.184 MeV et de 3.560 MeV).

24.5. Etude des interactions des deutérons avec les éléments légers

G. Bruno, J. Decharge, A. Perrin, G. Surget, C. Thibault

Dans le cadre des recherches entreprises sur les interactions produites par les deutérons sur les éléments légers, nos travaux ont porté sur les points suivants:
Etude de la diffusion élastique des deutérons par le Lithium, le carbone, l'oxygène pour des énergies comprises entre 4 MeV et 7 MeV.
Etude de réaction (d,α) sur le Lithium et sur l'oxygène pour des énergies comprises entre 1 et 2 MeV et entre 3 et 7 MeV.
Etude de réaction (d,p) pour divers niveaux du noyau résiduel sur le Lithium, le carbone, l'oxygène pour des énergies comprises entre 1 et 2 MeV et entre 3 et 7 MeV.
Ces résultats feront l'objet de publications.

24.5.1. Diffusion inélastique des deutérons

Les deutérons accélérés par un Van de Graaff tandem de 12 MeV arrivent sur un diffuseur constitué par une cible autoportée de ^{12}C de 25 à 50 $\mu g/cm^2$ sur laquelle on a fait un dépôt de Lithium par évaporation sous vide. Les détecteurs sont des jonctions diffusées. Pour la diffusion sur le ^{6}Li une coincidence entre le deutéron et le noyau de ^{6}Li de recul permet d'éliminer l'influence des réactions parasites. Les fonctions d'excitation ont été mesurées aux angles 115° et 120° (système du laboratoire): à titre d'exemple, la fig. 24.13. présente nos résultats pour le carbone.

24.5.2. Réactions (d,α)

Pour le Lithium, l'utilisation intensive d'un Van de Graaff de 2 MeV nous a permis d'obtenir des résultats assez complets dans la gamme d'énergie comprise entre 1 et 2 MeV, nous donnons en particulier les sections efficaces de production d'α (réaction $^{6}Li + d \rightarrow 2\alpha$) en valeur absolue.
Nos distributions angulaires comprennent toutes la valeur 0°

et s'étendent jusqu'à 170° (Laboratoire). La fig. 24.14. compare nos valeurs des coefficients A2 et A4 avec les valeurs publiées par ailleurs. Pour le ^{7}Li, les études en cours sont axées sur la réaction $^{7}Li + d \rightarrow \alpha_1 + {}^{5}He \rightarrow \alpha_2 + n$ qui nous permet d'atteindre le ^{5}He. Pour l'oxygène nos résultats sont très fragmentaires et sont limités pour l'instant à la valeur de la section efficace en fonction de l'énergie $\theta_{Labo} = 120°$ et Ed compris entre 3.5 MeV et 4.5 MeV et entre 5.7 MeV et 7.5 MeV.

24.5.3. Réaction (d,p)

Ici encore, nos résultats sur le Lithium sont assez complets entre 1 et 2 MeV et portent sur le fondamental et le premier niveau excité du noyau résiduel (^{7}Li, 0.478 keV). Les distributions angulaires s'étendent de 0° à 170° (Labo). Pour le carbone et l'oxygène, les résultats encore fragmentaires s'étendent de 4 à 7 MeV, pour des valeurs angulaires de 115° et 120° Labo. Ils portent sur les 4 premiers niveaux de ^{13}C et sur les 2 premiers niveaux de ^{17}O.

24.6. Etude des probabilités d'émission de neutrons prompts lors de la fission spontanée du ^{252}Cf

E. Baron, J. Frehaut, F. Ouvry, M. Soleilhac

Notre mesure utilise les techniques du scintillateur liquide associé à un détecteur de fragments de fission.

24.6.1. Principe

Nous enregistrons le nombre d'évènements (neutrons plus bruit de fond) vus par les 12 photomultiplicateurs du scintillateur liquide (Nuclear Enterprise) dans les 50 microsecondes qui suivent l'instant de fission. Nous avons vérifié, en mesurant la probabilité de capture d'un neutron en fonction du temps après l'instant de fission, qu'un neutron s'il est détecté à 99.28 chances sur 100 d'être enregistré dans les 50 microsecondes qui suivent son émission. 200 microsecondes après une fission, nous enregistrons le bruit de fond détecté pendant 50 microsecondes.

24.6.2. Résultats

Les résultats expérimentaux doivent être corrigés pour tenir compte de trois phénomènes:

Le bruit de fond (mesuré).
L'empilement de 2 neutrons en une seule impulsion produit par le temps mort imposé de l'électronique (110 nanosecondes). Nous avons vérifié que la correction d'empilement d'ordre multiple était superflue tant que le temps mort était inférieur à 200 nanosecondes.
La correction d'efficacité, obtenue en prenant comme valeur de référence du $\bar{\nu}$ du ^{252}Cf : 3.784 ± 0.020.
Pour déterminer la précision des mesures de P(n) nous tenons compte de 3 types d'erreur:

a) L'erreur due à l'incertitude sur le temps mort et sur l'intégrale de la probabilité de capture d'un neutron en fonction du temps.
b) L'erreur due à l'imprécision sur la valeur de référence du $\bar{\nu}$.
c) Les fluctuations statistiques sur le nombre d'évènements enregistrés pour chaque probabilité.

Les résultats portant sur 1.700.000 fissions sont rassemblés dans le tableau 24.1. La première colonne donne les P(n), les trois suivantes les 3 types d'erreurs, a), b), c), la quatrième l'erreur globale obtenue en faisant la moyenne quadratique des 3 précédentes, la cinquième colonne donne cette même erreur en % du P(n) correspondant.
Les paramètres de la distribution des P(n) sont les suivants:
la variance:

$$D = \langle \nu^2 \rangle - \bar{\nu}^2 = 1.61778$$

L'écart quadratique moyen de la distribution continue:

$$\sigma = \sqrt{D - 1/12} = 1.23873$$

reliant les points expérimentaux:
Le facteur

$$\Gamma_2 = (\langle \nu^2 \rangle - \bar{\nu}) / \bar{\nu}^2 = 0.84871$$

Efficacité du scintillateur liquide:

$$\epsilon = 0.8819 \pm \begin{cases} 0.0022 & \text{a)} \\ 0.0047 & \text{b)} \\ 0.0029 & \text{c)} \end{cases} \text{, cas}$$

TABLEAU 24.1.: Probabilités d'émission de neutrons prompts lors de la fission spontanée du ^{252}Cf.

N	P(n)	a)	b)	c)	erreur globale	%
0	0.00217	0.00005	0.00013	0.00009	0.00016	7.4
1	0.02454	0.00027	0.00116	0.00029	0.00123	5.0
2	0.12251	0.00027	0.00300	0.00065	0.00308	2.5
3	0.27135	0.00040	0.00215	0.00090	0.00237	0.87
4	0.30504	0.00062	0.00150	0.00085	0.00183	0.60
5	0.18726	0.00001	0.00277	0.00080	0.00288	1.54
6	0.06883	0.00021	0.00161	0.00065	0.00175	2.54
7	0.01569	0.00018	0.00048	0.00036	0.00063	4.02
8	0.00236	0.00004	0.00008	0.00026	0.00027	11.44

24.6.3. Conclusion

Les résultats permettent d'affirmer que la distribution des P(n) est légèrement différente d'une courbe de Gauss qui aurait même variance.

L'erreur la plus importante est constituée par l'erreur apportée par le $\bar{\nu}$ de référence.

Des mesures analogues ont été faites pour les fissions spontanées du ^{240}Pu, elles ne sont pas entièrement exploitées à ce jour.

Des essais en fissions provoquées par des neutrons de 3 MeV, ont été faits sur le ^{239}Pu et l'^{235}U. La faible statistique fission obtenue dans les essais préliminaires permet simplement de constater la concordance de nos résultats avec ceux déjà publiés.

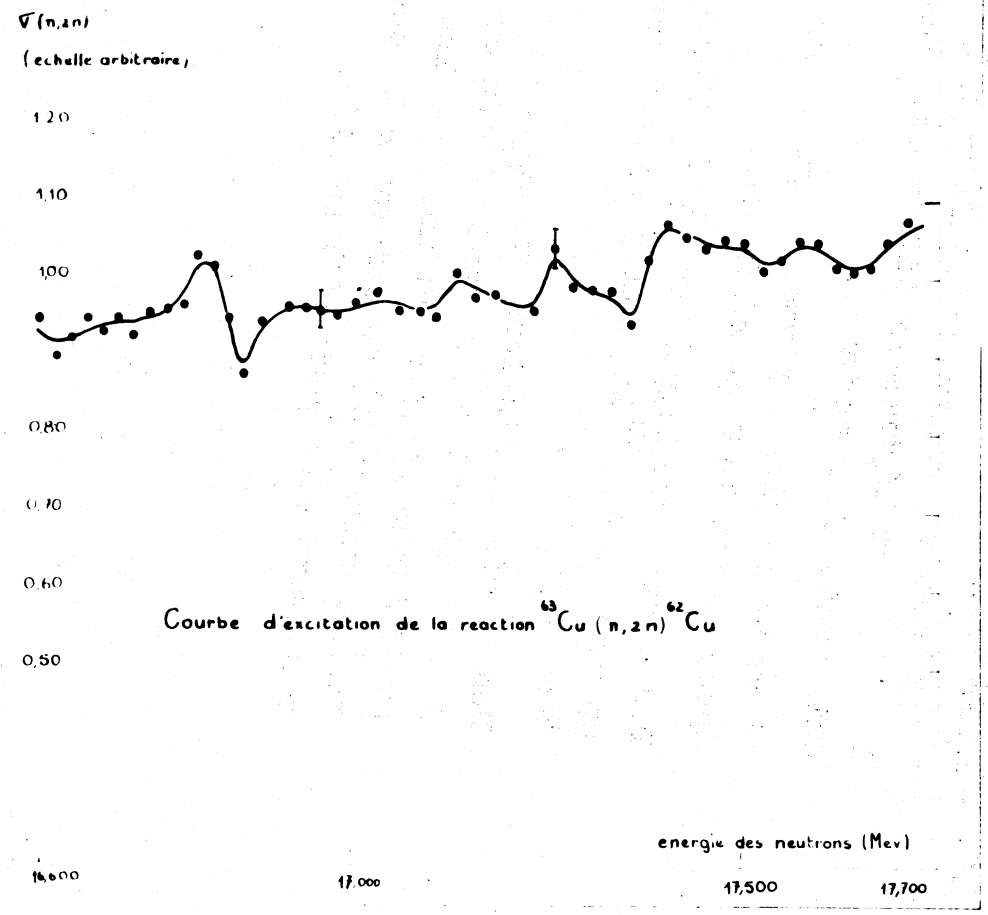

Fig. 24.1.

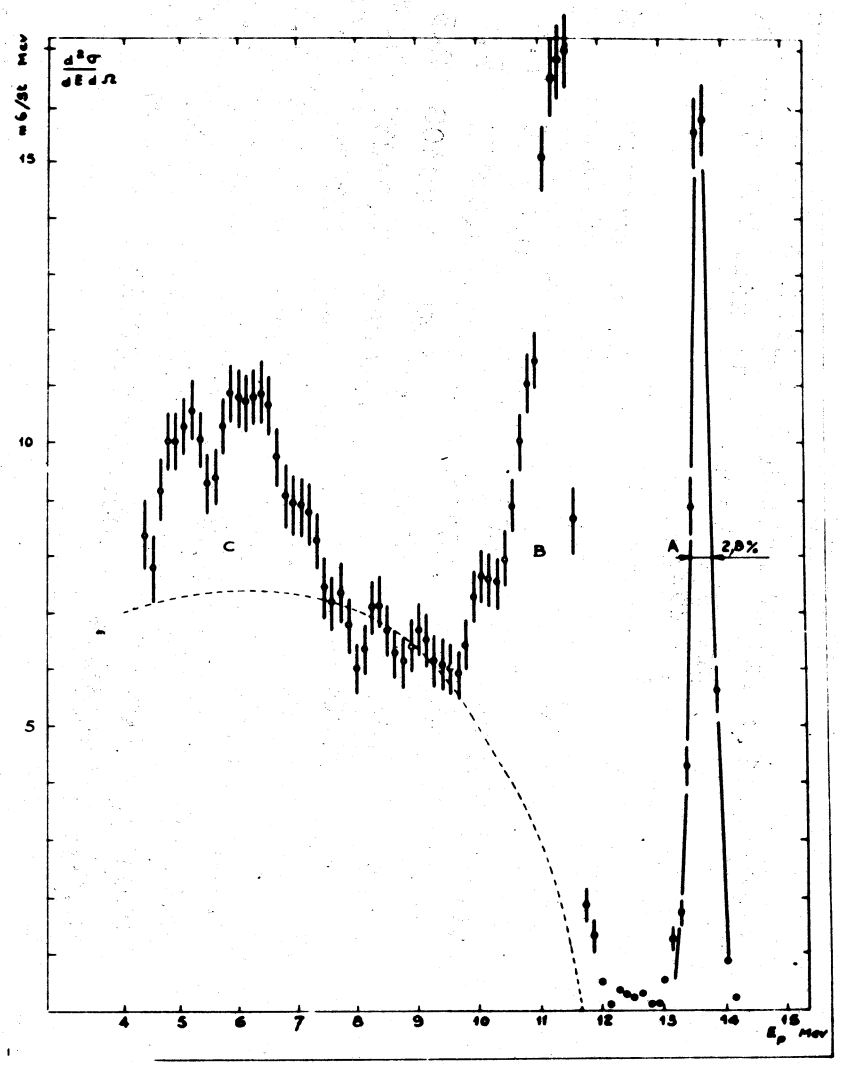

Fig. 24.2.

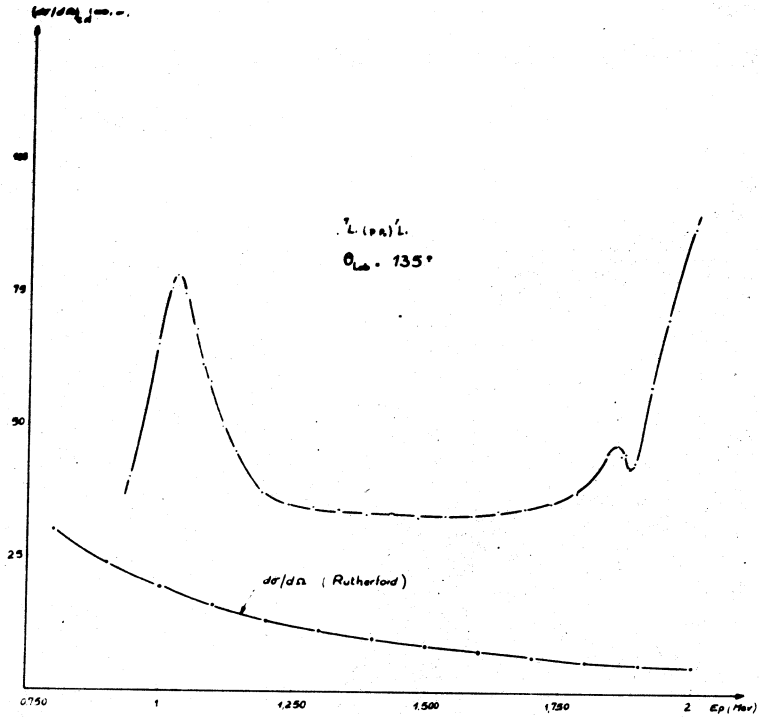

Fig. 24.3.

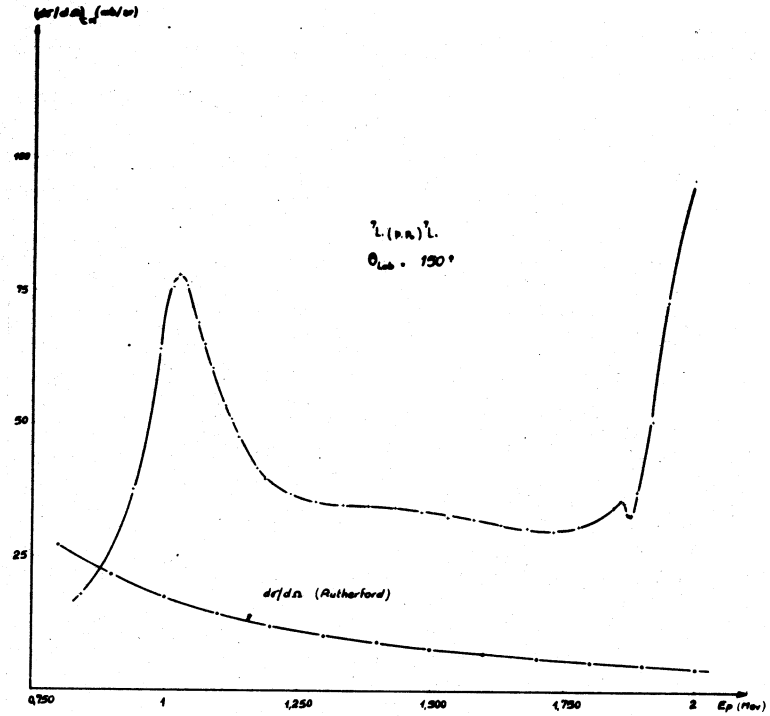

Fig. 24.4..

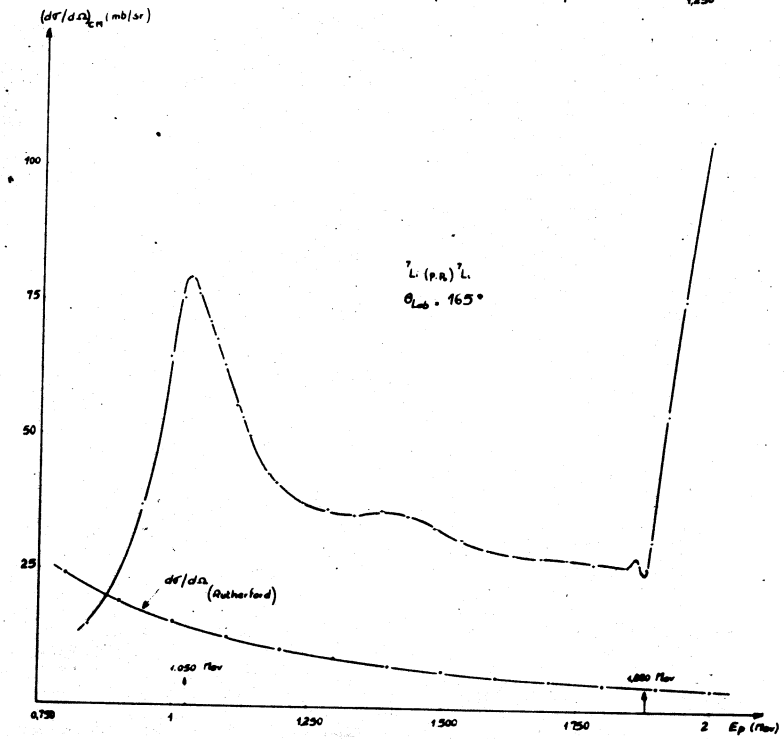

Fig. 24,5.

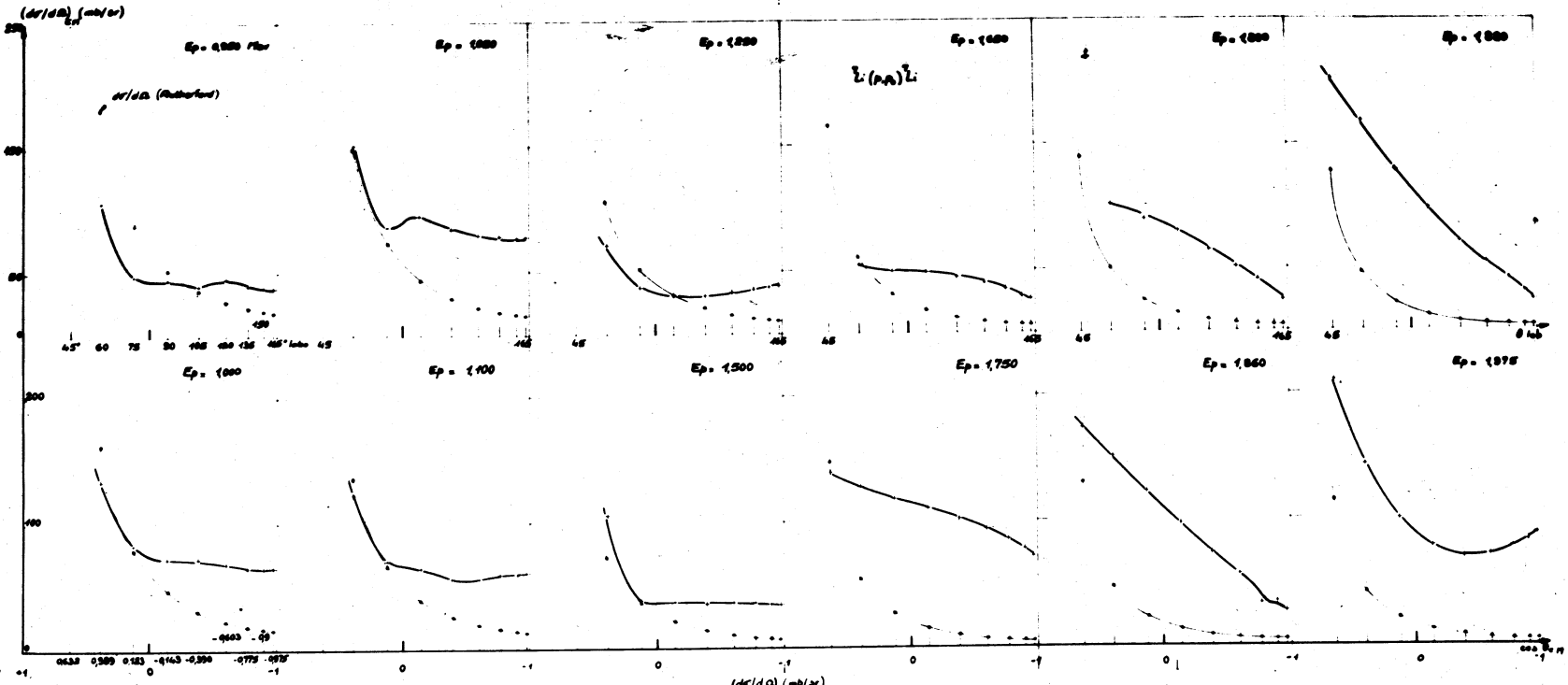

Fig.24.6.

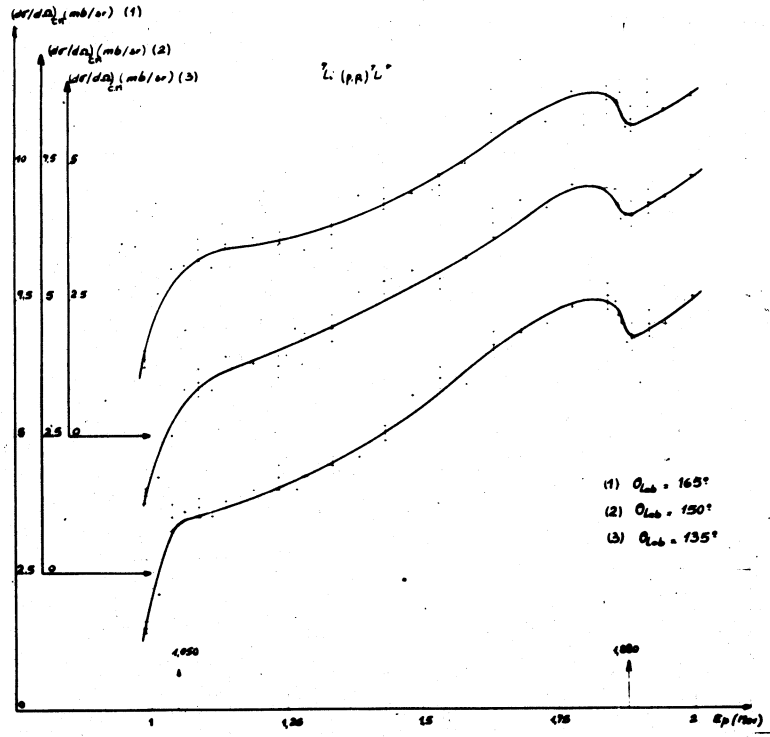

Fig. 24.7.

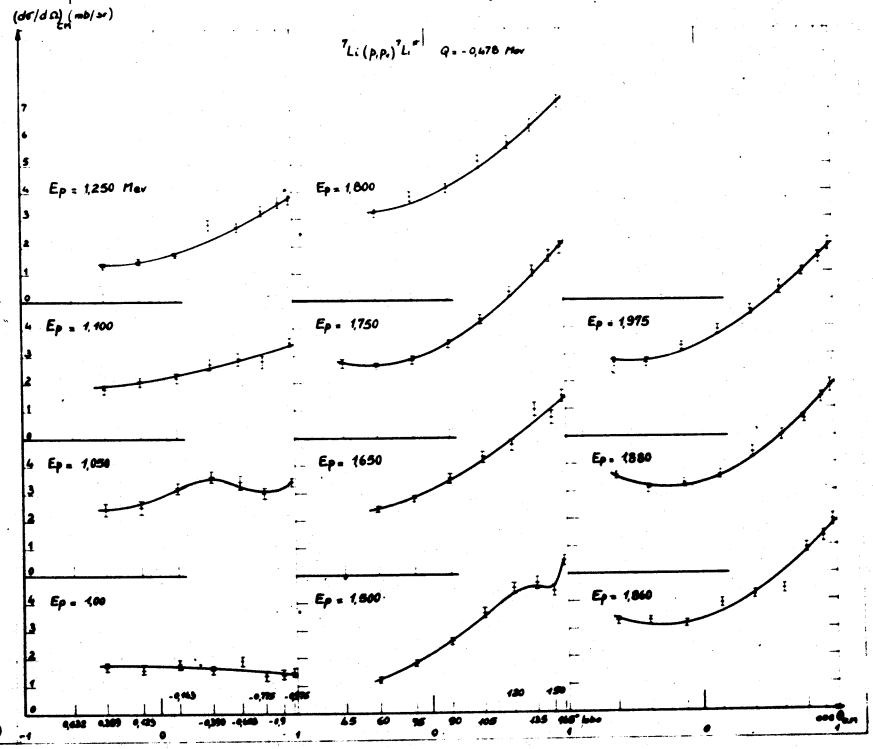

Fig.24.8.

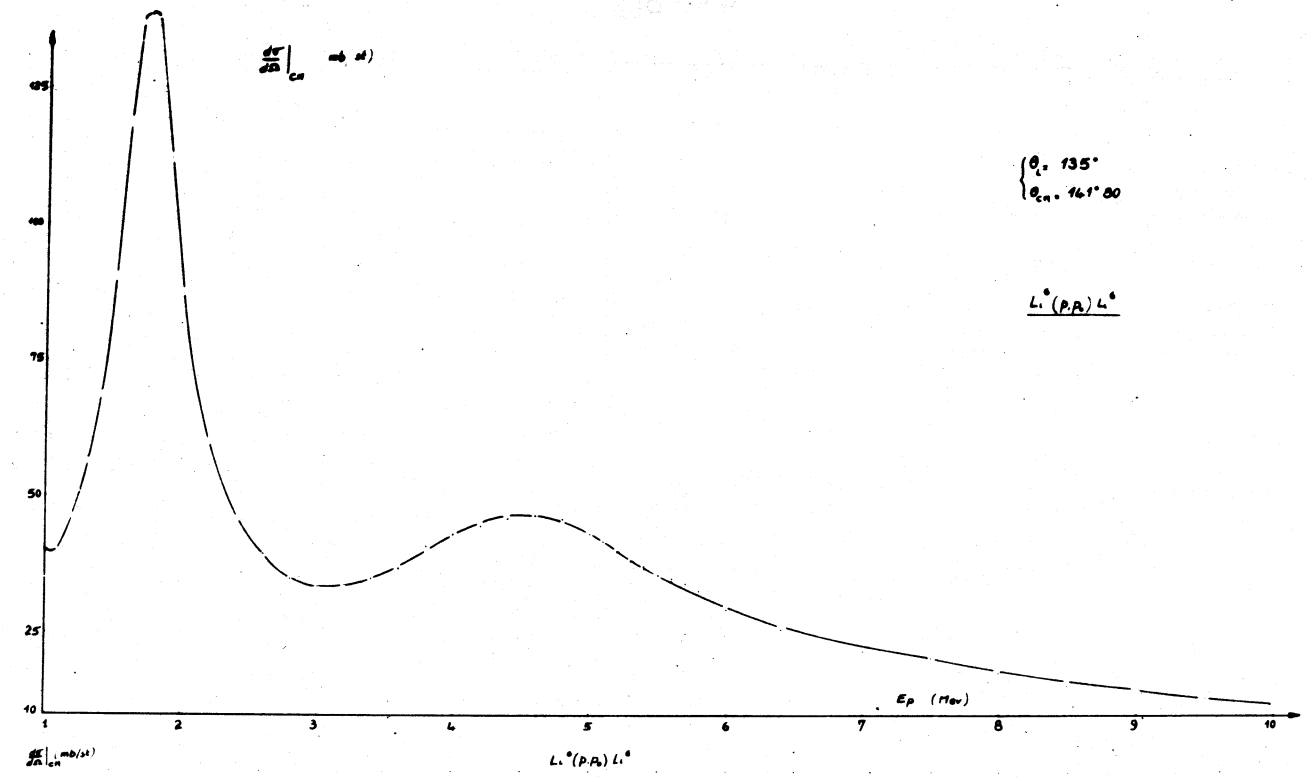

Fig. 24.9.

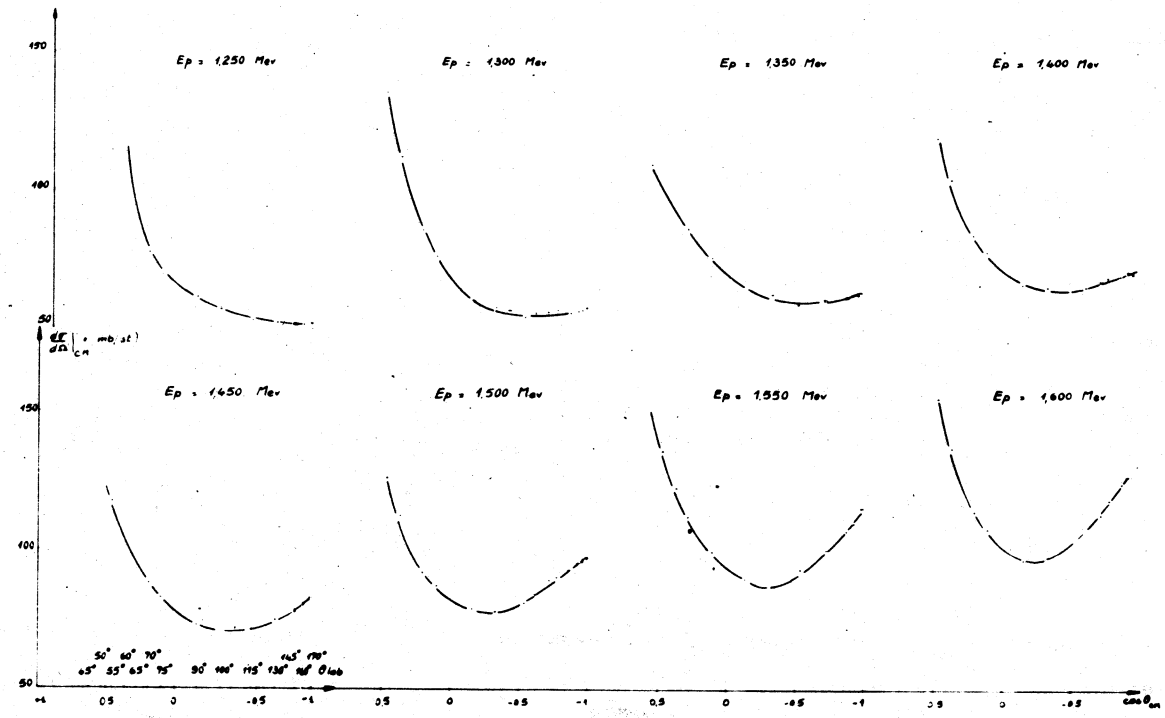

Fig. 24.10.

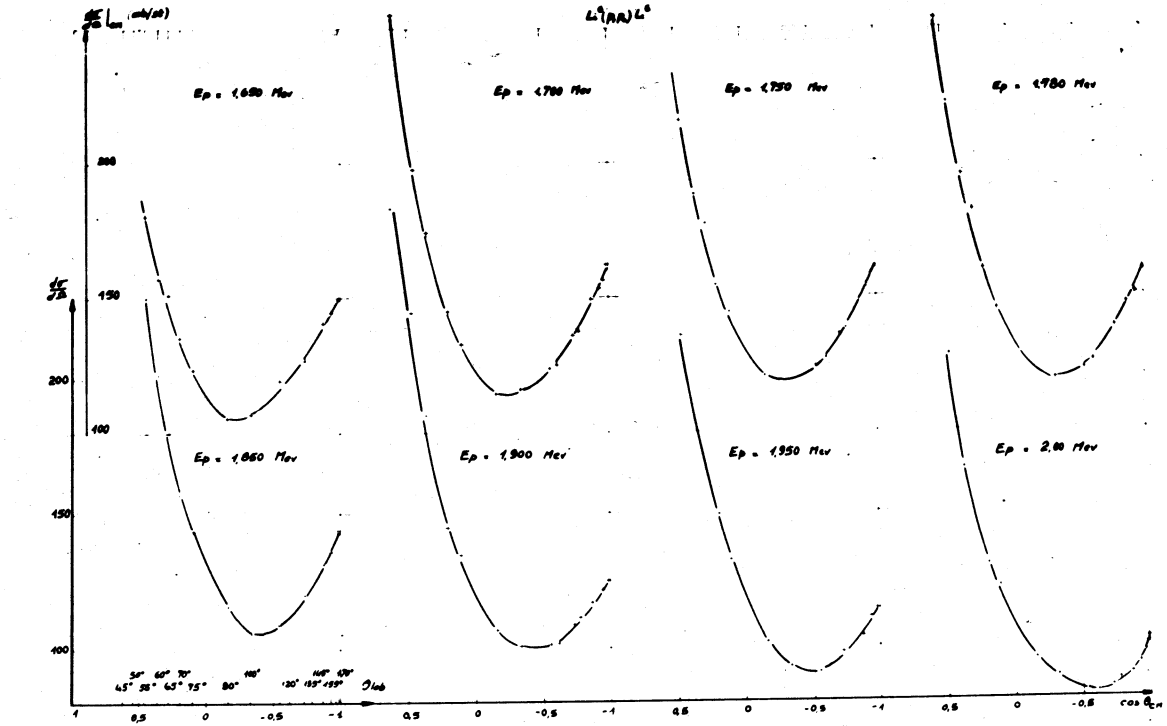

Fig. 24.11.

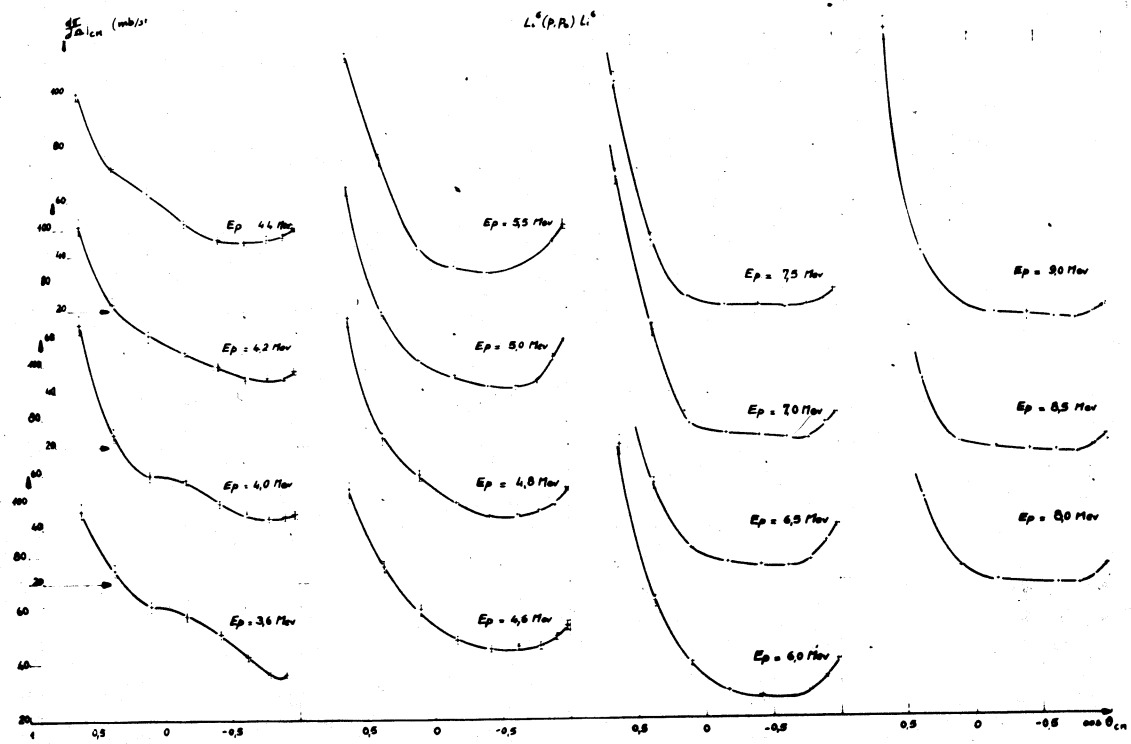

Fig. 24.12.

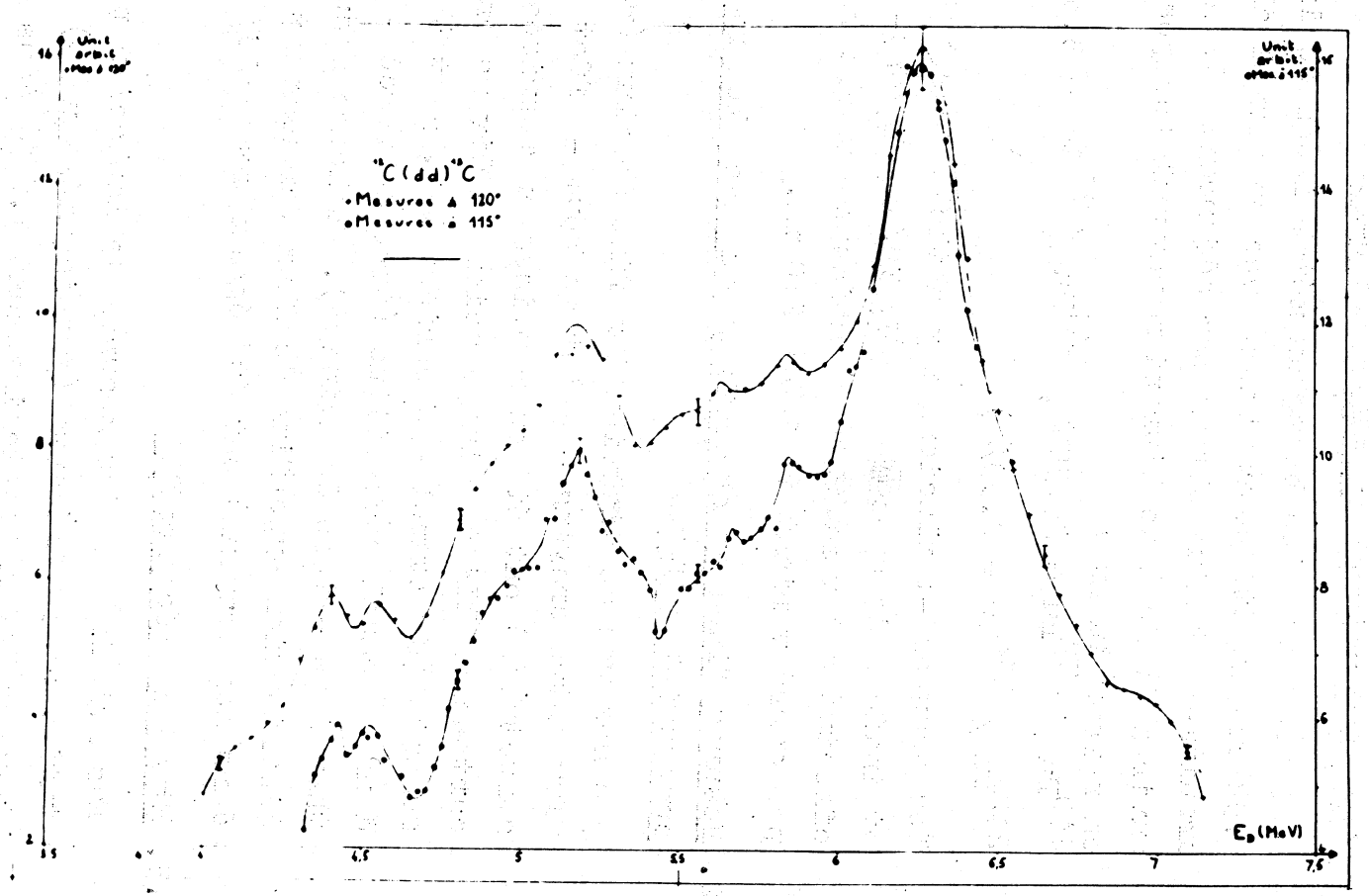

Fig. 24.13.

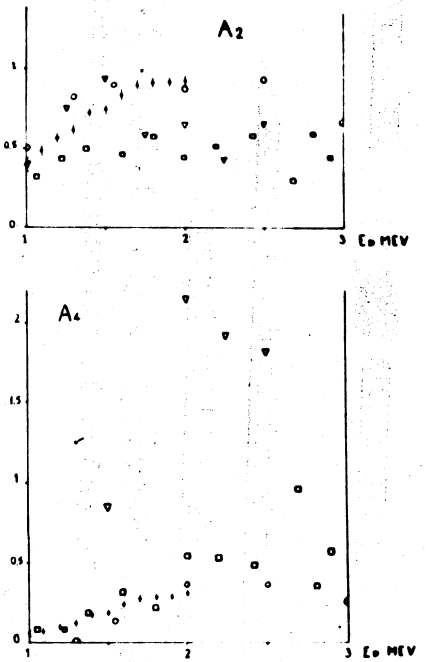

Variations des coefficients A_2 et A_4 avec E_D

$\sigma(\theta_{cm}) = \sigma(90°)\,[1 + A_2 \cos^2\theta + A_4 \cos^4\theta]$

- NP HEYDENBURG et al (1)
- YP ANTOUFIEV (4)
- JMF JERONIMO (5)
- nos résultats

Fig. 24.14.

25. SERVICE DES EXPERIENCES NEUTRONIQUES, CEA (FRANCE)

D. Breton

25.1. Physique experimentale des reacteurs

25.1.1. Réseaux modérés à l'eau lourde

Les études décrites sous 25.1.1.1./2./3. sont effectuées dans le cadre de programme de mesures sur AQUILON II

25.1.1.1. Etudes systématiques sur des barreaux cylindriques d'uranium naturel ou d'alliage U-Pu

Ces études sur des barreaux métalliques de diamètre 2.92 cm ont été poursuivies avec un nouvel alliage uranium-plutonium obtenu par adjonction de 0.047 % environ de Pu à de l'uranium naturel (composition en noyaux du Pu :
^{240}Pu / ^{239}Pu = 24.55% , ^{241}Pu / ^{239}Pu = 3.32% ,
^{242}Pu / ^{239}Pu = 0.39%).

Les mesures -laplaciens par méthode de substitution et indices de spectre (Pu/U, Lu/Mn, In/Mn)- ont été effectuées à température ambiante sur des réseaux à pas carré variant de 120 à 210 mm.

25.1.1.2. Mesures fines et hyperfines sur des éléments combustibles EL4

Des mesures de distribution fine de flux (rapport de flux entre crayons - effet de bout - effet des structures) ont été entreprises ou reprises sur des cartouches EL4 à gainage acier de divers enrichissements (U naturel - U enrichi à 1.35 et à 1.65%) dans un canal reconstitué (tube de force - isolement thermique - tube de guidage). Quelques mesures de distribution hyperfine de flux (creusement de flux dans les crayons) ont été également réalisées.

25.1.1.3. Etude de réseaux EL4

Essentiellement des mesures de laplacion par substitution de 32 éléments (empoisonnés au Cu) à 4 cartouches EL4 A (enrichissement 1.65%) dans des réseaux à pas carré de 210, 230 et 250 mm.

25.1.1.4. Mesures sous contrat

Une semaine a été consacrée à des mesures hyperfines dans un élément combustible à carbure d'uranium (Euratom, projet Essor).

25.1.1.5. Expérience critique EOLE

L'expérience critique EOLE a divergé le 2.12.65 au Centre d'Etudes Nucléaires de CADARACHE. EOLE est destiné à des mesures sur des réseaux à eau lourde et permettra de compléter les connaissances acquises à SACLAY sur AQUILON.

25.1.2. Réseaux modérés à l'eau légère

ALIZE est en cours de transformation en vue d'études pour le réacteur franco-allemand à haut flux.

25.1.3. Réseaux modérés au graphite

25.1.3.1. CESAR

Les essais d'ensemble ont montré que l'homogénéité de la répartition des températures et la stabilité thermique étaient excellentes jusqu'à la température maximale (450°C graphite).

Le réseau de référence (uranium de diamètre 35 mm) a été étudié par cartes de flux aux paliers 20°C, 200°C et 300°C, avec mesure du coefficient de température différentiel à chacun de ces paliers. Des combustibles classiques (barreaux et tubes) ont été étudiés par substitution aux trois températures. Un second réseau de référence, Ø 35 dégavé 1/3, a été étudié à 20°C. La zone de substitution a été successivement chargée en graphite, réalisant ainsi une colonne thermique interne utilisée pour l'étalonnage des couples de détecteurs d'indice de spectre, et en réseaux EDF2 (gavés, dégavés 1/3 et 1/12). Dans ces réseaux ont été menés des étalonnages d'absorbants, des mesures de structures fines et d'indice de spectre, des études d'hétérogénéités entrainées par la présence de divers types de combustibles annulaires de grandes dimensions.

25.1.3.2. MARIUS

Cette expérience critique a été transférée de MARCOULE à CADARACHE où elle a divergé le 17 mai 1965. Après l'étude du réseau de référence (pas 224 mm, canal Ø 110 mm, uranium Ø 31 mm), des substitutions accompagnées de structures fines ont été menées sur quelques types de combustible; en particulier on a étudié l'effet de gaines d'épaisseur variable.

Une campagne d'oscillation de combustible a été réalisée ensuite : étude de combustible synthétique Ø 29.2 mm à diverses teneurs en ^{235}U et plutonium, ce plutonium pouvant avoir lui-même des teneurs isotopiques différentes, par comparaison à des combustibles en uranium naturel additionné de bore et à des combustibles en uranium légèrement enrichi ou appauvri; étude de combustibles irradiés Ø 28 mm par la même méthode. Les irradiations des cartouches s'étalaient entre 700 et 4000 MWJ/T.

25.1.3.3. Mesures physiques sur les réacteurs de puissance

Le Service des Expériences Neutroniques a développé la technique des neutrons pulsés pour mesurer quelques antiréactivités caractéristiques sur de gros réacteurs. La mise au point de sources de forte intensité a été poursuivie, et une méthode de dépouillement utilisée pour extraire les différents modes harmoniques de la répartition du flux neutronique dans les grands milieux.

La détection du flux neutronique à bas niveau par semiconducteurs a été systématiquement utilisée au démarrage des réacteurs à graphite. Cette technique permet, moyennant une adaptation particulière des circuits électroniques associés à la diode détectrice, de mesurer des flux de façon continue, en augmentant la cadence des relevés dans une très forte proportion.

25.1.4. Piles à neutrons rapides

Les spécifications du coeur de démarrage de MASURCA ont été retenues (volume: de l'ordre de 200 l ; composition: alliage U-Pu-Fe et graphite).

La préparation de l'expérimentation est actuellement

en cours. Les expériences porteront entre autres sur la mesure du flux, des indices de spectre, de la réactivité et de l'effet Doppler.

25.2. Etude du graphite par la technique de la source pulsée de neutrons

L'étude du graphite plein a été terminée en 1965, les résultats en ont été présentés au Colloque de Karlsruhe (rapport SM 62/80). 53 massifs de graphite ont été étudiés, dans la gamme de laplaciens 5.6 m^{-2} à 156 m^{-2}, et les valeurs obtenues, ramenées à un graphite de densité 1.6, sont les suivantes:

libre parcours de transport: $\lambda_t = (2.606 \pm 0.01)$ cm
coefficient de refroidissement: $C = (41 \pm 3)\ 10^5\ cm^4\ s^{-1}$
anisotropie: $\lambda_{\parallel}/\lambda_{\perp} = 1.014 \pm 0.004$

Un programme d'étude de l'anisotropie de réseaux de canaux vides, au pas de 20 cm, dans le graphite, a commencé au second semestre et se terminera en 1966. Les diamètres des canaux utilisés sont 30, 50, 70, 90, 110 et 140 mm.

25.3. Mesure des sections efficaces par la méthode d'oscillation

25.3.1. Mesure des sections efficaces effectives d'échantillons fissiles

Ce travail est effectué dans le cadre du contrat EURATOM "Recyclage du Plutonium" n° 002 - 64 - 9 TRUF (RD).

Les mesures à MINERVE ont porté sur des échantillons constitués par des alliages d'uranium naturel ou légèrement appauvri (0.65%) contenant environ 0.05 et 0.075% de plutonium avec des teneurs isotopiques en ^{240}Pu de 1, 3, 6, 8 et 20% et quelques alliages d'uranium très appauvri (0.22% et 0.45%) contenant 0.25; 0.30 et 0.30% de Pu à 8 % et 20 % de ^{240}Pu.

Ces échantillons sont des cylindres métalliques de 29.2 mm de diamètre.

L'ensemble de ces résultats, qui sont en cours de dépouillement, permettra de déterminer les sections efficaces effectives d'absorption et de fission du plutonium de différentes composition aussi que le η de ces combustibles.

Les résultats sont obtenus avec une précision sur les sections efficaces de ± 1% et sur le η de l'alliage de ± 200 pcm.

Un soin particulier doit être apporté aux fabrications des échantillons, en particulier sur leur géométrie et sur l'analyse de la teneur en plutonium.

Parallèlement à ces mesures, des études ont été effectuées pour interpréter les perturbations locales de flux et en particulier les effets de répartition radiale des absorbeurs, des matériaux fissiles et aussi des corps résonnants.

25.3.2. Mesure des intégrales de résonance sur MINERVE

Les résultats d'une nouvelle série de mesures portent sur des échantillons métalliques de matériaux peu capturants et très diffusants qui ont été publiés dans le rapport CEA n° R 2840: R. VIDAL et E. MARTINHO "Mesure des intégrales de résonance d'absorption (Mn, Fe, Ni, Cu, Zr, Mo)".

Les résultats obtenus pour l'intégrale de résonance au-dessus de la partie 1/v correspondant à la dilution infinie sont les suivants:

Manganèse	: 10.5	± 1	b
Fer	: 1.1	± 0.3	b
Cobalt	: 50.5	± 4	b
Nickel	: 1.0	± 0.4	b
Cuivre	: 2.2	± 0.3	b
Molybdène	: 22.7	± 1	b
Zirconium	: 1.06	± 0.14	b

25.3.3. Mesure des sections efficaces thermiques sur ZOE

De nouvelles mesures des sections efficaces de capture thermique ont été reprises par la méthode d'oscillation de phase sur ZOE. Les résultats provisoires sont les suivants:

Zirconium	: = 182	± 2	mb
Cobalt	: = 38.0	± 0.3	b
Molybdène	: = 2.60	± 0.05	b
Nickel	: = 4.35	± 0.05	b

Des études sont actuellement en cours pour mesurer et calculer les coefficients d'autoabsorption et de dépression de flux à adopter dans le cas des mesures sur des échantillons sous forme de plaques et de cylindres placés dans différents modérateurs.

25.3.4. Mesures sur des combustibles irradiés

Deux méthodes de mesures sont actuellement en cours de mise au point. L'une porte sur la mesure du nombre de fissions par spectrométrie γ en analysant les pics du ^{144}Pr et du ^{137}Cs, l'autre sur la teneur en ^{240}Pu par comptage des neutrons produits par les fissions spontanées.

Ces études se font directement sur des cartouches d'uranium naturel irradiées dans les réacteurs de puissance.

26. LABORATOIRE DE PHYSIQUE NUCLEAIRE, CENTRE D'ETUDES NUCLEAIRES DE GRENOBLE - COMMISSARIAT A L'ENERGIE ATOMIQUE - ET UNIVERSITE DE GRENOBLE (FRANCE)

R. Bouchez.

Collision des neutrons rapides de 14 MeV sur noyaux legers

26.1. $^{6}Li(n,n')$

Sections efficaces totales calculées

$Q = 0$, $\sigma_e = (850 \pm 90)$ mb

$Q = -2.18$ MeV, $\sigma_{2.18} = (100 \pm 25)$ mb

Publications

F. Merchez, Nguyen Van Sen, V. Regis, R. Bouchez,

Excitation des premiers niveaux du ^{6}Li par des neutrons de 14 MeV, C.R. Acad. Sc., Paris, 260, 3922-2925 (1965).
Communication au Colloque sur les Noyaux Légers, Lyon, 26-28.1.1966.

Résumé

On a mis en évidence par diffusion $^{6}Li(n,n')$, outre le premier niveau de 2.18 MeV, l'excitation des niveaux 1 + (3.56 MeV) et 2 + (4.52 MeV), à l'aide d'un spectromètre par temps-de-vol (résolution totale: 1.3 ns à 1 mètre). Les sections efficaces différentielles, élastique et pour le premier niveau (2.18 MeV), ont été mesurées de 15° à 150°(L) et corrigées de la diffusion multiple.

Fig. 26.1.

Section efficace différentielle (centre de masse, corrigée de la diffusion multiple) de 10° à 150° de la diffusion élastique $^{6}Li(n,n')$ avec des neutrons de 14 MeV;
Section efficace différentielle (centre de masse, corrigée de la diffusion multiple) de 20° à 150° de la diffusion inélastique $^{6}Li(n,n')^{6}Li^{*}$ (2.18 MeV), $E_n = 14$ MeV.

26.2. $^{7}Li(n,n')$

Sections efficaces totales calculées

$\sigma_{(n,n')el+0.48\ MeV} = (1100 \pm 100)$mb

$\sigma_{(n,n')el} = (1020 \pm 100)$mb*

$\sigma_{(n,n')4.63\ MeV} = (150 \pm 20)$mb

*En adoptant pour $\sigma_{(n,n')0.48\ MeV}$ la valeur de (80 ± 10)mb[3].

Publications

V. Regis, Nguyen Van Sen, A. Fiore, Pham Dinh Lien, R. Bouchez,

Excitation du niveau 5.7 MeV du ^{7}Li par diffusion (n,n') à 14 MeV, Communication à Colloque sur les Noyaux Légers, Lyon, 26-28.1.1966 (J. Phys. à paraître).

Résumé

La diffusion des neutrons rapides de 14 MeV sur le ^{7}Li a été étudiée par une méthode de temps-de-vol avec une résolution de 1.2 ns. Le niveau de 0.48 MeV n'a pas été séparé du pic de diffusion élastique; des niveaux supérieurs, seul le 4.63 MeV apparaît excité. Les distributions angulaires ont été faites de 15° à 130° pour $^{7}Li(n,n')$ (Q = 0 + Q = -0.48 MeV) et Q = -4.63 MeV.

Les sections efficaces $\sigma_{(n,n')el+0.48\ MeV}$ et $\sigma_{(n,n')4.63\ MeV}$ ont été calculées et sont en accord avec celles trouvées par Anderson et al.(1) et Armstrong et al.(2).

Références

(1) Wong, Anderson and McClure, Nuclear Physics, 33, 680 (1962).
(2) Armstrong, Gammel, Rosen, Nuclear Physics, 52, 505 (1964).
(3) Benveniste, Mitchell, Schrader and Zenger, Nuclear Physics, 38, 300 (1962).

Fig. 26.2.

Section efficace différentielle moyenne sur l'état fondamental Q = 0 et sur le premier niveau excité 0.478 MeV.
Section efficace différentielle de la diffusion inélastique sur le deuxième niveau de 4.63 MeV.

26.3. $^{9}Be(n,2n)$

Sections efficaces

$\sigma_{(n,2n)}$ = 540 mb
σ_{t} = 1.51 b

Publications

R. Bouchez, J.C. Gondrand, P. Perrin, C. Perrin, A. Giorni, P. Quivy, M. Dubus, Mise en évidence d'états excités du ^{9}Be et du ^{8}Be dans la réaction $^{9}Be(n,2n)$ avec des neutrons de 14 MeV, C.R. Acad. Sc., Paris, 259, 3501-3503, (1964).

R. Bouchez, C. Perrin, A. Giorni, R. Darves-Blanc, Evidence d'interactions à deux corps dans la réaction $^{9}Be(n,2n)$ à 14 MeV, C.R. Acad. Sc., Paris, 261, 1269-1272, (1965).
C. Perrin, Interaction à deux corps dans la réaction $^{9}Be(n,\alpha\alpha nn)$ à 14 MeV - I. Mise en évidence des états résonnants. Thèse 3° cycle, Grenoble, 1965, n° 570.
A. Giorni, Interaction à deux corps dans la réaction $^{9}Be(n,\alpha\alpha nn)$ à 14 MeV. II. Mesure des sections efficaces. Thèse 3° cycle, Grenoble 1965, n° 571.

Résumé

A l'aide d'un spectromètre à double temps-de-vol, on a observé que la réaction $^{9}Be(n,2n)$ se produit principalement avec formation d'états résonnants du $^{9}Be^{*}$ (6.76 MeV; 7.94 MeV ...) et a lieu faiblement par le processus direct $^{8}Be(0) + n_1 + n_2$, correspondant à l'éjection par un neutron incident de 14.5 MeV du neutron périphérique peu lié (1.66 MeV) dans le ^{9}Be. Les mesures effectuées aux angles $\phi_1 = -\phi_2 = 30°$, 60°, 80° et $\phi_1 = 15°$, $\phi_2 = -30°$ ont montré une anisotropie de la réaction n,2n avec prédominance vers les angles avant.

Fig. 26.3.

Répartition des évènements pour E = (7.35±0.75)MeV correspondant à la désexcitation du niveau de 6.76 MeV du ^{9}Be, montrant la formation d'états résonnants.

Fig. 26.4.

Répartition des évènements dans la bande $^{8}Be(0)$ corrigée du bruit-de-fond et de l'efficacité.

26.4. $^{9}Be(n,n')$

Sections efficaces totales calculées

Q = 0	σ_e = 948±45 mb
Q = -2.43	σ = 150±30 mb

Publications

R. Darves-Blanc, Interaction à deux corps dans la réaction $^{9}Be(n,nn)\alpha\alpha$ à 14 MeV - part. III: niveaux du ^{9}Be. Thèse 3° cycle (à paraître).

Résumé

On a mesuré par diffusion des neutrons de 14 MeV sur ^{9}Be,

les sections efficaces différentielles élastiques de 10° à 140° et inélastique sur le niveau de 2.43 MeV de 20° à 140° corrigées de la diffusion multiple.

Fig. 26.5.

Sections efficaces différentielles de la diffusion élastique de 10° à 140° (centre de masse) corrigées de la diffusion multiple.

Fig. 26.6.

Sections efficaces différentielles de la diffusion inélastique de 20° à 140° (centre de masse) également corrigée de la diffusion multiple.

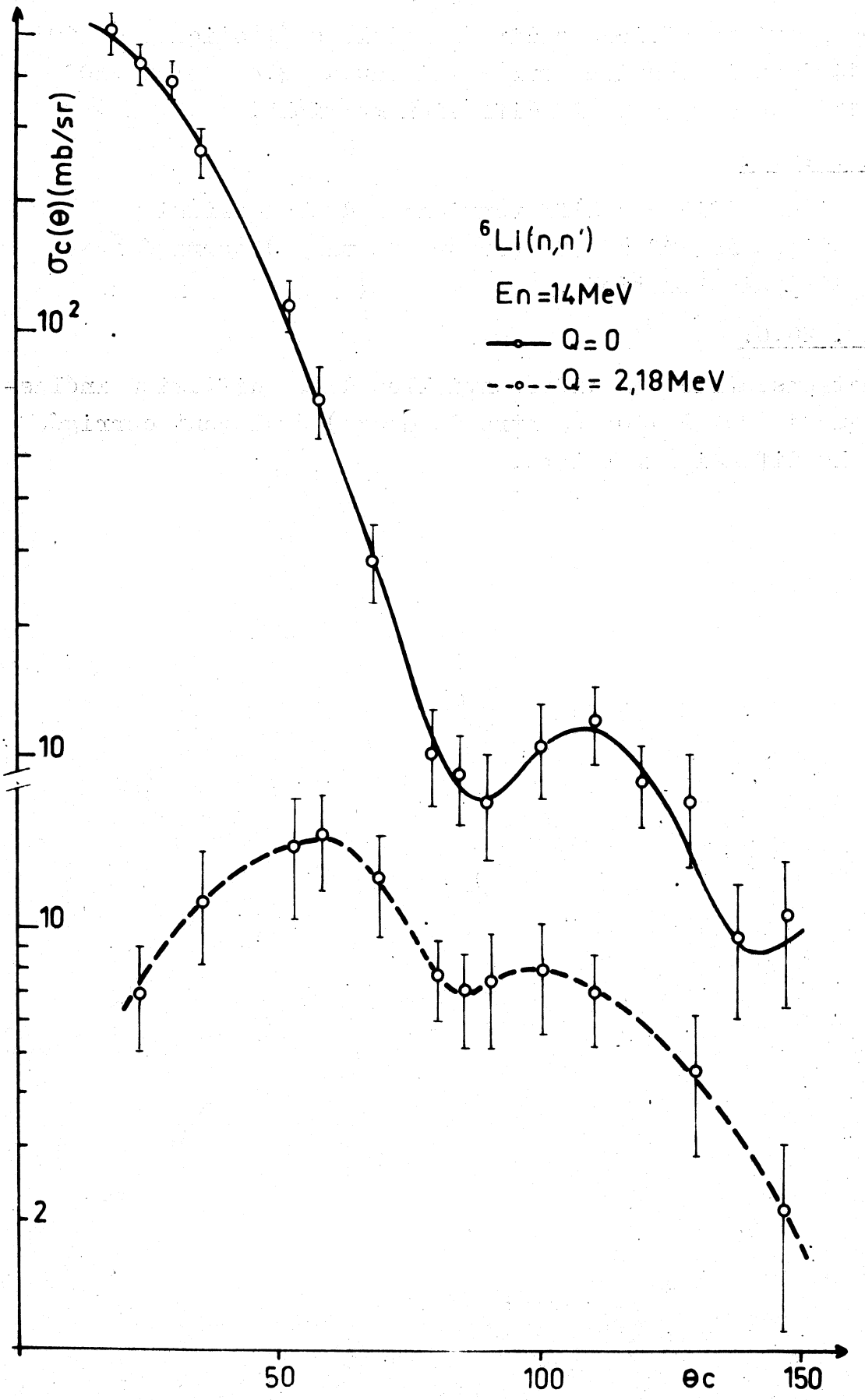

Fig. 26.1.

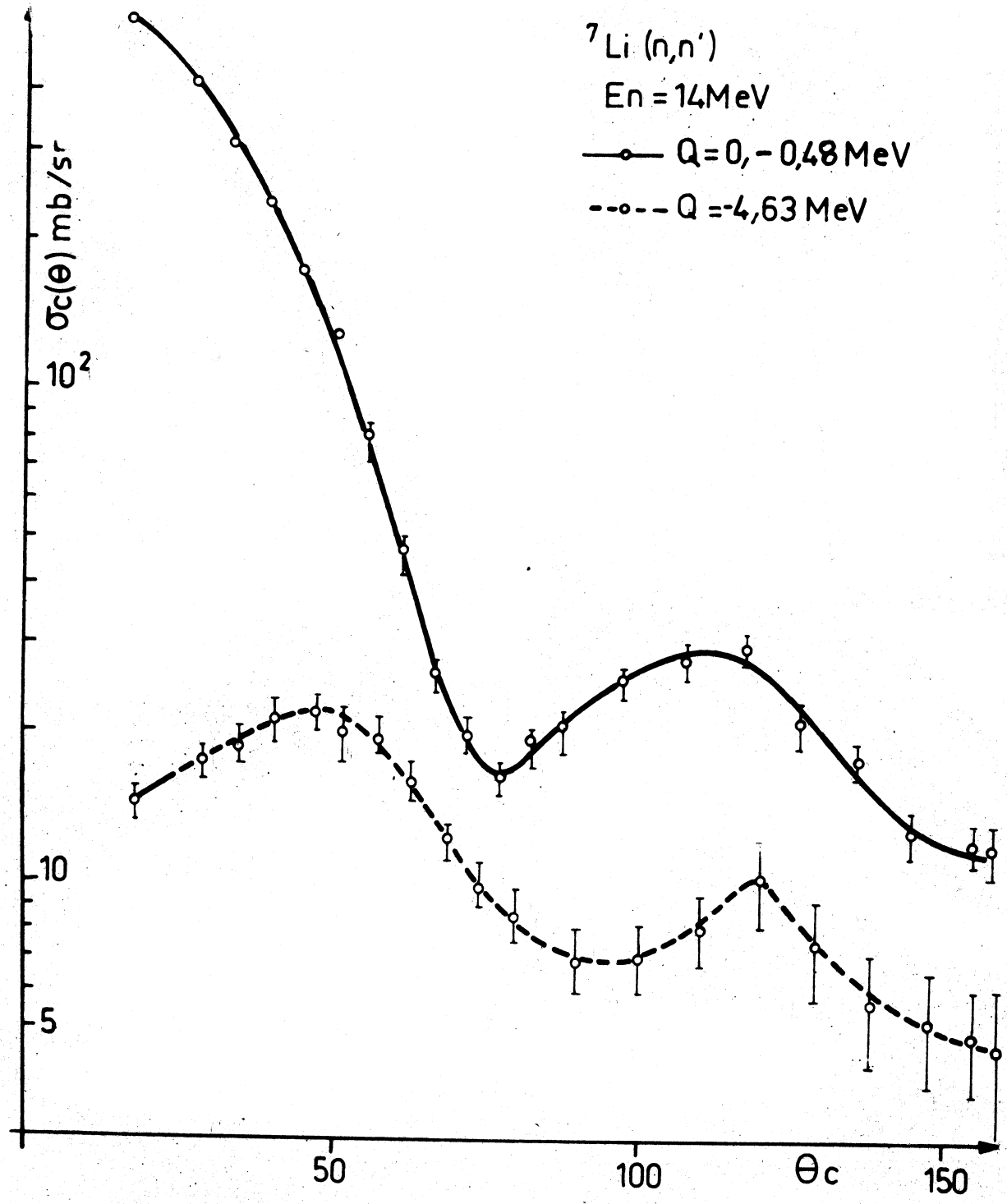
^{7}Li (n,n')
En = 14MeV
Q = 0, - 0,48 MeV
Q = -4,63 MeV
σc(θ) mb/sr
10²
10
5
50
100
θc
150

Fig. 26.2.

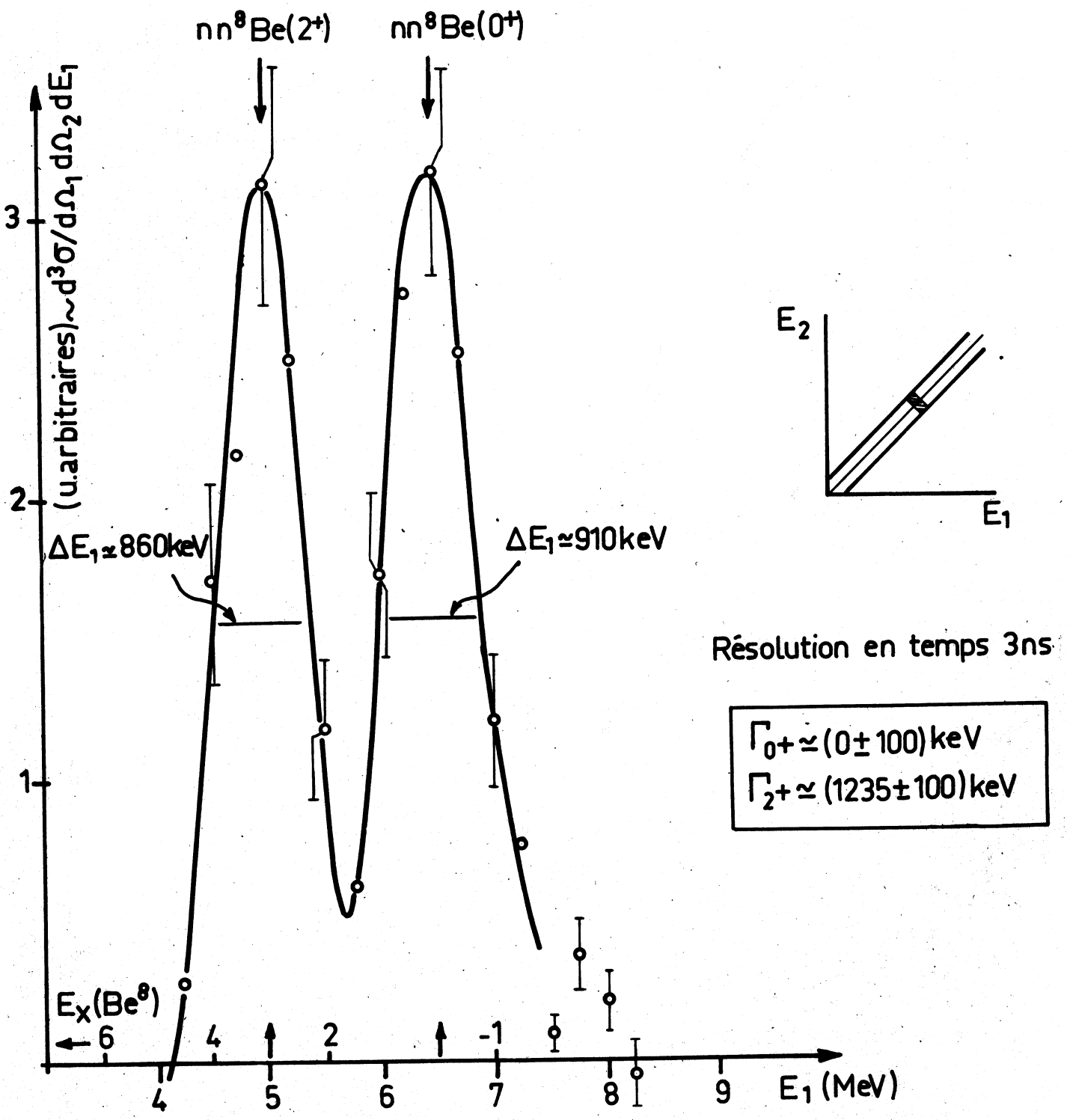
nn^{8}Be(2$^+$)
nn^{8}Be(0$^+$)
(u.arbitraires)~d$^3\sigma$/dΩ_1dΩ_2dE$_1$
3
2
1
ΔE$_1$≃860keV
ΔE$_1$≃910keV
E$_2$
E$_1$
Résolution en temps 3ns
Γ$_{0^+}$≃(0±100)keV
Γ$_{2^+}$≃(1235±100)keV
E$_x$(Be^8)
6
4
2
-1
4
5
6
7
8
9
E$_1$ (MeV)

Fig. 26.3.

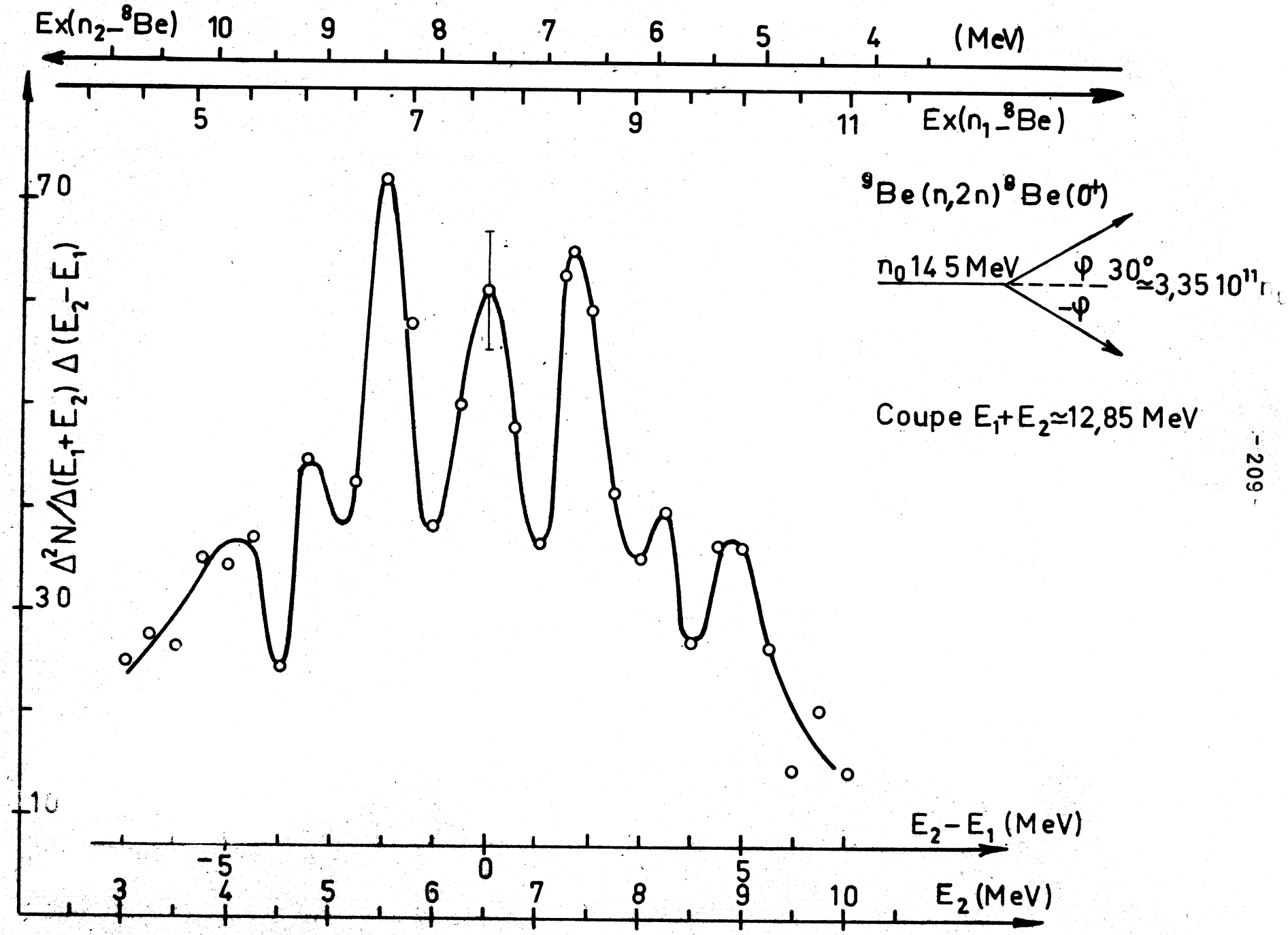
Ex(n2–8Be) 10 9 8 7 6 5 4 (MeV)
5 7 9 11 Ex(n1–8Be)
9Be(n,2n)8Be(0+)
n0 14 5 MeV
φ 30°
-φ
≃3,35 10^11 n
Coupe E1+E2≃12,85 MeV
70
30
10
Δ²N/Δ(E1+E2) Δ(E2–E1)
E2–E1 (MeV)
-5 0 5
3 4 5 6 7 8 9 10 E2 (MeV)

Fig. 26.4.

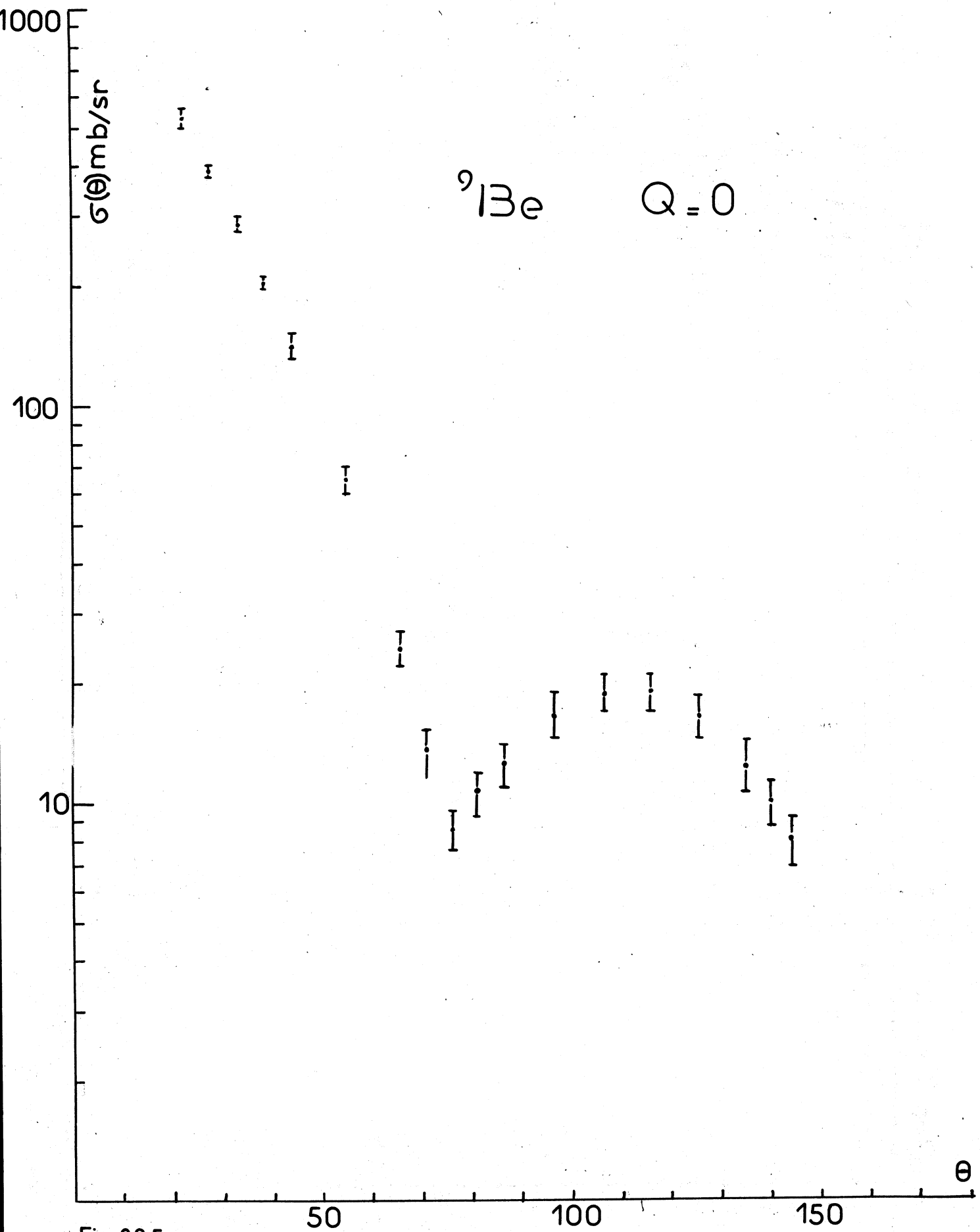

Fig. 26.5.

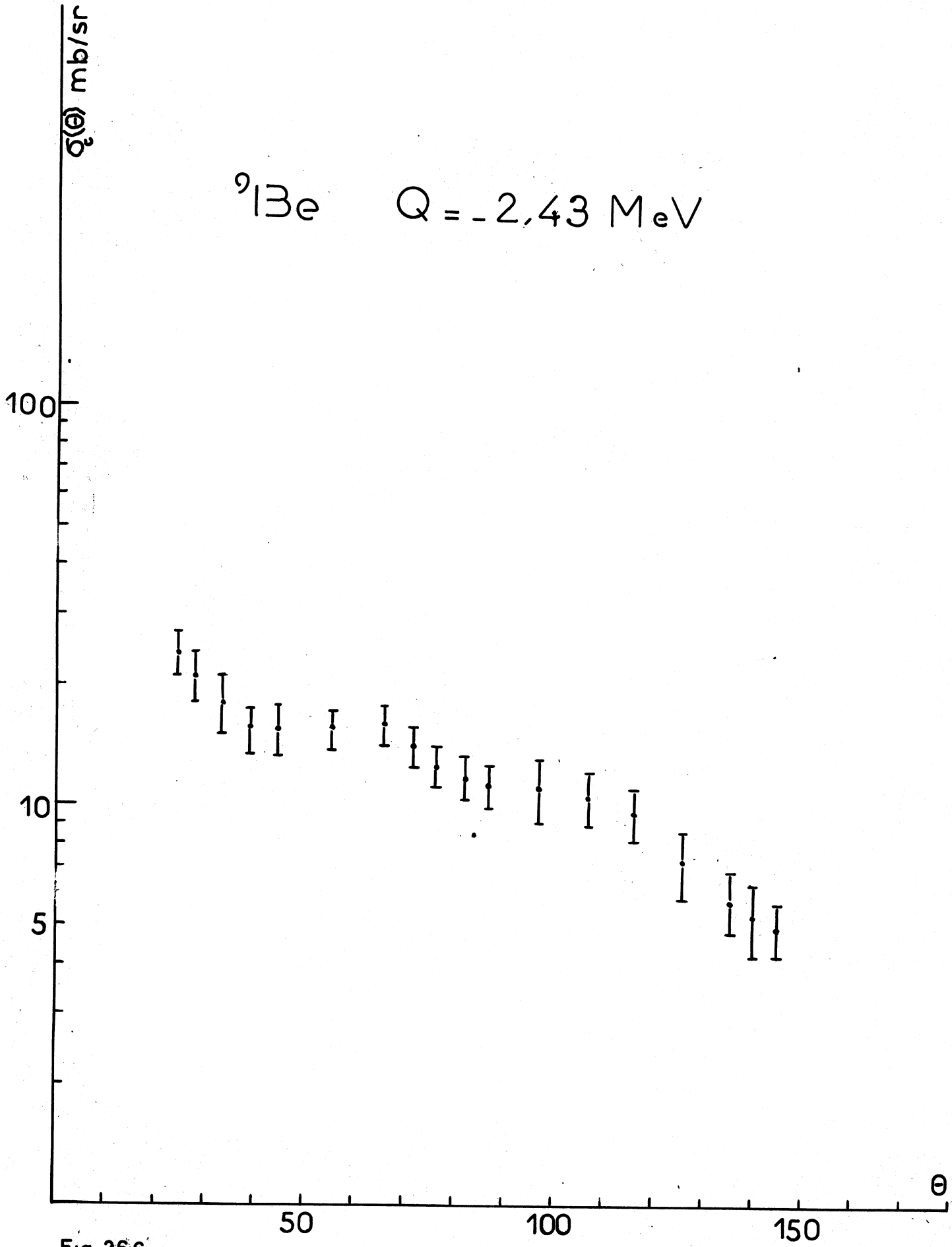

Fig. 26.6.